

MOLECULAR CHARACTERIZATION OF MURINE MODELS OF ASTROCYTOMA

Mark Vitucci

A dissertation submitted to the faculty of the University of North Carolina at Chapel Hill in partial fulfillment of the requirements for the degree of Doctor of Philosophy in the Curriculum in Genetics and Molecular Biology.

Chapel Hill
2013

Approved by:

Channing J. Der, Ph.D.

Timothy R. Gershon, M.D., Ph.D.

William Y. Kim, M.D.

C. Ryan Miller M.D., Ph.D.

Charles M. Perou, Ph.D.

© 2013
Mark Vitucci
ALL RIGHTS RESERVED

ABSTRACT

Mark Vitucci: Molecular Characterization of Murine Models of Astrocytoma
(Under the direction of C. Ryan Miller M.D., Ph.D.)

Astrocytomas are some of the most lethal diffuse gliomas, and glioblastoma (GBM, Grade IV astrocytoma) has a median survival of 12-15 months with therapy. The last decade has seen increased efforts to define the molecular landscape of human GBM, and led to a focus on genetic abnormalities within the receptor tyrosine kinase (RTK), RB cell cycle, and P53 signaling pathways. Genetically-engineered mouse (GEM) models have been designed based upon the data from these studies and have helped determine some of the requirements for gliomagenesis depending on the cellular and developmental context. Despite these efforts gliomagenesis requirements and progression are not completely defined, and more importantly, it is often unclear which molecular subtype is modeled by these GEM. In this work, we employ GEM with conditional, inducible mutations in the RB cell cycle, MAPK, and PI3K pathways to effect astrocytoma initiation followed by stochastic progression in astrocytes throughout the brain in adult mice. We define the requirements for astrocytoma initiation and the effect they have on gene expression and copy number. Stochastic progression to high-grade astrocytoma (HGA) and GBM are characterized by detection via contrast-enhancing MRI, rapid growth, genotype-dependent survival, acquisition of copy number abnormalities (CNA), and gene expression subtypes that resemble human GBM. These subtypes correlate with brain region rather than original genotype.

In parallel, we isolated astrocytes from pups containing the same genetic mutations and induced recombination in culture to create G1/S-defective astrocytes with activated *Kras* and/or *Pten* deletion.

We examined how these individual and combined mutations affected gene expression and phenotypic hallmarks of astrocytoma tumorigenesis including cell growth, migration, and invasion. Combined disruption of MAPK and PI3K signaling led to the most aggressive, invasive astrocytes (TRP) with stem-like and proneural expression profiles. These TRP astrocytes were confirmed to have stem cell properties *in vitro* and *in vivo*. After orthotopic injection into syngeneic mice, these TRP astrocytes formed HGA with high incidence, short latency, and reproducible survival, supporting its utility as a preclinical model. We replicated standard of care GBM treatment consisting of radiation with concurrent temozolomide and showed that TRP allografts were susceptible to radiation but not temozolomide. Similar to TRP astrocytes *in vitro*, the allograft HGA expression profiles were proneural, but after radiation treatment most were most similar to the mesenchymal subtype. Overall, this research defines the requirements for astrocytoma in adult murine astrocytes and raises important questions about whether mutations, cell type, or location determines molecular subtype. We develop several models which will be useful to further elucidate the molecular nuances of astrocytoma and their effects on initiation, progression, and signaling pathways. These models will also serve as the basis for future subtype specific preclinical models in which to develop novel gene signatures, biomarkers, and molecularly targeted therapies.

TABLE OF CONTENTS

LIST OF FIGURES	VII
LIST OF TABLES	X
LIST OF ABBREVIATIONS	XI
CHAPTER I: INTRODUCTION	1
Gene expression profiling of gliomas: Merging genomic and histopathological classification for personalized therapy	1
Genetically-engineered mouse models of diffuse gliomas	15
CHAPTER II: PROGRESSION FROM LOW- TO HIGH-GRADE ASTROCYTOMA IS CHARACTERIZED BY TRANSCRIPTOMAL HETEROGENEITY AND GENOMIC NUMBER COPY CHANGES.	37
Introduction	37
Materials and methods.....	40
Results.....	47
Discussion	57
CHAPTER III: COOPERATIVITY BETWEEN MAPK AND PI3K SIGNALING ACTIVATION IS REQUIRED FOR GLIOBLASTOMA PATHOGENESIS	205
Introduction	205
Materials and methods.....	208
Results.....	216
Discussion	226

CHAPTER IV: RADIATION, BUT NOT TEMOZOLOMIDE, IS EFFECTIVE IN AN ORTHOTOPIC ALLOGRAFT OF PRONEURAL GLIOBLASTOMA.....	260
Introduction	260
Materials and methods.....	261
Results.....	266
Discussion	271
CHAPTER V: DISCUSSION	282
REFERENCES	290

LIST OF FIGURES

Figure 1.1. Overall survival of patients with newly-diagnosed gliomas.	30
Figure 2.1. GFAP-CreER mediates recombination throughout the brain	63
Figure 2.2. Effects of initiating genotype and brain region on LGA tumorigenesis.	64
Figure 2.3. LGA transcriptomes show driver mutation- and brain region-associated signatures.	65
Figure 2.4. KrasG12D facilitates malignant progression to HGA.	66
Figure 2.5. LGA stochastically progress to rapidly proliferative, lethal HGA after acquisition of CNA.	67
Figure 2.6. GEM HGA transcriptomes are heterogeneous, mimic human GBM subtypes, and are reminiscent of distinct neural cell types.	69
Figure S2.1. RB pathway genes are altered in nearly all human GBM.	70
Figure S2.2. GFAP-CreER mediates recombination throughout the brain.	71
Figure S2.3. GFAP-CreER targets astrocytes.	72
Figure S2.4. GFAP-CreER does not target neurons.	73
Figure S2.5. Initiating oncogenic mutations (genotype) influence LGA tumor burden.	74
Figure S2.6. Morphometric analysis of nuclear density in phenotypically wild-type and LGA-containing mice.	75
Figure S2.7. Ablation of all Rb family members is required for tumorigenesis in adult murine astrocytes.	76
Figure S2.8. Cortical TRP+/- LGA burden increases over time.	77
Figure S2.9. TRP+/- mice develop LGA in all brain regions.	78
Figure S2.10. Perineuronal satellitosis increases over time in TRP+/- LGA.	79
Figure S2.11. Local proliferation of transformed cortical astrocytes produces hypercellular TRP+/- astrocytoma foci.	80

Figure S2.12. LGA transcriptomes cluster according to initiating genotype and brain region.	81
Figure S2.13. LGA have silent genomic landscapes, but transcriptional dysregulation of cell cycle genes.	82
Figure S2.14. Transformed TRP+/- astrocytes re-express p16.	83
Figure S2.15. KrasG12D potentiates malignant progression.....	84
Figure S2.16. Initiating genotype and astrocyte location influence CNA acquired upon malignant progression in TR(P) HGA.....	85
Figure S2.17. TR(P) HGA transcriptomes are heterogeneous and consist of three subtypes.....	86
Figure S2.18. HGA transcriptomes are distinct from LGA and subtypes correlate with anatomic location.	87
Figure S2.19. GEM HGA and human GBM have similar transcriptomes.	88
Figure S2.20. Copy number landscapes of GEM HGA models with and without p53 deletion are distinct.....	89
Figure S2.21. Heterozygous deletion of p53 accelerates tumorigenesis in T(RP) mice.....	90
Figure S2.22. T(RP) astrocytomas with p53 deletion show minimal CNA.	91
Figure S2.23. p53 deletion contributes to widespread genomic instability.....	92
Figure 3.1. MAPK and PI3K signaling and growth of G1/S-defective astrocytes with activated Kras and/or Pten deletion.....	231
Figure 3.2. Kras activation and Pten loss increase G1/S-defective astrocyte migration.	232
Figure 3.3. Pten deletion is necessary for maximum G1/S-defective astrocyte invasion.....	233
Figure 3.4. Restoration of Pten expression limits growth, migration, and invasion in TRP-/- astrocytes.	234
Figure 3.5. Gene expression profiling of G1/S-defective astrocytes with activated Kras and/or Pten deletion.	235
Figure 3.6. A PI3K signature defined in TRP-/- astrocytes upon release from PI-103-mediated inhibition of PI3K signaling is enriched in human	

proneural GBM.	236
Figure 3.7. G1/S-defective astrocytes form astrocytomas upon orthotopic injection into syngeneic, immunocompetent mouse brains.	237
Figure S3.1. MAPK and PI3K signaling and apoptosis in wild-type and G1/S-defective astrocytes.	238
Figure S3.3 Pharmacologic effects on signaling and viability.	240
Figure S3.4. Restoration of Pten reduces invasion in TP-/- astrocytes.	241
Figure S3.5. Consensus clustering of the transcriptomes of G1/S-defective astrocytes with and without activated Kras and Pten deletion.	242
Figure S3.6. Pharmacologic inhibition of PI3K pathway signaling in TRP-/- astrocytes.	243
Figure S3.7. Histopathological features of astrocytomas derived from G1/S-defective astrocytes.	244
Figure S3.8. Incidence of astrocytomas over the first four weeks post-injection.	245
Figure 4.1: TRP cells function as glioma stem cells in vitro and in vivo	274
Figure 4.2. TRP allografts develop rapidly proliferating GBM	275
Figure 4.3. TRP cells are sensitive to ionizing radiation and TMZ <i>in vitro</i>	276
Figure 4.4. TRP allografts response to radiation but not temozolomide therapy	277
Figure S4.1. TRP astrocytes express stem cell markers.	278
Figure S4.2. Orthotopic allograft injections have reproducible survival.	279
Figure S4.3. TRP astrocytes are insensitive to temozolomide.	280
Figure S4.4. Bioluminescent Imaging in U87 and TRP cells.	281

LIST OF TABLES

Table 1.2 Summary of glioma microarray studies.....	33
Table 1.3. Diffuse glioma GEMM.....	36
Table S2.1. TRP LGA cohort: Mice sacrificed at 2 m after induction.	97
Table S2.2. GFAP-CreER mice with Rb1 deletion \pm KrasG12D \pm Pten deletion or Nf1 deletion \pm T121 \pm Pten deletion.....	102
Table S2.3. One versus rest SAM analysis of T(RP) LGA transcriptomes at 2 m after induction.....	169
Table S2.4. KrasG12D immune LGA signature.....	176
Table S2.5. TRP HGA cohort: Mice aged to neurological morbidity.	178
Table S2.6. CNA in Rb, RTK, MAPK, PI3K, and Trp53 pathway genes in TR(P) HGA.	180
Table S2.7. CNA in spatially distinct TR(P) HGA show evidence of clonal evolution	183
Table S2.8. TR(P) HGA transcriptome samples.....	185
Table S2.9. HGA subtypes S1-S3 600-gene classifier.....	198
Table S2.10. Gene ontology (GO) terms from TR(P) HGA subtype SAM analyses.	201
Table S2.11. Transcriptomal subtypes in GEM HGA test set.....	202
Table S2.12. GFAP-CreER mice with p53 deletion and combinations of T121, KrasG12D, Pten deletion.	204
Table S3.1. ssGSEA ROC and P-values for the fifteen most and least enriched MSigDB gene expression signatures in Class 1-3 G1/S defective astrocytes.	246
Table S3.2. GSA scores and statistical significance of murine neural ontology and human HGA signatures for Class 1-3 G1/S defective astrocytes	247
Table S3.3 PI3K signature genes (N=518) defined by release of TRP ^{-/-} G1/S defective astrocytes from PI-103 inhibition.	248

LIST OF ABBREVIATIONS

4OHT	4-hydroxy-tamoxifen
A2	Low-grade astrocytoma, grade 2
A3	Anaplastic astrocytoma, grade 3
aCGH	Array comparative genomic hybridization
ANOVA	Analysis of variance
BS	Brain stem
CNA	Copy number abnormality
CSC	Cancer stem cell
CTX	Cortex
DI	Diencephalon
EGFR	Epidermal growth factor receptor
GBM	Glioblastoma
GEM	Genetically-engineered mice
GEP	Gene expression profiling
GFAP	Glial fibrillary acidic protein
GSEA	Gene set enrichment analysis
H&E	hematoxylin and eosin
HGA	High-grade astrocytoma
LGA	Low-grade astrocytoma
MAPK	Mitogen activated protein kinase
MRI	Magnetic resonance imaging

NF1	Neurofibromatosis type 1
NSC	Neural stem cell
OFB	Olfactory bulb
OPC	Oligodendrocyte precursor cells
P	Pten
PTEN	Phosphatase and tensin homolog
R	Kras ^{G12D}
RB	Retinoblastoma
RTK	Receptor tyrosine kinase
SVZ	Subventricular zone
T	N-terminal 121 amino acid truncation mutant of SV40 large T antigen
TCGA	The Cancer Genome Atlas
TMZ	Temozolomide
WHO	World Health Organization
XRT	External beam radiation therapy

CHAPTER I

Introduction

GENE EXPRESSION PROFILING OF GLIOMAS: MERGING GENOMIC AND HISTOPATHOLOGICAL CLASSIFICATION FOR PERSONALIZED THERAPY^{1,2}

Summary

The development of DNA microarray technologies over the past decade has revolutionized translational cancer research. These technologies were originally hailed as more objective, comprehensive replacements for traditional histopathological cancer classification systems based on microscopic morphology. Although DNA microarray-based gene expression profiling (GEP) remains unlikely in the near term to completely replace morphological classification of primary brain tumors, specifically the diffuse gliomas, GEP has confirmed that significant molecular heterogeneity exists within the various morphologically-defined gliomas, particularly glioblastoma (GBM). Herein we provide a ten year progress report on human glioma GEP, with a focus on development of clinical diagnostic tests to identify molecular subtypes uniquely responsive to adjuvant therapies. Such progress may lead to a more precise classification system that accurately reflects the cellular, genetic, and molecular basis of

¹A version of this work was previously published as Vitucci M, Hayes DN, Miller CR. Gene expression profiling of gliomas: merging genomic and histopathological classification for personalised therapy. Br J Cancer. 2011;104(4):545-53.

² A version of this work was previously published as Schmid RS, Vitucci M, Miller CR. Genetically engineered mouse models of diffuse gliomas. Brain Res Bull. 2012;88(1):72-9

gliomagenesis, a prerequisite for identifying subsets uniquely responsive to specific adjuvant therapies and ultimately in achieving individualized clinical care of glioma patients.

Introduction

Morphological evaluation of cancers by light microscopy has been the foundation for diagnosis, prognostication, and therapeutic stratification for well over a century. Yet patients with morphologically identical tumors can have significantly different clinical outcomes. To address the pressing medical need for more accurate outcome predictions, a variety of transformative technologies have been developed over the last four decades – electron microscopy, molecular biology, immunohistochemistry, and quantitative RT-PCR – to refine traditional cancer classification or as outright replacements. The newest such technology, DNA microarrays, was introduced in 1995, and its potential clinical utility in oncology was quickly recognized. In fact, the Director of the U.S. National Cancer Institute issued a challenge to the scientific community in 1999 (1) to “harness the power of comprehensive molecular analysis technologies to make the classification of tumors vastly more informative. This challenge is intended to lay the groundwork for *changing the basis* (emphasis added) of tumor classification from morphological to molecular characteristics.”

The response from the cancer research community has been intense: nearly 14,000 publications have utilized DNA microarrays for genome-wide gene expression profiling (GEP) in all aspects of cancer research, from basic to translational to clinical. GEP has unequivocally established that significant molecular heterogeneity exists within morphologically-defined cancers and that potentially clinically-relevant molecular subtypes can be identified. Yet to date, only two molecular diagnostic tests developed using DNA microarrays have either been approved by the U.S. Food and Drug Administration (MammaPrint®) or incorporated into practice guidelines (Oncotype Dx®) for clinical use in breast cancer (2).

This discordance between scientific productivity and clinical implementation over the course of a decade is not unexpected, given the stringent sample requirements, pace of technology development, data volume and complexity, continually evolving data analysis techniques, lack of defined best practices for analysis, and levels of evidence required for clinical use. A number of excellent review articles have discussed these and other impediments to implementing GEP clinically (2-4). Herein, we review a decade of DNA microarray-based GEP on the most common and biologically aggressive group of primary brain tumors, the diffuse gliomas (hereafter referred to simply as gliomas). The discussion will revisit morphological classification and address the potential role of GEP in identifying clinically-relevant molecular subtypes of gliomas. We will then primarily focus on studies that have examined the prognostic impact of multi-gene signatures for the most deadly glioma, glioblastoma (GBM).

Morphological classification of gliomas

Bailey and Cushing established the first diagnostic classification system for primary brain tumors in 1926, based upon their understanding of the histogenetic basis of brain development and the morphological resemblance of primary brain tumors to their presumed developmental counterparts by light microscopy. This system has been refined periodically, culminating in the current World Health Organization (WHO) scheme (5). Seven gliomas are currently recognized as distinct clinicopathological entities, each characterized by cytological and immunohistochemical evidence of differentiation along astrocytic, oligodendroglial, or both glial lineages (Table 1.1). Further refinement into distinct prognostic groups is dictated by histological grading (II-IV) based on morphological features associated with more aggressive biology, including mitoses, microvascular proliferation, and necrosis (6). Molecular and genetic features constitute an additional level of detail utilized not only to diagnostically differentiate among these entities, but increasingly to predict clinical outcomes and response to adjuvant therapies.

The prognostic power of the current WHO glioma classification has facilitated its widespread adoption for clinical patient management. However, it has long been recognized that individual patients within each diagnostic category can have vastly different outcomes that are not otherwise accounted for by established prognostic factors, including age, Karnofsky performance status (KPS), and therapy. This prognostic variability can be visualized using the 95% confidence intervals of Kaplan-Meier survival curves (Fig. 1.1). The extent to which prognostic factors account for outcome variability in multivariate Cox proportional hazards models can be quantified with metrics such as Harrell's C statistic (Table 1.1) (7). Using these two measurements, prognostic variability is least pronounced in astrocytic gliomas (Fig. 1.1A), particularly GBM, and is substantially higher in mixed (Fig. 1.1B) and pure oligodendroglial (Fig. 1.1C) gliomas. Prognostic variability is most pronounced among the lower grade gliomas (Fig. 1.1D, E). For these gliomas in particular, accurate classification and prognostication have become increasingly dependent on molecular assays. The most notable test detects co-deletion of chromosomal arms 1p and 19q, a genetic signature and favorable prognostic factor strongly associated with oligodendroglial differentiation (7). Yet even with ancillary molecular testing, classification of a subset of morphologically-ambiguous grade II and III gliomas remains challenging, even among experienced neuropathologists (6, 7). Clearly, more objective, molecular methods for diagnostic discrimination among gliomas are needed.

The clinicopathological variables central to the WHO 2007 classification - patient age at diagnosis, differentiation (cytology), histological grade, and 1p19q co-deletion status - account for 70-80 percent of the prognostic variability among each of the three major types of gliomas, based on the C index (Table 1.1). Inclusion of additional clinical factors (e.g. KPS, therapy) not otherwise available in this retrospective dataset would likely account for even more of the prognostic variability. Despite the inability to accurately predict outcomes for individual patients, this example clearly illustrates that existing clinicopathological factors account for the vast majority of prognostic variability in gliomas. It is

in this context – the ability to provide prognostic information independent of established factors - that the clinical utility of GEP must be defined (3). The key for clinical implementation of GEP will therefore be to quantify the remaining 20-30% of prognostic variability by one of two means: 1) utilizing GEP as a diagnostic adjunct to more accurately classify morphologically-ambiguous gliomas, or 2) to identify prognostically distinct molecular subtypes within otherwise morphologically-homogeneous gliomas.

Molecular classification of gliomas

The earliest GEP studies utilized class comparison to identify differentially expressed genes among morphologically-defined gliomas. Such genes were found in low-grade versus high-grade astrocytomas (8), high-grade oligodendrogliomas versus GBM (9, 10), primary versus secondary GBM (11-13), adult versus pediatric GBM (14), or a variety of morphologically-defined glioma subtypes (12, 13, 15). Using primarily hierarchical clustering on differentially expressed genes, transcriptomal profiles of individual tumors were shown to be most similar to those from the same diagnostic category, i.e. gliomas of similar differentiation and grade. These studies confirmed that morphological differences among gliomas are reflected at the mRNA transcript level and that differentially-expressed genes could be utilized to distinguish among morphologically-defined subtypes. However, discordance between morphological diagnosis and GEP-defined molecular subtype was frequent, likely due in part to inclusion of difficult-to-classify, morphologically-ambiguous gliomas.

Nutt, Louis, and colleagues provided a glimpse of the potential clinical utility of GEP as an ancillary diagnostic test for more accurate glioma classification (9). These investigators identified genes significantly correlated with either morphologically classical GBM or anaplastic oligodendroglioma in a training set of 21 tumors and built a class prediction model that showed 86% accuracy in assigning 29 diagnostically-challenging GBM and anaplastic oligodendrogliomas to their respective diagnostic categories. More importantly, a statistically significant difference in overall survival for the GEP- but not

the morphologically-defined groups was found, suggesting that GEP may provide more accurate classification and prognostication, particularly for morphologically-ambiguous gliomas. These findings were confirmed by Shirahata and colleagues (10), who identified 168 differentially-expressed genes from PCR array data on 32 GBM and anaplastic oligodendrogliomas and a weighted voting algorithm to develop a 67-gene diagnostic assay with 96.6% accuracy in distinguishing between these two prognostically-distinct high-grade gliomas using the published Nutt dataset (9) for validation.

Li, Fine, and colleagues provided the first report of a comprehensive, molecular classification of all gliomas (16). These authors utilized two unsupervised machine learning methods on a large training set (N=159) of WHO grade II-IV gliomas from all three histological categories. Guided only by molecular data, without influence of prior morphological diagnosis, they identified six hierarchically nested subtypes, divided into two main categories (O and G). The first category contained two subgroups (OA and OB) and the second had four nested subgroups (GA1, GA2, GB1, and GB2). These data confirmed that morphological differences among gliomas are reflected at the mRNA transcript level. Survival analyses showed that the O and G main groups and the OA and OB subgroups of O-type tumors, but not the four G subgroups, were prognostically distinct. Importantly, the prognostic impact of the two main subgroups was confirmed in an independent dataset from The Cancer Genome Atlas (TCGA) consisting entirely of GBM (17), while that of the six subgroups was confirmed in the REMBRANDT and Phillips, et al. datasets consisting of all seven gliomas (18, 19). However, the concordance between GEP-defined subtypes and histopathological diagnoses was not assessed and multivariate survival analyses with known prognostic factors were not conducted.

In retrospect, the aforementioned studies utilized small (N<100 per diagnostic category), ostensibly convenience cohorts of previously banked, frozen gliomas. As such, individual studies were statistically underpowered to assess the diagnostic discriminatory power of GEP vis-à-vis morphological classification. Moreover, the relatively small sample sizes and lack of data on known prognostic

covariates precluded comprehensive multivariable analyses. Particularly for the earlier studies, the prognostic impact of GEP signatures could not be validated in large, external datasets (4). Fortunately, most data have been deposited in publically-available online repositories, including the Gene Expression Omnibus and REMBRANDT (19). These data have already been instrumental in both novel hypothesis-driven, mechanistic studies (20) and subsequent GEP studies described below. Only through collection of GEP data on a sufficient number of all seven morphologically-defined gliomas will it be possible to assess whether GEP will be diagnostically robust enough to *replace* morphology as the *basis* for glioma classification.

GEP identifies prognostically-distinct molecular subtypes of gliomas

A number of GEP studies have identified prognostically-distinct molecular subtypes of gliomas. In 2004, Freije, Nelson, and colleagues analyzed 74 gliomas from four histological types and identified 595 differentially-expressed genes that correlated with overall survival (21). Hierarchical clustering showed four molecular subtypes (labeled HC1A, HC1B, HC2A, and HC2B) that segregated into two distinct (P=0.00011) survival clusters (SC): SC1 (93% HC1A/B and 62% non-GBM) and SC2 (76% HC2A/B and 89% GBM) with 4.8 and 0.6 year (y) median overall survival, respectively. Prognostic significance was confirmed in the independent Nutt dataset (9) and multivariate analysis showed that survival cluster was independent of patient age and histological grade. Functional annotation of the gene lists showed that HC1A subtype tumors were enriched for genes involved in neurogenesis (22), suggesting a more differentiated phenotype. In contrast, the poor survival subtypes were enriched for proliferation (HC2A) and extracellular matrix/invasion-related (HC2B) genes. A similar list of survival-related genes implicated in neurogenesis was identified by Liang, et al. (23), who also showed that GBM could be divided into two prognostically distinct molecular subtypes (median overall survival 2.1 vs. 0.3 y).

In 2006, Phillips, Aldape, and colleagues analyzed 76 high-grade astrocytomas and identified 108 differentially-expressed genes significantly associated with overall survival (18). Hierarchical and k-means clustering with those genes showed three distinct subtypes termed proneural, proliferative, and mesenchymal based upon functional annotation of representative genes. Like Frieje HC1A, the proneural subtype was defined by genes implicated in neurogenesis, composed predominantly (69%) of non-GBM, and associated with significantly more favorable median overall survival (3.6 vs. ≤ 1.3 y), independent of histological grade. In contrast, the proliferative and mesenchymal gene signatures were enriched for proliferation- and extracellular matrix/invasion-related genes, similar to the Frieje HC2A and HCA2B subtypes, respectively. Prognostic significance of molecular subtype was validated in an independent cohort of 184 gliomas of various histological types. Taken together, these results suggest that 1) the molecular subtype of a majority of WHO grade II-III gliomas is HC1A/proneural, and 2) HC1A/proneural GBM may be more prognostically favorable.

Using published datasets and new GEP data on 86 GBM, a subsequent meta-analysis by Lee, et al. utilized 377 differentially-expressed genes that divided GBM into four distinct subtypes on hierarchical clustering: HC1A/proneural, HC2A/proliferative, HC2B/mesenchymal, and a fourth with hybrid HC2A/HC2B features termed ProMes (24). Survival analysis confirmed the more favorable prognosis of HC1A/proneural GBM versus the remaining three molecular subtypes (median 1.4 vs. 0.9 y). With this larger dataset of 267 GBM, the authors also confirmed an association first identified by Phillips (18), namely that the mean age at diagnosis of proneural GBM patients was significantly younger (51 vs. 55 y, $P=0.02$). Moreover, in multivariable analyses, only molecular subtype, but not age, was significantly associated with overall survival. These data suggest a molecular basis for the known association of younger age with improved overall survival in GBM patients.

However, it is of critical note that none of these prognostic studies distinguished among recognized morphological variants of GBM. As shown in **Table 1.1**, GBM with oligodendroglial features occur in

younger patients and have a significantly prolonged overall survival compared to their GBM counterparts ($P < 0.0001$). Similarly, another morphological variant of GBM, small cell GBM (6), characterized by frequent gains of chromosome 7 (*EGFR*) and loss of chromosome 10q (*PTEN*), is morphologically similar to the prognostically more favorable anaplastic oligodendroglioma but lacks 1p19q codeletion. The recent recognition of these morphological patterns of GBM (5, 6), prognostically-distinct from anaplastic oligoastrocytoma and anaplastic oligodendroglioma, respectively, raises the possibility that earlier studies were “contaminated” with tumors known to have different prognoses. In addition, at least two significant design flaws were common in these studies (3, 4): 1) subtype-specific signature genes were identified using heterogeneous training sets composed of various histological subtypes (e.g. anaplastic astrocytoma and GBM) with known differences in overall survival (**Table 1.1**) and 2) signature genes were defined based upon their association with outcome in training sets and their prognostic significance was reanalyzed in independent test sets, raising the possibility that the correlation between GEP-defined subtypes and overall survival were a consequence of prior selection for outcome-related genes (3). To avoid the first problem, future studies should ideally define prognostic signatures in morphologically- and hence prognostically-homogeneous cohorts of gliomas. Moreover, consensus diagnosis among multiple, experienced neuropathologists and/or utilization of ancillary molecular testing such as 1p19q status for accurate assignment of morphologically-ambiguous cases into established diagnostic categories will be important quality control measures.

The second problem is likely mitigated by two recently published studies that have identified the HC1A/proneural subset of GBM using gene signatures defined completely by unsupervised methods. In the largest single-institution study conducted to date (25), Gravendeel and colleagues defined molecular subtypes for 276 gliomas of all histological types. Using 5,000 genes with highly-variable expression, these authors identified six molecular subtypes with distinct prognoses. GBM largely (73-86%) fell into three clusters (18, 22, and 23) and these tumors showed inferior prognosis relative to GBM in other

clusters (9, 16, 17) (median overall survival 0.7 vs. 2.1 y). Cluster 9 consisted primarily (86%) of oligodendroglial neoplasms and the vast majority (82%) appropriately harbored combined 1p19q loss-of-heterozygosity (LOH). Notably, the prognostically superior cluster 17 (median overall survival 3.3 and 2.1 y for all C17 gliomas and GBM, respectively) significantly (97%) overlapped with the Phillips proneural subtype, suggesting that detection of a subgroup of GBM with improved prognosis and transcriptional profiles similar to lower grade gliomas was not a consequence of prior selection of outcome-related genes (18). Notably, cluster 22 was enriched (38%) for secondary GBM, tumors that progress from lower grade precursors, arise in younger patients (6), and feature *IDH1* mutations (26), but lack *EGFR* amplification (5). These findings confirm those from a previous study that demonstrated distinct molecular profiles in primary versus secondary GBM (11). Clusters 18 and 23 contained predominantly GBM (78 and 86%, respectively) and showed significant overlap with Phillips proliferative (52%) and mesenchymal (93%) subtypes (18). Upon analysis of data (27) from the definitive phase III clinical trial that established concomitant chemoradiotherapy and adjuvant temozolomide as the standard-of-care for newly-diagnosed GBM patients (28), these clusters were found to selectively benefit from combined chemoradiation versus radiation alone. Importantly, multivariate analysis included most known prognostic factors, including age, gender, histological type, grade, KPS, surgery, chemotherapy, *EGFR* amplification, 1p19q status, and *IDH1* mutation (26). Only molecular subtype, KPS, and gender were significant, independent prognostic factors in this dataset ($P \leq 0.02$), suggesting that molecular subtyping may be more prognostically accurate than morphological classification. Moreover, these authors validated the prognostic significance of their signatures in four independent datasets (16, 18, 19, 29).

The TCGA, established by the U.S. National Cancer Institute and National Human Genome Research Institute in December 2005 with the mission of understanding “the molecular basis of cancer through the application of genome analysis technologies,” selected GBM as its first cancer type for study, based

on its uniformly poor prognosis and limited treatment options. As part of this multi-institutional project, we analyzed 200 GBM on three different GEP platforms (17). Unsupervised hierarchical cluster analysis defined four subtypes, termed proneural, neural, classical, and mesenchymal based on functional gene annotation and prior convention (18). Significant overlap in molecular subtypes was found for TCGA mesenchymal/Phillips mesenchymal/Freije HC2B and TCGA proneural/Phillips proneural/Freije HC1A (18, 21). Unlike previous studies, the TCGA proneural subtype was not associated with improved prognosis in the TCGA dataset consisting solely of GBM, but was in the validation datasets (18, 19) containing lower grade gliomas. Conversely, reanalysis of the TCGA GBM data with Phillips molecular subtype designations confirmed a slightly more favorable prognosis of the Phillips proneural GBM (median overall survival 1.2 y) relative to Phillips mesenchymal/proliferative GBM subtypes (1.0 and 0.6 y, respectively, $P=0.03$). These findings suggest that subtyping based on prognosis-defined, but not “intrinsic”, unsupervised gene signatures may identify a subset of GBM with more favorable prognosis. However, similar to previous findings (25), the TCGA classical and mesenchymal subtypes showed significantly improved overall survival after conventional chemoradiation or \geq four cycles of cytotoxic chemotherapy ($P=0.02$), suggesting that these subtypes may be particularly sensitive to DNA damaging agents. These hypotheses will be tested further in two ongoing phase III clinical trials conducted by the Radiation Therapy Oncology Group (RTOG), as discussed below.

Capitalizing on the unprecedented level of molecular data available for these tumors (29), we identified recurrent genomic aberrations in each molecular subtype. The classical subtype was characterized by frequent *EGFR* amplification and EGFRvIII mutations, *CDKN2A* deletion, and a lack of *TP53* mutations, while the mesenchymal subtype was characterized by *NF1*, *TP53*, and *PTEN* mutations. Consensus neuropathological review of a subset of TCGA cases has shown that the proneural, classical, and mesenchymal subtypes are enriched for GBM with oligodendroglial features, small cell GBM, and gliosarcoma (a morphological variant of GBM with mesenchymal differentiation (6)), respectively

(Cameron Brennan, personal communication). Moreover, pseudopalisading necrosis and to a lesser extent florid microvascular proliferation are frequent in mesenchymal GBM, but the proneural subtype typically lacks necrosis. These findings suggest that mesenchymal GBM may be uniquely susceptible to angiogenesis inhibitors, a hypothesis currently being tested in the RTOG 0825 trial discussed below. The proneural subtype, which like previous studies (18, 24) was found in younger patients, harbored frequent *PDGFRA* amplification and mutations in *IDH1*, *TP53*, and *PIK3CA/PIK3R1*, suggesting susceptibility to PDGFRA- and PI3K-targeted therapies. A recent proteomic analysis confirmed protein- and phosphorylation-level signaling abnormalities in the EGFR, PDGFR, and NF1 pathways in classical, proneural, and mesenchymal subtypes of GBM, respectively, further suggesting that these GBM subtypes may be uniquely susceptible to targeted agents (20).

A recent TCGA effort utilized methylation profiling to identify a GBM CpG island methylator phenotype (G-CIMP) in a significant fraction (29%) of proneural GBM, particularly secondary, *IDH1* mutation-positive GBM that progressed from lower grade tumors (30). This implies that G-CIMP might be common in lower-grade gliomas, the vast majority of which cluster with the proneural molecular subtype of GBM (18, 25). To further investigate this hypothesis, Noushmehr and colleagues analyzed eight G-CIMP gene regions in seven hypermethylated loci in an independent cohort of 152 WHO grade II and III gliomas by a MethyLight real-time PCR assay and found 46% of astrocytomas and 93% of oligodendrogliomas to be G-CIMP-positive. Furthermore, G-CIMP-positive GBM patients were younger (median 36 vs. 59 y, $P < 0.0001$) and survived longer than G-CIMP-negative GBM of both proneural and non-proneural subtypes (median overall survival 2.9 vs. 0.8 and 1.0 y, $P = 7 \times 10^{-7}$). Importantly, G-CIMP positivity was independent of age and histological grade on multivariable analysis. These findings suggest that G-CIMP defines a subset of proneural GBM and can be utilized to further refine expression-defined subtypes. The co-occurrence of G-CIMP/*IDH1* mutation positivity in the proneural, neurogenesis-related subtype further suggests that *IDH1* mutation and/or G-CIMP may confer

neoplastic susceptibility to a common neuron/oligodendrocyte precursor cell-of-origin (22), a hypothesis supported by the comparative expression profiling data that showed enrichment of genes expressed in purified, cultured murine oligodendrocytes in proneural GBM (17).

Clinical implementation of GEP for glioma classification

GEP-based diagnostic tests are currently being evaluated in prospective, randomized clinical trials in breast cancer (2). Similar progress in clinical neuro-oncology has recently been made. Based upon a previous report (18), Colman, Aldape, and colleagues (31) identified a consensus 38-gene signature from four independent datasets and from this set chose 9 genes (*AQP1*, *CHI3L1*, *EMP3*, *GPNMB*, *IGFBP2*, *LGALS3*, *OLIG2*, *PDPN*, and *RTN1*) based on their survival correlation and technical compatibility, for development of a quantitative, reverse transcription-polymerase chain reaction assay. Based on the logistical difficulties in obtaining fresh frozen tumors for DNA microarray-based assays, such an assay is absolutely critical for successful clinical implementation with formalin-fixed, paraffin-embedded (FFPE) GBM, which constitute the vast majority of clinical samples. The prognostic impact of this 9-gene profile was uniformly associated with both progression-free and overall survival and independent of clinical (age and KPS) and molecular factors, including *MGMT* methylation status. This assay is currently being tested in two prospective, randomized, phase III clinical trials conducted by the RTOG. RTOG0525 is investigating the use of dose-intensive adjuvant temozolomide versus standard-of-care (28) in patients stratified on the basis of *MGMT* promoter methylation status. Prospectively-banked FFPE tissue from this trial will be retrospectively analyzed using the 9-gene predictor to confirm its prognostic significance relative to *MGMT* status in a uniformly-treated patient population. RTOG0825 is investigating the benefit of adjuvant bevacizumab, a humanized, anti-angiogenesis monoclonal antibody, to standard-of-care and will prospectively randomize patients on the basis of both *MGMT* methylation status and the 9-gene assay. The study will address, as a secondary end-point, the hypothesis that mesenchymal GBM

will selectively benefit from the addition of bevacizumab to standard-of-care. Results from these important clinical trials are expected in 2011-2012. In summary, molecular subtyping now has the potential to become a readily implemented clinical test that may guide future treatment decisions, particularly in identifying those patients most likely to benefit from standard-of-care versus novel, molecularly targeted agents.

Conclusion

As we have outlined above and summarized in Table 1.2, tremendous progress in DNA microarray-based GEP of gliomas has been made over the past decade. In the next decade, next-generation sequencing technologies such as RNA-seq (32) promise to accelerate the pace and depth of discovery, further strengthening GEP as a method for cancer classification by directly determining transcript identity, structure, and abundance at the single-base level. Yet while GEP has provided significant insights into the molecular heterogeneity of morphologically-defined gliomas, its role in clinical neuro-oncology still remains to be established. Thus, ten years after the Director's Challenge, the need for a "vastly more informative classification system" for gliomas still exists. In this review, we have argued that GEP and the established morphological classification system are complementary, not mutually exclusive. The most clinically appropriate uses of GEP will be as a diagnostic adjunct to more accurately classify morphologically-ambiguous gliomas and the identification of molecular subtypes within otherwise morphologically-homogeneous gliomas. There has been substantial progress in defining molecular subtypes of GBM. However, unlike commercially-available genomic tests for breast cancer, molecular subtyping in GBM is unlikely to be utilized for risk stratification due to this tumor's limited prognostic variability. Rather, as illustrated by the RTOG clinical trials, molecular subtyping in GBM shows promise in identifying subsets that may be uniquely responsive to specific adjuvant therapies.

Thus, the recent merger of genomic and histopathological classification bodes well for the future of personalized medicine in neuro-oncology.

GENETICALLY-ENGINEERED MOUSE MODELS OF DIFFUSE GLIOMAS

Summary

Over the last decade, genetically-engineered mouse models have been extensively used to dissect the genetic requirements for neoplastic initiation and progression of diffuse gliomas. While these models faithfully recapitulate the histopathological features of human gliomas, comparative genomic analyses are increasingly being utilized to comprehensively assess their fidelity to recently identified molecular subtypes of these tumors. Future progress with these models will rely on incorporating insights not only from oncogenomics studies of cancer, but also from the developmental neuroscience and stem cell biology fields to design accurate and experimentally tractable models for use in translational cancer research, particularly for experimental therapeutics studies of molecularly defined subtypes of gliomas.

Introduction

Diffuse gliomas are the most common primary brain tumors (33, 34). They are classified clinically into three histological subtypes and malignancy grades (35, 36) and together account for more than 80% of all malignant brain tumors in the US (37). Gliomas represent some of the most devastating and difficult-to-treat of all human cancers. In fact, median survival for glioblastoma (GBM), the most common and biologically-aggressive glioma, has not improved significantly over the last four decades and still averages 12-15 months (37, 38). Currently, standard therapy for newly-diagnosed GBM patients

consists of surgical resection followed by fractionated radiotherapy with concomitant and adjuvant temozolomide (TMZ) chemotherapy, a regimen that results in a modest, three month improvement in median overall survival compared to radiation alone, but invariably fails to prevent tumor recurrence (28). Although effective treatment is complicated by the blood-brain barrier and the intrinsic resistance of tumor cells to radiation and cytotoxic chemotherapy (39), development of more successful treatment regimens has largely been impaired by the lack of understanding of glioma biology. Genetically-engineered mouse models (GEMM) of gliomas that faithfully recapitulate the genetics and biology of their human counterparts have therefore emerged as an essential experimental tool not only for the investigation of the genetics and cell and molecular biology of glioma initiation and progression, but also for the development of novel therapies (reviewed in (40-46)).

In this review, we will briefly describe our current understanding of the pathology and genetics of human gliomas and how this knowledge has fueled development of GEMM, particularly with regard to the genes involved in dysregulated cell-autonomous intracellular signaling pathways in human gliomas and the cell(s) from which they may arise. We will then review the advantages and disadvantages of existing glioma GEMM, and lastly, identify recent and new directions for translational research using these important model systems.

Histopathological classification of human gliomas

Modeling human gliomas in mice must carefully aim to approximate the complex genetics and biology of both the human tumor and its microenvironment. Gliomas show marked heterogeneity in their cellular morphology and identity, differentiation potential, proliferation rate, prognosis, and therapeutic response (47, 48). Based upon the latest World Health Organization (WHO) classification, gliomas are grouped into seven distinct clinicopathological entities by cytological and immunohistochemical evidence of differentiation along astrocytic, oligodendroglial, or both glial

lineages (35). Histological grading (II-IV) based upon the presence of morphological features associated with more aggressive biology, including mitoses, microvascular proliferation, and necrosis, yields further refinement into distinct prognostic groups (36, 48), with WHO grade IV GBM representing the most malignant glioma. Two distinct neoplastic progression pathways for GBM have been recognized: primary GBM constitute over 95% of all GBM and arise without evidence of a previously-existing lower-grade glioma, and secondary GBM develop through progression from low-grade or anaplastic gliomas. Though histopathologically indistinguishable, the molecular pathology of primary and secondary GBM differs (35). Primary GBM are characterized by frequent *EGFR* amplification and *PTEN* mutations, whereas secondary GBM typically contain *TP53* mutations and *MDM2* gene amplifications (35). Both frequently harbor DNA copy number and sequence abnormalities in G1 cell cycle checkpoint pathway genes (64% in (49) and 87% in (29)), including *RB1*, *CDK4*, *CCND1* (cyclin D1), and *CDKN2A* (*p16^{INK4A}*), and PI3K/PTEN/AKT pathway genes (50% in (49) and 53% in (29)), including *PTEN* loss of heterozygosity and *PIK3CA* mutation (29, 49).

Molecular genetic classification of human gliomas

Over the last decade, molecular genetic analyses have identified significant molecular heterogeneity within various morphologically-defined human gliomas and have helped identify biologically distinct human glioma subtypes (48). For instance, gene expression profiling via microarrays has been used to identify genes differentially expressed between GBM and anaplastic oligodendroglioma (9, 10), prognostically distinct molecular subtypes of anaplastic astrocytoma and GBM (17, 18, 21), and molecular subtypes of all diffuse gliomas (16, 25). Most molecular characterization efforts though have focused solely on GBM. In the largest molecular profiling effort conducted to date, The Cancer Genome Atlas (TCGA) project (17, 29) has generated a comprehensive molecular catalog of human GBM and confirmed that recurrent genomic abnormalities occur in genes involved in four key intracellular

signaling pathways: cell cycle, mitogenic (receptor tyrosine kinase (RTK)), pro-survival (PI3K-PTEN), and TP53 pathways (17, 29, 30). Notably, specific genomic abnormalities were associated with one of four molecular subtypes (proneural, neural, classical, and mesenchymal), and the mesenchymal and classical subtypes showed improved survival after intense adjuvant therapy (17). Proneural GBM contained a subset of tumors that shared a genomic hypermethylation phenotype with lower grade gliomas, occurred in younger patients, showed improved overall survival, and were associated with *IDH1* mutations (30). Taken together, these reports have convincingly shown the biological heterogeneity within human GBM. However, profiling human tumor samples only provides a static perspective of genomic alterations and cannot yet readily differentiate molecular genetic “drivers” of gliomagenesis from “passenger” events that occur during neoplastic progression (50). While sophisticated bioinformatic analyses can provide critical clues to possible cell(s) of origin and the genetics of tumor initiation and progression, experimental models are required to definitively address these important issues. GEMM are uniquely suited to fill this need. For example, the heterozygous *IDH1/2* mutations frequently found in the majority of low-grade gliomas and secondary GBM have been proposed to be involved in glioma initiation (26, 49), a question GEM modeling is ideally suited to address.

To date, GEMM have defined the importance in neoplastic initiation and progression of the frequently-altered genes in four key intracellular signaling pathways observed in human gliomas (40, 46). Although model design, cellular targets, and specific genetic modifications vary considerably, the entire morphological spectrum of diffuse gliomas has been recapitulated in these model systems (Table 1.3).

Human gliomas and the cancer stem cell hypothesis

The cancer stem cell (CSC) hypothesis postulates that tumor initiation and maintenance is governed by a subpopulation of tumor cells with the functional properties of normal stem cells, namely unlimited

self-renewal and multi-lineage differentiation potential (51). GBM was among the first solid cancers where evidence of a hierarchy of phenotypically distinct tumor cells was identified. Employing principles and methods from the study of normal and neoplastic hematopoiesis, several groups identified a subpopulation of GBM cells (brain tumor stem cells, BTSC) with NSC-like properties (52, 53). Moreover, these BTSC could initiate tumors that phenotypically resembled the GBM from which they were isolated upon orthotopic injection of as few as 100 BTSC into the brains of immunodeficient mice (54). Subsequent work showed that CD133+ BTSC from human GBM displayed enhanced DNA repair capacity relative to CD133- cells and resistance to radiation *in vitro* and *in vivo* (55). Moreover, the percentage of CD133 immunoreactive cells in WHO grade II-IV gliomas has been shown to inversely correlate with progression-free and overall survival as well as the time-to-recurrence for grades II and III gliomas (56). Despite debate over the suitability of xenotransplantation assays (see below), the poorly characterized function of CD133 and controversy over its use to prospectively identify human BTSC (57), the CSC hypothesis has transformed glioma research in at least two ways: 1) in contrast to the stochastic model of tumorigenesis in which all tumor cells are assumed capable of initiating and maintaining tumorigenesis, it suggests that BTSC are unique in these capabilities and thus their specific therapeutic targeting will be required for prevention of tumor recurrence and improving patient outcomes; and 2) it suggests that the elusive cell-of-origin for gliomas may be a true NSC or a more terminally-differentiated glial cell that has reacquired NSC-like properties through de-differentiation (57-60).

Developmental neurobiology and the glioma cell(s) of origin

Though recent scientific and technical advances have yielded much progress, cellular targets for glioma initiation, progression, and maintenance remain the focus of intense investigation and debate (61, 62). It is widely accepted that identification of the differences and similarities between the cell(s) from which a tumor arises (cell(s) of origin) and their normal counterparts would permit development of

new therapeutic approaches to overcome the lack of success with currently available treatments (reviewed in (63)). In support of the hypothesis that gliomas arise from cells with NSC-like properties, developmentally-important transcription factors required for NSC self-renewal and multipotency have been shown to be reactivated in gliomas (reviewed in (64)) and gene expression signatures in GBM have been shown to match developmental templates (17, 27).

The largest germinal region in the adult brain resides in the subventricular zone (SVZ), located between the ependymal layer of the lateral ventricles and the parenchyma of the striatum. The SVZ contains astrocyte-like stem cells, which can be identified by the astroglial marker GFAP. Thus, the SVZ is widely viewed as a potential source of glioma initiating cells (59, 65-67). In support of this hypothesis, a recent clinical study has found that 93% of gliomas contacted at least one region of the lateral ventricular wall (68). However, more research is required to establish the relationships between CSC and NSC and whether the latter can serve as cell(s) of origin for gliomas (reviewed in (58, 61, 62, 69). Recently, support for the NSC or progenitor cell origin of both astrocytomas (67, 70) and oligodendrogliomas (71) has been obtained using GEMM. Most glioma GEMM have utilized human glial fibrillary acid protein (hGFAP), nestin, or S100 β promoters (Table 1.3), all of which are active in multiple cell types in the developing and adult brain. It would be highly desirable to target specific subpopulations of stem or progenitor cells to further define their potential for tumor initiation and maintenance. More specific lineage-restricted promoters that have been utilized in neurodevelopmental genetic fate mapping and lineage tracing studies will be important tools for addressing these issues in the future (72, 73).

Glioma GEMM design

It has become evident that overall design, the targeted cells and their inherent differentiation capacity, and the specific genetic modification(s) and pathways targeted are required to achieve

accurate modeling of human gliomas (46). In general, glioma GEMM have been constructed using seven design strategies: 1) traditional knockout models in which exons of a tumor suppressor gene are deleted; 2) knock-in models whereby oncogenes are replaced by mutant, constitutively active alleles within their native locus, under control of endogenous promoter elements; 3) transgenic models in which expression of an oncogene is spatially restricted to specific cell types through use of a cell type-specific promoter; 4) spatially restricted induction models that employ localized viral delivery to induce either somatic gene transfer in non-transgenic animals or cell type-specific gene transfer in transgenic animals engineered to express the cognate viral receptor under control of a cell type-specific promoter; 5) spatially restricted induction of conditional genetic events through viral vector delivery of a DNA recombinase; 6) conditional models in which genetic events are induced through cell-specific expression of a DNA recombinase using cell type-specific promoters; and 7) conditional, systemic induction models that employ cell type-specific expression of drug-inducible DNA recombinase activity. Choice of model design influences the timing and cellular targets of genetically-induced oncogenesis, specifically during development or adulthood, as well as experimental tractability, i.e. how easily the model system is manipulated in labs with variable technical capabilities, which in turn influences model dissemination through the research community and the utility of GEM for preclinical studies.

Dissecting the genetics of glioma initiation and progression in GEMM

The first glioma GEMM utilized knockout or conventional transgenic strategies (46). In contrast to the majority of cancers that develop sporadically, these models more accurately mimic inherited tumor predisposition syndromes in which initiating mutations are present throughout the body. Although some of these GEMM showed increased susceptibility to gliomagenesis, embryonic or early post-natal lethality, widespread neoplasia in various organ systems, incomplete penetrance (<100% of GEMM develop tumors of interest), and long latency (time to development of tumors of interest) posed

significant hurdles to investigation of organ-specific genetic mechanisms of neoplasia. For example, homozygous deletion of *Pten*, one of the most frequently mutated genes in human gliomas (29), proved to be embryonically lethal, whereas heterozygous loss induced tumors or pre-neoplastic changes in colon, gonads, prostate, skin, and thyroid, but not the brain (74). Similarly *Ink4a/Arf* deletion produced largely sarcomas or lymphomas, but no brain tumors (75). One of the first GEMM that specifically developed gliomas utilized simultaneous (cis) deletion of the *Nf1* and *Trp53* tumor suppressor genes (76). Spatial restriction of transgenic oncogene expression using cell-specific regulatory elements improved, but did not completely eliminate these problems. Transgenic expression of the oncogene *v-Src* from a murine GFAP promoter uniformly led to perinatal astrogliosis, but only 14% subsequently developed low-grade astrocytomas, leading the authors to conclude that *v-Src* alone was insufficient for astrocytoma initiation (77, 78). Simultaneous inactivation of pRb, p107, and p130 in hGFAP+ cells engineered to express an N-terminal SV40 large T antigen (T₁₂₁) truncation mutant transgene led to perinatal death from neurodevelopmental abnormalities in 10 of 13 founder mice (79). hGFAP-directed expression of constitutively active HRAS alone rapidly induced low-grade astrocytomas in 85-100% of mice and these tumors invariably progressed to high-grade astrocytomas upon spontaneous acquisition of karyotypic abnormalities (80), *Trp53* mutation, or loss of INK4A or PTEN protein expression (80-82).

Several groups have utilized viral gene transfer to spatially restrict induction of oncogenesis. The advantages and disadvantages of this modeling approach have been reviewed in detail elsewhere (46, 83). The main advantages to this approach are the targeting of somatic cells in adult animals and experimental flexibility, specifically the ability to transfer multiple genes, either simultaneously or sequentially, in specific regions of the brain. One of the original GEMM employing this design strategy utilized Maloney murine leukemia retrovirus (MoMuLV) to deliver *Pdgfb* (PDGFβ protein) into dividing cells in the forebrains of newborn mouse pups (84), which resulted in tumors with a wide range of

histologies, 14-29 week latency, and 40% penetrance. More recently, GEMM utilizing avian retroviral (RCAS) vectors have been generated. In contrast to the traditional retroviral system, RCAS requires the use of conventional transgenic GEM engineered to express its cognate receptor, *tva*, typically with spatial restriction to specific cell types using either hGFAP or nestin promoters (G-*tva* or N-*tva*, respectively) (85). Histologically diverse gliomas form in these GEMM, with tumor type, penetrance, and latency dictated by the oncogene(s) delivered and the cell types targeted. For example, RCAS-mediated expression of PDGF β in either GFAP⁺ or nestin⁺ cells yielded low- to high-grade oligodendrogliomas, with histological grade, penetrance, and latency depending on the injected viral dose (86, 87). In contrast, RCAS-delivery of constitutively active KRAS and AKT1 produced GBM in ~25% of injected mice when targeted to nestin⁺ cells, but did not initiate gliomagenesis when targeted to GFAP⁺ cells (88, 89). In both of these model systems, concomitant loss of one or both *Ink4a/Arf* alleles accelerated tumor progression, generally with increased penetrance and shorter latency (89, 90).

Conditional GEMM, the latest models developed to explore the genetic mechanisms of glioma initiation and progression, more faithfully mimic sporadic tumor development. As reviewed in detail elsewhere (46, 91), these models employ mice (*Cre*-drivers) engineered to express a transgenic DNA recombinase, mostly commonly the bacteriophage Cre enzyme, driven by cell-specific regulatory elements. Whereas embryonic lethality in conventional transgenic and knockout mice precluded investigation of many important genes in gliomagenesis, conditional GEMM utilized oncogenes preceded by transcriptional stop elements flanked (floxed) by Cre recognition sequences (loxP sites), or floxed exons of tumor suppressor genes, to phenotypically silence these genetic modifications during development. Crossbreeding with a transgenic Cre-driver mouse or somatic induction via viral delivery of Cre thus permitted investigation of tissue-specific genetic mechanisms of neoplasia. An additional advantage of this latter technique has been the targeting of spatially- and biologically-distinct areas of the brain (70).

A variety of conditional glioma GEM models have been described. One of the first utilized T_{121} to selectively inactivate pRb, p107, and p130 in GFAP+ cells (79). Whereas embryonic expression of conventional transgenic GFAP- T_{121} was lethal, conditional expression using a β -actin *Cre*-driver induced WHO grade III anaplastic astrocytomas, with decreased latency upon simultaneous, conditional, heterozygous deletion of *Pten*. Similar results were obtained upon somatic induction of *Pten* loss through stereotactic injection of retroviral (MSCV)-*Cre* into floxed GFAP- T_{121} /*Pten* mouse brains, where ~75% developed GBM (92). Conditional deletion of the *Nf1* tumor suppressor, a negative regulator of RAS signaling and frequent mutational target in human GBM (29), specifically in GFAP+ astrocytes resulted in development of optic nerve astrocytomas (93). When combined with loss of *Trp53* (94) or *Pten* (95), conditional *Nf1* deletion in GFAP+ cells resulted in progression to high-grade gliomas, including GBM, with complete penetrance. The conditional modeling approach has recently been extended to include oncogenes. In particular, conditional transgenic over-expression of wild-type *EGFR* or a constitutively active extracellular domain truncation mutant of *EGFR*, events frequently found in human GBM (29), resulted in de novo GBM formation within 5-12 weeks of adenoviral-*Cre*-mediated recombination in the presence, but not absence, of simultaneous deletion of *Ink4a/Arf* and *Pten* (96).

The newest development in glioma GEMM modeling has been the use of drug-inducible *Cre*-drivers, which permit tight spatial as well as temporal control of somatic recombination. The most common system utilizes *Cre* recombinase genetically fused to a mutated estrogen receptor ligand-binding domain (Cre^{ERT2}) (97), an enzyme that remains unresponsive to endogenous estrogens such as estradiol (98), but is activated upon systemic administration (intraperitoneal injection) of the synthetic estrogen 4-hydroxy-tamoxifen (4OHT). This system requires minimal technical expertise and provides control over the timing of genetic induction. We have utilized this system with a GFAP- Cre^{ERT2} driver that directs gene expression in GFAP+ cells throughout the neuroaxis, with no activity in non-astrocytic cell populations (99), and a series of six GEMM with conditional alleles that inactivate RB (T_{121}) and/or PTEN

and/or constitutively activate KRAS specifically in adult astrocytes (40). All models with inactivated RB (T_{121} expression) were fully penetrant and resulting tumors showed the histopathological features of human astrocytomas, including perineuronal and perivascular satellitosis. A similar approach using conditional deletion of *Pten* and *Trp53*, with or without *Rb1* deletion, in GFAP+ cells resulted in development of high-grade (WHO grade III and IV) astrocytomas (100) which acquired widespread genomic copy number abnormalities during tumor progression (see Section 9 below).

Glioma GEMM in translational cancer research: comparative oncogenomics

With the advent of sophisticated molecular technologies, such as high-throughput, genome-wide microarray-based analyses and genomic re-sequencing, cross-species comparisons between GEMM and their corresponding human cancers have recently become feasible. As previously discussed, genomic techniques have identified heretofore unrecognized molecular heterogeneity in otherwise histologically homogeneous tumor types, including gliomas such as GBM (48). Thus, the next generation of cancer GEMM will require not only standard comparative histopathology, but genomic molecular analyses to identify “best-fit” GEMM with specific molecular subtypes of their corresponding human cancers. Integration of mouse modeling and bioinformatics has been proposed to investigate coordinate gene regulation, discovery of novel biomarkers, and development of targeted drug therapy based upon prominent cancer signaling pathways in molecularly defined GEMM (101).

With the exception of one recent study described below, comprehensive, genome-wide molecular characterization of the majority of glioma GEMM has yet to be performed. However, progress has been made in other tumor types and these studies provide a blueprint for future work using glioma GEMM. In the most straightforward analyses, cancer GEMM have been validated by showing similar patterns of co-expressed genes as their human counterparts. Sawyers and colleagues defined differentially expressed genes between wild-type murine prostate and a transgenic *Myc*-driven prostate cancer

GEMM and identified a subset of these in *MYC*-driven human prostate cancers that co-expressed *PIM1*, a kinase known to cooperate with *MYC* in tumorigenesis (102). A similar type of comparison using a *Kras*-driven lung cancer GEMM identified a *KRAS* expression signature in human lung adenocarcinomas that was unidentifiable based on *KRAS* mutational status alone (103). Wong and colleagues performed gene expression profiling on primary *Lkb1*-deficient/*Kras*-mutated GEM lung cancers and their corresponding spontaneous metastases to define a metastasis signature that showed prognostic significance in human lung adenocarcinomas and identify a subset of LKB1-deficient human cancers that may be amenable to combined inhibition of SRC, PI3K, and MEK signaling pathways (104). These findings suggest that genomic analyses of GEMM tumors can be used to discover novel genes co-expressed with signature mutations in human cancers.

In an effort to define “best-fit” GEMM for molecular subtypes of hepatocellular carcinoma (HCC), Thorgerirsson and colleagues performed comparative gene expression profiling of seven GEMM and two molecularly-defined, prognostically-distinct subtypes of human HCC (105). They discovered three GEMM with expression profiles similar to human HCC with better prognosis and two GEMM similar to the subtype with poor prognosis. This same experimental design was subsequently applied to breast cancer (106), where several GEMM showed gene expression profiles similar to either basal-like or luminal subtypes of human breast cancer. Subsequent comparative GEMM/human gene expression profiling has suggested luminal, but not basal progenitor cells to be the likely cell of origin for sporadic basal-like and hereditary *BRCA1*-deficient breast cancers (107).

Two recently published reports have utilized comparative genomics to study human gliomas. The TCGA utilized transcriptomal profiles of fluorescent-activated cell sorting (FACS)-purified neurons, astrocytes, and oligodendrocytes from a transgenic GEM that expressed enhanced green fluorescent protein from the *S100 β* promoter (108), a GEM previously used in neurodevelopmental fate mapping studies (109), to identify potential lineage relationships among the four distinct molecular subtypes of

human GBM (17). Baker and colleagues performed microarray-based gene expression profiling and copy number analysis on two GEMM of adult high-grade astrocytomas with conditional inactivation of *Pten* and *Trp53*, with or without concomitant *Rb1* deletion (100). The murine tumors cluster into three groups that show similarity to molecularly-defined subtypes of human GBM (17, 18). Notably, brain region-, but not genotype-specific signatures were evident in these murine tumors, suggesting that regional differences in gene expression profiles within the adult brain (110), or possibly the cell(s) of origin, may dictate molecular subtype-specification. Regardless, this first comparative genomics between GEMM and human glioma represents a significant milestone (111). However, more comparative genomics studies using of GEMM and human tumors, similar in design to the one cited above for breast cancer (107), will be required to define the role of different cell(s) of origin or brain regions on molecular subtype-specification of human gliomas. The extensive GEMM resources of the developmental neuroscience community will thus be critical not only for defining the cell of origin for specific molecular subtypes of human gliomas, but also the identification of “best-fit” glioma GEMM of these subtypes for future translational studies.

Glioma GEMM in translational cancer research: experimental therapeutics

Preclinical cancer drug development has relied upon immunodeficient mouse xenografts of human tumor cell lines since the 1950s (112, 113). For gliomas in particular, cell lines such as U87MG (114) have been widely used in both subcutaneous and orthotopic xenograft experiments because of their reproducible growth rates and uniformly high penetrance, which enables generation of large tumor-bearing cohorts for experimental therapeutics (reviewed in (42)). However, there are several serious flaws with this approach. The most important shortcomings are the requirement for immunodeficient host and genetic and phenotypic divergence from the original tumor after *in vitro* cell culture (115). Moreover, these systems are poorly predictive of drug efficacy (reviewed in (45)) and ill-suited for

continued use in prioritizing drugs for clinical development, particularly for molecularly defined tumor subtypes. Although much has been written about the promise of GEMM in this regard (45, 116, 117), they remain experimentally less amenable to therapy studies (118) and their utility in prioritizing drug candidates for human clinical trials has not been systematically examined. Progress has been hampered by variable penetrance and latency *in vivo*, the requirement for small animal imaging to monitor spontaneous GEM tumor development, and the lack of GEM tumor cell culture systems for *in vitro* drug screening.

With their highly penetrant, short latency tumor development in the appropriate anatomical location of immunocompetent hosts, the latest glioma GEMM overcome some of these shortcomings. Multiple groups have utilized small animal imaging, including conventional magnetic resonance imaging (119) and bioluminescence imaging (120-122), to longitudinally monitor the growth of GEM gliomas and investigate the efficacy of either standard cytotoxic drugs like TMZ (120) or novel targeted agents (121, 122). However, these GEMM have yet to be used to define chemotherapeutic efficacy of specific molecular subtypes of gliomas.

Non-germline glioma GEMM for experimental therapeutics

Recently, non-germline GEMM (nGEMM) have been proposed as an important resource for translational and preclinical experimental therapeutics studies due to their flexibility, speed and reduced cost (reviewed in (123)). These models utilize germline GEM as the source of specific genetically-engineered cell populations, including stem/progenitor and terminally-differentiated cells, and orthotopic implantation into syngeneic, immunocompetent hosts to investigate the cellular and molecular requirements for tumor initiation and maintenance. Cortical injection of *Ink4a/Arf*-null neural stem cells (NSC) or primary astrocytes transfected with an activated EGFR into SCID mice produced invasive, high-grade astrocytomas within 2 months (124). Similarly, injection of *Ink4c/Trp53-null*

cerebellar granular precursor cells (CGPCs) into the cortex of *nude* mice produced medulloblastomas with gene expression profiles similar to those that arose spontaneously in these GEM (125). While these two examples illustrate the utility of nGEMM, these studies suffer from one issue that has plagued conventional human tumor xenograft studies, specifically the use of immunodeficient recipients (45). To overcome this issue, we have recently developed a completely syngeneic nGEMM system (40) which should prove to be more amenable to preclinical experimental therapeutics studies than conventional GEMM.

Summary and conclusions

Major improvements in GEM modeling over the last decade have produced a variety of glioma GEMM that faithfully recapitulate the genetics and biology of their human counterparts. Coupled with increasingly sophisticated histopathological and comparative genomic analyses, insights from developmental neuro- and stem cell biology will fuel development of the next generation of experimentally tractable GEMM not only to further define the cellular and molecular basis of gliomagenesis, but to develop novel targeted therapeutics for specific molecular subtypes of gliomas.

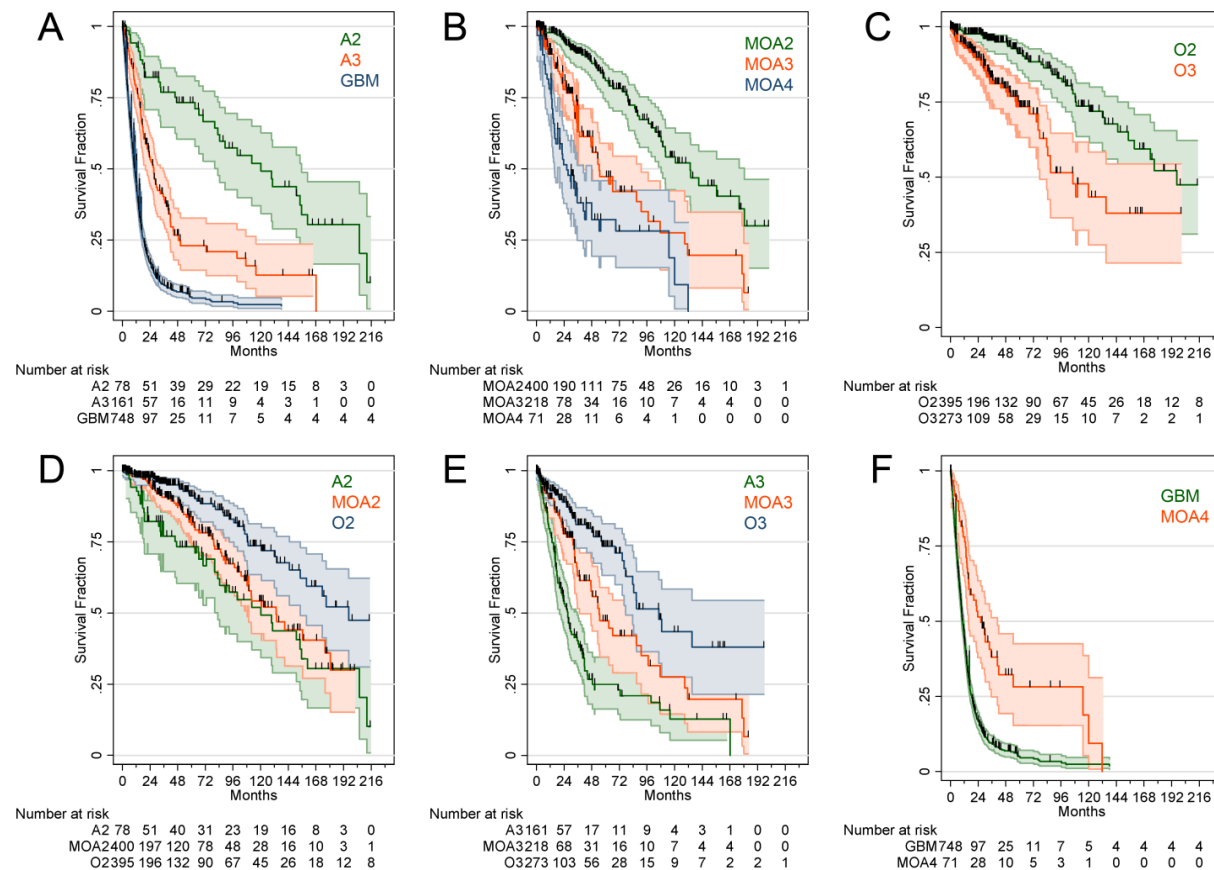


Figure 1.1. Overall survival of patients with newly-diagnosed gliomas. Overall survival of patients with newly-diagnosed gliomas grouped on the basis of the two main components of the WHO classification system: differentiation (cytology) - astrocytic (A), mixed oligoastrocytic (B), or oligodendroglial (C); and histological grade - WHO grade II (D), III (E), or IV (F). Clinicopathological parameters, statistics, and abbreviations are listed in Table 1.1.

Table 1.1. Prognostic utility of the WHO 2007 classification for diffuse gliomas

Table 1. Prognostic utility of the WHO 2007 classification for diffuse gliomas							
	WHO Grade			Multivariate analysis			
	II	III	IV	Prognostic factor	HR	P value	ΔC or Overall C*
Astrocytomas							
	DA, A2	AA, A3	GBM, A4				
N	78	161	748	Grade	1.9	< 0.001	0.61
Median OS (y)	10.0	2.2	0.9	Age**	1.9	<0.001	0.08
95% CI	6.9-13.0	1.7-2.7	0.8-1.0	All (N=987)			0.69
Mean age	33	39	57				
Grading criteria		Mitoses	MVP ± necrosis				
Oligoastrocytomas							
	OA, MOA2	AOA, MOA3	GBM-O, MOA4***				
N	400	218	71	1p19q code1	2.6	<0.001	0.54
Median OS (y)	11.1	3.9	2.2	Age**	2.1	< 0.001	0.15
95% CI	9.0-15.0	2.8-4.6	1.3-3.4	Grade	2.2	0.007	0.10
Mean age	38	42	48	All (N=559)			0.79
Grading criteria		Mitoses ± MVP	Necrosis				
Oligodendrogliomas							
	ODG, O2	AO, O3					
N	395	273		1p19q code1	2.1	0.020	0.54
Median OS (y)	16.4	8.8		Age**	2.4	<0.001	0.17
95% CI	12.9-21.1	6.5-ND		Grade	2.5	0.004	0.03
Mean age	40	44		All (N=539)			0.74
Grading criteria		Mitoses ± MVP ± necrosis					
All diffuse gliomas							
N	2344			1p19q code1	1.9	0.002	0.63
Median OS (y)	2.9			Age**	1.8	<0.001	0.13
95% CI	2.5-3.6			Cytology	1.7	<0.001	0.04

Mean age

46

Grade

2.0

<0.001

0.03

All (N=1363)

0.83

Abbreviations: anaplastic astrocytomas (AA, A3); anaplastic oligodendroglioma (AO, O3); co-deletion (codel); confidence interval (CI); diffuse astrocytoma (DA, A2); hazard ratio (HR); glioblastoma (GBM, A4); glioblastoma with oligodendroglial features (GBM-O, MOA4); mixed oligoastrocytoma (OA, MOA2); mixed anaplastic oligoastrocytoma (AOA, MOA3); microvascular proliferation (MVP); oligodendroglioma (ODG); overall survival (OS); years (y).

Data from adult patients (≥ 20 y) with newly diagnosed gliomas at Washington University School of Medicine (1977-2009 and (Miller *et al*, 2006)).

* Harrell's C statistic for the multivariable Cox proportional hazards model with all factors (C) or ΔC for each individual factor in the model (Miller *et al*, 2006).

** Age at diagnosis trichotomized as follows: ≤ 40 , 40-60, ≥ 60 y (Miller *et al*, 2006).

***Note that GBM-O (MOA4) is not currently recognized as a distinct clinicopathological entity by the WHO; instead, it is considered a morphological pattern of GBM with a slightly more favorable prognosis (Louis *et al*, 2007).

Table 1.2 Summary of glioma microarray studies

Table 2. Summary of glioma microarray studies							
Reference	Gliomas Analyzed			Source	Findings	Genes (N)	Biological Process or Molecular Subtype
	Dataset	Histology*	Total (N)				
Rickman, 2001		19 PA, 21 GBM	40		<ul style="list-style-type: none"> Distinguishes PA and GBM. 	360	
Nutt, 2003	T	7 O3, 14 GBM	21		<ul style="list-style-type: none"> Distinguishes O3 and GBM. 		
	V	15 nonclassic O3 14 nonclassic GBM	29		<ul style="list-style-type: none"> 86% predictive accuracy for morphologically-ambiguous cases. Improved prognostic stratification vs. histological classification. 	19	
Shai, 2003		5 A2, 3 O2, 18 priGBM, 9 secGBM	35		<ul style="list-style-type: none"> Distinguishes among histological subtypes. 	170	
van den Boom, 2003	T	6 A2, 2 MOA2 → 4 secGBM, 2 A3, 2 MOA3	16		<ul style="list-style-type: none"> Correlates with malignant progression. 	66	
	V	9 A2, 10 A3, 17 priGBM, 7 secGBM	43		<ul style="list-style-type: none"> Progression-associated signature confirmed. 	9	
Godard, 2003	T	12 A2, 14 priGBM, 5 secGBM	31		<ul style="list-style-type: none"> Confirmed findings of Shai, 2003 and van den Boom, 2003. Distinguishes A2/secGBM and priGBM. 	9	Angiogenesis
	V	12 A2, 4 pri GBM, 4 secGBM	20		<ul style="list-style-type: none"> 93% prediction accuracy. 	13	Immune response
Tso, 2006		4 A2, 9 A3, 8 O2, 11 O3, 46 priGBM, 14 secGBM	92		<ul style="list-style-type: none"> Distinguishes priGBM and non-GBM astrocytomas. Distinguishes secGBM and non-GBM astrocytomas. 	58	Cell cycle
					<ul style="list-style-type: none"> 84% predictive accuracy for 25 similarly-treated priGBM and secGBM. 	21	ECM
Faury, 2007		32 pediatric GBM 7 adult GBM	39		<ul style="list-style-type: none"> Distinguishes 2 molecular subtypes of pediatric GBM based on Ras-Akt activation status. Distinguishes pediatric and adult GBM. 	1437	
						1569	
Shirahata, 2007	T	12 O3, 20 GBM	32		<ul style="list-style-type: none"> Distinguishes among Ras-Akt ± pediatric GBM and adult GBM. 	108	Phillips, 2006 proliferative
	V	22 O3, 28 GBM	50	Nutt, 2003	<ul style="list-style-type: none"> Distinguishes O3 and GBM. 96.6% predictive accuracy. Improved prognostic stratification vs. histological classification, confirming Nutt, 2003. 	168	
Li, 2009	T	52 A2, 29 A3, 55 GBM, 11 O2, 11 O3, 1 MOA2	159		<ul style="list-style-type: none"> Defined 6 hierarchically-nested molecular subtypes with 3 distinct prognoses. 92% prediction accuracy. 	54	G-O
	V	7 A2, 18 A3, 68 GBM, 12 O2, 9 O3, 7 MOA2, 68 gliomas	187		<ul style="list-style-type: none"> Reproduced six molecular subtypes. 	69	OA-OB
	V	21 A3, 55 GBM	76	Phillips, 2006	<ul style="list-style-type: none"> Prognostic significance confirmed. O subtype perfectly overlapped Phillips proneural GBM, but with 2 distinct prognoses. 	352	GA1-GA2-GB1-GB2
	V	265 GBM	265	TCGA	<ul style="list-style-type: none"> Prognostic significance confirmed. 		
Freije, 2004	T	8 A3, 7 O2, 9 O3, 50 GBM	74		<ul style="list-style-type: none"> Defined 4 molecular subtypes with 2 distinct prognoses. Improved prognostic stratification vs. histological classification. Prognostic independence from patient age and histological grade. 	595→ 44	Survival HC1A – neurogenesis HC1B – synaptic transmission HC2A – proliferation HC2B – ECM
	V	22 O3, 28 GBM	50	Nutt, 2003	<ul style="list-style-type: none"> Prognostic independence from patient age and histological grade. 	344	
Liang, 2005		2 O2, 4 MOA2, 25 GBM	31		<ul style="list-style-type: none"> Defined 2 prognostic GBM subtypes, 1 similar to HC1A from Freije, 2004. 	70	Survival
Phillips, 2006	T	21 A3, 55 GBM	76		<ul style="list-style-type: none"> Defined 3 molecular GBM subtypes with 2 distinct prognoses. 	108→ 35	
	V	22 O3, 28 GBM	50	Nutt, 2003	<ul style="list-style-type: none"> Prognostic significance validated. 		Survival Proneural – neurogenesis Proliferative – cell cycle Mesenchymal – ECM
	V	31 A3, 1 O2, 13 O3, 7 MOA3, 132 GBM	184		<ul style="list-style-type: none"> Prognostic independence from patient age and histological grade. 89% of 73 WHO grade III gliomas are proneural. Proneural subtype correlates with younger age at diagnosis. 	35	
Murat, 2008	T	80 GBM from TMZ/XRT→TMZ phase II/III clinical trials	80		<ul style="list-style-type: none"> Prognostic independence from patient age and MGMT methylation. HOX signature associated with resistance to TMZ/XRT→TMZ. 	18	HOX, self-renewal
	V	35 A3, 9 O3, 102 GBM	146	Freije, 2004 Phillips, 2006	<ul style="list-style-type: none"> Prognostic independence from patient age and histological grade. 	10	EGFR

Lee, 2008		86 GBM 181 GBM from previous studies	267	Mischel, 2003 Nutt, 2003 Shai, 2003 Freije, 2004 Rich, 2005 Phillips, 2006	<ul style="list-style-type: none"> Defined 4 molecular GBM subtypes: 3 from Freije, 2004 and 1 hybrid ProMes. Proneural subtype correlates with younger age at diagnosis. Prognostic independence from patient age. 	595→ 377	Survival HC1A-Proneural HC2A-Proliferative (Pro) HC2B-Mesenchymal (Mes) ProMes
Gravendeel, 2009	T	8 PA, 13 A2, 16 A3, 106 priGBM, 53 secGBM, 8 O2, 44 O3, 3 MOA2, 25 MOA3	276		<ul style="list-style-type: none"> Defined 6 “intrinsic” molecular subtypes with distinct prognoses. Cluster 9 prognostically favorable, enriched for oligodendroglial neoplasms. Cluster 17 prognostically intermediate, histologically diverse, overlapped with Phillips, 2006 proneural. Clusters 18 and 23 prognostically inferior, enriched for GBM, overlapped with Phillips, 2006 proliferative and mesenchymal. Prognostic independence from Karnofsky performance status and gender. 		
	V	80 GBM	80	Murat, 2008	<ul style="list-style-type: none"> Clusters 18 and 23 selectively benefitted from TMZ/XRT→TMZ. 	5000	
	V	76 gliomas 296 gliomas 236 GBM		Phillips, 2006 Li, 2009 Madhavan, 2009 TCGA	<ul style="list-style-type: none"> Prognostic significance confirmed. 		
Verhaak, 2010	T	200 GBM	200	TCGA	<ul style="list-style-type: none"> Defined 4 “intrinsic” molecular subtypes; not prognostic in TCGA dataset. Proneural: frequent <i>PDGFRA</i> amplification and mutations in <i>IDH1</i>, <i>TP53</i>, and <i>PIK3CA/PIK3R1</i>. Classical: frequent <i>EGFR</i> amplification, EGFRvIII mutations, and <i>CDKN2A</i> deletions. Mesenchymal: frequent mutations in <i>NF1</i>, <i>TP53</i>, and <i>PTEN</i>. TCGA proneural, Phillips proneural, and Freije HC1A overlap. TCGA mesenchymal, Phillips mesenchymal, and Freije HC2B overlap. 		Proneural – neurogenesis Neural – synaptic transmission Classical – EGFR Mesenchymal – immune response
	V	173 GBM 21 A3, 56 GBM 23 A3, 36 O2/3, 76 GBM 44 GBM 70 GBM	499	TCGA Phillips, 2006 Sun, 2006 Beroukhi m, 2007 Murat, 2008	<ul style="list-style-type: none"> Prognostic significance in five datasets with both GBM and lower grade gliomas. Molecular subtypes reproducible in four independent datasets. Proneural subtype correlates with younger age at diagnosis. Molecular subtype-copy number correlations confirmed in Beroukhi, 2007 dataset. Intensive therapy benefitted classical and mesenchymal GBM from TCGA and Murat, 2008. 	840	
Noushmehr, 2010	T	272 GBM	272	TCGA	<ul style="list-style-type: none"> GBM CpG island methylator phenotype (G-CIMP) in 29% of proneural GBM. G-CIMP correlated with younger age at diagnosis and more favorable prognosis. Prognostic independence from patient age and histological grade. 	1503	
	V	60 and 92 WHO grade II and III gliomas	152		<ul style="list-style-type: none"> G-CIMP positivity in WHO grade II/III astrocytomas (45%) and oligodendrogliomas (93%). 	8	
Colman, 2010	T	110 GBM	110	Nutt, 2003 Freije, 2004 Nigro, 2005 Phillips, 2006	<ul style="list-style-type: none"> Defined consensus 38-gene signature using top 200 survival-associated genes from each of four datasets. 	38	Survival
	V	68 GBM with FFPE tissues	68		<ul style="list-style-type: none"> Selected 9 genes based on survival correlation and technical compatibility with FFPE tissues. Prognostic significance confirmed for both progression-free and overall survival. 	9	
	V	101 GBM from patients treated with standard-of-care TMZ/XRT→TMZ	101		<ul style="list-style-type: none"> Prognostic independence from <i>MGMT</i> methylation status in the 101 GBM validation dataset. 		

- Prognostic independence from patient age and Karnofsky performance status in both validation datasets.

Studies listed in order of appearance in the text. *See Table 1.1 for histological subtype abbreviations. Abbreviations: concomitant temozolomide/radiation therapy and adjuvant temozolomide (TMZ/XRT→TMZ); dataset types: training (T), validation (V); extracellular matrix (ECM); formalin-fixed, paraffin-embedded (FFPE); primary GBM (priGBM); secondary GBM (secGBM).

Table 1.3. Diffuse glioma GEMM

Cell-of-origin	Genetic modification(s) in key signaling pathways					Ref(s)
	RB	RTK	PI3K	TP53	Other	
GFAP+		KRAS ^{G12D}				(126)
All	INK4A/ARF ⁻	FIG-ROS				(127)
GFAP+	RB1 ^{-/-}		PTEN ^{-/-}	TP53 ^{-/-}		(100)
Nestin+ or GFAP+	INK4A ^{-/-} ARF ^{-/-} INK4A/ARF ^{-/-}	PDGFβ KRAS ^{G12D}	Akt-Myr-Δ11-60		IGFBP2	(86, 87, 90, 128)
GFAP+	INK4A/ARF ^{-/-}	KRAS ^{G12V}		TP53 ^{-/-}		(129)
GFAP+		¹² V-Ha-Ras EGFRvIII				(80-82, 130)
Nestin+ or GFAP+		KRAS ^{G12D}	Akt-Myr-Δ11-60		MYC	(88, 89, 131)
Nestin+ or GFAP+	INK4A/ARF ^{+/- or -/-} CDK4	EGFRvIII bFGF		TP53 ^{+/-}		(132)
GFAP+	middle T			middle T		(133)
Nestin+		KRAS ^{G12D}	PTEN ^{-/-} Akt-Myr-Δ11-60			(134)
GFAP+		NF1 ^{+/-}	PTEN ^{+/-}	TP53 ^{+/-}		(95)
GFAP+	RB _f (T ₁₂₁)	KRAS ^{G12D}	PTEN ^{+/-} PTEN ^{-/-}			(40)
S100β+	INK4A/ARF ^{+/-}	v-erbB ¹² V-Ha-Ras		TP53 ^{+/-}		(71, 135)
All		NF1 ^{+/-}		TP53 ^{+/-}		(76, 136)
GFAP+	RB1 ^{+/-}	v-src		TP53 ^{+/-}		(77, 78)
Nestin+ or GFAP+	INK4A/ARF ⁻	KRAS ^{G12D}	Akt-Myr-Δ11-60			(89)
Nestin+ or GFAP+	INK4A ⁻ or ARF ⁻	KRAS ^{G12D}	Akt-Myr-Δ11-60			(137)
GFAP+		¹² V-Ha-Ras EGFRvIII	PTEN ^{+/-} PTEN ^{-/-}			(82)
GFAP+	RB _f (T ₁₂₁)		PTEN ^{+/-}	TP53 ^{+/-}		(79, 92)
Col1a1+	INK4A/ARF ^{-/-}	EGFR EGFRvIII	PTEN ^{-/-}			(96)
GFAP+		NF1 ^{+/-} NF1 ^{-/-}		TP53 ^{-/-}		(94)

CHAPTER II

Progression from low- to high-grade astrocytoma is characterized by transcriptomal heterogeneity and genomic number copy changes.

INTRODUCTION

Diffuse astrocytomas, the most common brain cancers, are characterized by extensive morphological, molecular, genomic, and biological heterogeneity. Patients with the most frequent histological subtype, glioblastoma (GBM, WHO Grade IV), have a median survival of 12-15 m (138). The dismal survival of GBM patients has fueled research to define its sources of heterogeneity. Numerous studies within the last decade have shown that gene expression profiling can differentiate between various histological subtypes of gliomas, including low-grade and high-grade gliomas and primary and secondary GBM (reviewed in (48)). The Cancer Genome Atlas (TCGA) utilized array comparative genomic hybridization (aCGH) and DNA sequencing to define commonly mutated genes in primary GBM and concluded that GBM tumorigenesis requires genetic alterations in three core signaling pathways: the RB regulated G1/S cell cycle checkpoint, receptor tyrosine kinase (RTK) signaling, and TP53 signaling (29). TCGA also examined the genomic heterogeneity of primary GBM and defined four transcriptomal subtypes – proneural, neural, classical, and mesenchymal (17) – that were similar to subtypes previously identified in multiple histological subtypes of gliomas (16, 18, 25). Putative oncogenic driver mutations were enriched in each GBM subtype, but none were exclusive. These data suggest that factors other than driver mutations may significantly contribute to GBM transcriptomal heterogeneity. Such factors include the differentiation state and fate potential of the cells harboring tumor-initiating mutations, and the genetic and epigenetic mutations that transformed cells acquire during malignant progression.

Defining the sources of genomic heterogeneity in GBM requires tractable model systems where oncogenic driver mutations and their cellular targets can be experimentally defined to induce de novo tumorigenesis in the complex microenvironment of the brain. In this regard, genetically engineered mouse (GEM) models have proven critical in understanding the genetic and cellular basis of GBM pathogenesis (reviewed in (139)). A number of GEM models with core signaling pathway mutations have established the roles of these genes in astrocytoma initiation and/or progression.

Most astrocytoma GEM models disrupted the G1/S checkpoint using *Cdkn2a* (*Ink4a/Arf*) or *Rb1* deletion mutations. Functional inactivation of three Rb family proteins in embryonic/neonatal mice led to astrocytoma tumorigenesis that was accelerated in a *Pten*-null background (79) and focal, somatic *Pten* deletion increased angiogenesis and invasion in this model (92). Others showed that conditional deletion of *Pten* and *Trp53* in adult murine astrocytes led to development of high-grade astrocytomas (HGA) with shortened latency in the presence of *Rb1* deletion, but that *Rb1* and *Pten* deletions failed to produce astrocytomas in the absence of *Trp53* deletions (100). To activate the MAPK pathway, most GEM models used constitutively activated *Kras* or *Nf1* deletion. *Nf1* deletion alone is insufficient to initiate astrocytoma tumorigenesis (94, 140), but *Kras* activation in embryonic/neonatal neural progenitors inefficiently produces low-grade astrocytomas (LGA) (126). In contrast, *Kras* activation requires additional oncogenic mutations, such as *Ink4a/Arf* with or without *Trp53/Pten* deletions, to form HGA in adult GFAP-positive astrocytes (129). To activate the PI3K pathway, the majority of GEM models used *Pten* deletion. Whereas deleting *Pten* in embryonic and adult mouse brains does not produce astrocytomas (100, 141), *Pten* cooperates with *Trp53* and *Nf1* deletion in embryonic and adult neural stem cells to produce HGA (70).

However, because no oncogenic driver mutations are exclusive to any of the four human GBM subtypes, it is difficult to classify GEM as subtype-specific models based solely on their oncogenic driver mutations. Therefore, it remains unclear how the majority of GEM recapitulate the underlying

molecular features of the human disease, including genome-wide gene expression, copy number, and mutational landscapes. Studies comparing expression profiles of GBM GEM to their human counterparts have only recently begun to emerge (100, 142-145) and only one of these examined genomic copy number abnormalities (CNA) (100). Furthermore, all three of these reports only examined tumors harvested from terminally-aged mice. Thus, the molecular features of astrocytoma initiation and progression in adult mice have yet to be characterized using genomic methods.

There are at least three potential sources of genomic heterogeneity in GBM: the oncogenic mutations that initiate tumorigenesis and drive malignant progression, the intrinsic biology and fate potential of the mutated cell (the cell of origin), and the developmental stage during which transformation occurs. In the current report, we used conditional, inducible GEM models to target constitutive RTK effector pathway ($Kras^{G12D}$ and/or *Pten* deletion) mutations in G1/S checkpoint-defective adult mouse astrocytes with *GFAP-CreER* (99). We examined the influence of cell of origin, specifically with regard to regional astrocyte heterogeneity in the adult mouse brain (146), on the genomic heterogeneity of astrocytomas before and after malignant progression.

MATERIALS AND METHODS

Genetically-engineered mice

Heterozygous *TgGZT*₁₂₁ (79), *Kras*^{G12D+/Isl} (147), *GFAP-CreER* (99), and *Rosa26-tdTomato* mice (148) as well as homozygous *Pten*^{loxP/loxP} (149), *p53*^{loxP/loxP} (150), *Rb1*^{loxP/loxP} (150), and *Nf1*^{loxP/loxP} (151) mice were maintained on a C57/Bl6 background. PCR genotyping was performed as previously described (79, 99, 147-151). All experimental animals were >94% C57/Bl6. Animal studies were approved by the University of North Carolina Institutional Animal Care and Use Committee.

Tamoxifen induction

Cre-mediated recombination in adult mice at approximately 3 m of age was induced with 1 mg of 4-hydroxytamoxifen (4OHT) (Sigma, St. Louis, MO) per day for five consecutive days by intraperitoneal injection. Kaplan-Meier plots and log-rank analyses were conducted in Stata 12 (College Station, TX). Comparisons at $\alpha \leq 0.05$ were considered significant.

Histopathological evaluation

Serial sagittal sections (4 μ m) of formalin-fixed, paraffin embedded brains were stained with hematoxylin and eosin (H&E) on a Leica Autostainer XL (Buffalo Grove, IL). Histopathological grading was performed according to WHO 2007 criteria for human astrocytomas (5) and defined as LGA (WHO grade II) or HGA (WHO grade III and IV (GBM)) by CRM, who was blinded to initiating genotype, induction status, and survival.

Quantification of LGA burden

H&E stained slides were scanned on an Aperio ScanScope XT (Vista, CA) using a 20X objective and the resulting svf files were imported into an Aperio Spectrum web database. Brains were manually segmented into cortex, diencephalon, brainstem, and olfactory bulb regions with Aperio ImageScope using the Allen Brain Atlas as a reference (152). Quantification of nuclei was performed as previously

described with the following modifications (153). The Aperio color deconvolution v9 algorithm was used to quantify the area occupied by hematoxylin-positive nuclei in each region on 1-3 serial sagittal brain sections per mouse (mean 1.9, SEM 0.4). Because LGA was detected in the cerebellum of 1 of 282 (0.4%) 4OHT-induced, GFAP-CreER mice with T, R, and/or P alleles examined histologically (Tables S2.1 and S2.5), the cerebellum was excluded from further analyses. Percent nuclear area was calculated as hematoxylin-positive pixels divided by total region pixels for each section and graphed as mean \pm SEM. Because regional nuclear density could be affected by the distance of the section from the sagittal midline, the brains from three wild-type C57Bl/6 mice were completely serially sectioned and every odd numbered section was scanned and analyzed as described above. The distance from midline was estimated using the Allen Brain Atlas. Although no significant distance-related effects were evident for the cortex, diencephalon, and brainstem by linear regression (Fig. S2.6C, $P \geq 0.21$), OFB nuclear density significantly decreased after 300 μ m lateral to sagittal midline. Therefore, only sections within the medial-most 300 μ m were used for morphometric analyses in Figs. 2B and S6. No significant differences in nuclear density of the cortex, diencephalon, brainstem, or olfactory bulb were evident in genotypes with histologically normal brains (N=25, Figs. S6AB, one-way ANOVA $P \leq 0.15$), therefore relative LGA burden was calculated as the regional nuclear area for each LGA-bearing mouse (N=19, Figs. 2B, S6D, and Table S2.1) relative to the mean for all non-tumor bearing genotypes (N=25, Fig. S2.6AB and Table S2.1). The effects of initiating genotype and brain region on LGA burden in Figs. 2B and S6A were analyzed using two-way ANOVA and the effects of genotype for each of the four regions in Fig. 2.6D were analyzed using one-way ANOVA in GraphPad Prism 5 (San Diego, CA).

Genetic lineage tracing and fate mapping

GFAP-CreER; Rosa26-tdTomato with or without *TgGZT₁₂₁*; *Kras*^{G12D+/Isl}; *Pten*^{+/-loxP} were induced with 4OHT at 3.5 m of age (mean 105, SD 38 d) as described above. Phenotypically wild-type *GFAP-*

CreER; *Rosa26-tdTomato* mice were sacrificed 7 d (N=3) and *GFAP-CreER^{T2}*; *Rosa26-tdTomato*; *TgGZT₁₂₁*; *Kras^{G12D+/Isl}*; *Pten^{+/-loxP}* mice were sacrificed approximately 3 w (N=3, mean 18.7 d) and 2 m (N=2, mean 60 d) post-induction. All mice received a single intraperitoneal injection with EdU (5mg/kg) 4 h before perfusion. Mice were perfused with 4% paraformaldehyde and their brains were immersion fixed in 4% paraformaldehyde overnight. Fixed brains were embedded in agarose and sagittal 50 μ m sections cut using a Leica VT1000S vibratome.

Immunofluorescence staining

Floating brain sections were permeabilized and blocked for 1 h using phosphate buffered saline (PBS) with 0.5% Triton X-100, 0.01 M glycine, and 5% goat serum. Primary antibodies were added for 18 h in staining buffer (PBS with 0.1% Triton X-100 and 0.5% bovine serum albumin) using the following concentrations: BLBP (rabbit 1:1000, Millipore, #ABN-14), GFAP (chicken 1:2000, Aves, #GFAP), GFAP (rabbit 1:1000, DAKO, #Z0334), Ki-67 (mouse 1:1000, Cell Signaling Technologies, #9449S), MAP2 (chicken 1:1000, Thermo #PA1-16751), NeuN (mouse 1:500, Chemicon, #MAB377), NSE (chicken 1:250, AbCam, #ab39369), P16 (mouse 1:500, Santa Cruz, #sc-1661), Sox2 (rabbit 1:500, Chemicon, #ab5603), and SV40 T antigen (mouse, 1:100, Calbiochem, #DP02). Sections were rinsed twice with wash buffer (PBS with 0.1% Triton X-100) and then washed twice for 30 min. Slices were stained for 4 h with DAPI (1:2000) and the following secondary antibodies: Alexa Fluor 488 (anti-rabbit A11034, anti-mouse A11029, and anti-chicken A11039, 1:1000), Alexa Fluor 568 (anti-rabbit A11036, 1:1000), Alexa Fluor 633 (anti-mouse, A21236, 1:500) and Alexa Fluor 647 (anti-rabbit A21071 and anti-chicken, A21103, 1:500). EdU was detected using the Invitrogen Click-iT EdU Cell Proliferation Assay (#C10338) according to the manufacturer's instructions. Sections were washed and mounted onto glass slides. Images were acquired using a Zeiss LSM 710 confocal microscope (Thornwood, NY).

Immunofluorescence quantification

Four random images of the cortex, diencephalon, brainstem, and olfactory bulb, and two images of the subventricular zone (SVZ), were taken using a 20X objective from each of three consecutive sagittal sections, located approximately 1.35 mm lateral to midline, from N=2-3 replicate mice per genotype and time point examined. TdTomato- and DAPI-positive nuclei were counted using ImageJ and their ratio was calculated to determine the percent tdTomato-positive cells for each image. The mean percent tdTomato-positive cells \pm SEM from 24-36 images was then calculated for each brain region. The percent EdU-positive cells were calculated similarly from 1-3 consecutive sagittal sections (mean 1.6, SEM 0.4 sections/mouse), located approximately 0.875 mm lateral to midline, for each mouse brain. The effects of genotype and time from induction on % tdTomato- (Fig. 2.2C) or EdU-positive cells (Fig. 2.2D) were analyzed using two-way ANOVA in GraphPad Prism 5. To determine GFAP-CreER recombination efficiency and specificity for astrocytes, the percentages of BLBP-positive astrocytes and NeuN-positive neurons in the cortex, diencephalon, brainstem, and olfactory bulb that were tdTomato/BLBP- and tdTomato/NeuN-double positive were determined from 2-5 random images/region in a sagittal brain slice from a 4OHT-induced *GFAP-CreER; Rosa26-tdTomato* mouse.

Microarrays

Total DNA or RNA was isolated from flash frozen brains or tumors (Tables S2.1, S2.5, S2.8, and S2.13) using DNeasy® or RNeasy® Mini Kits (Qiagen, Valencia, CA). RNA quality was confirmed on an Agilent Bioanalyzer (RNA Integrity Number > 7) and labeled using the Agilent Low RNA Input Linear Amplification Kit (Santa Clara, CA). RNA from mouse brains harvested 2 m after 4-OHT induction were hybridized to Agilent Whole Mouse Genome 4x44K microarrays (G4122F) while tumors and brains from terminally sacrificed mice were hybridized to 4x44Kv2 (G4846A) per the manufacturer's protocol. Stratagene Universal Mouse Reference RNA (Agilent, #740100) was co-hybridized to each array as a

reference. DNA was hybridized to Agilent Mouse 244A microarrays (G4415A) using a pooled DNA reference made from wild-type C57/Bl6 and syngeneic, phenotypically wild-type littermates. DNA labeling and hybridization were performed in the UNC LCCC Genomics Core using Agilent CGH ULS Protocol v.3.1 according to manufacturer's instructions. Microarrays were scanned on an Agilent DNA Microarray Scanner (G2565CA). Images were analyzed using Agilent Feature Extraction Software.

Microarray analyses

All original raw microarray data are publically available at both the UNC Microarray Database (<http://genome.unc.edu>) and the NCBI GEO (GSE49269). Microarray data was normalized using Lowess. Analyses were performed on data present in at least 70% of experimental samples using genes with an absolute signal intensity of at least 10 units in both the Cy3 and Cy5 channels (154). Replicate probes were collapsed to genes by averaging. Further analyses were performed in R (R Development Core Team, <http://www.R-project.org>). For the 2 m LGA cohort, 78 olfactory bulb and prosencephalon samples (Table S2.1) from eight microarray batches were combined in CombatR (155) using a parametric adjustment to remove batch effects and form a data matrix on which all further analyses were performed. Forty-three HGA (Table S2.5) from three microarray batches were analyzed similarly. Probes were annotated with gene symbols using Agilent eArray (<https://earray.chem.agilent.com/earray>). Cluster v3.0 and JavaTreeview were used for hierarchical clustering analyses (156, 157). Genes were median centered and the 2000 and 5000 most variable genes across all samples were identified by median absolute deviation (MAD) scores. Consensus clustering (158) was performed using the R package ConsensusClusterPlus (159) with 1000 iterations and an 80% resample rate and gave identical results using 2000 and 5000 genes. Core subtype membership was verified by silhouette width analysis (17, 160). ClaNC was used to define a 600 gene classifier (200 per subtype) to distinguish among three (S1-S3) HGA subtypes (161). Single sample Gene

Set Enrichment Analysis (ssGSEA) was performed as previously described (162, 163). For human TCGA GBM signatures, the 250 genes most highly expressed in each subtype, as determined by TCGA in one versus rest comparisons, were used (17). The murine neural lineage dataset GSE9566 was downloaded from NCBI GEO. Neural lineage-specific gene signatures were the top 500 genes associated with each cell type (108). The human lower-grade astrocytoma dataset GSE35158 was downloaded from NCBI GEO and signature genes were taken from Table S2.3 of Gorovets, et al. (164). For comparison to human gene sets, mouse genes were converted to the human orthologs using the MGI database (<ftp://ftp.informatics.jax.org/pub/reports/index.html#orthology>).

Array CGH analyses

Lowess-normalized data were analyzed and plotted using the R script SWITCHdna (165) with $\alpha=16$ and $F_{\text{thresh}}=12$. Probe level analysis of the *Pten* locus indicated that loss of exon 5 was detectable in LGA with deleted *Pten*, suggesting tumor cell density was sufficient to detect potential CNA in LGA. Raw Agilent 244A copy number data from GSE22927 (100) was downloaded from NCBI GEO, normalized, and analyzed similarly.

Prediction of TCGA GBM subtypes in GEM HGA

TCGA GBM subtypes of 42 core TR(P) HGA (Fig. S2.15) were predicted using the murine orthologs of the TCGA GBM ClANC 840 gene classifier (17, 163). Murine HGA and TCGA GBM mRNA expression data were combined using Distance Weighted Discrimination (DWD) (166). Heat maps were limited to the 840 classifier genes and samples were ordered according to their predicted subtype.

GEM HGA validation set analyses

Three adult murine HGA datasets were downloaded from NCBI GEO (GSE22927, GSE35917, and GSE29458; Table S2.11) (100, 142, 144). Data were limited to 8105 genes common to all three datasets and batch effects were removed using parametric adjustment in CombatR using the TCGA GBM subtype predictions determined in the original manuscripts as covariates. Hierarchical clustering and single sample prediction of S1-S3 HGA subtypes using the ClANC 600 gene classifier defined in the discovery set were performed on the validation set.

Significance analysis of microarrays (SAM)

Genes significant to LGA versus normal brain or LGA with and without Kras^{G12D} were determined by one versus rest SAM with a false discovery rate (FDR) of 0.001 (Table S2.3). Genes significant to each murine HGA subtype were determined by one versus rest SAM with FDR of 0.001, 0.01, and 0 for S1, S2, and S3, respectively (Table S2.9). FDR were chosen in order to define 1000-2000 of the most significant differentially expressed genes.

G1/S checkpoint (RB pathway) mutations in human GBM

Data from 236 TCGA human GBM with aCGH, sequencing, and mRNA and protein expression data were analyzed using the cBio Cancer Genomics Portal (167). Copy number abnormalities were determined by GISTIC 2.0; mRNA and protein expression Z-scores beyond ± 2 were considered significant. Fisher's exact tests were performed to assess co-occurrence or mutual exclusivity.

RESULTS

G1/S cell cycle checkpoint genes are mutated in virtually all human GBM

Significant alterations in G1/S cell cycle checkpoint (RB pathway) genes occur in 98% of adult human GBM in the TCGA dataset (Fig. S2.1). Reduced *RB1* mRNA or protein expression, inactivating mutations, or copy number losses trend towards co-occurrence with similar alterations in its pocket protein family members *RBL1* or *RBL2*, suggesting that functional compensation amongst these proteins may require elimination to disrupt the G1/S checkpoint in the absence of *CDKN2A/CDKN2B* alterations, which occur in 68-70% of cases. *Rb1* deletion in adult GFAP-positive mouse brain cells fails to initiate astrocytoma tumorigenesis, in both the presence and absence of concomitant *Pten* deletion (100). However, inactivation of all three Rb family proteins (Rb1, p107, p130) by T₁₂₁ expression in GFAP-positive embryonic brain cells is sufficient for LGA development and tumorigenesis is accelerated when combined with heterozygous *Pten* deletion (79). We have recently shown that T₁₂₁ expression ablates the G1/S checkpoint in murine astrocytes (163). It remains unknown whether functional ablation of Rb family members in the adult mouse brain is sufficient for astrocytoma development and whether concomitant *Pten* loss accelerates tumorigenesis in this developmental context. To study the individual and combined loss of Rb family and Pten activity in adult mouse brains, we used conditional, inducible transgenic *GFAP-CreER* mice (99).

GFAP-CreER targets astrocytes in multiple regions of the adult mouse brain

Genetic lineage tracing in 3 m adult *GFAP-CreER; Rosa26-tdTomato* mice showed that 4OHT induced recombination throughout the brain (Figs. 2.1, S2.2). Multiplex immunofluorescence showed that recombination occurred in $59 \pm 2\%$ of BLBP-positive astrocytes in the cortex, diencephalon, and brainstem (Fig. S2.3). In contrast, only $0.2 \pm 0.1\%$ of NeuN-positive neurons in these regions co-expressed tdTomato (Fig. S2.4).

Ablation of all Rb family members is sufficient for tumorigenesis in adult murine astrocytes

GFAP-CreER;T₁₂₁ ± *Pten*^{loxP/loxP} mice were induced to generate *GFAP-CreER*;T₁₂₁ ± *Pten*^{-/-} mice (hereafter referred to as T and TP^{-/-}, respectively). T and TP (TP^{+/-} and TP^{-/-}) mice were sacrificed 2 m after induction and the effects of these mutations on astrocytoma initiation and penetrance were analyzed. All mice remained neurologically asymptomatic, but histopathological analysis showed 100% incidence of LGA throughout the brain (Figs. 2.2A, S2.5). In contrast, *Pten* deletion alone was insufficient for tumorigenesis, as P mice displayed no hypercellularity, nuclear atypia, or abnormal brain architecture (Table S2.1), consistent with a previous report (100). Quantification of nuclei showed that T and TP^{-/-} mice had similar overall hypercellularity, but different regional LGA distribution (Figs. 2.2B, S2.5).

Kras^{G12D} potentiates tumorigenesis in G1/S-defective adult murine astrocytes

Because RTK genes such as *EGFR*, *PDGFRA*, *ERBB2*, and *MET* are commonly overexpressed, amplified, or mutationally activated in human GBM and uniformly activate Ras signaling (168), we used a conditional *Kras*^{G12D} knock-in allele to model the downstream RAS-MAPK pathway activation elicited by RTK gene alterations. *KRAS* mutations occur in only 2% of human GBM (29), but *KRAS* and other *RAS/RAF* genes are gained and overexpressed in both human GBM and cell lines (168, 169) and the negative RAS regulator *NF1* is deleted or mutationally inactivated in 17% of GBM (29). *Kras*, but not other Ras isoforms, is activated upon *Nf1* deletion in murine astrocytes, and *Kras*^{G12D} phenocopies *Nf1* deletion *in vitro* and *in vivo* (170). Moreover, we have recently shown that *Kras*^{G12D} potentiates MAPK signaling, growth, migration, and invasion of G1/S-defective murine astrocytes expressing T₁₂₁ *in vitro* and facilitates development of GBM in syngeneic mouse brains (163).

Kras^{G12D} has been shown to inefficiently induce LGA in neonatal mouse neural progenitors (126). To investigate whether Kras^{G12D} alone was tumorigenic or cooperated with Rb family and/or Pten dysfunction in adult murine astrocytes, we crossed *GFAP-CreER;Kras^{G12D+/Isl} ± T₁₂₁ ± Pten^{loxP/loxP}* mice, induced recombination, and sacrificed R, RP, TR, and TRP mice at 2 m after induction. In this context, Kras^{G12D} alone or in combination with *Pten* deletion was insufficient for tumorigenesis, as R and RP mice displayed no increased cellularity and had normal brain architecture (Fig. S2.6AB and Table S2.1). Both TR and TRP mice developed neurologically asymptomatic LGA with 100% incidence (Figs. 2.2A, S2.5). In contrast to *Pten* deletion, Kras^{G12D} significantly increased LGA burden in T mice (18% in TR versus 11% in TP^{-/-}) (Figs. 2.2B, S2.5, S2.6D). TRP^{-/-} mice had the highest LGA burden and 25% harbored anaplastic astrocytomas (WHO Grade III) after 2 m (Figs. 2.2AB, S2.5, S2.6D). ANOVA showed that both initiating genotype and brain region significantly affected tumor burden. These findings demonstrate that Kras^{G12D} potentiates tumorigenesis in G1/S-defective astrocytes and that *Pten* deletion further increases LGA burden throughout the adult mouse brain.

Ablation of all Rb family members is required for tumorigenesis in adult murine astrocytes

Rb1 deletion, *Rb1;Pten* co-deletion ± Kras^{G12D}, or *Nf1 ± Rb1 ± Pten* co-deletion showed no evidence of tumorigenesis in adult astrocytes. In contrast, similar to TR(P), all T mice with *Nf1 ± Pten* deletions developed astrocytomas (Fig. S2.7, Table S2.2). Collectively, these results demonstrate that *Rb1* deletion alone is insufficient for tumorigenesis, even in the presence of activating MAPK (Kras^{G12D} or *Nf1* deletion) and PI3K (*Pten* deletion) pathway mutations. Rather, they suggest that inhibition of all three Rb family proteins is required to ablate the G1/S checkpoint and initiate astrocytoma tumorigenesis in adult murine astrocytes. These results also demonstrate that Kras^{G12D} and *Nf1* deletion have similar tumorigenic effects in G1/S-defective, adult murine astrocytes.

TRP-transformed astrocytes maintain their astrocytic identity and develop into hypercellular foci over time

In order to fate map transformed astrocytes, we used fluorescent lineage tracing with *GFAP-CreER*; *Rosa26-tdTomato* crossed with *TRP^{+/-}* mice. TRP significantly increased tdTomato cell density from 4-6% in the normal cortex, diencephalon, brainstem, and olfactory bulb at 7 d to 18-27% and 42-47% in these regions 21 and 60 d after induction (Fig. 2.2C, S2.8, S2.9). A temporal increase in perineuronal satellitosis, a histopathological hallmark of human astrocytomas, was also evident (Figs. S2.10 and S2.11D). Furthermore, these cells expressed T₁₂₁ (Fig. S2.11AB) and the astrocytic markers BLBP (Fig. S2.11C) and Gfap (data not shown) and hypercellular foci developed by 60 d (Fig. S2.11E). A single pulse labeling with EdU showed increased proliferation of tdTomato-positive cells in all brain regions over time (Fig. 2.2D, S2.9). Ki-67 staining showed that proliferation was heterogeneous at 60 d (43-52% CV). Hypercellular foci had 5-fold increased proliferation relative to surrounding diffuse astrocytoma (Fig. S2.11DE). These results show that TRP initiates tumorigenesis in astrocytes in four distinct brain regions, that transformed cells maintain their astrocytic identity, and that proliferation and histopathological hallmarks of human astrocytomas increase over time. The fact that hypercellular areas with markedly increased proliferation develop suggests that these foci progress to HGA upon stochastic acquisition of additional mutations.

T(RP) LGA transcriptomes have *Kras*^{G12D} oncogenic driver- and astrocyte location-specific signatures

To understand how Rb, Kras, and Pten affect tumorigenesis at the molecular level, we examined gene expression and copy number in high tumor burden areas - olfactory bulbs and forebrains - harvested from mice at 2 m after induction (Table S2.1). Principal components analysis (PCA) showed separation of normal olfactory bulb, normal forebrain, and LGA in both regions. Moreover, LGA with

and without $Kras^{G12D}$ grouped separately in both locations (Fig. 2.3A), but there was no $Kras^{G12D}$ effect in non-tumor olfactory bulbs (Fig. 3B). Consensus clustering (158) of transcriptome data confirmed the distinction between brain regions and LGA with or without $Kras^{G12D}$ (Fig. S2.12). Notably, there were minimal and infrequent copy number alterations (CNA) in LGA, including those with $Kras^{G12D}$ (Fig. S2.13A). These findings demonstrate that T(RP) LGA have not acquired significant CNA, and their transcriptomes have $Kras^{G12D}$ oncogenic driver- and astrocyte location-specific signatures.

T(RP) LGA transcriptomes recapitulate subtypes of non-GBM astrocytomas

Significance analysis of microarray (SAM) (171) was conducted to identify genes differentially expressed between T(RP) LGA and normal brain (Table S2.3). Gene ontology (GO) analysis showed that the most highly expressed LGA genes functioned in multiple cell cycle checkpoints (Fig S2.13B). We confirmed aberrant G1/S signaling by performing p16 immunofluorescence. At 5 m, p16 is normally absent in wild-type cortical murine astrocytes, but is expressed in neurons (172). Unlike wild-type mice, TRP induced p16 expression in transformed astrocytes, consistent with microarray data (Fig. S2.14). Upregulation of G1/S checkpoint genes is consistent with Rb pathway disruption in T(RP) LGA. SAM and GO analysis of LGA with versus without $Kras^{G12D}$ showed that the most highly expressed genes were enriched in immune response and cell membrane biology (Table S2.3). To determine if this $Kras^{G12D}$ signature was differentially expressed among human astrocytomas, we assessed its enrichment in non-GBM human astrocytomas (164). The $Kras^{G12D}$ signature was highly expressed in the pre-glioblastoma (PG) subtype (Fig. 2.3C), which has shorter survival than neuroblastic and early progenitor-like subtypes, contains mostly HGA (anaplastic astrocytomas), and has a genomic landscape similar to GBM, including frequent *EGFR* amplification and *CDKN2A* and chromosome 10 (*PTEN*) deletions (164). Taken together, these data suggested that murine LGA with $Kras^{G12D}$ would rapidly progress to HGA and show worse survival than LGA without $Kras^{G12D}$.

LGA with $Kras^{G12D}$ stochastically progress to HGA and acquire CNA

To determine whether LGA progress to HGA, we induced recombination in all LGA-bearing genotypes and aged mice until neurological morbidity. Astrocytoma incidence was 100% for all six T-containing genotypes (Fig. 2.4A). LGA in T and TP mice infrequently progressed to high-grade anaplastic astrocytoma (WHO Grade III), but none of these mice exhibited neurological symptoms when sacrificed up to 18 m after induction. Furthermore, terminal T and TP LGA contained few and infrequent CNA (Fig. 2.5I). Taken together with the two-month LGA aCGH data (Fig. S2.13A), these results indicate that T(P) LGA rarely acquire CNA regardless of their age.

In contrast, TR mice frequently progressed to HGA, including GBM (Fig. 2.4A), and median survival was 4.5 m after induction. (Fig. 2.4B). These results indicate that while Rb family dysregulation is required to initiate tumorigenesis in adult murine astrocytes, $Kras^{G12D}$ facilitates progression to HGA. Furthermore, deleting *Pten* in $TRP^{+/-}$ and $TRP^{-/-}$ mice resulted in frequent HGA progression. Although the frequencies of HGA in TRP mice were not statistically different from TR, *Pten* deletion led to increased incidence of GBM, which all contained pseudopalisading necrosis, but rarely microvascular proliferation (Figs. 2.4A, S2.15, 2.5A-F). $TRP^{+/-}$ and $TRP^{-/-}$ mice survived a median of 4.0 and 2.8 m, respectively (Fig. 2.4B), and HGA occurred in all brain regions except cerebellum (Fig. S2.15).

The variable survival in TR(P) mice with HGA suggested that progression occurred stochastically. We therefore monitored the development of HGA in $TRP^{+/-}$ mice with contrast-enhanced magnetic resonance imaging (MRI) over time. HGA, but not LGA were visible by T1- and T2-weighted MRI and enhanced with gadolinium. Therefore, contrast enhancement (Fig. 2.5A) was used as a surrogate for histological progression. All mice had MRI-undetectable LGA (Fig. 2.5B-F), but also developed focal, contrast-enhancing HGA (Fig. 2.5B-F) at 3-5 m after induction. Onset was variable, but HGA growth and

lethality were uniformly high (Fig. 2.5G-H). These findings suggest that TRP LGA progress into rapidly proliferating, lethal HGA upon the stochastic acquisition of additional mutations.

Because HGA had variable onset and grew rapidly after initial MRI identification, we performed copy number analysis to investigate genomic instability. Array CGH of 41 terminal TR(P) HGA detected abnormalities throughout the genome (Fig. 2.5J-L). All three genotypes had prevalent copy number gains throughout chromosome 6, which contains the established oncogenes *Braf*, *Kras*, and *Met*. Among Rb, RTK/MAPK/PI3K, and Trp53 pathway genes, *Ccnd2*, *Stat1*, *Met*, *Braf*, *Kras*, *Raf1*, and *Mdm4* were gained in >20% of HGA. Other notable, but less frequent CNA were gains of *Egfr*, *ErbB2*, *Pdgfrb*, and *Pik3ca* oncogenes and loss of *Pten*, *Cdkn2a*, and *Trp53* tumor suppressors (Table S2.6). TRP^{-/-} HGA had the lowest frequency of these CNA. Similar chromosomal distributions of CNA were evident in TR and TRP^{+/-} HGA, but CNA were more frequent in TR HGA (Fig. S2.16). Only 3 HGA (7%) had no CNA and all were from TRP^{-/-} mice with short, 1.9-2.1 m survivals, including one asymptomatic TRP^{-/-} mouse sacrificed for inclusion in the 2 m cohort that harbored a grossly visible mass. These results suggest that most HGA acquire CNA during malignant progression.

Gene expression profiling identifies three HGA subtypes that correlate with astrocyte location

In order to examine the heterogeneity of murine HGA gene expression, we performed microarray-based expression profiling on 43 terminal TR(P) HGA and identified three subtypes using consensus clustering (Fig. S2.17). Silhouette width analysis (160) identified 42 core HGA samples with expression profiles most representative of each subtype (Fig. S2.17D). HGA subtype did not correlate with initiating oncogenic mutations (Table S2.8). Similarly, no *Pten* deletion-related effect was evident in LGA transcriptomes (Figs. 2.3AB and S2.12), suggesting that *Pten* deletion does not significantly contribute to transcriptomal heterogeneity either before or after malignant progression in this model. Whereas initiating genotype correlated with survival (Fig. 2.4B), HGA subtype did not (Fig. S2.18A). However,

HGA subtype correlated with brain region (Fig. S2.18B). Subtype 1 (S1) tumors were primarily located in the brainstem (72%), some of which developed as exophytic masses that extended into the fourth ventricle. Subtype 2 (S2) tumors were primarily located in the olfactory bulb (50%). Subtype 3 (S3) tumors were located in all brain regions. These results suggest that GFAP-positive astrocytes in different brain regions give rise to transcriptomally distinct HGA.

Moreover, HGA transcriptomes were distinct from their genotype-matched LGA counterparts (Fig. S2.18C). This finding confirms that, despite identical initiating oncogenic mutations, progression from LGA to HGA is associated with significant transcriptomal changes. These results are consistent with the transcriptomal differences between non-genotype-matched human LGA and HGA (12, 13, 15) and suggest that the secondary mutations acquired during malignant progression significantly influence astrocytoma transcriptomes.

Murine HGA phenocopy human HGA transcriptomal subtypes

A classifier consisting of 600 genes, the 200 most representative of each subtype, correctly predicted subtype with 0% cross validation and error rates (Fig. 2.6A, Table S2.9). In order to further characterize these subtypes, we examined differentially expressed genes using SAM (171) and defined their biological functions using gene ontology analyses (Table S2.11). Immune and cytokine response, NF- κ B pathway, and extracellular matrix genes were significantly expressed in S1, suggesting that this subtype was similar to human mesenchymal HGA (17, 18). We therefore predicted the human GBM subtype of individual murine HGA using the 840-gene TCGA classifier and found that 94% of S1 HGA were predicted as mesenchymal GBM (Figs. 2.6C, S2.19, and Table S2.8). S1 HGA were also enriched in a cultured murine astrocyte signature (108) (Fig. 2.6E), similar to human mesenchymal GBM (17).

Cell cycle, proliferation, and RNA processing genes were significantly expressed in S2 HGA. The majority (75%) of S2 HGA were predicted as proneural GBM using the TCGA classifier. S2 HGA also

expressed a previously identified proliferation signature (173) and a murine oligodendrocyte precursor signature (108), similar to human proneural GBM (17).

Genes highly expressed in S3 HGA were enriched in synaptic transmission, ion channel and glutamate signaling, and other neuronal processes. TCGA classifier predicted 65, 29, and 6% of S3 HGA as human neural, proneural, and mesenchymal GBM, respectively, and all were enriched in a murine neuronal signature (108). These results imply that the transcriptomes of S3 HGA are the most heterogeneous, but are most similar to human neural GBM.

Seven TR(P) mice developed two distinct HGA in different brain regions; of these, four had different S1-S3 HGA subtypes (Table S2.8). Six of these HGA pairs were analyzed by aCGH and none contained identical genomic copy number landscapes (Table S2.7). Together, these data suggest that CNA acquired stochastically during malignant progression significantly contribute to HGA transcriptomal heterogeneity.

Validation of S1-S3 HGA subtypes in different adult GEM HGA models

S1-S3 HGA subtypes were validated in an independent test set of transcriptome data from adult GEM HGA models with different initiating oncogenic mutations (100, 142, 144). The 600-gene classifier showed similar expression in both the discovery and test sets (Figs. 2.6AB). Furthermore, test set samples clustered by both predicted human GBM and mouse HGA subtypes. Similar to the results with TR(P) HGA, S1, S2, and S3 HGA in the test set were primarily predicted as mesenchymal, proneural, and neural GBM, respectively (Fig. 2.6D, Table S2.11). Two datasets contained normal brain samples and these clustered with neural S3 HGA. This finding recapitulates the clustering of human non-neoplastic brain with neural GBM (17).

Deletion of p53 affects the CNA landscapes of murine HGA upon malignant progression

Because HGA from both TR(P) and *Rb1/Pten/p53* triple KO (100) models reproduce multiple human GBM subtypes, we compared their CNA landscapes. *Rb1/Pten/p53* triple KO HGA harbored CNA in all autosomes, but the chromosomal pattern of CNA was more restricted in TR(P) HGA (Fig. S2.20). Because the role of p53 in maintenance of genomic integrity is well established (174), we hypothesized that *p53* deletion contributed to the difference between genomic landscapes in these models. To test this hypothesis, we bred a floxed *p53* allele into T(RP) mice (Table S2.12). At 2-6 m after induction, all T(RP);*p53*^{+/-} mice harbored LGA and 4/14 had progressed to HGA (Fig. S2.21). Similar to T(RP) mice without p53 deletion (Fig. S2.13A), T(RP);*p53*^{+/-} astrocytomas harvested 2 m after induction were largely devoid of CNA (Fig. S2.22). In contrast to T mice without *Kras*^{G12D} in which LGA failed to progress (Fig. 2.4A) and lacked CNA even when aged over a year (Fig. 2.5I), at 11 m after induction, a T;*p53*^{+/-} mouse developed GBM with widespread CNA similar to *Rb1/Pten/p53* triple KO HGA (Fig. S2.23). These data support the conclusion that heterozygous *p53* deletion results in widespread genomic instability during malignant progression.

DISCUSSION

In this study, we genetically disrupted Rb, Ras, and Pten signaling in adult murine astrocytes and systematically investigated tumorigenesis in all relevant genotype combinations. Functional ablation of the Rb family of pocket proteins was sufficient for low-grade astrocytoma (LGA) initiation throughout the brain, but Kras^{G12D}, deletions of *Rb1*, *Nf1*, and *Pten*, and double and triple combinations of these mutations were insufficient for tumorigenesis. LGA transcriptomes were distinct from histologically normal brains and clustered by anatomic brain region and Kras^{G12D} status. We identified a Kras^{G12D}-associated immune response signature that was enriched in the pre-glioblastoma subtype of human lower-grade astrocytomas. When aged to neurological morbidity, mice with Rb pathway and Kras \pm Pten dysfunction developed contrast enhancing HGA with variable latency, rapid growth kinetics, and CNA in Rb, RTK/MAPK/PI3K, and Trp53 pathway genes. Three transcriptomal HGA subtypes were identified and subsequently validated in an independent test set of HGA from adult GEM models with different initiating oncogenic mutations. These murine HGA subtypes phenocopy human GBM transcriptomes and were enriched for similar biological processes and showed human subtype-specific signatures. Single sample prediction using human GBM subtype-specific genes, single sample gene set enrichment, and hierarchical clustering with combined mouse and human expression data, confirmed the similarities between murine HGA and human GBM transcriptomal subtypes.

The role of Rb family proteins in astrocytoma initiation and progression

In contrast to previous studies that inactivated Rb family proteins in embryonic mice (79) or conditionally deleted *Rb1* in adult mouse brains (100), we found that inactivation of the Rb family of pocket proteins – Rb1, Rbl1/p107, and Rbl2/p130 – with T₁₂₁ was sufficient to initiate astrocytoma tumorigenesis in adult murine astrocytes. Deletion of *Rb1* alone could not substitute for T₁₂₁ or combine with Kras^{G12D}, *Nf1* deletion, or *Pten* deletion to initiate tumorigenesis. Together, this evidence suggests

that functional compensation amongst Rb pocket proteins renders *Rb1* deletion insufficient for astrocytoma initiation in adult murine astrocytes, even when paired with MAPK or PI3K pathway mutations. G1/S cell cycle checkpoint function is critical for cell growth regulation; thus, virtually all human GBM acquire RB pathway mutations. Although *RBL1* and *RBL2* are infrequently mutated, their decreased expression tends to co-occur with inactivating *RB1* mutations in human GBM that lack *CDKN2A/CDKN2B* mutations. These findings suggest that functional compensation amongst Rb family proteins may require elimination to disrupt the G1/S checkpoint in both humans and mice. While T_{121} was sufficient for initiation, *RB1* mutations are generally thought to be a late event during malignant glioma progression in humans (175). Whether these findings reflect a fundamental difference between mice and humans or indicate an unappreciated role for functional compensation amongst Rb pocket proteins in human gliomas remains unclear.

We provide the first report of murine LGA gene expression and CNA data in adult, conditional GEM. Expression profiling showed that LGA are distinct from non-tumorigenic brains and can be separated into two subtypes based on *Kras*^{G12D}, but not *Pten* deletion. These data suggest that in G1/S-defective adult murine astrocytes, *Kras*^{G12D} has greater effect on gene expression than *Pten* deletion and are consistent with a recent study in which multiple fragments of individual human GBM were sequenced to examine clonal evolution (176). The authors suggest that PTEN loss is a late event in human GBM progression and occurs after primary genetic events such as RB and RAS pathway mutations. Murine LGA transcriptome analysis also distinguished between the profiles of LGA that would frequently progress to HGA versus those that would not. One notable difference between this murine subtype and its potential human counterpart—the pre-glioblastoma subtype predicted to become GBM (164)—is that murine LGA have relatively silent genomes, but human pre-glioblastomas have genomic copy number profiles similar to GBM. The lack of CNA may be attributable to fewer A3 in mice at 2 m versus many A3 in human pre-GBM, but it is noteworthy that gene expression indicates LGA with GBM

potential before progression. Additionally, we showed that, regardless of time after induction or genotype, all LGA genomes were relatively absent of CNA. These data suggest that transcriptomal signatures may be better conserved across species than patterns of chromosomal instability or mutations.

A detailed genomic and transcriptomal characterization of murine LGA can be used as a foundation for further studies. This model is particularly suited to examining the effects of standard radiotherapy and temozolomide on histological and genomic tumor progression and survival. Progression and adaptation studies would only be possible in humans with detailed follow-ups, and long survival of patients with A2 makes such studies logistically difficult. In contrast, this murine LGA model provides a unique opportunity to examine treatment induced biological responses in a reasonable timeframe.

Modeling human subtypes and the influence of the cell of origin

Human GBM have been characterized based on their transcriptomal variation with the ultimate hope that subtype-specific features can be used to realize the potential of targeted therapy and personalized medicine (16-18, 25). Using GEM to determine the cellular origin(s) of the four transcriptomal GBM subtypes has been complicated by the fact that a variety of different methods and genes are used to drive GEM tumorigenesis, and that many GEM employ GFAP or Nestin Cre drivers in the developmental context where they have overlapping cellular specificity (139). As a result, direct comparisons between models, cells, and transcriptomes are difficult.

Proneural-like murine HGA and GBM have been described in a model that embryonically deleted *p53/Nf1* with GFAP-, Nestin-, or NG2-Cre in fluorescently labeled cells (143), a model that employs PDGF and Cre-expressing viral injections in 6-8 w floxed *Pten* or *Pten/p53* mice (142), and a GFAP-CreER-driven adult GEM with floxed *Pten/p53* \pm floxed *Rb1* (100). Here, adult GFAP-driven S2 proneural-like HGA often occurred in the olfactory bulb and all S2 HGA were enriched in an OPC signature, suggesting a

potential cell of origin. If OPC are the origin it indicates that proneural-like HGA progress similarly in embryonic and adult GEM, in that initiating mutations occur in NSC but OPC are the tumorigenic cell lineage (143). However, we cannot yet determine the specific cell of origin for olfactory bulb S2 proneural-like HGA despite confirmation that GFAP-Cre targets SVZ cells, but we suspect they originate from neural stem cells of the SVZ that travel through the RMS in addition to local olfactory bulb astrocytes. TRP brains have RMS tumors, and GFAP-positive proliferation and tumorigenesis occurs in the inner region of the olfactory bulb where the RMS deposits. Ongoing studies involve a detailed origin and fate characterization of these cells.

We also described S1 mesenchymal-like HGA which often occurred in the brainstem and expressed signatures resembling cultured astrocytes. Mesenchymal-like HGA have been described in two other adult HGA models—the Baker group deleted *Pten/p53 ± Rb1* in GFAP-positive cells (100), and the Verma group injected lentivirus expressing *Hras*^{V12} and p53-shRNA into SVZ, cortex, and hippocampus of GFAP-Cre, mice or into the cortex of Syn1-Cre mice (144). However, when Nestin-Cre mice were used hippocampal injections generated neural-like HGA. The result of different subtypes based on alternate Cre-drivers indicates that subtle differences in GFAP and Nestin hippocampal cellular specificity lead to transcriptomally distinct HGA even when using identical tumorigenic driver genes. Notably, none of these mesenchymal mouse models included *Nf1* deletion, often thought to be a hallmark of mesenchymal GBM. Together, these three adult HGA models show that a variety of driver mutations in astrocytes and neurons can form mesenchymal HGA.

Lastly, we described S3 neural-like HGA that occurred in the cortex, diencephalon, brainstem, and olfactory bulb. S3 neural-like HGA had the most heterogenous transcriptomes—neuron signature genes were enriched in S3 HGA, but individual HGA also highly expressed OPC, astrocyte, and oligodendrocyte signatures. Similar transcriptomal heterogeneity existed in neural-like HGA from the Verma group even though all those HGA were initiated in the same location in Nestin-Cre mice (144). These two examples

of neural-like HGA suggest hippocampal NSC and differentiated astrocytes as potential sources. We have yet to define the origin of S1 or S3 HGA, but based on the knowledge that most cortical astrocytes in mice originate from local proliferation of postnatal astrocytes rather than from glial progenitors migrating from the SVZ (177), we suspect that cortical and brainstem HGA arise from locally transformed astrocytes and not NSC.

The classical GBM subtype has been more difficult to reproduce in GEM. We and others (100) showed a few tumors that predicted as classical, but these are part of the S2-proneural subtype rather than a unique group like human classical GBM. However, classical GBM might be one subtype that can be more easily defined by its oncogenic mutations because *CDKN2A* loss, *EGFR* gain, and *EGFR* increased expression are nearly universal in classical GBM. Unfortunately comprehensive analysis was precluded in the adult HGA GEM that used these genetic drivers because it lacked a brain-specific promoter and transcriptome analysis (96).

Determining how astrocytoma cells of origin, initiating mutations, acquired genomic changes, and microenvironment contribute to HGA and GBM has been difficult in part because human GBM transcriptomes have not been as instructive as other cancers such as medulloblastoma, where, human subtype signatures suggested key driver mutations, which were later confirmed to drive subtype specificity when initiated in specific cells of origin in GEM (178). Yet despite different Cre-drivers, initiating mutations, and degrees of CNA, S1-S3 GFAP-Cre TR(P) HGA cover the transcriptomal diversity present in previous HGA GEM. These data suggest that while initiating oncogenic drivers and/or acquired CNA, no doubt, contribute to genome-wide transcription, the promoter driving the model, and thus brain region and/or cell of origin, play a more prominent role in defining murine HGA subtype.

In summary, this is the first study to validate murine glioma transcriptome subtypes using a test set composed of adult glioma models with diverse oncogenic mutations. It shows inherent heterogeneity that reproduces both the transcriptomal diversity of human GBM and encapsulates the transcriptomal

diversity of three recent adult GEM GBM cohorts, each with distinct combinations of oncogenic mutations and putative cells of origin. This study builds on previous GEM genomic analysis to suggest that there can be multiple GBM cells of origin and that to discover the conditions for astrocytoma transcriptomal heterogeneity researchers must understand the cellular context of tumorigenic mutations. Advances using developmental neurobiology and lineage tracing to identify brain cellular hierarchies should facilitate this task. It will allow researchers to further define the requirements for subtype specificity by targeting initiating mutations in different cellular lineages within spatially distinct brain regions.

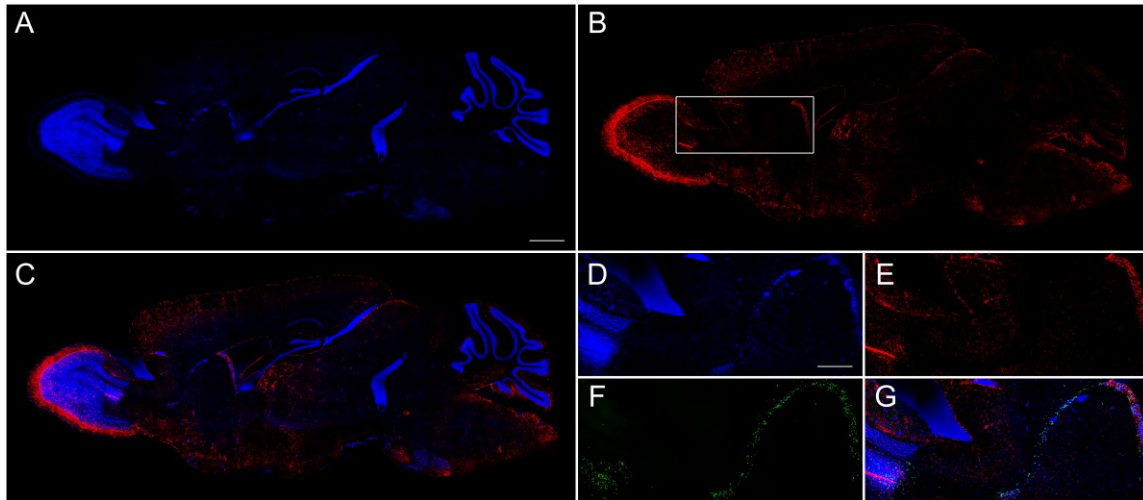


Figure 2.1. GFAP-CreER mediates recombination throughout the brain Genetic lineage tracing in a *GFAP-CreER;Rosa26-tdTomato* mouse at 7 d after induction. DAPI (A, D), tdTomato (B, E), and merged (C, G). Only cells in neurogenic brain regions (panels D-G from the boxed region in B), including the SVZ and rostral migratory stream, incorporate EdU (F).

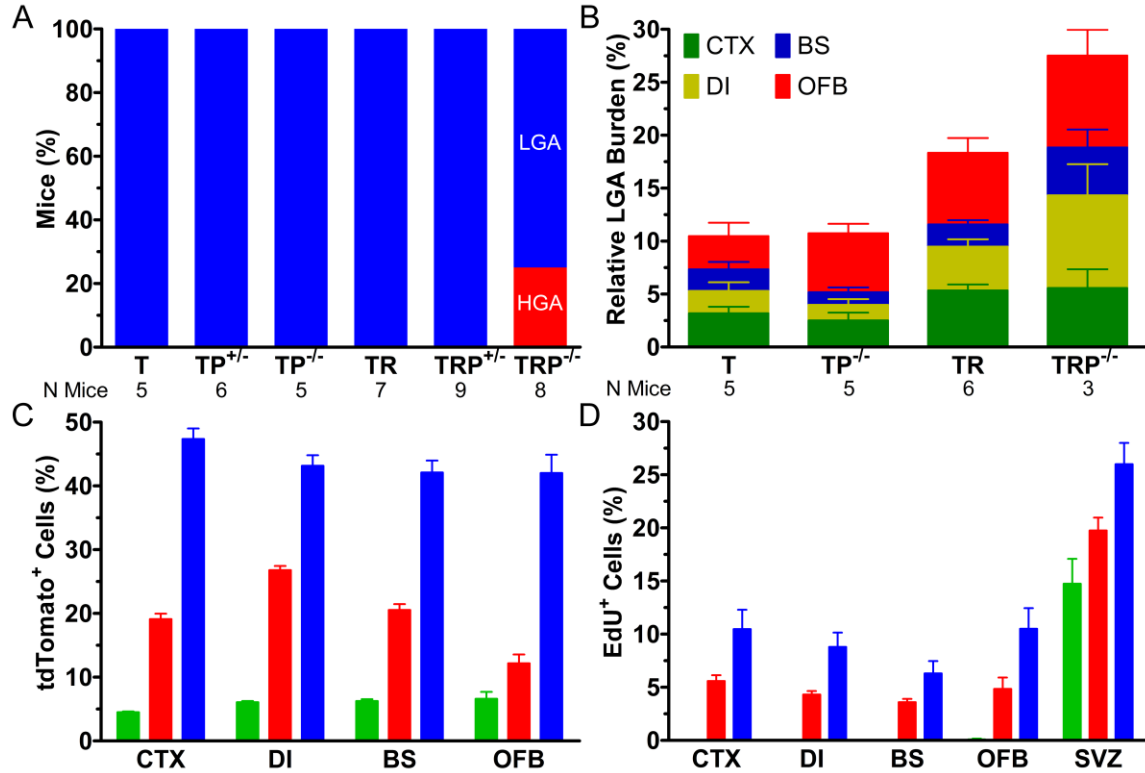


Figure 2.2. Effects of initiating genotype and brain region on LGA tumorigenesis. All mice harbored LGA (blue) and only 25% of TRP^{-/-} mice had progressed to HGA (red) at 2 m after induction (A). Nuclear density in the cortex (CTX), diencephalon (DI), brainstem (BS), and olfactory bulb (OFB) was examined for each genotype and compared to phenotypically wild-type controls (Fig. S2.6). T and TP^{-/-} mice had similar overall hypercellularity, but regional distribution differed: TP^{-/-} mice harbored significantly greater OFB LGA (one-way ANOVA $P=0.002$). Regional differences were not evident between TP^{-/-} and TR or TR and TRP^{-/-}, but both initiating genotype and brain region significantly affected LGA burden overall (two-way ANOVA $P\leq 0.002$). Genetic lineage tracing in *GFAP-CreER;Rosa26-tdTomato* (green) and *GFAP-CreER;Rosa26-tdTomato;TRP^{+/-}* (red, blue) mice at 7 (green), 21 (red), and 60 (blue) d showed an increase in tdTomato- (C) and proliferating, EdU-positive cells (D) over time in all four brain regions. Only tdTomato-positive cells in the subventricular zone (SVZ) proliferated in the presence and absence of TRP^{+/-}. Both initiating genotype/time and brain region significantly affected tdTomato- and EdU-positive cell density (two-way ANOVA $P\leq 0.0001$).

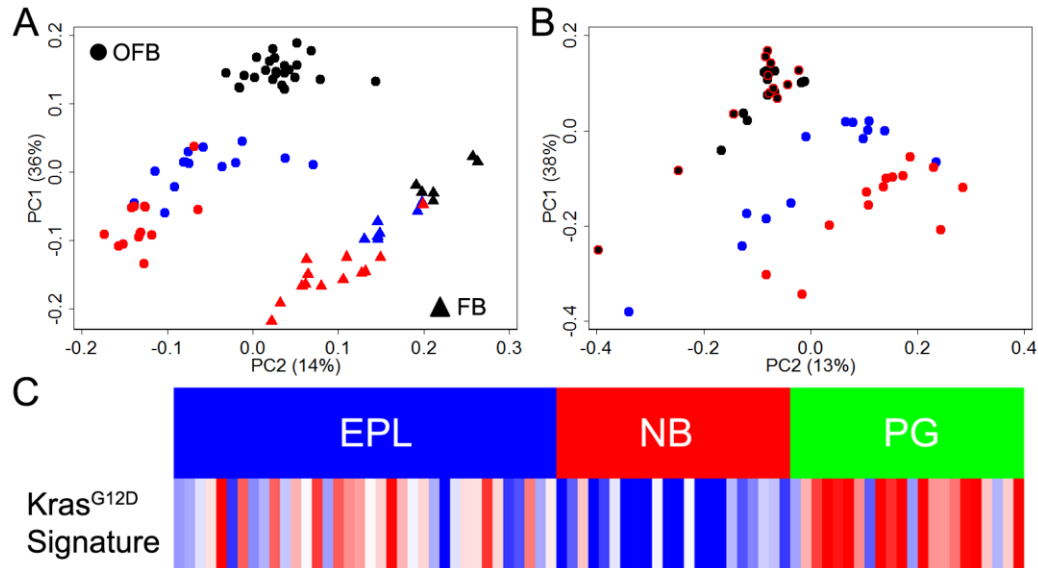


Figure 2.3. LGA transcriptomes show driver mutation- and brain region-associated signatures.

Principal component analysis (PCA) shows that normal (black) and LGA-containing (red, blue) olfactory bulbs (OFB) and forebrains (FB) have distinct transcriptomes, as phenotypically wild-type mice (normal brains, Table S) clustered separate from T, TR, TP, TRP LGA (A). Transcriptomes of OFB and CTX LGA with (red) and without (blue) Kras^{G12D} are also distinct. Although OFB transcriptomes from histologically normal mice with (black with red outlines) and without (black) Kras^{G12D} were indistinguishable, the transcriptomes of OFB LGA with Kras^{G12D} (red) were distinct from those without (blue) (B). A Kras^{G12D}-related OFB LGA gene signature was enriched in the pre-glioblastoma (PG), but not the neuroblastic (NB) or early progenitor-like (EPL) subtypes of human non-GBM astrocytomas.

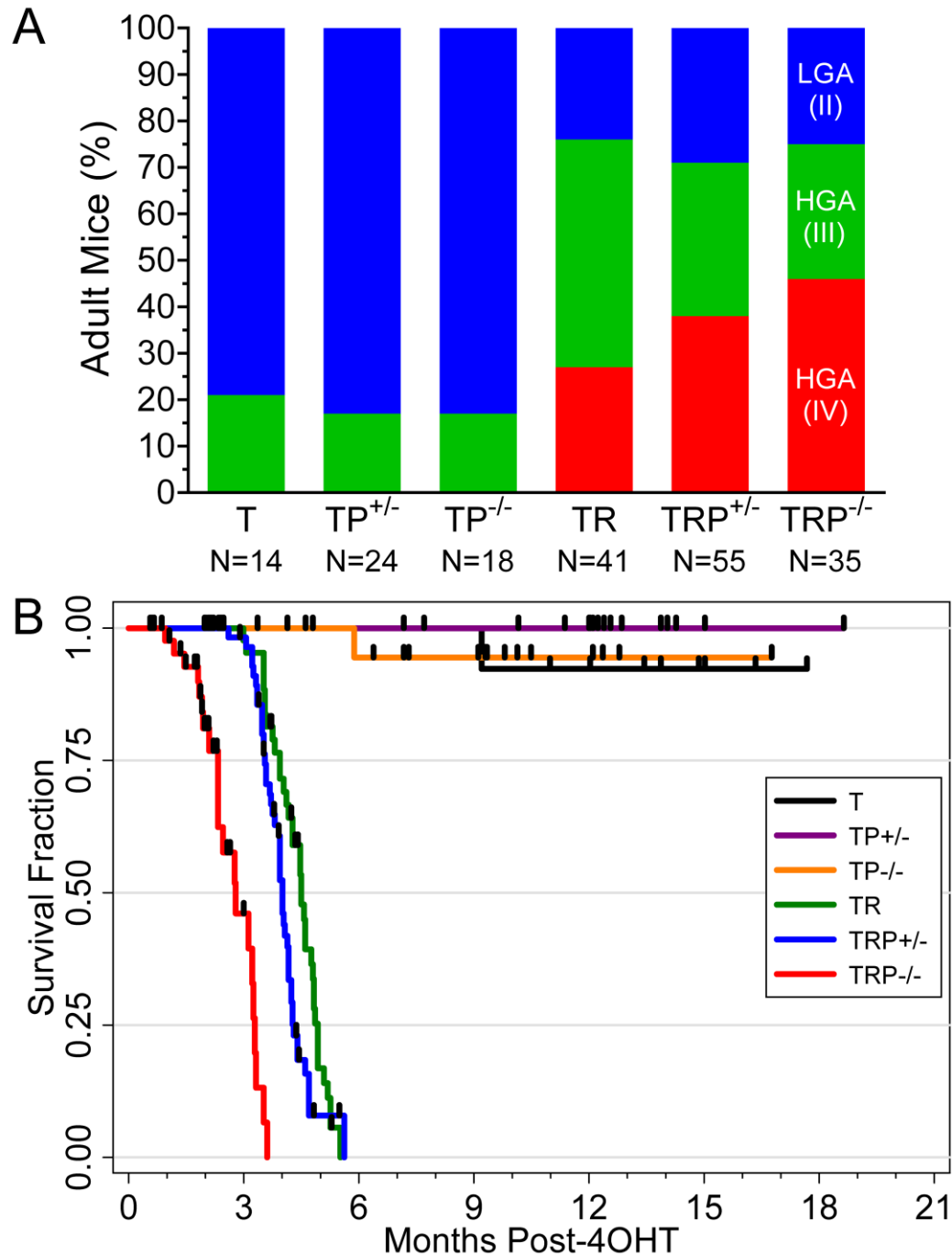


Figure 2.4. KrasG12D facilitates malignant progression to HGA. Histopathological examination of brains from aged mice (A) showed that only 17-21% of T, TP^{+/-}, and TP^{-/-} mice harbored HGA (all A3). In contrast, 71-76% of TR, TRP^{+/-}, and TRP^{-/-} mice harbored HGA [Chi-squared $P \leq 0.001$, TR(P) vs. T(P)]. GBM developed in 35, 54, and 62% of TR, TRP^{+/-}, and TRP^{-/-} mice (Chi-squared $P = 0.065$, TRP^{-/-} vs. TR). Whereas TR, TRP^{+/-}, and TRP^{-/-} mice developed HGA-related neurological morbidity and showed significantly decreased median survivals of 4.5, 4.0, and 2.8 m, respectively (Log-rank $P < 0.009$ for all pairwise comparisons), all T, TP^{+/-}, and TP^{-/-} mice were neurologically asymptomatic when sacrificed 7-19 m after induction.

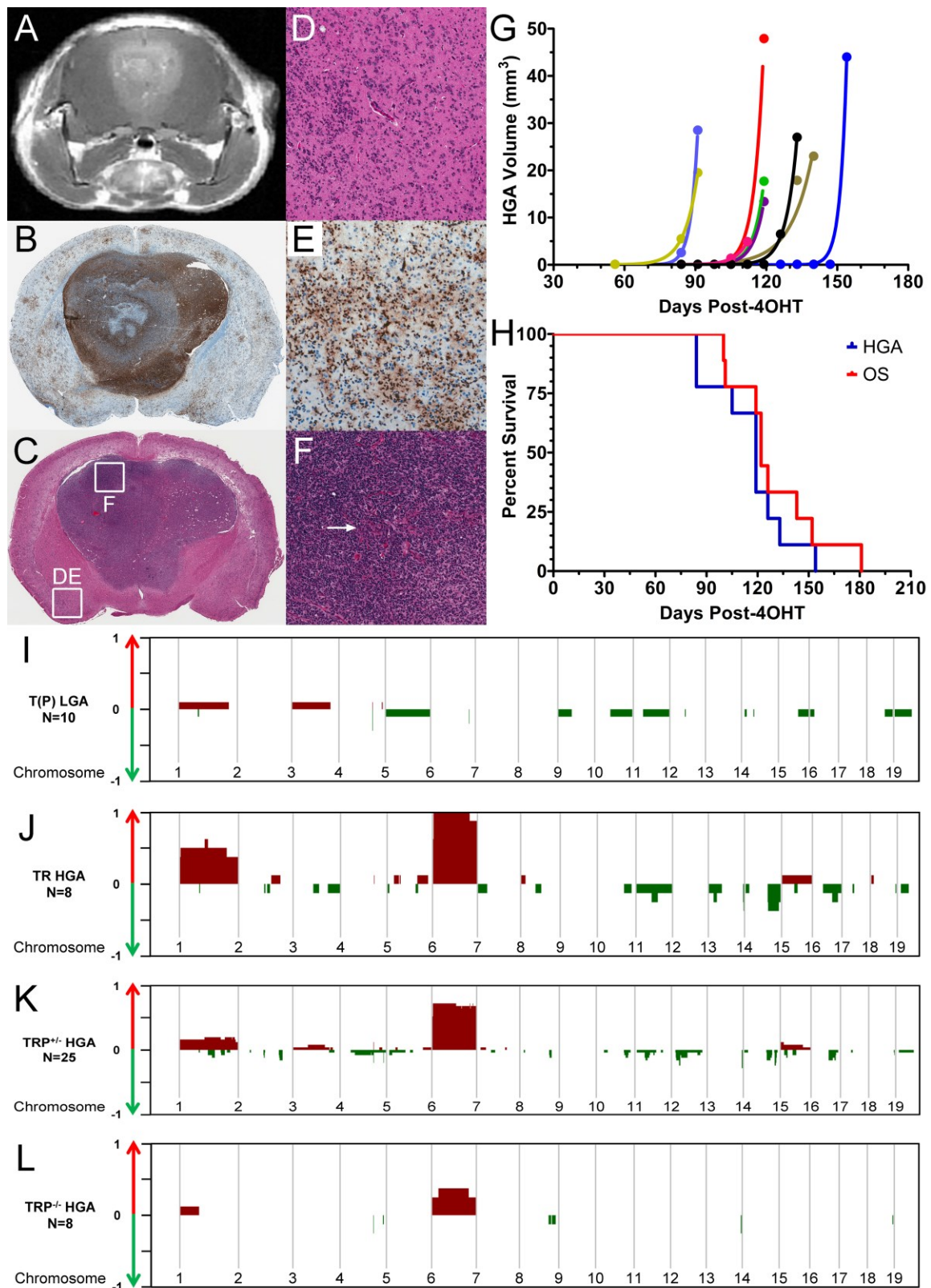


Figure 2.5. LGA stochastically progress to rapidly proliferative, lethal HGA after acquisition of CNA. Gadolinium contrast enhancing (A), T_{121} -positive (B) HGA (C) develop focally in the context of widespread LGA (C, D, E). A representative GBM with microvascular proliferation (F) from a $TRP^{+/-}$

mouse is shown (A-F). Quantification of T2-weighted serial magnetic resonance images showed logarithmic increases in HGA volume in 9 TRP^{+/-} mice with mean doubling of 3±1 d (G). Median time to first HGA mass appearance, median survival, and mean time to death after appearance of HGA was 119±7 (range 84-154), 122±2, and 14±3 d, respectively (H). Frequency plots of aCGH data show that terminal LGA (> 1 year survival) rarely acquire CNA (I). All TR HGA (J) showed gains of chromosome 6, but only 64-72% TRP^{+/-} HGA (K) show similar gains (Fisher $P=0.15$). Half of TR, but only 16-20% of TRP^{+/-} HGA showed chromosome 1 gains (Fisher $P=0.17$). TRP^{-/-} HGA (L) acquire the least CNA and have the lowest frequency (13-25%) of chromosome 6 gains (Fisher $P\leq 0.04$).

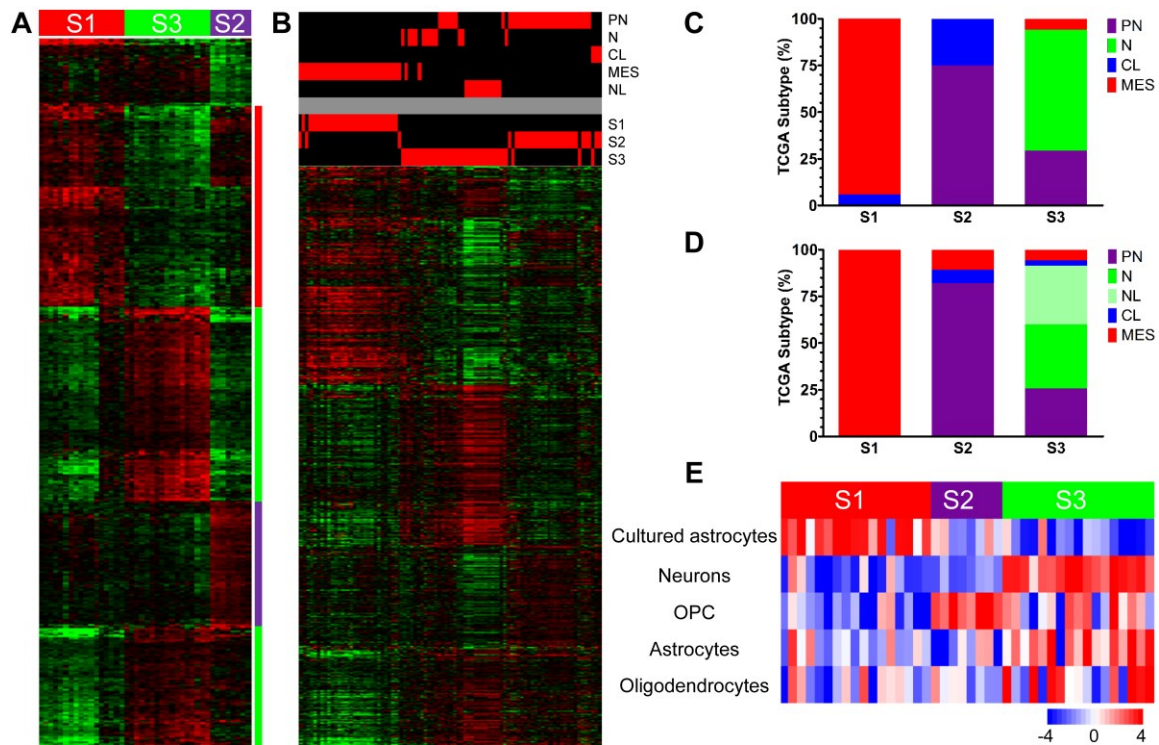


Figure 2.6. GEM HGA transcriptomes are heterogeneous, mimic human GBM subtypes, and are reminiscent of distinct neural cell types. Hierarchical clustering of TR(P) HGA discovery set using a 600-gene classifier (200 per subtype) shows transcriptomal heterogeneity (A). Hierarchical clustering of an independent test set composed of 3 adult GEM HGA models with different initiating mutations shows the 600-gene classifier accurately clusters samples according to their predicted TR(P) HGA S1-S3 subtypes (B). HGA subtypes S1-S3 correlate with distinct TCGA human GBM subtypes (C, Fisher $P=2.2 \times 10^{-12}$). Similar S1-S3 subtype associations with human GBM subtypes were evident in the GEM HGA test set (D). ssGSEA of discovery set samples shows enrichment of distinct neural cell lineage signatures (E). S1, S2, and S3 HGA are enriched in cultured astrocytes, oligodendrocyte precursor cells (OPC), and neurons, respectively.

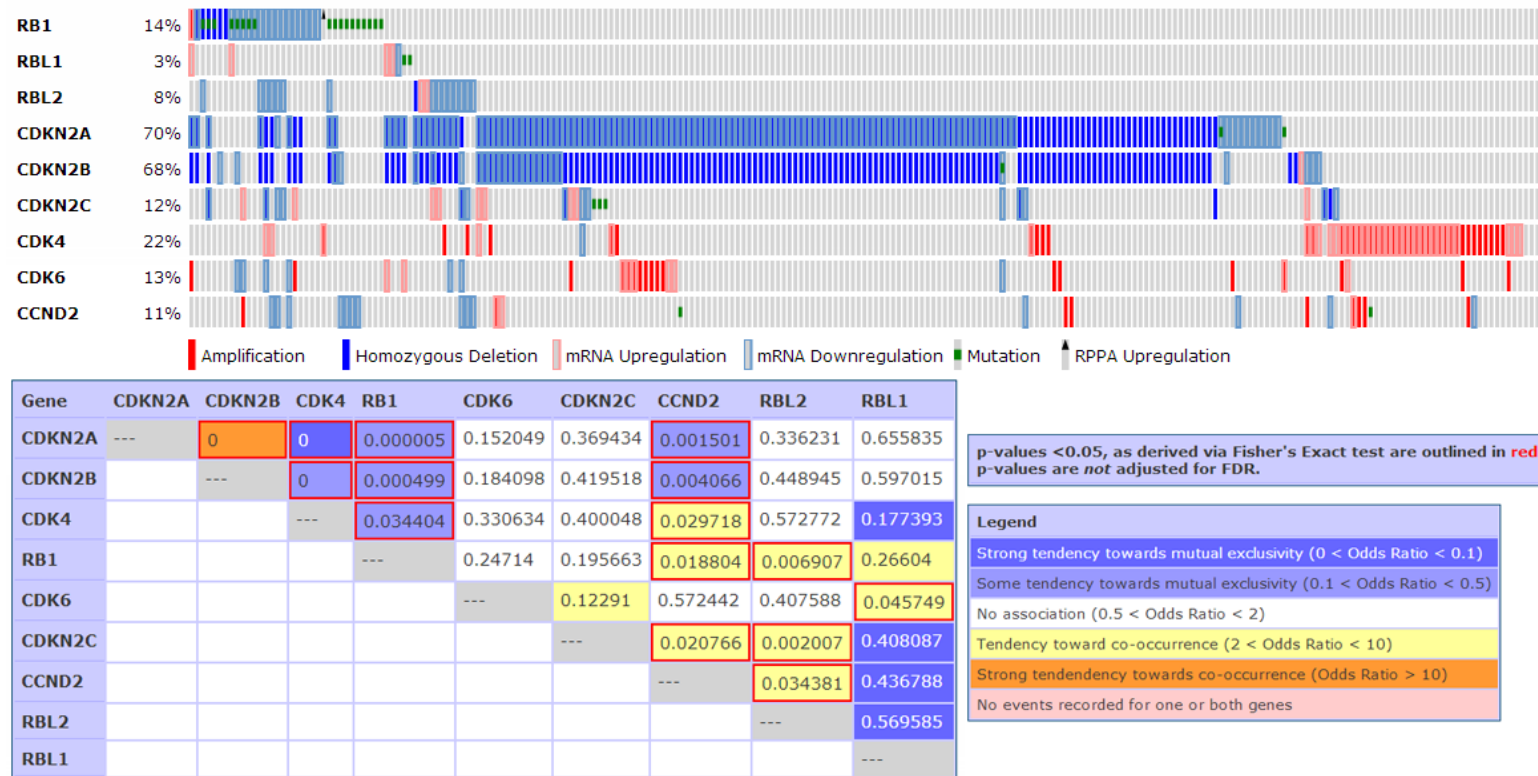


Figure S2.1. RB pathway genes are altered in nearly all human GBM. TCGA GBM with mRNA and protein expression, aCGH, and sequencing data (N=236) were analyzed using the cBio Portal for Cancer Genomics (167). Ninety-eight percent (N=232) harbored one or more significant RB pathway gene alteration(s). *RB1* alterations trend towards co-occurrence with alterations in its pocket protein family members, *RBL1* or *RBL2* ($P=0.27$ and $P=0.007$, respectively).

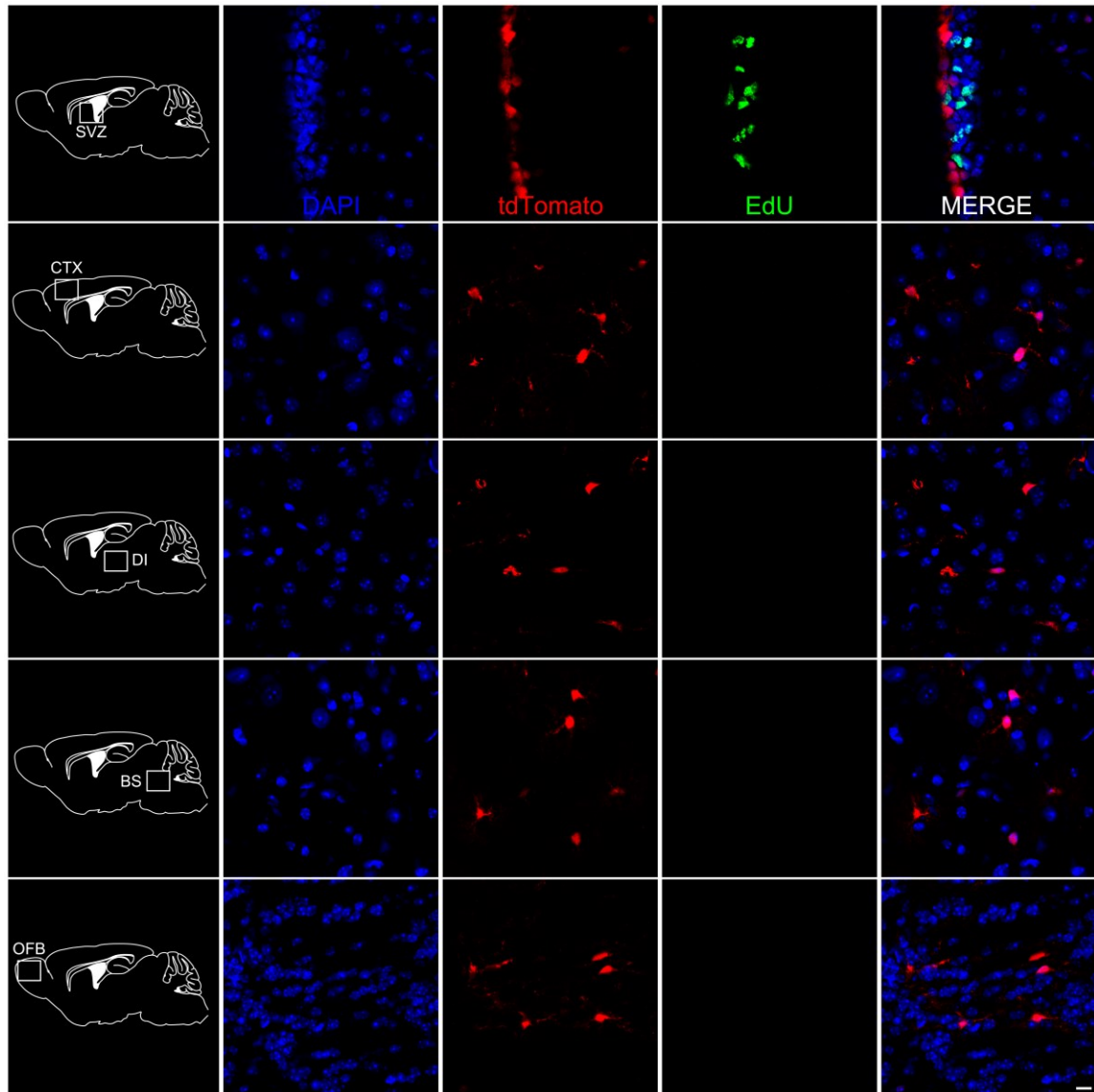


Figure S2.2. GFAP-CreER mediates recombination throughout the brain. Genetic lineage tracing in a *GFAP-CreER;Rosa26-tdTomato* mouse at 7 d after induction (Fig. 1) shows recombination (tdTomato expression) in the subventricular zone (SVZ), cortex (CTX), diencephalon (DI), brainstem (BS), and olfactory bulb (OFB). Only cells in the SVZ incorporate EdU. Scale bar 10 μ m.

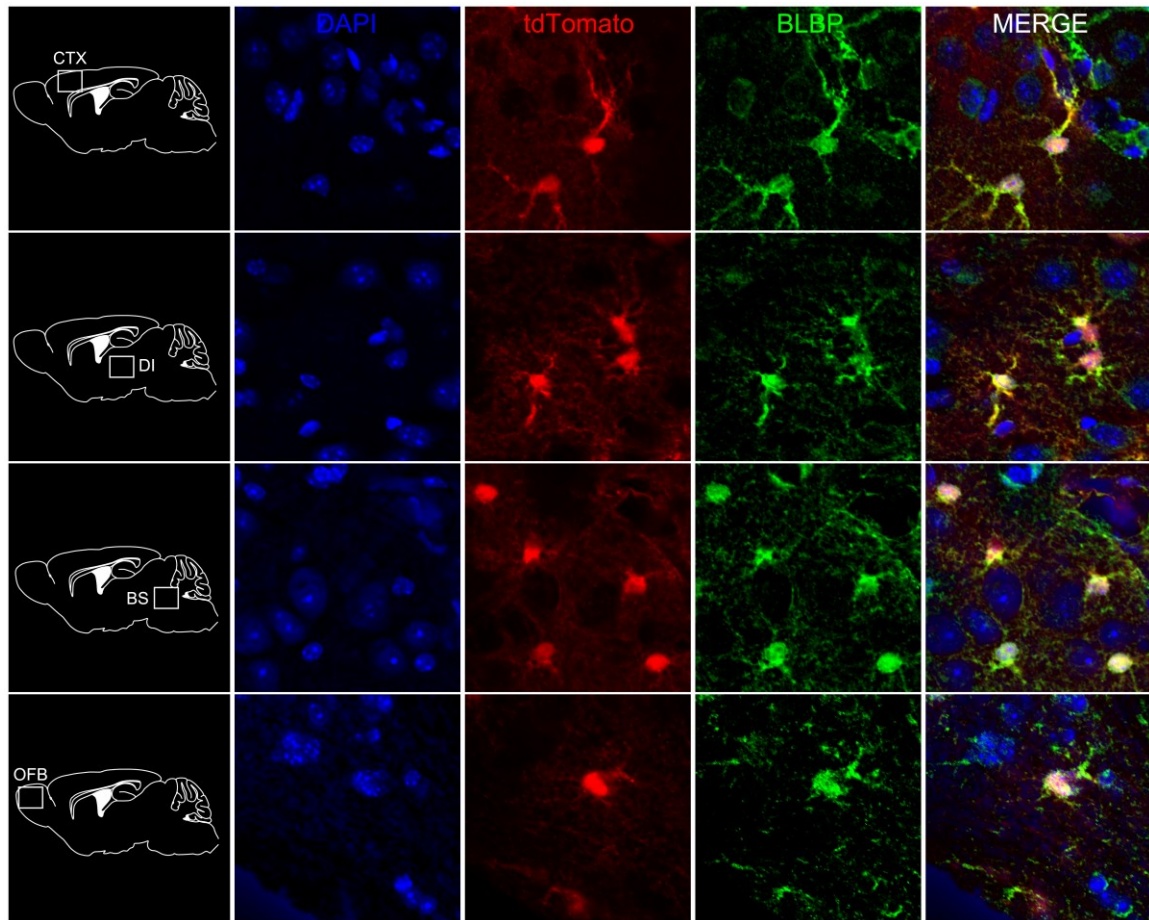


Figure S2.3. GFAP-CreER targets astrocytes. Genetic lineage tracing in a *GFAP-CreER;Rosa26-tdTomato* mouse at 7 d after induction shows recombination (tdTomato expression) in cortical (CTX), diencephalic (DI), brainstem (BS), and olfactory bulb (OFB) astrocytes as defined by their stellate cellular morphology and co-expression of brain lipid binding protein (BLBP).

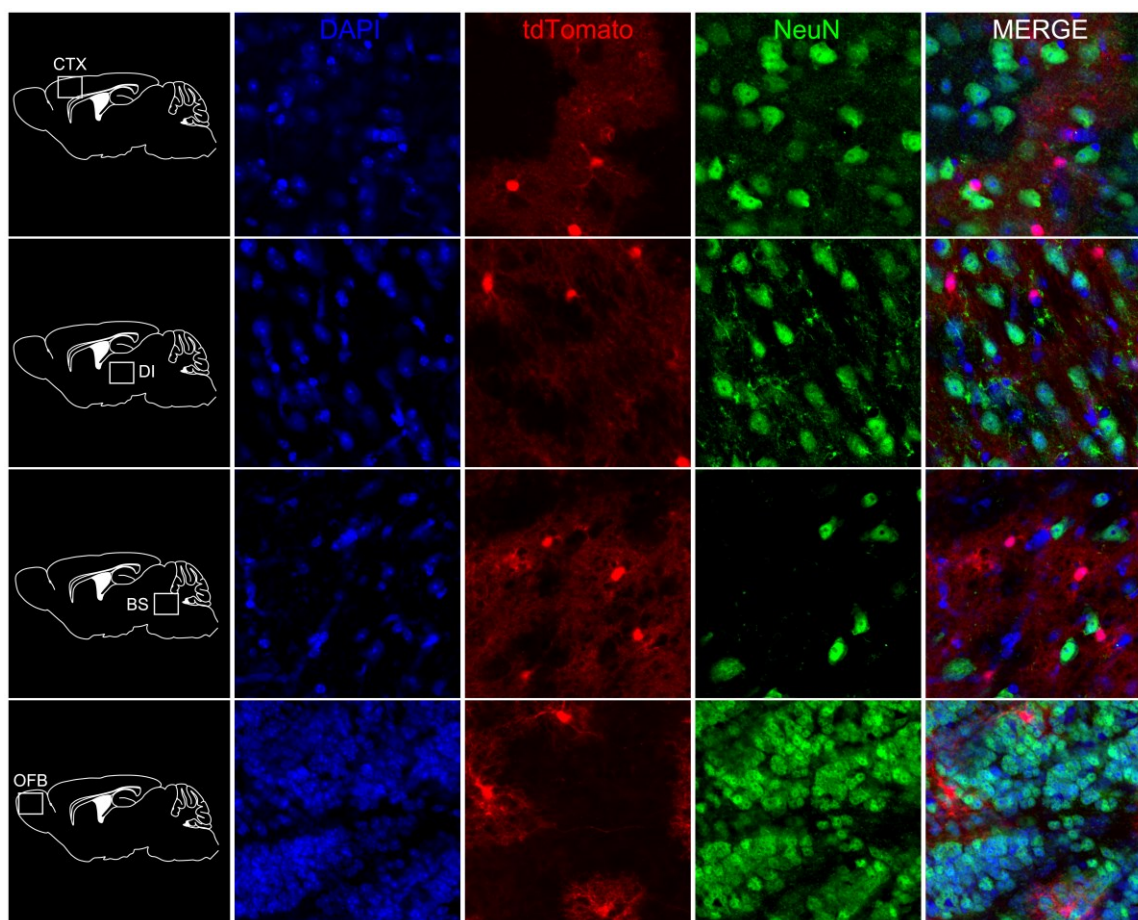


Figure S2.4. GFAP-CreER does not target neurons. Genetic lineage tracing in a *GFAP-CreER;Rosa26-tdTomato* mouse at 7 d after induction shows minimal recombination (tdTomato expression; $0.2 \pm 0.1\%$) in cortical (CTX), diencephalic (DI), brainstem (BS), and olfactory bulb (OFB) neurons as defined by their cellular morphology and co-expression of NeuN.

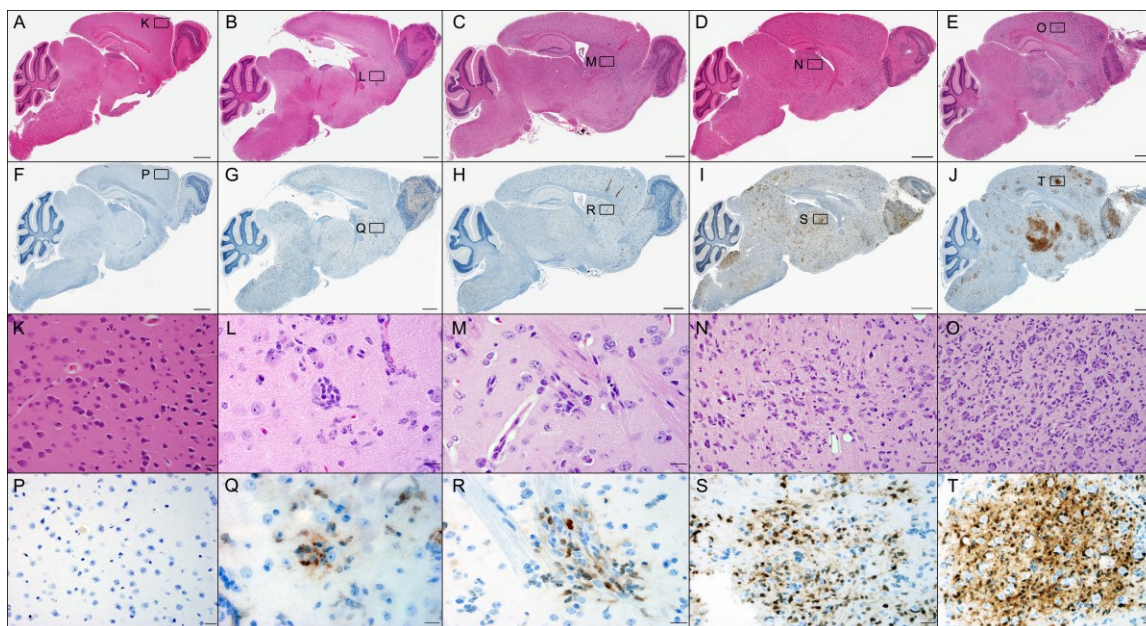


Figure S2.5. Initiating oncogenic mutations (genotype) influence LGA tumor burden.

Representative H&E (A-E, K-O) and T_{121} immunohistochemistry (F-J, P-T) images in wild-type (A, F, K, P), T (B, G, L, Q), $TP^{-/-}$ (C, H, M, R), TR (D, I, N, S), and $TRP^{-/-}$ (E, J, O, T) mice at 2 m after induction. T and $TP^{-/-}$ mice have similar LGA burden. TR mice have increased LGA burden. $TRP^{-/-}$ mice have the greatest LGA burden and show small hypercellular LGA foci (Fig. 2B). Scale bars 1 mm (A-J) and 20 μ m (K-T).

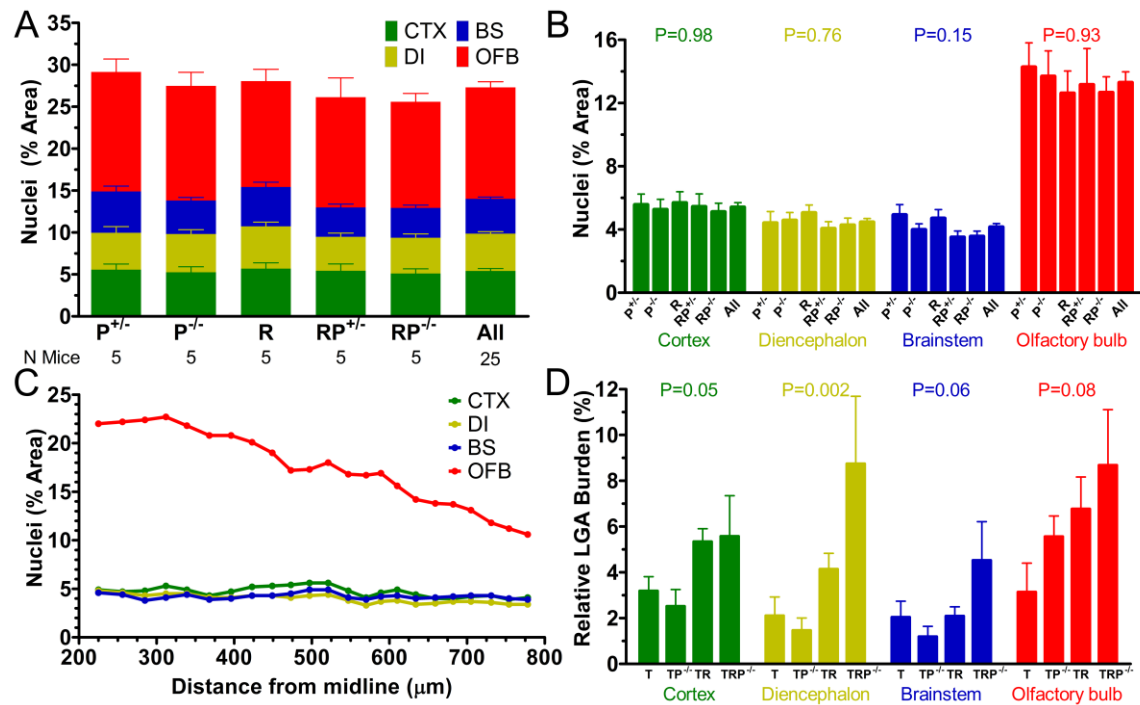


Figure S2.6. Morphometric analysis of nuclear density in phenotypically wild-type and LGA-containing mice. Adult P^{+/+}, P^{-/-}, R, RP^{+/+}, and RP^{-/-} mice sacrificed at 2 m after induction showed no evidence of astrocytoma tumorigenesis and were phenotypically wild-type (A, Table S2.1). No differences in cortical (CTX), diencephalic (DI), brainstem (BS), and olfactory bulb (OFB) nuclear densities were evident across these genotypes (one-way ANOVA $P \geq 0.34$), but nuclear density in the OFB was significantly greater than the other 3 brain regions (B, two-way ANOVA $P < 0.0001$). The effect of distance from sagittal midline on nuclear density was examined in 3 wild-type C57Bl/6 mice (C). Data from Fig. 2B are re-graphed in D to highlight the effects of genotype on LGA burden in all four brain regions (one-way ANOVA $P \leq 0.08$).

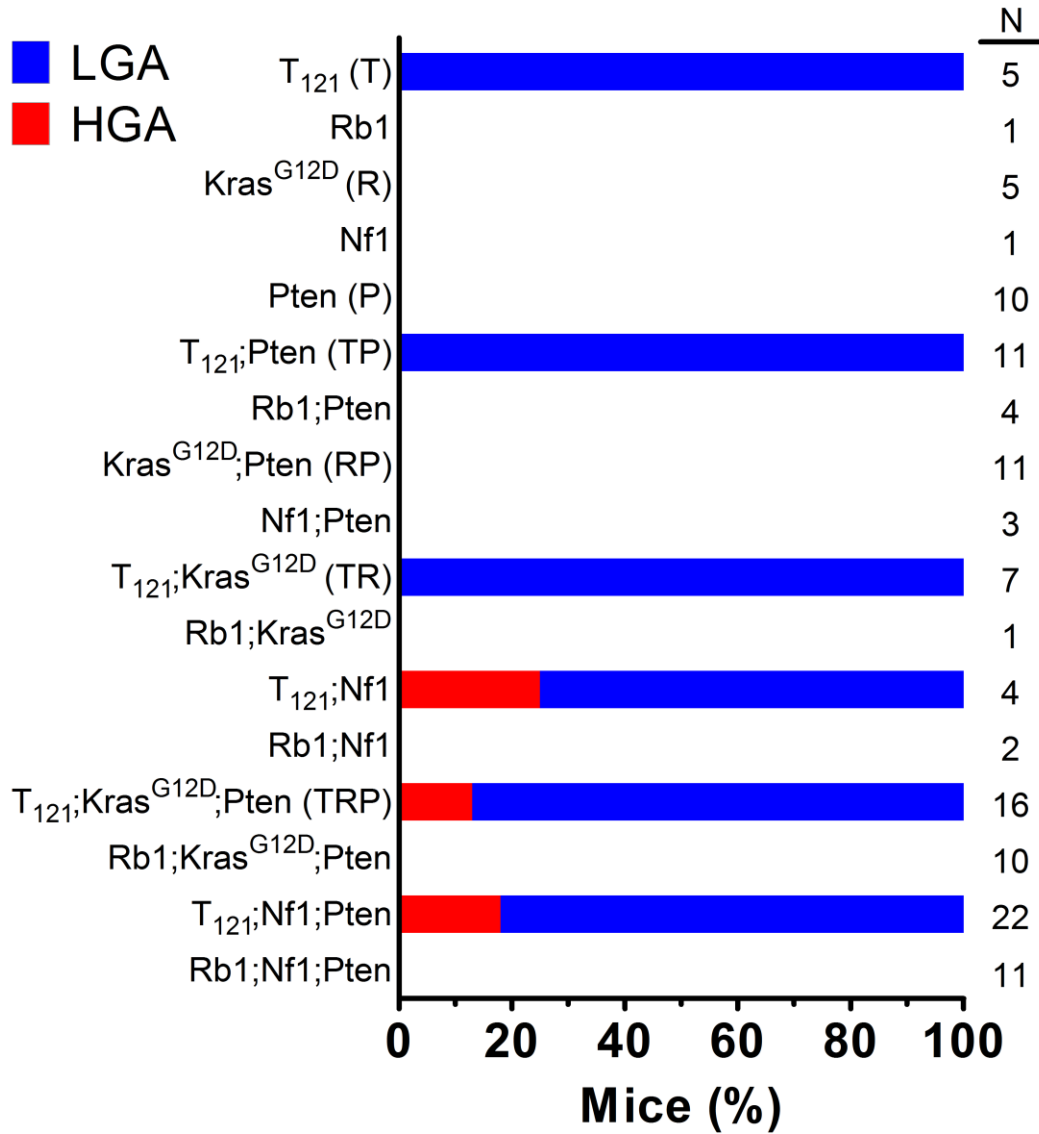


Figure S2.7. Ablation of all Rb family members is required for tumorigenesis in adult murine astrocytes. Histological examination of GFAP-CreER mouse brains with combinations of T₁₂₁ or Rb1 deletion, Kras^{G12D} or Nf1 deletion, and Pten deletion (Table S2.2) showed low- or high-grade astrocytomas only in T mice with combinations of Kras^{G12D}, Nf1 or Pten deletions.

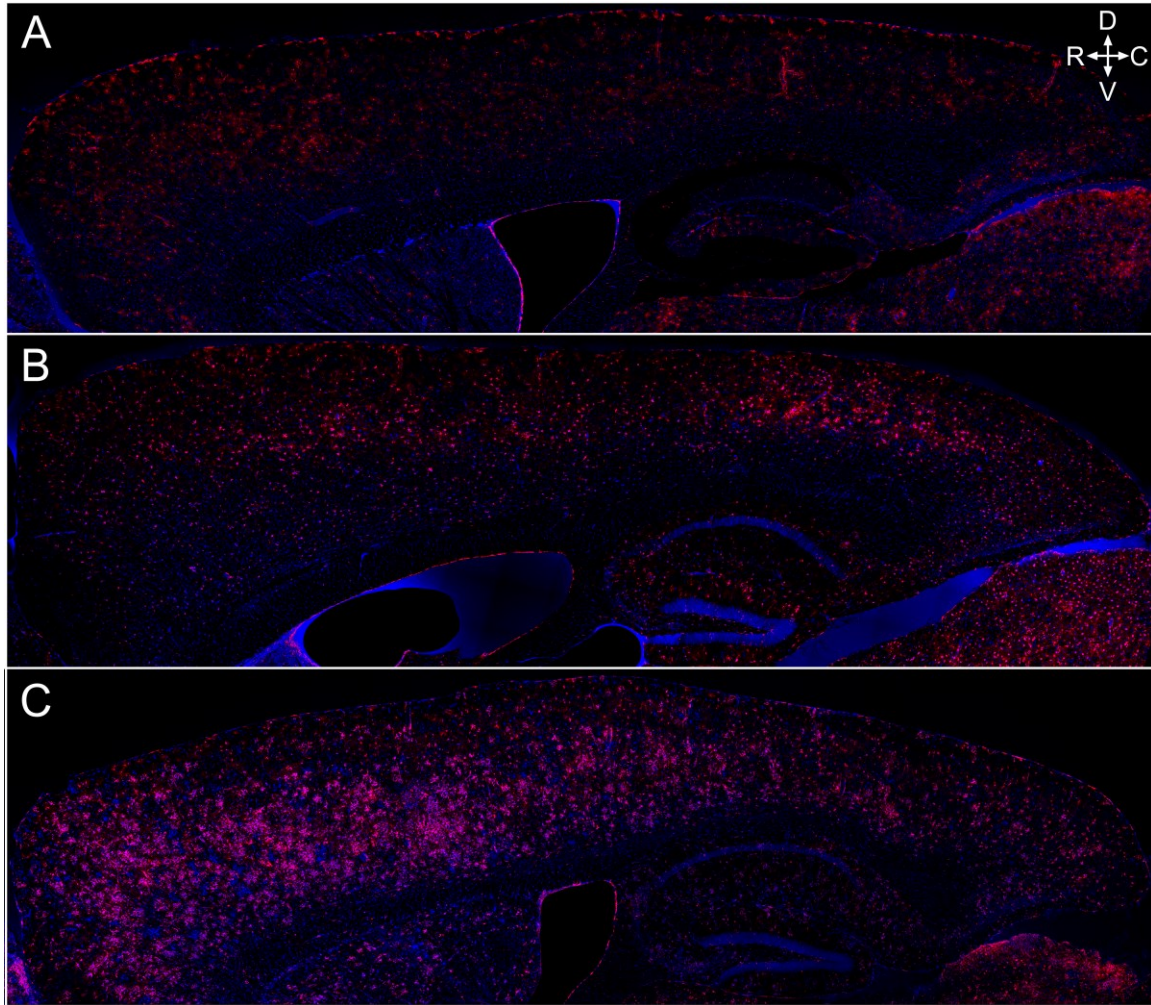


Figure S2.8. Cortical TRP^{+/-} LGA burden increases over time. Genetic lineage tracing in *GFAP-CreER;Rosa26-tdTomato* (A) and *GFAP-CreER;Rosa26-tdTomato;TRP^{+/-}* (B, C) mice at 7 (A), 21 (B), and 60 (C) d after induction showed a time-dependent increase in TRP^{+/-} LGA burden throughout the cortex. Orientation: C, caudal; D, dorsal; R, rostral; V, ventral.

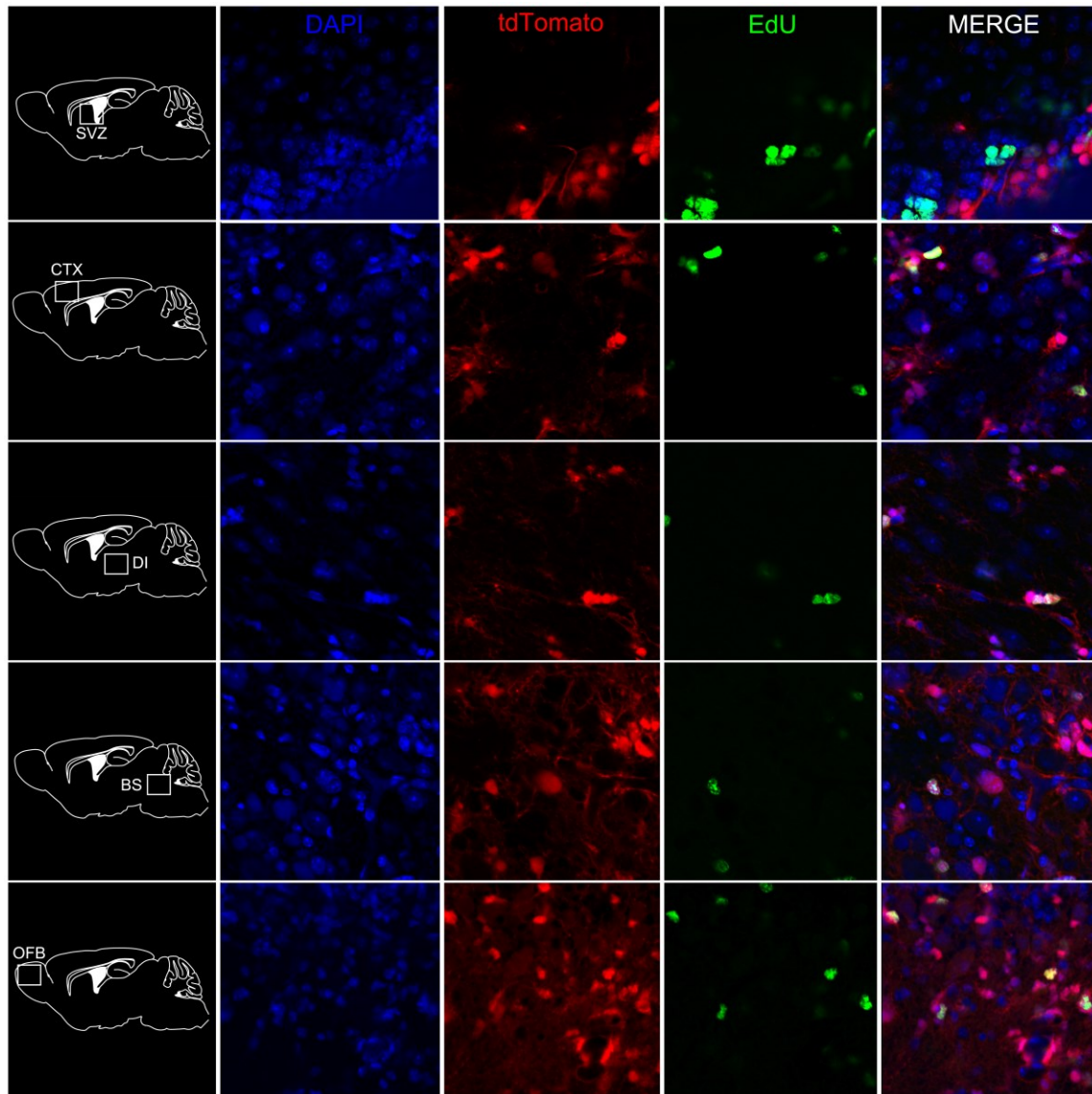


Figure S2.9. TRP^{+/-} mice develop LGA in all brain regions. Increased tdTomato- and proliferating, EdU-positive cells were evident in the subventricular zone (SVZ), cortex (CTX), diencephalon (DI), brainstem (BS), and olfactory bulb (OFB) in a representative *GFAP-CreER; Rosa26-tdTomato; TRP^{+/-}* mouse sacrificed 21 d after induction (compare to Fig. S2).

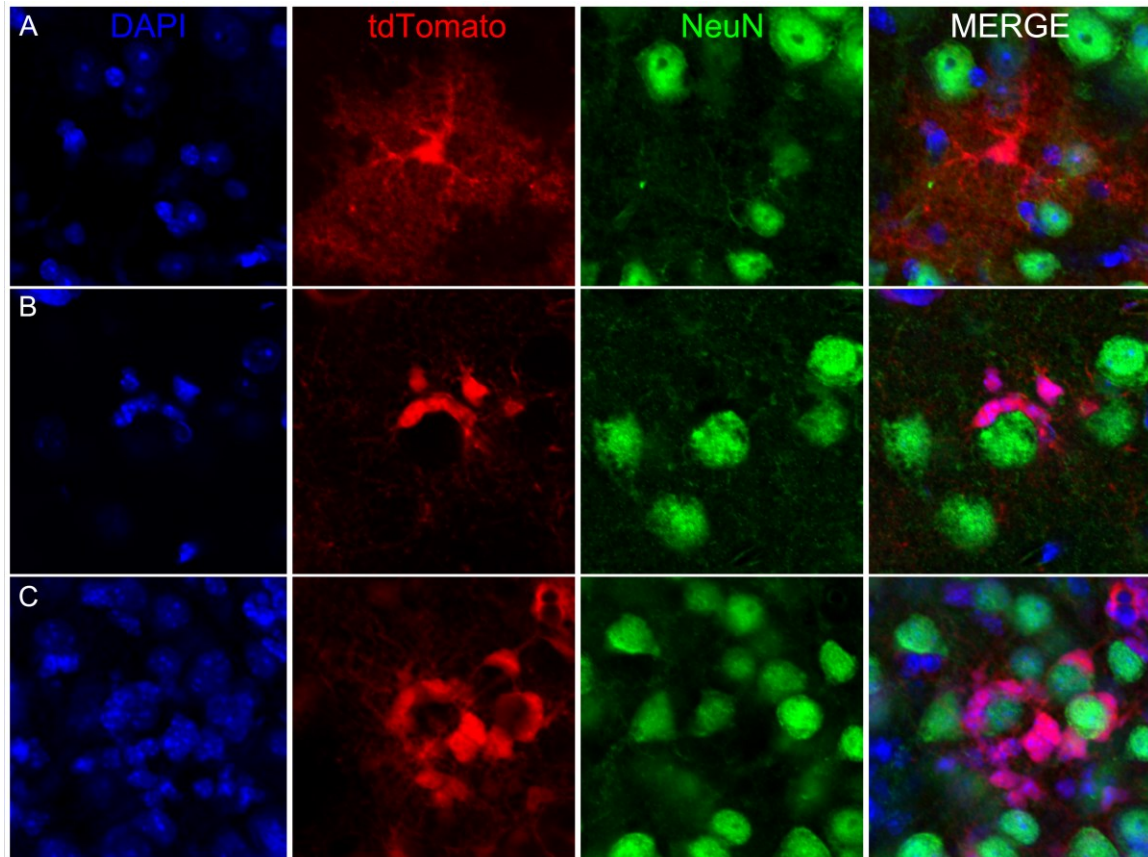


Figure S2.10. Perineuronal satellitosis increases over time in TRP^{+/-} LGA. Genetic lineage tracing in *GFAP-CreER;Rosa26-tdTomato* (A) and *GFAP-CreER;Rosa26-tdTomato;TRP^{+/-}* (B, C) mice at 7 (A), 21 (B), and 60 (C) d after induction showed a time-dependent increase in tdTomato⁺ cells surrounding NeuN⁺ cortical neurons.

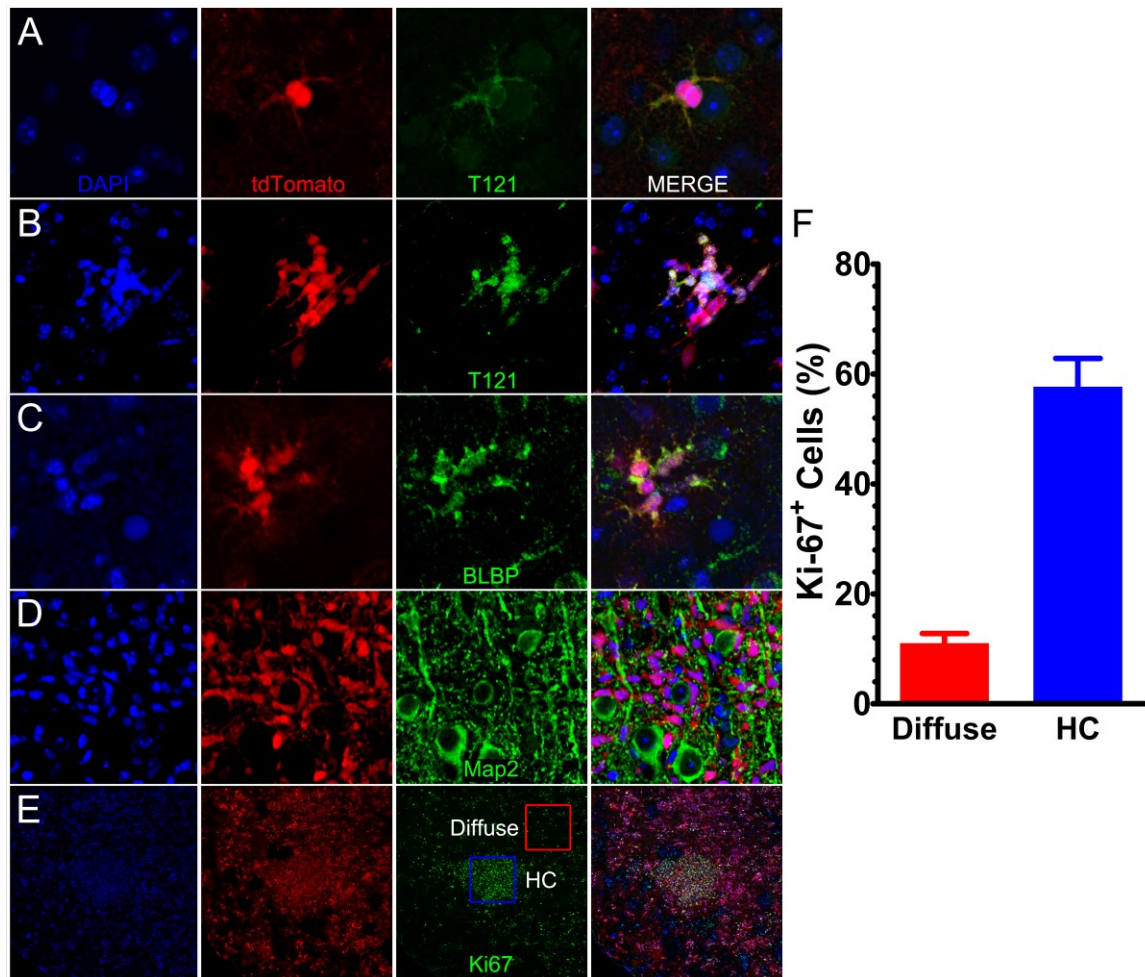


Figure S2.11. Local proliferation of transformed cortical astrocytes produces hypercellular TRP+/- astrocytoma foci. Genetic lineage tracing in *GFAP-CreER;Rosa26-tdTomato;TRP^{+/-}* mice at 21 (A-C) and 60 (D, E) d after induction shows a transformed tdTomato/ cortical astrocyte in telophase (A), development of small foci of T₁₂₁- (B) and BLBP-positive (C) cortical astrocytoma cells, dense satellitosis around Map2-positive cortical neurons (D), and larger hypercellular foci (E, blue box HC) of astrocytoma with 5-fold increased Ki67-positive cells (F) compared to surrounding diffuse cortical astrocytoma (E, red box).

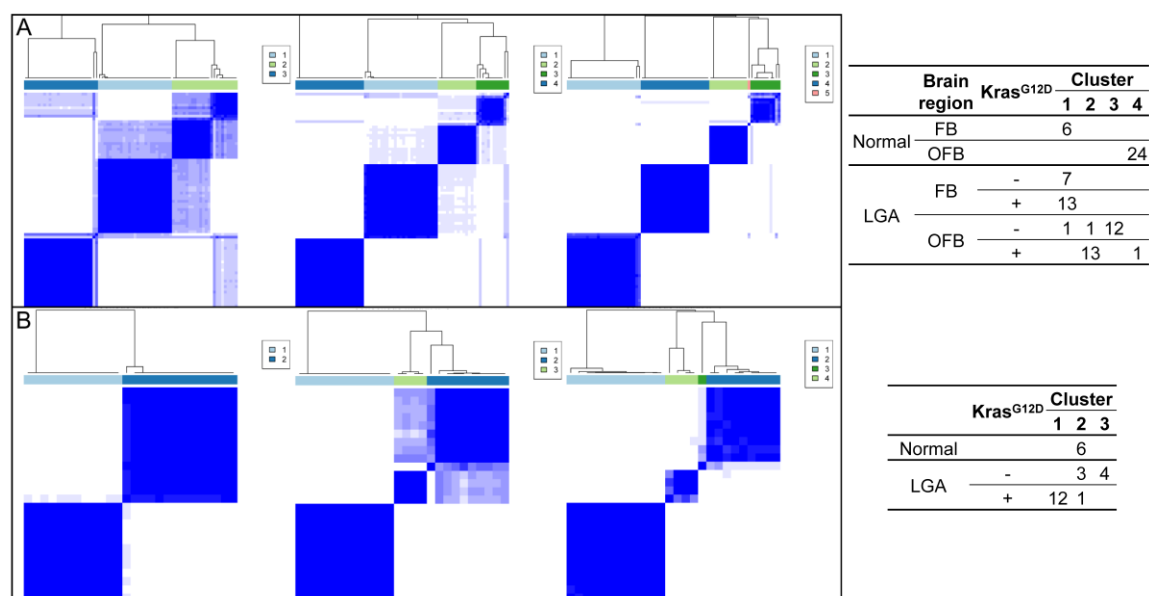


Figure S2.12. LGA transcriptomes cluster according to initiating genotype and brain region.

Consensus hierarchical clustering of olfactory bulb (OFB) and forebrain (FB) LGA transcriptomes (Fig. 3A, Table S2.1) with the 5000 most variable genes identified four clusters (A) composed largely of normal or LGA FB (cluster 1), OFB LGA with Kras^{G12D} (cluster 2), OFB LGA without Kras^{G12D} (cluster 3), and normal OFB (cluster 4). Consensus hierarchical clustering of only FB LGA transcriptomes (Fig. 3A, Table S2.1) showed 3 clusters (B) consisting of LGA with Kras^{G12D} (cluster 1), normal FB (cluster 2), and LGA without Kras^{G12D} (cluster 3), confirming that the influence of Kras^{G12D} on LGA transcriptomes is independent of brain region.

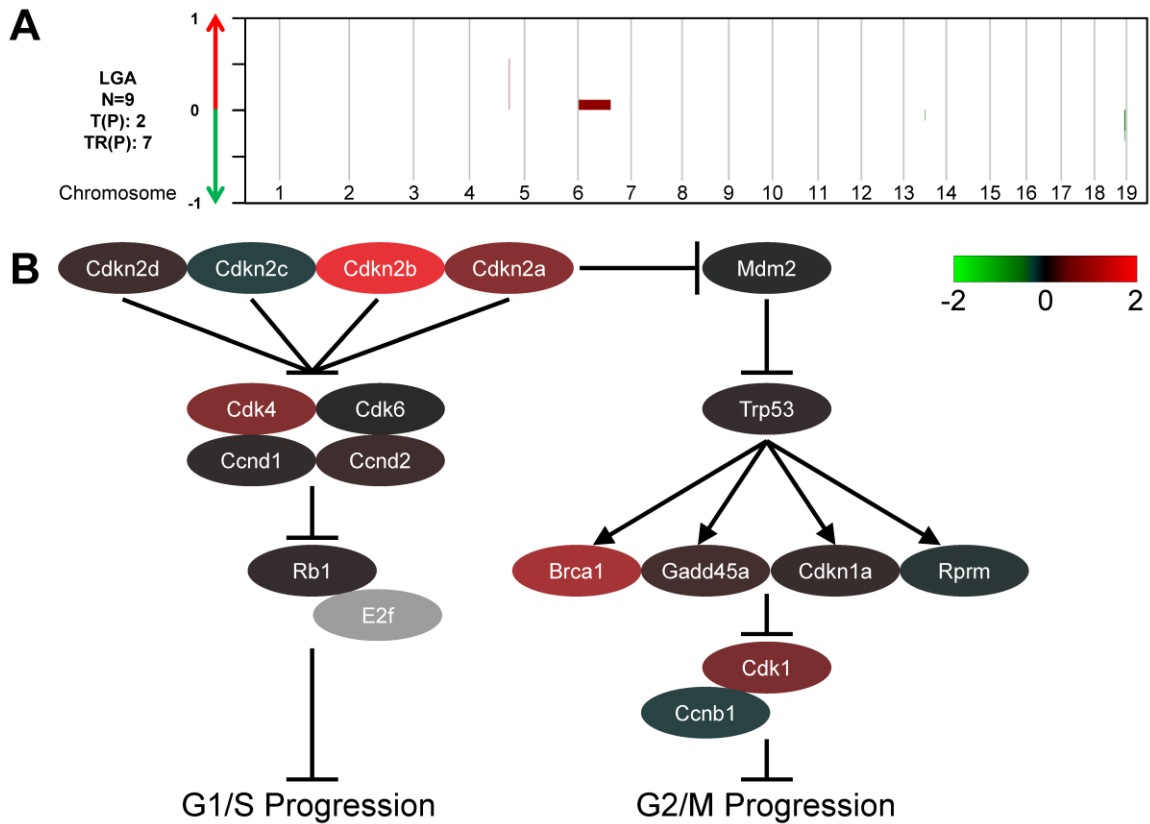


Figure S2.13. LGA have silent genomic landscapes, but transcriptional dysregulation of cell cycle genes. Frequency plot of aCGH data shows minimal acquisition of CNA in T(P) and TR(P) LGA at 2 m after induction (A). mRNA expression (Log2 median-centered) of G1/S and G2/M cell cycle checkpoint genes is dysregulated in OFB LGA compared to histologically normal OFB.

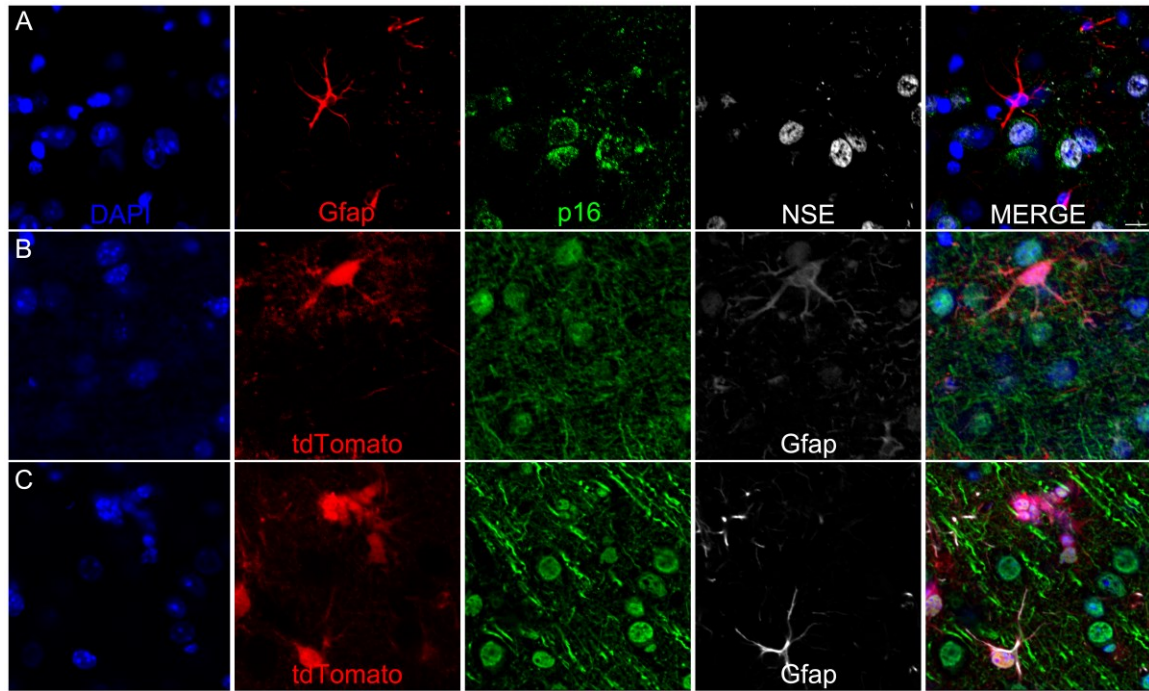


Figure S2.14. Transformed TRP^{+/-} astrocytes re-express p16. p16 is expressed in neuron-specific enolase (NSE)-positive cortical neurons, but not Gfap- or tdTomato-positive cortical astrocytes in 3 m adult wild-type, C57Bl/6 (A) and *GFAP-CreER;Rosa26-tdTomato* (B) mice, respectively. In contrast, p16 is expressed in transformed Gfap/tdTomato-positive cortical astrocytes from an age-matched *GFAP-CreER;Rosa26-tdTomato;TRP^{+/-}* mouse (C). Scale bar 10 μm.

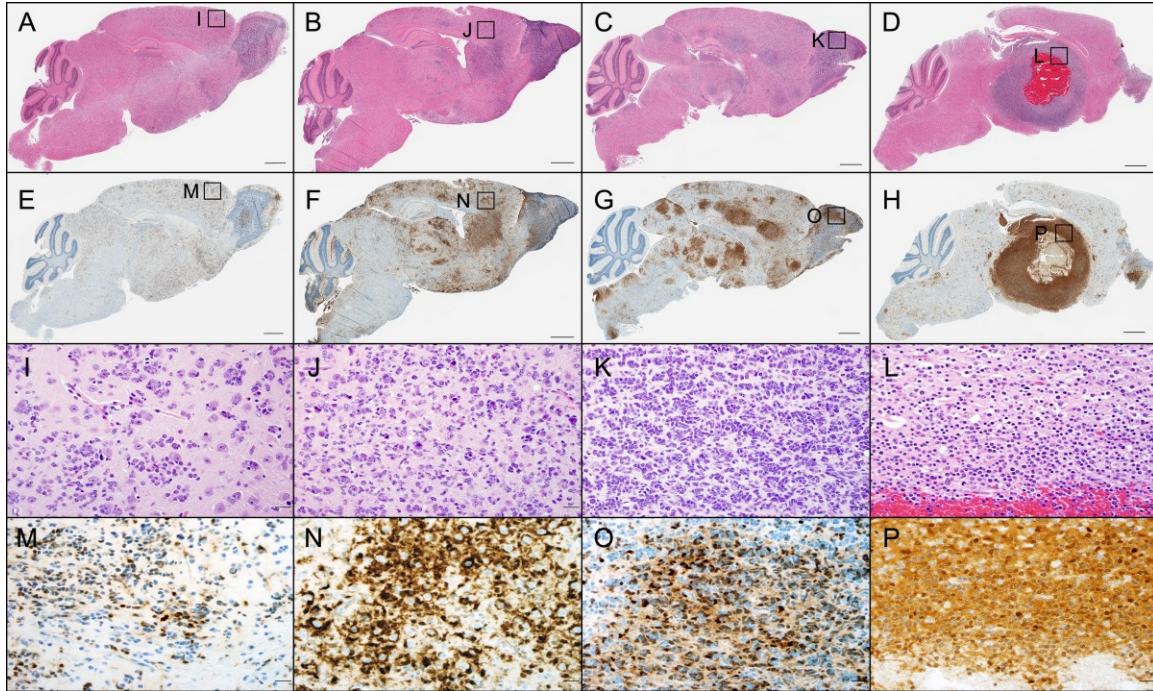


Figure S2.15. KrasG12D potentiates malignant progression. H&E (A-D, I-L) and T₁₂₁ immunohistochemistry (E-H, M-P) shows LGA throughout the brain in a neurologically asymptomatic T mouse sacrificed 13 m after induction (A, E, I, M). In contrast, multiple HGA (A3) foci are evident throughout the brain in symptomatic TR (B, F, J, N) and TRP^{-/-} (C, G, K, O) mice. A second symptomatic TRP^{-/-} mouse (D, H, L, P) developed a diencephalic GBM with central hemorrhage and necrosis. Scale bars 1 mm (A-H) and 20 μ m (I-P).

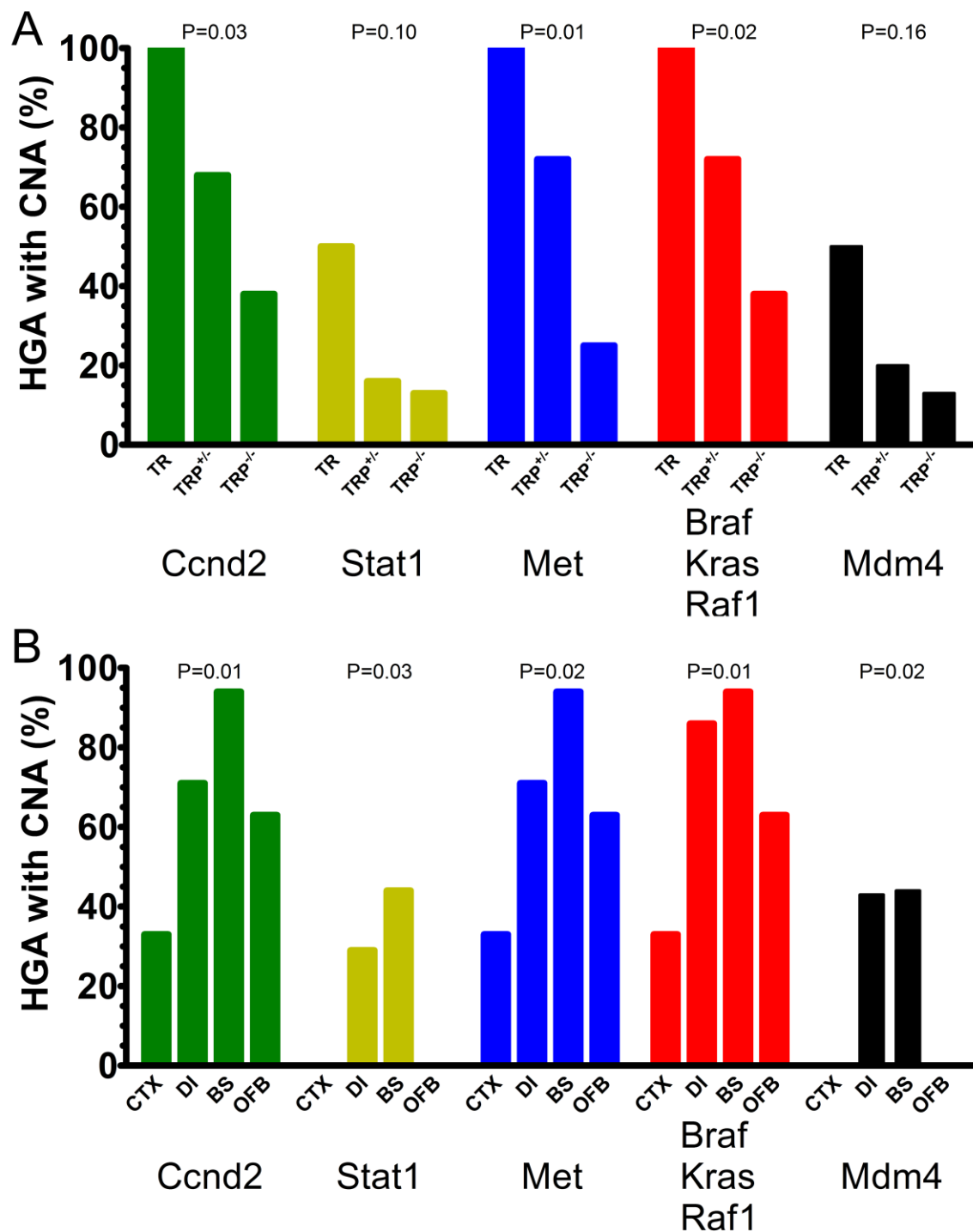


Figure S2.16. Initiating genotype and astrocyte location influence CNA acquired upon malignant progression in TR(P) HGA. Initiating genotype (A) and astrocyte location (B) significantly influence the development of CNA in recurrently altered (>20% of samples, Table S2.4) Rb, RTK/MAPK/PI3K, and p53 pathway genes (Fisher's $P \leq 0.16$).

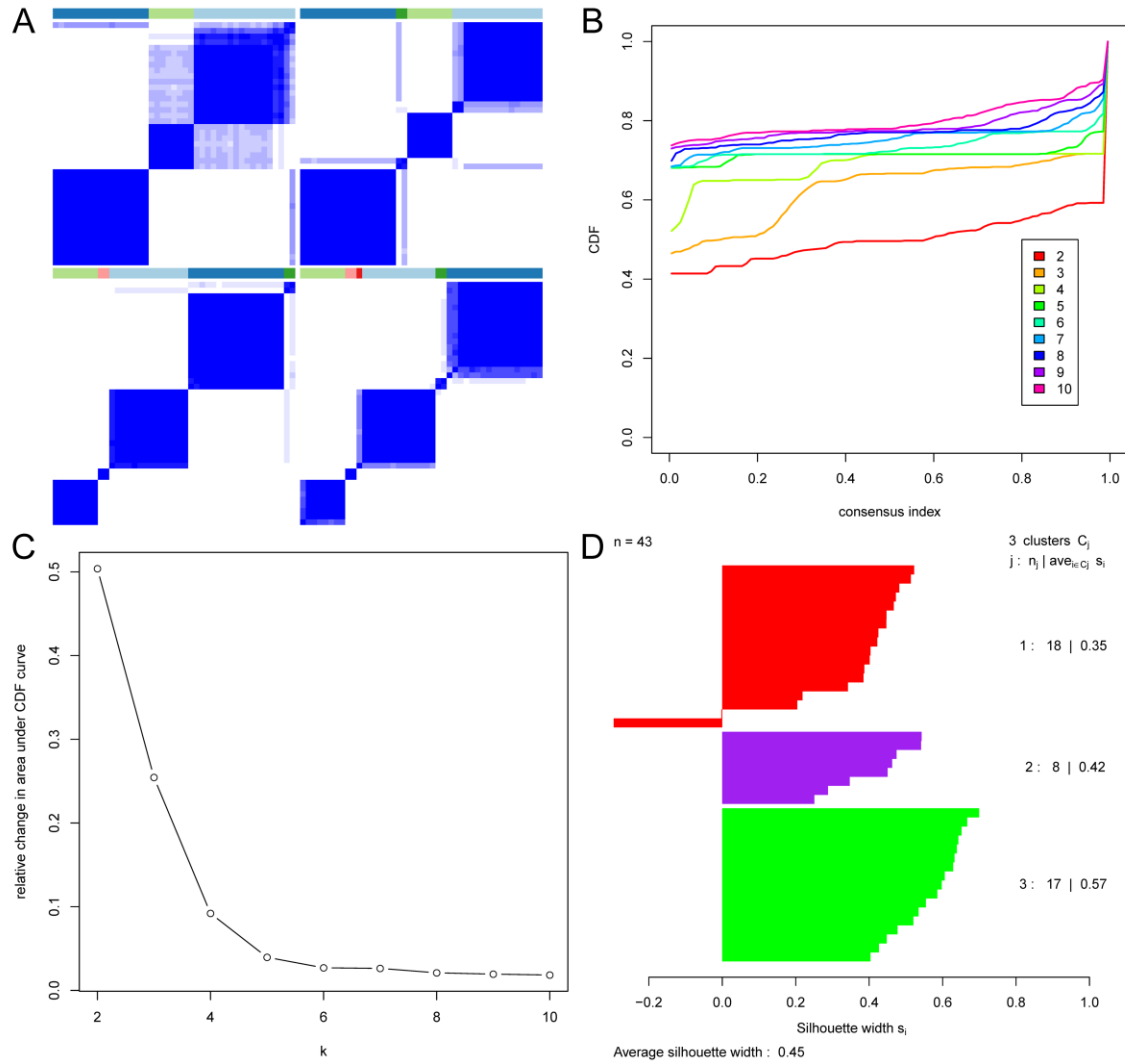


Figure S2.17. TR(P) HGA transcriptomes are heterogeneous and consist of three subtypes.

Consensus clustering using either 2000 or 5000 genes with highest median absolute deviation for $k=3-6$ (A). The bimodal distribution at 0 and 1 in the consensus index indicates well-defined subtypes (B). Consensus clustering reaches a local maximum at 6 clusters (C), but 3 contain 2 or fewer HGA (A, bottom right). Positive silhouette widths identify 42 of 43 HGA as core subtype members. One sample with negative silhouette width was excluded from subsequent analyses (Table S2.8).

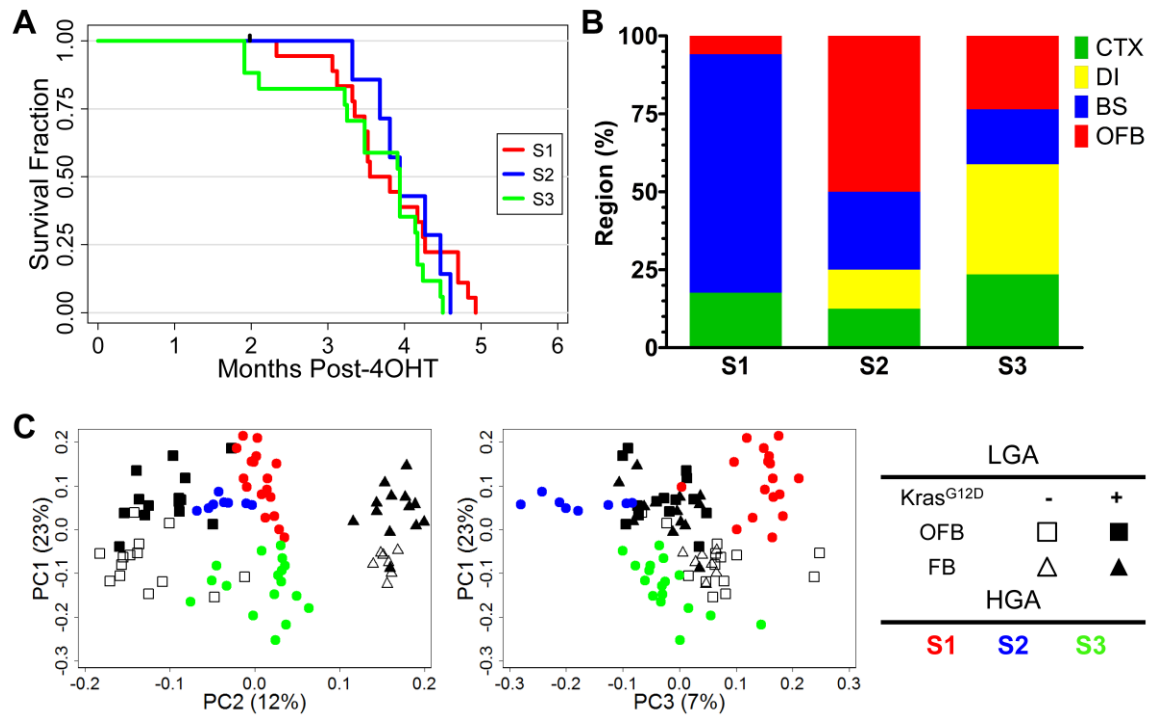


Figure S2.18. HGA transcriptomes are distinct from LGA and subtypes correlate with anatomic location. In contrast to initiating genotype (Fig. 4), HGA subtype does not influence survival (A, Log-rank $P=0.4$). S1 and S2 HGA subtypes are predominantly located in brainstem (BS) and olfactory bulb (OFB), respectively (B, Fisher $P=0.004$). S3 is composed of HGA from BS, OFB, cortex (CTX) and diencephalon (DI). PCA shows that LGA and HGA transcriptomes are distinct (C). Separation of OFB and forebrain (FB) LGA, LGA with and without Kras^{G12D} (Fig. 3A), and S1-S3 HGA subtypes (Figs. 6 and S17) are preserved when LGA and HGA transcriptome datasets are combined.

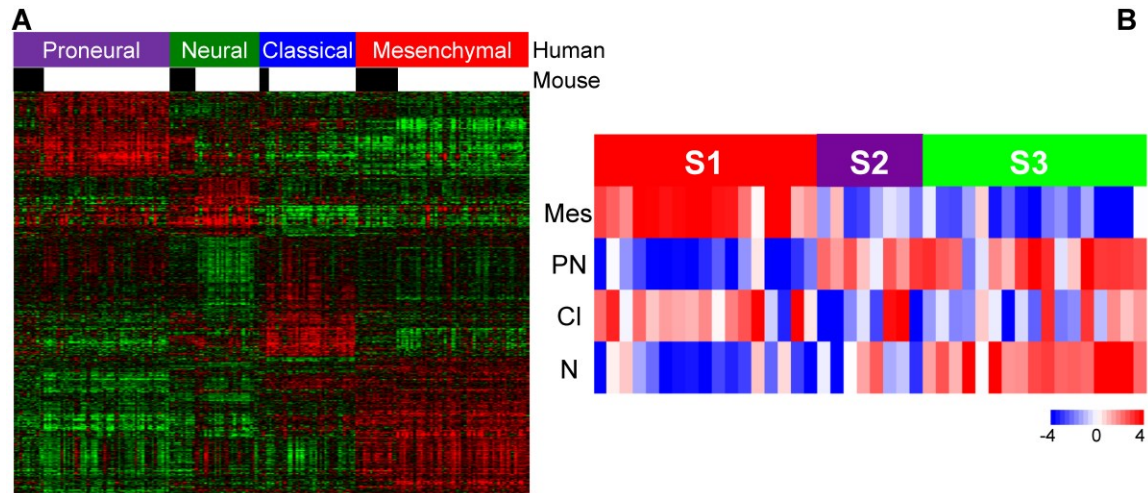


Figure S2.19. GEM HGA and human GBM have similar transcriptomes. GEM HGA (black bars) and human GBM (colored subtypes) express the TCGA GBM 840-gene classifier similarly (A). Murine HGA are grouped according to their predicted TCGA subtype. ssGSEA shows enrichment of mesenchymal, proneural, and neural/ proneural TCGA subtype signatures in S1, S2, and S3 TR(P) HGA, respectively (B).

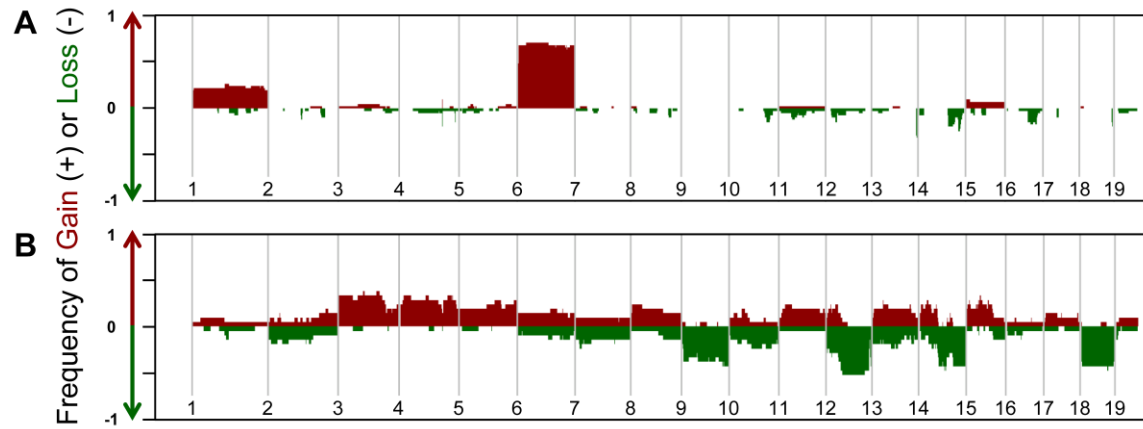


Figure S2.20. Copy number landscapes of GEM HGA models with and without p53 deletion are distinct. Frequency plots of aCGH data from TR(P) HGA show frequent CNA only on chromosomes 1 and 6 (A). In contrast, *Rb1/Pten/p53* triple KO HGA (GSE22927) show frequent CNA across the genome (B) (100), suggesting that *p53* deletion in *Rb1/Pten*-deleted murine astrocytes significantly affects the spectrum of CNA acquired during malignant progression.

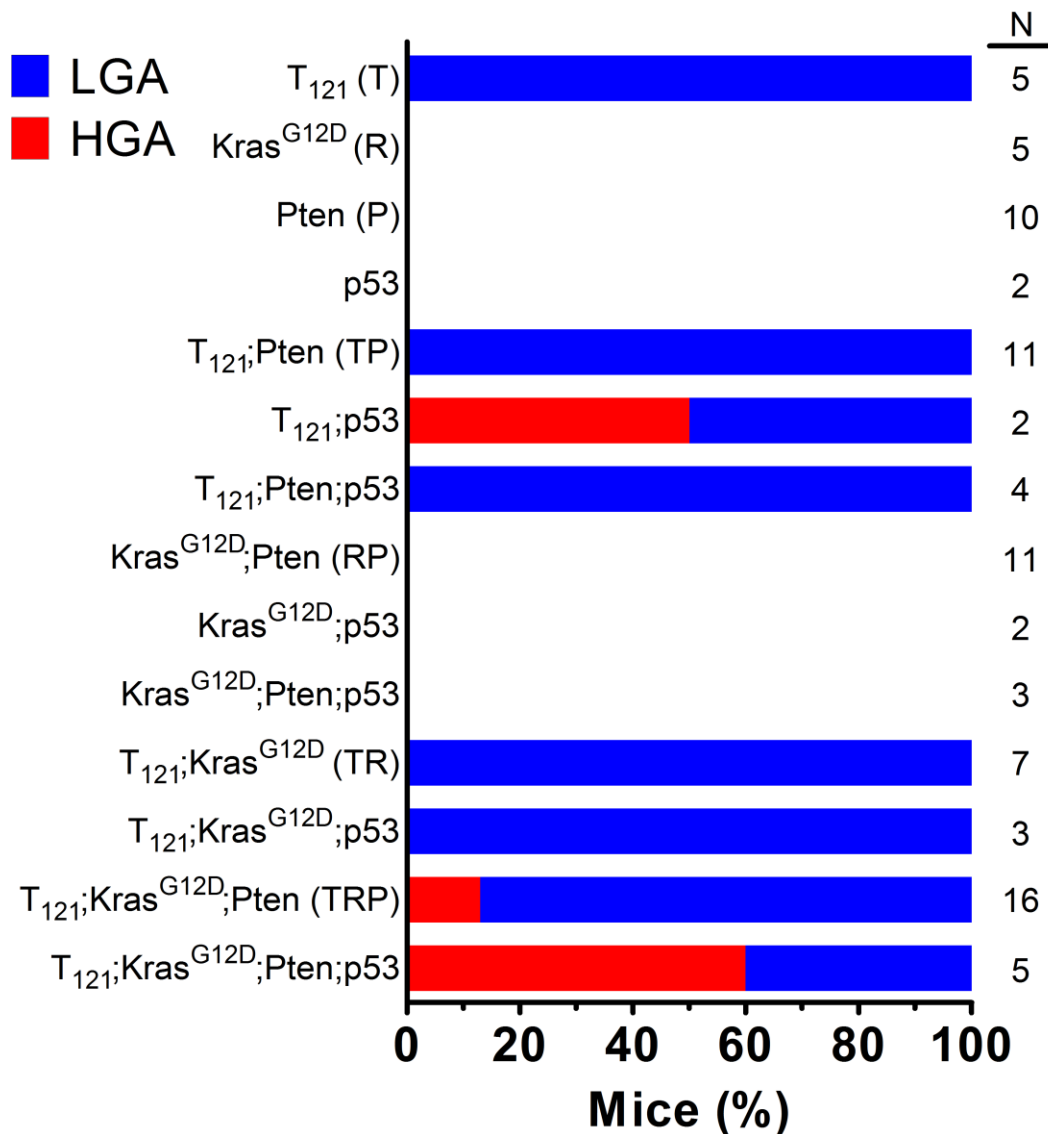


Figure S2.21. Heterozygous deletion of p53 accelerates tumorigenesis in T(RP) mice. Histological examination of 2 m T(RP);GFAP-CreER mouse brains with and without heterozygous p53 deletion (Table S2.12) showed that deletion of p53 induced tumorigenesis only in the context of T, but T;p53 and TRP;p53 mice developed HGA more frequently than T and TRP mice.

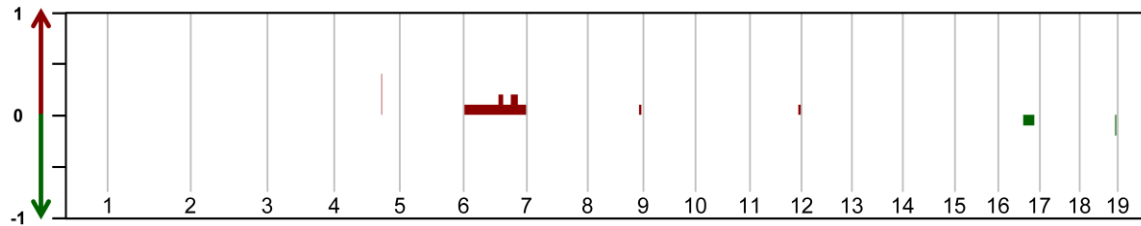


Figure S2.22. T(RP) astrocytomas with p53 deletion show minimal CNA. Frequency plot of aCGH data from 10 astrocytomas from 7 T(RP) mice with heterozygous *p53* deletion (Table S2.12) shows minimal CNA at ~2 m after induction.

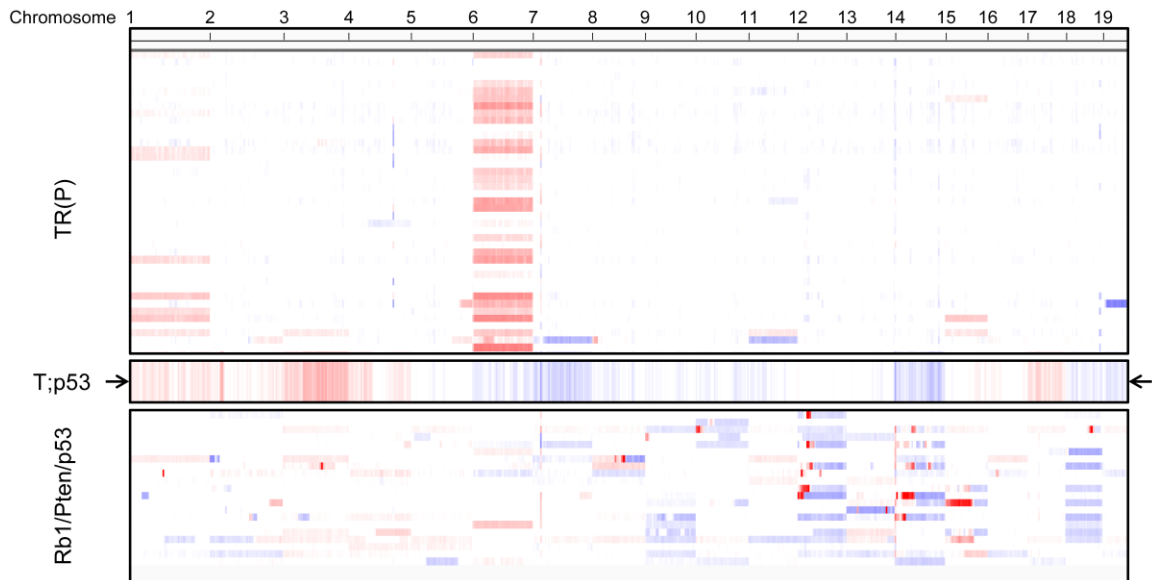


Figure S2.23. p53 deletion contributes to widespread genomic instability. IGV analysis of aCGH data from TR(P) (N=41, top, Fig. 5J-L) and *Rb1/Pten/p53* triple KO HGA (N=21, bottom, Fig. S20B) shows that their genomic CNA landscapes are distinct. One GBM (arrow) harvested from a terminally-aged, neurologically symptomatic T;p53^{+/-} mouse shows a CNA pattern more similar to *Rb1/Pten/p53* triple KO than TR(P) HGA, suggesting that *p53* deletion induces widespread genomic instability and variable CNA landscapes upon malignant progression.

Table S2.1. TRP LGA cohort: Mice sacrificed at 2 m after induction

ID	Genotype	GFAP-CreER	4OHT induction	Sex	Age at induction (days)	Survival (days)	Diagnosis (Fig. 2A)	LGA Burden (Figs. 2B, S6)	Olfactory bulb (OFB) or forebrain (FB) transcriptome samples (Fig. 3)
207979	TP ^{-/-}	No	Yes	M	61	67	Normal		
207967	TRP ^{-/-}	No	Yes	F	61	67	Normal		
221182	P ^{+/-}	Yes	No	M	100	66	Normal		FB
223979	R	Yes	No	F	127	74	Normal		OFB
217861	TP ^{+/-}	Yes	No	F	119	65	Normal		OFB, FB
220435	TRP ^{-/-}	Yes	No	M	111	66	Normal		OFB
221699	TRP ^{-/-}	Yes	No	M	90	66	Normal		OFB, FB
219892	P ^{-/-}	Yes	Yes	F	98	64	Normal	S6AB	OFB
219921	P ^{-/-}	Yes	Yes	M	101	64	Normal	S6AB	OFB
220057	P ^{-/-}	Yes	Yes	F	95	64	Normal	S6AB	OFB
221927	P ^{-/-}	Yes	Yes	M	116	63	Normal	S6AB	OFB
221928	P ^{-/-}	Yes	Yes	M	116	63	Normal	S6AB	OFB
214254	P ^{+/-}	Yes	Yes	F	63	70	Normal	S6AB	OFB
217463	P ^{+/-}	Yes	Yes	F	99	66	Normal	S6AB	OFB
217871	P ^{+/-}	Yes	Yes	M	92	66	Normal	S6AB	OFB, FB
219899	P ^{+/-}	Yes	Yes	M	98	64	Normal	S6AB	
220724	P ^{+/-}	Yes	Yes	F	107	66	Normal	S6AB	OFB
217708	R	Yes	Yes	M	94	66	Normal	S6AB	
219670	R	Yes	Yes	M	98	65	Normal	S6AB	OFB

220060	R	Yes	Yes	M	95	64	Normal	S6AB	
225561	R	Yes	Yes	F	87	74	Normal	S6AB	OFB
225567	R	Yes	Yes	F	87	74	Normal	S6AB	
215214	RP ^{-/-}	Yes	Yes	F	101	59	Normal	S6AB	OFB, FB
219159	RP ^{-/-}	Yes	Yes	F	104	65	Normal	S6AB	OFB
219898	RP ^{-/-}	Yes	Yes	M	98	64	Normal	S6AB	OFB
219918	RP ^{-/-}	Yes	Yes	M	101	64	Normal	S6AB	OFB
220062	RP ^{-/-}	Yes	Yes	M	98	45	Normal	S6AB	OFB
207970	RP ^{+/-}	Yes	Yes	F	61	67	Normal	S6AB	
214987	RP ^{+/-}	Yes	Yes	M	104	59	Normal	S6AB	OFB
215216	RP ^{+/-}	Yes	Yes	M	101	59	Normal	S6AB	OFB, FB
220061	RP ^{+/-}	Yes	Yes	M	95	64	Normal	S6AB	OFB
221181	RP ^{+/-}	Yes	Yes	M	100	66	Normal	S6AB	OFB
217872	T	Yes	Yes	M	92	66	A2	2B, 6D	
219147	T	Yes	Yes	F	104	65	A2	2B, 6D	OFB, FB
220727	T	Yes	Yes	F	107	66	A2	2B, 6D	OFB, FB
221184	T	Yes	Yes	M	100	66	A2	2B, 6D	OFB, FB
221940	T	Yes	Yes	M	114	63	A2	2B, 6D	OFB, FB
217857	TP ^{-/-}	Yes	Yes	F	91	66	A2	2B, 6D	OFB
219594	TP ^{-/-}	Yes	Yes	F	98	65	A2	2B, 6D	OFB
219595	TP ^{-/-}	Yes	Yes	M	98	65	A2	2B, 6D	OFB
219699	TP ^{-/-}	Yes	Yes	M	98	65	A2	2B, 6D	OFB
221180	TP ^{-/-}	Yes	Yes	M	100	66	A2	2B, 6D	OFB
215217	TP ^{+/-}	Yes	Yes	M	101	59	A2		OFB, FB
216188	TP ^{+/-}	Yes	Yes	F	85	59	A2		OFB, FB
219438	TP ^{+/-}	Yes	Yes	F	97	65	A2		OFB
219591	TP ^{+/-}	Yes	Yes	M	98	65	A2		OFB

219973	TP ^{+/-}	Yes	Yes	M	101	64	A2		OFB, FB
246036	TP ^{+/-}	Yes	Yes	F	98	63	A2		
214252	TR	Yes	Yes	F	63	70	A2	2B, 6D	OFB
222912	TR	Yes	Yes	M	147	74	A2	2B, 6D	FB
225569	TR	Yes	Yes	F	87	74	A2	2B, 6D	FB
225800	TR	Yes	Yes	M	82	74	A2	2B, 6D	
245121	TR	Yes	Yes	M	134	60	A2	2B, 6D	
245308	TR	Yes	Yes	F	129	60	A2		
245310	TR	Yes	Yes	F	129	60	A2	2B, 6D	
215534	TRP ^{-/-}	Yes	Yes	M	96	59	A2	2B, 6D	OFB, FB
215697	TRP ^{-/-}	Yes	Yes	M	94	59	A2	2B, 6D	OFB, FB
216103	TRP ^{-/-}	Yes	Yes	M	89	59	A2		FB
216498	TRP ^{-/-}	Yes	Yes	F	84	44	A2		OFB
243054	TRP ^{-/-}	Yes	Yes	M	129	63	A2		OFB, FB
246037	TRP ^{-/-}	Yes	Yes	M	98	63	A2		
214253	TRP ^{-/-}	Yes	Yes	F	63	70	A3	2B, 6D	OFB, FB
245665	TRP ^{-/-}	Yes	Yes	M	106	60	A3		
214828	TRP ^{+/-}	Yes	Yes	F	133	66	A2		OFB, FB
216175	TRP ^{+/-}	Yes	Yes	F	114	66	A2		OFB, FB
217494	TRP ^{+/-}	Yes	Yes	M	99	66	A2		OFB, FB
217703	TRP ^{+/-}	Yes	Yes	F	87	73	A2		
217706	TRP ^{+/-}	Yes	Yes	F	87	73	A2		OFB
219439	TRP ^{+/-}	Yes	Yes	F	97	65	A2		OFB, FB
219596	TRP ^{+/-}	Yes	Yes	F	70	66	A2		OFB, FB
219695	TRP ^{+/-}	Yes	Yes	F	98	65	A2		OFB, FB
219913	TRP ^{+/-}	Yes	Yes	F	101	64	A2		OFB

Summary						
GFAP-CreER	4OHT induction	Genotype	Diagnosis	Total transcriptome samples		Total Mice
				OFB	FB	
No	Yes	TP ^{-/-}	Normal			1
		TRP ^{-/-}				1
Yes	No	P ^{+/-}	Normal		1	1
		R		1		1
		TP ^{+/-}		1	1	1
		TRP ^{-/-}		2	1	2
	Yes	P ^{+/-}	Normal	4	1	5
		P ^{-/-}		5		5
		R		2		5
		RP ^{+/-}		4	1	5
		RP ^{-/-}		5	1	5
		T		4	4	5
		TP ^{+/-}		5	3	6
		TP ^{-/-}		5		5
		TR		1	2	7
		TRP ^{+/-}		8	6	9
		TRP ^{-/-}	LGA (A2)	4	4	6
			HGA (A3)	1	1	2
Total				52	26	72

	Mean	SD	Min	Max
Age at induction (days)	98.3	17.2	61	147
Post-induction survival (days)	64.7	5.3	44	74

Table S2.1. TRP LGA cohort: Mice sacrificed at 2 m after induction. Adult GFAP-CreER mice with combinations of T, R, and P alleles were induced with 4OHT at ~3 m of age (mean 98, SD 17 d) and sacrificed ~2 m (mean 65, SD 5 d) later. Uninduced GFAP-CreER mice (N=5), induced mice lacking GFAP-CreER (N=2), and induced GFAP-CreER mice with P, R, or RP (N=25) showed no evidence of tumorigenesis. In contrast, all induced GFAP-CreER mice with T(P) or TR(P) developed astrocytomas (N=40).

Table S2.2. GFAP-CreER mice with *Rb1* deletion \pm *Kras*^{G12D} \pm *Pten* deletion or *Nf1* deletion \pm T₁₂₁ \pm *Pten* deletion

Mouse ID	Genotype	Sex	Age at induction (days)	Cause of death	Survival (days)	Diagnosis
250564	Rb1 ^{+/-} ;Nf1 ^{+/-}	M	118	Sac	191	Normal
248559	Rb1 ^{+/-} ;Pten ^{+/-}	F	173	Sac	119	Normal
248590	Rb1 ^{+/-} ;Pten ^{+/-}	M	172	Sac	60	Normal
248916	Rb1 ^{+/-} ;Pten ^{+/-}	F	148	Sac	119	Normal
250700	Rb1 ^{+/-} ;Pten ^{+/-}	F	113	Sac	191	Normal
250012	Rb1 ^{+/-} ;Nf1 ^{+/-} ;Pten ^{+/-}	F	105	Sac	78	Normal
250630	Rb1 ^{+/-} ;Nf1 ^{+/-} ;Pten ^{+/-}	M	119	Sac	189	Normal
250013	Rb1 ^{+/-} ;Nf1 ^{+/-} ;Pten ^{-/-}	F	105	Sac	78	Normal
250773	Rb1 ^{+/-} ;Nf1 ^{+/-} ;Pten ^{-/-}	F	104	Sac	191	Normal
250358	Rb1 ^{+/-} ;Nf1 ^{-/-} ;Pten ^{+/-}	M	102	Sac	63	Normal
250016	Rb1 ^{+/-} ;Nf1 ^{-/-} ;Pten ^{+/-}	M	252	Sac	183	Normal
251062	Rb1 ^{+/-} ;Nf1 ^{-/-} ;Pten ^{-/-}	M	110	Sac	185	Normal
248558	Rb1 ^{+/-} ;Kras ^{G12D}	F	173	Sac	119	Normal
248915	Rb1 ^{+/-} ;Kras ^{G12D} ;Pten ^{+/-}	F	148	Sac	119	Normal
248922	Rb1 ^{+/-} ;Kras ^{G12D} ;Pten ^{+/-}	M	148	Sac	60	Normal
249182	Rb1 ^{+/-} ;Kras ^{G12D} ;Pten ^{+/-}	F	135	Sac	60	Normal
250362	Rb1 ^{+/-} ;Kras ^{G12D} ;Pten ^{+/-}	F	101	Sac	63	Normal
249234	Rb1 ^{+/-} ;Kras ^{G12D} ;Pten ^{-/-}	F	131	Sac	63	Normal
251580	Rb1 ^{+/-} ;Kras ^{G12D} ;Pten ^{-/-}	M	117	Sac	70	Normal
252508	Rb1 ^{+/-} ;Kras ^{G12D} ;Pten ^{-/-}	F	101	Sac	32	Normal

252661	Rb1 ^{+/-} ;Kras ^{G12D} ;Pten ^{-/-}	F	98	Sac	94	Normal
252666	Rb1 ^{+/-} ;Kras ^{G12D} ;Pten ^{-/-}	M	115	Sac	38	Normal
250561	Rb1 ^{-/-}	M	118	Sac	191	Normal
250628	Rb1 ^{-/-} ;Nf1 ^{+/-}	F	119	Sac	191	Normal
250356	Rb1 ^{-/-} ;Nf1 ^{+/-} ;Pten ^{+/-}	F	179	Sac	185	Normal
251054	Rb1 ^{-/-} ;Nf1 ^{+/-} ;Pten ^{-/-}	F	114	Sac	185	Normal
251276	Rb1 ^{-/-} ;Nf1 ^{+/-} ;Pten ^{-/-}	F	95	Sac	185	Normal
250017	Rb1 ^{-/-} ;Nf1 ^{-/-} ;Pten ^{-/-}	M	252	Sac	162	Normal
252660	Rb1 ^{-/-} ;Kras ^{G12D} ;Pten ^{-/-}	F	98	Sac	37	Normal
250631	Nf1 ^{-/-}	M	119	Sac	189	Normal
247642	Nf1 ^{+/-} ;Pten ^{+/-}	M	95	Sac	175	Normal
249594	Nf1 ^{+/-} ;Pten ^{-/-}	M	36	Sac	184	Normal
250612	Nf1 ^{-/-} ;Pten ^{+/-}	F	118	Sac	191	Normal
245449	T;Nf1 ^{+/-} ;Pten ^{+/-}	M	355	Brain tumor	99	GBM
246071	T;Nf1 ^{+/-} ;Pten ^{+/-}	M	312	Sac	184	A3
246522	T;Nf1 ^{+/-} ;Pten ^{+/-}	M	272	Sac	184	A3
247171	T;Nf1 ^{+/-} ;Pten ^{+/-}	F	147	Sac	175	A2
247472	T;Nf1 ^{+/-} ;Pten ^{+/-}	M	242	Sac	64	A2
247641	T;Nf1 ^{+/-} ;Pten ^{+/-}	M	95	Sac	175	A2
247658	T;Nf1 ^{+/-} ;Pten ^{+/-}	M	166	Sac	184	A2
247965	T;Nf1 ^{+/-} ;Pten ^{+/-}	M	73	Sac	175	A2
247967	T;Nf1 ^{+/-} ;Pten ^{+/-}	M	73	Sac	175	A2
248900	T;Nf1 ^{+/-} ;Pten ^{+/-}	F	81	Sac	184	A2
249328	T;Nf1 ^{+/-} ;Pten ^{+/-}	F	56	Sac	184	A2
249589	T;Nf1 ^{+/-} ;Pten ^{+/-}	F	155	Sac	63	A2
250615	T;Nf1 ^{+/-} ;Pten ^{+/-}	M	118	Sac	189	A2

249591	T;Nf1 ^{+/-} ;Pten ^{-/-}	F	155	Sac	63	A2
249870	T;Nf1 ^{+/-} ;Pten ^{-/-}	M	117	Sac	72	A2
250765	T;Nf1 ^{+/-} ;Pten ^{-/-}	M	144	Sac	232	A2
251496	T;Nf1 ^{+/-} ;Pten ^{-/-}	F	122	Sac	184	A2
245462	T;Nf1 ^{+/-}	M	355	Sac	184	A2
246372	T;Nf1 ^{+/-}	F	211	Sac	175	A2
247966	T;Nf1 ^{+/-}	M	73	Sac	175	A2
247640	T;Nf1 ^{-/-} ;Pten ^{+/-}	M	95	Sac	175	A2
249890	T;Nf1 ^{-/-} ;Pten ^{+/-}	M	116	Sac	72	A2
249871	T;Nf1 ^{-/-} ;Pten ^{-/-}	M	117	Sac	72	A2
249961	T;Nf1 ^{-/-} ;Pten ^{-/-}	M	117	Sac	72	A2
250898	T;Nf1 ^{-/-} ;Pten ^{-/-}	M	130	Brain tumor	169	A3
249593	T;Nf1 ^{-/-}	M	36	Sac	184	A3

Summary		
Genotype	Diagnosis	Total
Rb1 ^{+/-} ;Nf1 ^{+/-}	Normal	1
Rb1 ^{+/-} ;Pten ^{+/-}		4
Rb1 ^{+/-} ;Nf1 ^{+/-} ;Pten ^{+/-}		2
Rb1 ^{+/-} ;Nf1 ^{+/-} ;Pten ^{-/-}		2
Rb1 ^{+/-} ;Nf1 ^{-/-} ;Pten ^{+/-}		2
Rb1 ^{+/-} ;Nf1 ^{-/-} ;Pten ^{-/-}		1
Rb1 ^{+/-} ;Kras ^{G12D}		1
Rb1 ^{+/-} ;Kras ^{G12D} ;Pten ^{+/-}		4

Rb1 ^{+/-} ;Kras ^{G12D} ;Pten ^{-/-}		5
Rb1 ^{-/-}		1
Rb1 ^{-/-} ;Nf1 ^{+/-}		1
Rb1 ^{-/-} ;Nf1 ^{+/-} ;Pten ^{+/-}	Normal	1
Rb1 ^{-/-} ;Nf1 ^{+/-} ;Pten ^{-/-}		2
Rb1 ^{-/-} ;Nf1 ^{-/-} ;Pten ^{-/-}		1
Rb1 ^{-/-} ;Kras ^{G12D} ;Pten ^{-/-}		1
Nf1 ^{+/-} ;Pten ^{+/-}		1
Nf1 ^{+/-} ;Pten ^{-/-}	Normal	1
Nf1 ^{-/-}		1
Nf1 ^{-/-} ;Pten ^{+/-}		1
T;Nf1 ^{+/-}	LGA (A2)	3
	LGA (A2)	10
T;Nf1 ^{+/-} ;Pten ^{+/-}	HGA (A3)	2
	HGA (GBM)	1
T;Nf1 ^{+/-} ;Pten ^{-/-}	LGA (A2)	4
T;Nf1 ^{-/-}	HGA (A3)	1
T;Nf1 ^{-/-} ;Pten ^{+/-}	LGA (A2)	2
	LGA (A2)	2
T;Nf1 ^{-/-} ;Pten ^{-/-}	HGA (A3)	1
Total		59

Age at induction (days)

Mean	138.3
SD	67.1

Min	36
Max	355

Table S2.2. GFAP-CreER mice with Rb1 deletion ± KrasG12D ± Pten deletion or Nf1 deletion ± T121 ± Pten deletion. Adult GFAP-CreER mice were induced with 4OHT at ~4.5 m of age (mean 138, SD 67 d) and sacrificed ~4 m (mean 123, SD 60 d) later. *Rb1*-deleted mice, with or without *Kras*^{G12D}, *Nf1* or *Pten* deletions (N=29), and *Nf1*-deleted mice, with or without *Pten* deletion (N=4), showed no evidence of tumorigenesis. In contrast, all induced T;*Nf1*-deleted mice, with or without *Pten* deletion (N=26), developed astrocytomas.

Table S2.3. One versus rest SAM analysis of T(RP) LGA transcriptomes at 2 m after induction

Comparison	Up/Down	Gene	Row	d.value	stdev	rawp	q.value	R.fold
LGA versus normal brain	Down	Pdlim7	12262	-11.8648	0.048313	0	0	0.672115
LGA versus normal brain	Down	Srxn1	15484	-11.86238	0.061941	0	0	0.600915
LGA versus normal brain	Down	SrpK2	15459	-11.64601	0.037509	0	0	0.738754
LGA versus normal brain	Down	Mtor	10427	-11.579	0.038943	0	0	0.731576
LGA versus normal brain	Down	Klhl30	9014	-11.57341	0.110097	0	0	0.413454
LGA versus normal brain	Down	D030063E12	4869	-11.4376	0.045203	0	0	0.698818
LGA versus normal brain	Down	Adarb1	1812	-11.28855	0.083187	0	0	0.521572
LGA versus normal brain	Down	Inpp5a	8553	-11.28443	0.059095	0	0	0.629878
LGA versus normal brain	Down	Armc8	2469	-11.22809	0.042497	0	0	0.718391
LGA versus normal brain	Down	Atpaf1	2690	-11.17776	0.048432	0	0	0.68712
LGA versus normal brain	Down	Got2	7527	-11.1009	0.054372	0	0	0.65812
LGA versus normal brain	Down	Akap17b	2007	-11.04388	0.056799	0	0	0.647397
LGA versus normal brain	Down	Rcan2	13644	-10.99853	0.069494	0	0	0.588728
LGA versus normal brain	Down	Cish	4168	-10.8756	0.080631	0	0	0.544532
LGA versus normal brain	Down	Clip1	4245	-10.84813	0.05434	0	0	0.664577
LGA versus normal brain	Down	6030419C18Rik	1167	-10.80144	0.084588	0	0	0.530834
LGA versus normal brain	Down	Fam120b	6179	-10.72756	0.048818	0	0	0.695585
LGA versus normal brain	Down	Cited2	4171	-10.65492	0.060756	0	0	0.63845
LGA versus normal brain	Down	Slmap	15069	-10.63424	0.046931	0	0	0.707561
LGA versus normal brain	Down	Mfap3l	10011	-10.59715	0.068636	0	0	0.604012
LGA versus normal brain	Down	Npr3	11026	-10.55832	0.05708	0	0	0.658532
LGA versus normal brain	Down	Ell2	5849	-10.50984	0.051089	0	0	0.689233
LGA versus normal brain	Down	Ppp2r5b	12919	-10.49732	0.058299	0	0	0.654295
LGA versus normal brain	Down	Arhgef3	2420	-10.48864	0.053139	0	0	0.679547
LGA versus normal brain	Down	Cdc42se2	3851	-10.45468	0.044654	0	0	0.723545
LGA versus normal brain	Down	Cerk	4012	-10.41994	0.037036	0	0	0.765295

LGA versus normal brain	Down	Cyb5r4	4769	-10.35856	0.033562	0	0	0.785862
LGA versus normal brain	Down	Leprotl1	9273	-10.33641	0.032106	0	0	0.794512
LGA versus normal brain	Down	Rhobtb2	13788	-10.31214	0.046205	0	0	0.718734
LGA versus normal brain	Down	Cyt1l	4862	-10.28559	0.077127	0	0	0.577025
LGA versus normal brain	Down	Ptcd1	13225	-10.26615	0.054141	0	0	0.68027
LGA versus normal brain	Down	Igf1	8402	-10.18118	0.061668	0	0	0.647138
LGA versus normal brain	Down	Ube2f	16991	-10.15848	0.032359	0	0	0.796246
LGA versus normal brain	Down	Tex264	16029	-10.10401	0.034471	0	0	0.785509
LGA versus normal brain	Down	Impdh1	8527	-10.02706	0.057147	0	0	0.672208
LGA versus normal brain	Down	Slc9a3r2	15039	-10.01538	0.057703	0	0	0.669932
LGA versus normal brain	Down	Rnf128	13885	-10.00837	0.061156	0	0	0.654256
LGA versus normal brain	Down	Rabgap1l	13450	-9.980746	0.061244	0	0	0.654626
LGA versus normal brain	Down	Dnajc27	5383	-9.94855	0.050791	0	0	0.704515
LGA versus normal brain	Down	Pppde2	12939	-9.930312	0.034096	0	0	0.790819
LGA versus normal brain	Down	Zbtb4	17690	-9.92347	0.067191	0	0	0.629916
LGA versus normal brain	Down	B4galnt1	2816	-9.903721	0.061421	0	0	0.655972
LGA versus normal brain	Down	2310061104Rik	528	-9.90043	0.047184	0	0	0.723396
LGA versus normal brain	Down	Bag5	2855	-9.893671	0.044809	0	0	0.735435
LGA versus normal brain	Down	Tmtc1	16443	-9.861215	0.07646	0	0	0.592964
LGA versus normal brain	Down	Bace1	2846	-9.819497	0.053286	0	0	0.695806
LGA versus normal brain	Down	Slc2a6	14885	-9.814645	0.081365	0	0	0.574919
LGA versus normal brain	Down	Pptc7	12943	-9.809048	0.056409	0	0	0.681452
LGA versus normal brain	Down	Got1	7525	-9.807952	0.072166	0	0	0.612255
LGA versus normal brain	Down	Chchd7	4061	-9.795723	0.090205	0	0	0.542005
LGA versus normal brain	Down	2410016006Rik	550	-9.792571	0.050969	0	0	0.707541
LGA versus normal brain	Down	Cyp2s1	4824	-9.786391	0.059391	0	0	0.668397
LGA versus normal brain	Down	Tdrd9	15983	-9.78534	0.08718	0	0	0.553598
LGA versus normal brain	Down	Cdkl2	3918	-9.765427	0.097656	0	0	0.516322
LGA versus normal brain	Down	5830408C22Rik	1141	-9.754068	0.07844	0	0	0.588407
LGA versus normal brain	Down	Filip1	6578	-9.703105	0.095227	0	0	0.527046

LGA versus normal brain	Down	Rgs11	13753	-9.695361	0.067907	0	0	0.633589
LGA versus normal brain	Down	Nme1	10934	-9.687696	0.069177	0	0	0.628436
LGA versus normal brain	Down	Qrs1	13368	-9.676679	0.032099	0	0	0.806298
LGA versus normal brain	Down	Insig2	8565	-9.663531	0.044171	0	0	0.743887
LGA versus normal brain	Down	Edil3	5700	-9.66081	0.074427	0	0	0.607506
LGA versus normal brain	Down	Nceh1	10673	-9.650539	0.064162	0	0	0.651032
LGA versus normal brain	Down	Ube2o	17003	-9.648242	0.070726	0	0	0.623138
LGA versus normal brain	Down	6330406l15Rik	1183	-9.631188	0.081983	0	0	0.578508
LGA versus normal brain	Down	Ttll7	16877	-9.627232	0.084315	0	0	0.569704
LGA versus normal brain	Down	Ppp1r16b	12883	-9.541502	0.083358	0	0	0.576197
LGA versus normal brain	Down	Rab37	13415	-9.523755	0.083214	0	0	0.577338
LGA versus normal brain	Down	Prkar1a	13000	-9.518387	0.05484	0	0	0.69641
LGA versus normal brain	Down	Acsl1	1714	-9.487328	0.059224	0	0	0.677419
LGA versus normal brain	Down	Map2k1	9744	-9.484919	0.072884	0	0	0.619295
LGA versus normal brain	Down	Wwp1	17577	-9.4818	0.052368	0	0	0.708804
LGA versus normal brain	Down	Foxd1	6665	-9.477132	0.084251	0	0	0.574963
LGA versus normal brain	Down	Tmem57	16383	-9.430053	0.040275	0	0	0.768547
LGA versus normal brain	Down	Chchd10	4055	-9.429511	0.062068	0	0	0.666524
LGA versus normal brain	Down	Fkbp1b	6590	-9.426683	0.082913	0	0	0.581722
LGA versus normal brain	Down	Aars2	1558	-9.400453	0.052055	0	0	0.71235
LGA versus normal brain	Down	Fbxo28	6444	-9.390135	0.033295	0	0	0.805165
LGA versus normal brain	Down	Cul3	4723	-9.38448	0.030901	0	0	0.817906
LGA versus normal brain	Down	Pdk3	12255	-9.376205	0.055265	0	0	0.698254
LGA versus normal brain	Down	Asb11	2522	-9.375862	0.090556	0	0	0.555154
LGA versus normal brain	Down	Abca5	1573	-9.374138	0.060237	0	0	0.676111
LGA versus normal brain	Down	Thbd	16090	-9.342069	0.095662	0	0	0.538238
LGA versus normal brain	Down	Dnajb12	5357	-9.338725	0.039087	0	0	0.776458
LGA versus normal brain	Down	Usp31	17174	-9.316142	0.081427	0	0	0.591076
LGA versus normal brain	Down	Cmas	4284	-9.308657	0.065685	0	0	0.654544
LGA versus normal brain	Down	Ufsp1	17067	-9.293136	0.063176	0	0	0.665676

LGA versus normal brain	Down	Ppm1j	12858	-9.283068	0.089481	0	0	0.562274
LGA versus normal brain	Down	Mapre3	9796	-9.280378	0.072519	0	0	0.627201
LGA versus normal brain	Down	Acvr1b	1749	-9.275793	0.053084	0	0	0.710843
LGA versus normal brain	Down	Zfp667	17992	-9.269356	0.07397	0	0	0.621723
LGA versus normal brain	Down	Stk24	15593	-9.257199	0.03205	0	0	0.814116
LGA versus normal brain	Down	Scyl2	14340	-9.256841	0.038068	0	0	0.783285
LGA versus normal brain	Down	Pgam1	12347	-9.249432	0.043836	0	0	0.754995
LGA versus normal brain	Down	Cul5	4726	-9.246629	0.038759	0	0	0.780036
LGA versus normal brain	Down	Tmem87b	16409	-9.235527	0.060842	0	0	0.677406
LGA versus normal brain	Down	Ryr1	14187	-9.23483	0.074295	0	0	0.62153
LGA versus normal brain	Down	Slc30a9	14897	-9.223927	0.04847	0	0	0.733523
LGA versus normal brain	Down	Lancl3	9180	-9.22268	0.115299	0	0	0.478513
LGA versus normal brain	Down	Has1	7907	-9.222039	0.082247	0	0	0.591118
LGA versus normal brain	Down	Mdh1	9901	-9.220326	0.054003	0	0	0.708123
LGA versus normal brain	Down	Cox5a	4472	-9.21586	0.044524	0	0	0.752452
LGA versus normal brain	Down	Il34	8503	-9.204648	0.077093	0	0	0.611484
LGA versus normal brain	Down	Fam110c	6164	-9.203584	0.069343	0	0	0.642512
LGA versus normal brain	Down	Tm6sf1	16193	-9.20118	0.091427	0	0	0.558166
LGA versus normal brain	Down	Mef2a	9948	-9.184175	0.05995	0	0	0.682738
LGA versus normal brain	Down	Fhdc1	6561	-9.182867	0.067427	0	0	0.651043
LGA versus normal brain	Down	Ecsit	5688	-9.179111	0.035131	0	0	0.799699
LGA versus normal brain	Down	Mrv1	10331	-9.175415	0.07052	0	0	0.638584
LGA versus normal brain	Down	Stim1	15584	-9.173184	0.051662	0	0	0.720011
LGA versus normal brain	Down	Pip4k2c	12501	-9.166473	0.055877	0	0	0.701157
LGA versus normal brain	Down	Napepld	10631	-9.162846	0.056072	0	0	0.700383
LGA versus normal brain	Down	Asb2	2526	-9.159581	0.086106	0	0	0.578867
LGA versus normal brain	Down	Gnl3l	7493	-9.147765	0.060457	0	0	0.681579
LGA versus normal brain	Down	Ube2k	16998	-9.108882	0.034689	0	0	0.803306
LGA versus normal brain	Down	Creld1	4555	-9.108	0.054151	0	0	0.710443
LGA versus normal brain	Down	Ttpal	16882	-9.107162	0.034641	0	0	0.803582

LGA versus normal brain	Down	Jhdm1d	8735	-9.099067	0.054439	0	0	0.709394
LGA versus normal brain	Down	Cnrip1	4340	-9.097265	0.041833	0	0	0.768137
LGA versus normal brain	Down	Sema6b	14427	-9.088583	0.080695	0	0	0.601482
LGA versus normal brain	Down	Mctp1	9894	-9.086801	0.095934	0	0	0.546489
LGA versus normal brain	Down	Tmem163	16286	-9.086452	0.048034	0	0	0.738945
LGA versus normal brain	Down	Ap3s2	2272	-9.080996	0.046362	0	0	0.746899
LGA versus normal brain	Down	Cnnm2	4320	-9.080891	0.052257	0	0	0.719697
LGA versus normal brain	Down	Slc36a2	14929	-9.069554	0.111344	0	0	0.4966
LGA versus normal brain	Down	1810074P20Rik	404	-9.069125	0.031553	0	0	0.820084
LGA versus normal brain	Down	Gls2	7072	-9.068891	0.081719	0	0	0.598284
LGA versus normal brain	Down	D230025D16Rik	4920	-9.058861	0.054368	0	0	0.710788
LGA versus normal brain	Down	Brms1l	3164	-9.04856	0.034527	0	0	0.805292
LGA versus normal brain	Down	Dcun1d4	5095	-9.044323	0.070917	0	0	0.641093
LGA versus normal brain	Down	Cacna1h	3359	-9.037544	0.036683	0	0	0.794695
LGA versus normal brain	Down	Icam4	8325	-9.014051	0.08733	0	0	0.579471
LGA versus normal brain	Down	Dcaf11	5050	-9.009606	0.0316	0	0	0.820911
LGA versus normal brain	Down	Ypel5	17652	-8.998006	0.06653	0	0	0.660376
LGA versus normal brain	Down	Hmga1	8102	-8.961743	0.056162	0	0	0.705487
LGA versus normal brain	Down	Arhgap22	2385	-8.958193	0.059799	0	0	0.68983
LGA versus normal brain	Down	Xylt2	17622	-8.9535	0.043835	0	0	0.761819
LGA versus normal brain	Down	Smarca1	15090	-8.950305	0.070987	0	0	0.643782
LGA versus normal brain	Down	4931408A02Rik	985	-8.949974	0.057533	0	0	0.699831
LGA versus normal brain	Down	Fam53c	6312	-8.93955	0.046415	0	0	0.750056
LGA versus normal brain	Down	2310044G17Rik	511	-8.935273	0.040016	0	0	0.780488
LGA versus normal brain	Down	Hecw2	7981	-8.931817	0.063246	0	0	0.676001
LGA versus normal brain	Down	Lpgat1	9463	-8.92651	0.079994	0	0	0.609601
LGA versus normal brain	Down	Kcnab2	8789	-8.915434	0.092512	0	0	0.564565
LGA versus normal brain	Down	Znrf1	18175	-8.903776	0.050551	0	0	0.731996
LGA versus normal brain	Down	Atp6v0a1	2661	-8.901728	0.047449	0	0	0.746194
LGA versus normal brain	Down	Gpr12	7574	-8.882743	0.058969	0	0	0.695532

LGA versus normal brain	Down	Zswim1	18199	-8.872768	0.065762	0	0	0.667347
LGA versus normal brain	Down	Morc4	10182	-8.867319	0.045331	0	0	0.756825
LGA versus normal brain	Down	Col4a3bp	4393	-8.860035	0.029864	0	0	0.832434
LGA versus normal brain	Down	Ptger3	13241	-8.859932	0.119789	0	0	0.479193
LGA versus normal brain	Down	Socs5	15243	-8.85248	0.06415	0	0	0.674603
LGA versus normal brain	Down	Ccl25	3676	-8.849706	0.077522	0	0	0.621553
LGA versus normal brain	Down	Uhrf1bp1l	17085	-8.848564	0.050244	0	0	0.734796
LGA versus normal brain	Down	Rassf4	13567	-8.825291	0.047368	0	0	0.748441
LGA versus normal brain	Down	Lrp11	9494	-8.821638	0.085704	0	0	0.592114
LGA versus normal brain	Down	Ugcg	17069	-8.814562	0.067031	0	0	0.663952
LGA versus normal brain	Down	Ptger2	13240	-8.809445	0.083861	0	0	0.599249
LGA versus normal brain	Down	Wnk4	17546	-8.806278	0.087662	0	0	0.585613
LGA versus normal brain	Down	Snx21	15220	-8.804535	0.031296	0	0	0.826137
LGA versus normal brain	Down	Gphn	7554	-8.79952	0.032582	0	0	0.819771
LGA versus normal brain	Down	Ccbl1	3545	-8.796207	0.042503	0	0	0.771712
LGA versus normal brain	Down	Fbxo25	6442	-8.7956	0.063445	0	0	0.679227
LGA versus normal brain	Down	Pdlim3	12259	-8.782783	0.077569	0	0	0.623615
LGA versus normal brain	Down	Grb10	7676	-8.78222	0.066794	0	0	0.665909
LGA versus normal brain	Down	Mapk14	9776	-8.779496	0.038106	0	0	0.79303
LGA versus normal brain	Down	Nap1l3	10626	-8.779168	0.086501	0	0	0.590738
LGA versus normal brain	Down	Pgap3	12352	-8.776104	0.06051	0	0	0.692055
LGA versus normal brain	Down	B130024G19Rik	2761	-8.773361	0.077683	0	0	0.623501
LGA versus normal brain	Down	Csrnp2	4639	-8.76294	0.053284	0	0	0.723504
LGA versus normal brain	Down	Obfc2a	11225	-8.761831	0.048235	0	0	0.746064
LGA versus normal brain	Down	Bcat1	3008	-8.760209	0.057961	0	0	0.703319
LGA versus normal brain	Down	Pparg	12818	-8.74777	0.079705	0	0	0.616749
LGA versus normal brain	Down	Tle2	16169	-8.738574	0.073077	0	0	0.642343
LGA versus normal brain	Down	Sema3a	14411	-8.728358	0.067991	0	0	0.662757
LGA versus normal brain	Down	Adssl1	1873	-8.726025	0.077837	0	0	0.624506
LGA versus normal brain	Down	Myoz1	10560	-8.717993	0.085286	0	0	0.597279

LGA versus normal brain	Down	Prdm6	12964	-8.714792	0.090916	0	0	0.577418
LGA versus normal brain	Down	Luzp1	9613	-8.705747	0.05251	0	0	0.72843
LGA versus normal brain	Down	Synrg	15751	-8.703848	0.074252	0	0	0.638928
LGA versus normal brain	Down	Sphk1	15359	-8.695349	0.089793	0	0	0.582051
LGA versus normal brain	Down	Phlda1	12412	-8.690931	0.041193	0	0	0.780241
LGA versus normal brain	Down	Narf	10635	-8.676213	0.052816	0	0	0.727872
LGA versus normal brain	Down	Dlat	5291	-8.673149	0.037264	0	0	0.799295
LGA versus normal brain	Down	1700054N08Rik	305	-8.667779	0.074999	0	0	0.637246
LGA versus normal brain	Down	Tm7sf2	16195	-8.663482	0.059336	0	0	0.700249
LGA versus normal brain	Down	Dexi	5209	-8.661544	0.049369	0	0	0.743492
LGA versus normal brain	Down	Yjefn3	17643	-8.659092	0.104854	0	0	0.532946
LGA versus normal brain	Down	Rybp	14185	-8.654406	0.030512	0	0	0.832737
LGA versus normal brain	Down	Slc23a2	14806	-8.651394	0.06931	0	0	0.659923
LGA versus normal brain	Down	Hmgxb3	8118	-8.648246	0.058538	0	0	0.704049
LGA versus normal brain	Down	Prkg2	13020	-8.639922	0.068876	0	0	0.662005
LGA versus normal brain	Down	Tubg2	16903	-8.636893	0.069775	0	0	0.658549
LGA versus normal brain	Down	Pdxk	12273	-8.635212	0.078376	0	0	0.625556
LGA versus normal brain	Down	Cltb	4274	-8.633047	0.044428	0	0	0.766549
LGA versus normal brain	Down	Ttc39c	16853	-8.630253	0.058583	0	0	0.704374
LGA versus normal brain	Down	lppk	8598	-8.62834	0.046126	0	0	0.758912
LGA versus normal brain	Down	Rnf214	13925	-8.61698	0.043141	0	0	0.772849
LGA versus normal brain	Down	4930555K19Rik	955	-8.607147	0.054982	0	0	0.720347
LGA versus normal brain	Down	Pthlh	13257	-8.598678	0.089072	0	0	0.588086
LGA versus normal brain	Down	Hagh	7893	-8.597616	0.063711	0	0	0.684082
LGA versus normal brain	Down	Vamp2	17222	-8.59724	0.050131	0	0	0.741753
LGA versus normal brain	Down	Socs2	15240	-8.59578	0.09087	0	0	0.581923
LGA versus normal brain	Down	Nars	10638	-8.595561	0.058508	0	0	0.705682
LGA versus normal brain	Down	Nr2f2	11049	-8.594259	0.075794	0	0	0.636664
LGA versus normal brain	Down	Scd1	14290	-8.585471	0.087833	0	0	0.592921
LGA versus normal brain	Down	Mgst3	10051	-8.584368	0.09237	0	0	0.577168

LGA versus normal brain	Down	Atp6v1h	2678	-8.578576	0.053734	0	0	0.726502
LGA versus normal brain	Down	Pdzd4	12280	-8.576401	0.065041	0	0	0.679327
LGA versus normal brain	Down	Dnajc5	5388	-8.57432	0.051175	0	0	0.737753
LGA versus normal brain	Down	Pip5k1b	12503	-8.573871	0.091134	0	0	0.581815
LGA versus normal brain	Down	Gcnt1	6933	-8.566603	0.071414	0	0	0.654392
LGA versus normal brain	Down	Atp2c1	2637	-8.565629	0.048919	0	0	0.747931
LGA versus normal brain	Down	Dnajib5	5363	-8.561469	0.050625	0	0	0.740502
LGA versus normal brain	Down	Tmod1	16425	-8.55622	0.08564	0	0	0.601753
LGA versus normal brain	Down	Rasa4	13541	-8.555415	0.049635	0	0	0.745022
LGA versus normal brain	Down	Wif1	17533	-8.553017	0.129741	0	0	0.463398
LGA versus normal brain	Down	Akap11	2004	-8.550952	0.076527	0	0	0.635348
LGA versus normal brain	Down	Btbd3	3189	-8.549091	0.068925	0	0	0.66469
LGA versus normal brain	Down	Slc6a8	15015	-8.546494	0.061473	0	0	0.694778
LGA versus normal brain	Down	Epm2aip1	5961	-8.540175	0.065525	0	0	0.678493
LGA versus normal brain	Down	Klhdc1	8984	-8.531225	0.056709	0	0	0.715092
LGA versus normal brain	Down	Cln3	4193	-8.527379	0.060972	0	0	0.697406
LGA versus normal brain	Down	Acsf4	1716	-8.50687	0.055385	0	0	0.721387
LGA versus normal brain	Down	Gdpd5	6956	-8.499838	0.081092	0	0	0.620169
LGA versus normal brain	Down	D17Wsu92e	4905	-8.487548	0.052718	0	0	0.733341
LGA versus normal brain	Down	Tbx18	15908	-8.485708	0.065138	0	0	0.681722
LGA versus normal brain	Down	Ogfrl1	11254	-8.483118	0.071504	0	0	0.656752
LGA versus normal brain	Down	Pvr	13331	-8.476956	0.042901	0	0	0.777183
LGA versus normal brain	Down	Rreb1	14102	-8.474225	0.045654	0	0	0.764781
LGA versus normal brain	Down	Aph1b	2293	-8.469501	0.056985	0	0	0.71567
LGA versus normal brain	Down	Cbln4	3523	-8.463623	0.096937	0	0	0.566269
LGA versus normal brain	Down	Kitl	8960	-8.463027	0.097443	0	0	0.564615
LGA versus normal brain	Down	1700012B15Rik	195	-8.450865	0.055606	0	0	0.722007
LGA versus normal brain	Down	Lrp12	9495	-8.441838	0.07616	0	0	0.640412
LGA versus normal brain	Down	Tspyl2	16806	-8.440306	0.056698	0	0	0.717698
LGA versus normal brain	Down	Fam19a3	6281	-8.433577	0.114084	0	0	0.513296

LGA versus normal brain	Down	Hs3st1	8227	-8.433339	0.095222	0	0	0.57314
LGA versus normal brain	Down	Pcdhb6	12148	-8.430208	0.045369	0	0	0.767125
LGA versus normal brain	Down	Zbtb8b	17706	-8.427379	0.078288	0	0	0.632982
LGA versus normal brain	Down	Galnt16	6860	-8.426899	0.076293	0	0	0.640417
LGA versus normal brain	Down	Snf8	15166	-8.425863	0.045615	0	0	0.766124
LGA versus normal brain	Down	Slc5a6	14999	-8.422896	0.050235	0	0	0.745807
LGA versus normal brain	Down	Bsdc1	3174	-8.422238	0.057855	0	0	0.713374
LGA versus normal brain	Down	Dennd5b	5195	-8.408107	0.060753	0	0	0.701823
LGA versus normal brain	Down	Atp6ap2	2660	-8.406415	0.070498	0	0	0.66313
LGA versus normal brain	Down	Eno2	5901	-8.405707	0.076011	0	0	0.642193
LGA versus normal brain	Down	Arrb1	2491	-8.399417	0.075371	0	0	0.644803
LGA versus normal brain	Down	Cacnb3	3367	-8.399082	0.084681	0	0	0.610794
LGA versus normal brain	Down	Slc35e2	14920	-8.398687	0.046784	0	0	0.761584
LGA versus normal brain	Down	Rnasek	13864	-8.389628	0.051518	0	0	0.741124
LGA versus normal brain	Down	Cpeb3	4498	-8.387539	0.041433	0	0	0.785932
LGA versus normal brain	Down	Tmeff2	16232	-8.3809	0.051075	0	0	0.743265
LGA versus normal brain	Down	Kcnk3	8836	-8.379609	0.066571	0	0	0.679321
LGA versus normal brain	Down	Ankrd12	2178	-8.379228	0.062173	0	0	0.696905
LGA versus normal brain	Down	Vps28	17372	-8.378391	0.029075	0	0	0.844633
LGA versus normal brain	Down	5430417L22Rik	1099	-8.374901	0.05175	0	0	0.740515
LGA versus normal brain	Down	Adck3	1820	-8.355657	0.062878	0	0	0.694771
LGA versus normal brain	Down	Myadml2	10479	-8.349049	0.066807	0	0	0.679349
LGA versus normal brain	Down	Gspt2	7748	-8.347266	0.071028	0	0	0.663012
LGA versus normal brain	Down	Fgf10	6529	-8.341845	0.098482	0	0	0.565845
LGA versus normal brain	Down	Whamm	17527	-8.338893	0.048762	0	0	0.754388
LGA versus normal brain	Down	Pard6b	12058	-8.338728	0.047156	0	0	0.761429
LGA versus normal brain	Down	Zfp169	17808	-8.337529	0.042212	0	0	0.783526
LGA versus normal brain	Down	Nptn	11030	-8.336904	0.074687	0	0	0.649473
LGA versus normal brain	Down	Fam117b	6175	-8.335441	0.04994	0	0	0.749359
LGA versus normal brain	Down	Ctgf	4672	-8.333133	0.081227	0	0	0.625517

LGA versus normal brain	Down	Rap1gds1	13518	-8.331519	0.053804	0	0	0.732923
LGA versus normal brain	Down	A330049M08Rik	1445	-8.328826	0.062848	0	0	0.695705
LGA versus normal brain	Down	Fam65b	6328	-8.326667	0.061046	0	0	0.703047
LGA versus normal brain	Down	Tchh	15942	-8.323226	0.113765	0	0	0.518748
LGA versus normal brain	Down	Ehd3	5767	-8.322545	0.0783	0	0	0.636549
LGA versus normal brain	Down	Tomm70a	16535	-8.311385	0.039488	0	0	0.796527
LGA versus normal brain	Down	Fmod	6630	-8.307093	0.107593	0	0	0.5382
LGA versus normal brain	Down	Apbb3	2284	-8.294144	0.061763	0	0	0.701117
LGA versus normal brain	Down	Mapre2	9795	-8.290694	0.071313	0	0	0.663775
LGA versus normal brain	Down	B4galt6	2824	-8.290041	0.077851	0	0	0.63932
LGA versus normal brain	Down	Gm10914	7113	-8.285936	0.091134	0	0	0.592493
LGA versus normal brain	Down	Plcx2	12593	-8.284349	0.081217	0	0	0.627276
LGA versus normal brain	Down	Tspan5	16798	-8.284204	0.042713	0	0	0.782497
LGA versus normal brain	Down	Syt7	15768	-8.283253	0.064026	0	0	0.69239
LGA versus normal brain	Down	Olfr745	11759	-8.279885	0.076921	0	0	0.643096
LGA versus normal brain	Down	Slc25a44	14849	-8.276694	0.047393	0	0	0.761937
LGA versus normal brain	Down	Prickle1	12986	-8.276408	0.07336	0	0	0.656488
LGA versus normal brain	Down	Abca7	1575	-8.274854	0.08384	0	0	0.618237
LGA versus normal brain	Down	BC037034	2958	-8.267058	0.049071	0	0	0.754884
LGA versus normal brain	Down	Tbcc	15887	-8.266525	0.034628	0	0	0.820031
LGA versus normal brain	Down	Spryd3	15417	-8.265413	0.073152	0	0	0.657638
LGA versus normal brain	Down	Fkrp	6600	-8.264617	0.060291	0	0	0.707951
LGA versus normal brain	Down	Rnft2	13949	-8.255343	0.056718	0	0	0.722853
LGA versus normal brain	Down	Crebl2	4551	-8.250365	0.067225	0	0	0.680831
LGA versus normal brain	Down	Ica1	8321	-8.249846	0.06319	0	0	0.696741
LGA versus normal brain	Down	Smg7	15120	-8.225836	0.029506	0	0	0.845155
LGA versus normal brain	Down	Tspan13	16787	-8.224132	0.092169	0	0	0.591311
LGA versus normal brain	Down	Terf2ip	16008	-8.214794	0.054454	0	0	0.733398
LGA versus normal brain	Down	Arhgef9	2428	-8.213854	0.072685	0	0	0.661115
LGA versus normal brain	Down	Wac	17416	-8.211896	0.040538	0	0	0.793942

LGA versus normal brain	Down	Tmem41a	16366	-8.209917	0.046467	0	0	0.767643
LGA versus normal brain	Down	Wdr37	17463	-8.199571	0.045641	0	0	0.771512
LGA versus normal brain	Down	Prkaa2	12993	-8.19296	0.052613	0	0	0.741719
LGA versus normal brain	Down	Prkg1	13019	-8.190365	0.096975	0	0	0.57664
LGA versus normal brain	Down	Tmx4	16452	-8.183888	0.075623	0	0	0.651171
LGA versus normal brain	Down	Kif26b	8933	-8.167232	0.046447	0	0	0.768787
LGA versus normal brain	Down	Npy5r	11034	-8.166729	0.113777	0	0	0.525153
LGA versus normal brain	Down	Ndfip1	10703	-8.163252	0.053025	0	0	0.740795
LGA versus normal brain	Down	2900052N01Rik	707	-8.154873	0.095778	0	0	0.581941
LGA versus normal brain	Down	Atp1b1	2628	-8.13789	0.093708	0	0	0.58944
LGA versus normal brain	Down	6430548M08Rik	1207	-8.137665	0.070757	0	0	0.670917
LGA versus normal brain	Down	Sema3f	14416	-8.135946	0.054096	0	0	0.737072
LGA versus normal brain	Down	Epb4.1l1	5930	-8.135614	0.079582	0	0	0.63841
LGA versus normal brain	Down	Plekha2	12605	-8.135034	0.050547	0	0	0.751996
LGA versus normal brain	Down	Map3k12	9754	-8.134599	0.050478	0	0	0.752299
LGA versus normal brain	Down	Tyrp1	16954	-8.131431	0.093331	0	0	0.59094
LGA versus normal brain	Down	Tmem180	16306	-8.125506	0.044024	0	0	0.7804
LGA versus normal brain	Down	Tmem151a	16279	-8.125106	0.095444	0	0	0.584189
LGA versus normal brain	Down	Proca1	13050	-8.120438	0.0993	0	0	0.571824
LGA versus normal brain	Down	Bin1	3079	-8.120231	0.050483	0	0	0.752656
LGA versus normal brain	Down	Nupl1	11190	-8.119588	0.042454	0	0	0.787468
LGA versus normal brain	Down	Deptor	5202	-8.118927	0.099058	0	0	0.572662
LGA versus normal brain	Down	Mrps5	10324	-8.115531	0.044013	0	0	0.780684
LGA versus normal brain	Down	Slc41a2	14963	-8.111607	0.057523	0	0	0.723668
LGA versus normal brain	Down	Abl2	1629	-8.110629	0.085231	0	0	0.619307
LGA versus normal brain	Down	Wisp1	17539	-8.10276	0.112092	0	0	0.53283
LGA versus normal brain	Down	Cbfa2t3	3514	-8.10217	0.125212	0	0	0.495005
LGA versus normal brain	Down	Smyd2	15142	-8.099884	0.052961	0	0	0.742789
LGA versus normal brain	Down	Prkacb	12997	-8.097358	0.066655	0	0	0.687901
LGA versus normal brain	Down	Atp6v0d1	2665	-8.096802	0.043701	0	0	0.782498

LGA versus normal brain	Down	Armcx3	2473	-8.095793	0.043546	0	0	0.783202
LGA versus normal brain	Down	Ush1g	17147	-8.090312	0.070755	0	0	0.672482
LGA versus normal brain	Down	Sema3e	14415	-8.083717	0.085432	0	0	0.619594
LGA versus normal brain	Down	Dctn6	5090	-8.081719	0.046726	0	0	0.769704
LGA versus normal brain	Down	Evl	6060	-8.077865	0.062776	0	0	0.703637
LGA versus normal brain	Down	Baz2a	2884	-8.077553	0.061821	0	0	0.707419
LGA versus normal brain	Down	Ipo13	8591	-8.072232	0.05995	0	0	0.715027
LGA versus normal brain	Down	Darc	5027	-8.070908	0.073076	0	0	0.664439
LGA versus normal brain	Down	Klhl18	9002	-8.067448	0.036385	0	0	0.8159
LGA versus normal brain	Down	Dgkd	5221	-8.050419	0.061509	0	0	0.709475
LGA versus normal brain	Down	Chmp2b	4095	-8.042801	0.057809	0	0	0.724499
LGA versus normal brain	Down	Setd4	14530	-8.039385	0.064035	0	0	0.699887
LGA versus normal brain	Down	Ankrd50	2208	-8.030483	0.09445	0	0	0.59112
LGA versus normal brain	Down	Selm	14408	-8.028467	0.096797	0	0	0.583527
LGA versus normal brain	Down	Phldb1	12415	-8.02511	0.055941	0	0	0.732586
LGA versus normal brain	Down	Zkscan14	18139	-8.016221	0.055641	0	0	0.734061
LGA versus normal brain	Down	Atg16l1	2590	-8.013374	0.059901	0	0	0.716973
LGA versus normal brain	Down	A930038C07Rik	1543	-8.012721	0.06764	0	0	0.686827
LGA versus normal brain	Down	Egln3	5758	-8.011347	0.061028	0	0	0.712558
LGA versus normal brain	Down	Dopey1	5443	-8.007227	0.05091	0	0	0.753852
LGA versus normal brain	Down	Tspan10	16784	-8.006526	0.110992	0	0	0.540116
LGA versus normal brain	Down	Mark1	9812	-8.005904	0.075285	0	0	0.658508
LGA versus normal brain	Down	Armcx1	2471	-8.003801	0.09484	0	0	0.590871
LGA versus normal brain	Down	Rab12	13387	-8.002665	0.036382	0	0	0.817247
LGA versus normal brain	Down	Txndc11	16932	-8.001486	0.03092	0	0	0.842408
LGA versus normal brain	Down	Rspo3	14133	-7.999499	0.092414	0	0	0.599045
LGA versus normal brain	Down	Pla2g6	12563	-7.992458	0.049759	0	0	0.759068
LGA versus normal brain	Down	3110057O12Rik	747	-7.981806	0.052172	0	0	0.749278
LGA versus normal brain	Down	Alk	2080	-7.979834	0.101562	0	0	0.570205
LGA versus normal brain	Down	ErbB3	5982	-7.97663	0.031779	0	0	0.838863

LGA versus normal brain	Down	Kcnab3	8790	-7.975942	0.066732	0	0	0.691474
LGA versus normal brain	Down	Hmgcll1	8110	-7.97576	0.06947	0	0	0.681094
LGA versus normal brain	Down	Slc6a6	15013	-7.972678	0.086578	0	0	0.619742
LGA versus normal brain	Down	Dok3	5436	-7.970527	0.076662	0	0	0.654728
LGA versus normal brain	Down	Arhgef15	2412	-7.965539	0.07164	0	0	0.673311
LGA versus normal brain	Down	Vdr	17254	-7.965073	0.076199	0	0	0.656591
LGA versus normal brain	Down	Numb	11167	-7.95577	0.038525	0	0	0.808603
LGA versus normal brain	Down	Btbd2	3188	-7.952137	0.038708	0	0	0.807867
LGA versus normal brain	Down	Csnk1g1	4628	-7.950725	0.047093	0	0	0.771415
LGA versus normal brain	Down	Trak2	16604	-7.950311	0.058697	0	0	0.723637
LGA versus normal brain	Down	Dnajc30	5386	-7.946636	0.032513	0	0	0.836032
LGA versus normal brain	Down	Parp6	12075	-7.932859	0.065438	0	0	0.6978
LGA versus normal brain	Down	Fam70a	6333	-7.931433	0.061454	0	0	0.713302
LGA versus normal brain	Down	Scoc	14325	-7.928258	0.057442	0	0	0.729299
LGA versus normal brain	Down	Stx3	15641	-7.92595	0.037855	0	0	0.812232
LGA versus normal brain	Down	Igsf3	8432	-7.921636	0.098272	0	0	0.582983
LGA versus normal brain	Down	Nfil3	10828	-7.918417	0.091121	0	0	0.606453
LGA versus normal brain	Down	Ghitm	6996	-7.917685	0.042597	0	0	0.791539
LGA versus normal brain	Down	Rufy2	14160	-7.917259	0.06877	0	0	0.685642
LGA versus normal brain	Down	Grb14	7677	-7.911089	0.068803	0	0	0.685721
LGA versus normal brain	Down	Klhl8	9023	-7.910227	0.05449	0	0	0.741733
LGA versus normal brain	Down	Krt222	9090	-7.909086	0.087352	0	0	0.619477
LGA versus normal brain	Down	Lmtk2	9376	-7.905735	0.092117	0	0	0.603634
LGA versus normal brain	Down	Zfand5	17773	-7.901581	0.053593	0	0	0.745628
LGA versus normal brain	Down	Bean1	3049	-7.899088	0.079047	0	0	0.648691
LGA versus normal brain	Down	BC057022	2980	-7.894846	0.066081	0	0	0.696549
LGA versus normal brain	Down	Hprt	8205	-7.892334	0.084347	0	0	0.630385
LGA versus normal brain	Down	Setd7	14533	-7.89104	0.063674	0	0	0.705906
LGA versus normal brain	Down	Cited4	4172	-7.890139	0.078703	0	0	0.650229
LGA versus normal brain	Down	Rad23b	13467	-7.88909	0.045856	0	0	0.778213

LGA versus normal brain	Down	Cox5b	4473	-7.888921	0.048712	0	0	0.766157
LGA versus normal brain	Down	Plekhm3	12628	-7.884476	0.034963	0	0	0.826071
LGA versus normal brain	Down	Snx14	15212	-7.876232	0.038047	0	0	0.812442
LGA versus normal brain	Down	Alx3	2105	-7.871299	0.069448	0	0	0.684611
LGA versus normal brain	Down	Usp3	17172	-7.870881	0.068572	0	0	0.687902
LGA versus normal brain	Down	Palm2	12024	-7.868996	0.106177	0	0	0.560386
LGA versus normal brain	Down	BC024659	2937	-7.865209	0.082742	0	0	0.636936
LGA versus normal brain	Down	Ttbk2	16822	-7.863768	0.051645	0	0	0.754647
LGA versus normal brain	Down	Mfn2	10019	-7.856126	0.08152	0	0	0.64152
LGA versus normal brain	Down	Cd47	3790	-7.851425	0.052053	0	0	0.753307
LGA versus normal brain	Down	Gabra3	6814	-7.842855	0.070467	0	0	0.681761
LGA versus normal brain	Down	Appl1	2335	-7.841077	0.035171	0	0	0.826003
LGA versus normal brain	Down	Nipal2	10878	-7.84086	0.076232	0	0	0.660795
LGA versus normal brain	Down	Steap2	15579	-7.840394	0.046862	0	0	0.775168
LGA versus normal brain	Down	Pclo	12165	-7.839118	0.081997	0	0	0.640474
LGA versus normal brain	Down	Yars2	17626	-7.838764	0.02941	0	0	0.852316
LGA versus normal brain	Down	Pwp2	13337	-7.837325	0.035059	0	0	0.826583
LGA versus normal brain	Down	Ppt2	12942	-7.833046	0.03299	0	0	0.836007
LGA versus normal brain	Down	Akap8l	2014	-7.82933	0.066685	0	0	0.696358
LGA versus normal brain	Down	ATP6	2658	-7.828071	0.058829	0	0	0.726726
LGA versus normal brain	Down	Trim44	16675	-7.825051	0.059427	0	0	0.724461
LGA versus normal brain	Down	Dcn	5076	-7.824636	0.120977	0	0	0.518854
LGA versus normal brain	Down	Mypop	10564	-7.824142	0.074524	0	0	0.667535
LGA versus normal brain	Down	Ankrd29	2191	-7.823321	0.066033	0	0	0.699019
LGA versus normal brain	Down	Fam65a	6327	-7.817669	0.080424	0	0	0.646745
LGA versus normal brain	Down	Rbp7	13635	-7.809569	0.090518	0	0	0.612631
LGA versus normal brain	Down	Amacr	2110	-7.809117	0.036304	0	0	0.821593
LGA versus normal brain	Down	Nacad	10600	-7.804731	0.063471	0	0	0.709378
LGA versus normal brain	Down	H2-Q1	7861	-7.803826	0.128323	0	0	0.499513
LGA versus normal brain	Down	Pacsin2	11998	-7.800065	0.066862	0	0	0.696634

LGA versus normal brain	Down	Gpr85	7638	-7.797741	0.077829	0	0	0.656612
LGA versus normal brain	Down	Prg4	12983	-7.797418	0.093497	0	0	0.603306
LGA versus normal brain	Down	Pak1	12015	-7.794743	0.079214	0	0	0.651821
LGA versus normal brain	Down	Col13a1	4374	-7.794171	0.080317	0	0	0.647967
LGA versus normal brain	Down	9630001P10Rik	1372	-7.792267	0.073612	0	0	0.671936
LGA versus normal brain	Down	Cnst	4341	-7.78689	0.060622	0	0	0.720938
LGA versus normal brain	Down	Wdr59	17479	-7.783472	0.050994	0	0	0.759482
LGA versus normal brain	Down	Uso1	17151	-7.77989	0.036243	0	0	0.822471
LGA versus normal brain	Down	Cds1	3937	-7.776377	0.08062	0	0	0.647552
LGA versus normal brain	Down	Lrrc24	9517	-7.771095	0.069556	0	0	0.687519
LGA versus normal brain	Down	Strbp	15624	-7.769865	0.053011	0	0	0.75164
LGA versus normal brain	Down	Slc2a5	14884	-7.762938	0.096443	0	0	0.595147
LGA versus normal brain	Down	2310046A06Rik	514	-7.762783	0.065743	0	0	0.702053
LGA versus normal brain	Down	Mef2d	9951	-7.762434	0.050411	0	0	0.762436
LGA versus normal brain	Down	Supt6h	15690	-7.761858	0.059975	0	0	0.724212
LGA versus normal brain	Down	Rnf113a1	13876	-7.759607	0.047276	0	0	0.775479
LGA versus normal brain	Down	Chrna2	4119	-7.758547	0.058923	0	0	0.72842
LGA versus normal brain	Down	4921507P07Rik	809	-7.756641	0.06301	0	0	0.712645
LGA versus normal brain	Down	Avpi1	2730	-7.75184	0.072529	0	0	0.677252
LGA versus normal brain	Down	Acot7	1694	-7.751547	0.08679	0	0	0.627305
LGA versus normal brain	Down	Syn3	15734	-7.751366	0.058403	0	0	0.730673
LGA versus normal brain	Down	Ryr3	14189	-7.746897	0.05794	0	0	0.732622
LGA versus normal brain	Down	Ube2q1	17004	-7.746268	0.037586	0	0	0.817249
LGA versus normal brain	Down	Grsf1	7729	-7.743323	0.03961	0	0	0.808482
LGA versus normal brain	Down	Ept1	5975	-7.74274	0.029674	0	0	0.852776
LGA versus normal brain	Down	March11	9800	-7.74022	0.069001	0	0	0.690599
LGA versus normal brain	Down	2310057M21Rik	523	-7.737921	0.047271	0	0	0.776051
LGA versus normal brain	Down	Ccdc92	3659	-7.734166	0.076489	0	0	0.663616
LGA versus normal brain	Down	Prkca	13004	-7.733444	0.075115	0	0	0.668547
LGA versus normal brain	Down	Prss53	13136	-7.733174	0.05283	0	0	0.753384

LGA versus normal brain	Down	Cyfp2	4779	-7.729828	0.061019	0	0	0.72113
LGA versus normal brain	Down	Npy1r	11033	-7.728783	0.093675	0	0	0.60542
LGA versus normal brain	Down	Chmp7	4101	-7.728741	0.030793	0	0	0.847924
LGA versus normal brain	Down	Prrt3	13110	-7.726481	0.065821	0	0	0.702921
LGA versus normal brain	Down	Shisa9	14652	-7.721198	0.074612	0	0	0.670777
LGA versus normal brain	Down	Pnrc1	12708	-7.7093	0.058858	0	0	0.730142
LGA versus normal brain	Down	Lrch1	9475	-7.708801	0.068453	0	0	0.693665
LGA versus normal brain	Down	Dusp14	5541	-7.707941	0.08896	0	0	0.621706
LGA versus normal brain	Down	Slc24a3	14809	-7.706827	0.073838	0	0	0.674057
LGA versus normal brain	Down	Gga3	6981	-7.705657	0.060766	0	0	0.722846
LGA versus normal brain	Down	Fam3a	6296	-7.704974	0.028079	0	0	0.860742
LGA versus normal brain	Down	Klf16	8974	-7.704075	0.058828	0	0	0.730413
LGA versus normal brain	Down	Ptprk	13300	-7.700587	0.031618	0	0	0.844706
LGA versus normal brain	Down	5730403B10Rik	1109	-7.699979	0.041307	0	0	0.802146
LGA versus normal brain	Down	Aph1c	2294	-7.699456	0.091358	0	0	0.61412
LGA versus normal brain	Down	Asb13	2523	-7.698616	0.038899	0	0	0.812553
LGA versus normal brain	Down	Cpeb1	4496	-7.696189	0.096605	0	0	0.597292
LGA versus normal brain	Down	Nkrf	10900	-7.690044	0.05749	0	0	0.736064
LGA versus normal brain	Down	Slc38a2	14939	-7.686994	0.049158	0	0	0.769569
LGA versus normal brain	Down	Bbs5	2898	-7.684531	0.068365	0	0	0.694788
LGA versus normal brain	Down	Entpd3	5919	-7.680281	0.115565	0	0	0.540522
LGA versus normal brain	Down	Dip2c	5277	-7.679495	0.078019	0	0	0.660146
LGA versus normal brain	Down	Ngfrap1	10852	-7.675597	0.050531	0	0	0.764263
LGA versus normal brain	Down	Mtap1a	10378	-7.675083	0.070456	0	0	0.687411
LGA versus normal brain	Down	Dgke	5222	-7.670892	0.075186	0	0	0.670475
LGA versus normal brain	Down	Cacna2d1	3362	-7.670146	0.095616	0	0	0.601489
LGA versus normal brain	Down	App	2333	-7.667023	0.071926	0	0	0.68233
LGA versus normal brain	Down	Tmem64	16391	-7.664168	0.051597	0	0	0.760252
LGA versus normal brain	Down	Zbtb7a	17702	-7.655281	0.065756	0	0	0.705452
LGA versus normal brain	Down	Atp5g1	2647	-7.654106	0.051568	0	0	0.760642

LGA versus normal brain	Down	Zfp523	17933	-7.651687	0.056935	0	0	0.73936
LGA versus normal brain	Down	Orai2	11890	-7.64826	0.060664	0	0	0.724986
LGA versus normal brain	Down	Rab3gap2	13424	-7.647851	0.051016	0	0	0.763045
LGA versus normal brain	Down	Fam110b	6163	-7.637202	0.076009	0	0	0.668735
LGA versus normal brain	Down	Farp2	6384	-7.636408	0.050338	0	0	0.766098
LGA versus normal brain	Down	Med16	9927	-7.63349	0.0572	0	0	0.738854
LGA versus normal brain	Down	Pitpna	12510	-7.6333	0.04748	0	0	0.777854
LGA versus normal brain	Down	Nr6a1	11057	-7.632658	0.076898	0	0	0.665757
LGA versus normal brain	Down	Ap4s1	2276	-7.631853	0.041762	0	0	0.801779
LGA versus normal brain	Down	Fabp3	6130	-7.614589	0.106197	0	0	0.570919
LGA versus normal brain	Down	Atp6v1d	2672	-7.614436	0.069542	0	0	0.692783
LGA versus normal brain	Down	B230337E12Rik	2787	-7.613838	0.091661	0	0	0.616473
LGA versus normal brain	Down	Ttc19	16831	-7.61341	0.060041	0	0	0.728441
LGA versus normal brain	Down	Ube2w	17012	-7.608726	0.048268	0	0	0.775256
LGA versus normal brain	Down	Epn1	5962	-7.608623	0.058076	0	0	0.736175
LGA versus normal brain	Down	Rnf150	13899	-7.603447	0.073228	0	0	0.679814
LGA versus normal brain	Down	Smtnl2	15136	-7.591068	0.114613	0	0	0.547134
LGA versus normal brain	Down	Scyl3	14341	-7.589163	0.04551	0	0	0.787099
LGA versus normal brain	Down	Rheb	13782	-7.587246	0.043527	0	0	0.795397
LGA versus normal brain	Down	Ppm1b	12852	-7.586352	0.038195	0	0	0.818039
LGA versus normal brain	Down	Tmem85	16405	-7.584679	0.045947	0	0	0.785405
LGA versus normal brain	Down	Grin1	7701	-7.58465	0.100166	0	0	0.590611
LGA versus normal brain	Down	2900056M20Rik	711	-7.582341	0.061697	0	0	0.723062
LGA versus normal brain	Down	Ttll11	16870	-7.57888	0.090394	0	0	0.62197
LGA versus normal brain	Up	Slc2a4	14883	27.42	0.12	0	0	10.46
LGA versus normal brain	Up	Rarres1	13534	26.60	0.10	0	0	6.76
LGA versus normal brain	Up	Nuf2	11163	26.58	0.12	0	0	8.50
LGA versus normal brain	Up	Ckap2	4174	26.57	0.13	0	0	10.52
LGA versus normal brain	Up	Pbk	12097	26.36	0.17	0	0	23.40
LGA versus normal brain	Up	Prc1	12954	26.02	0.12	0	0	8.19

LGA versus normal brain	Up	1190002F15Rik	87	25.70	0.13	0	0	9.83
LGA versus normal brain	Up	Mboat1	9854	25.02	0.10	0	0	6.16
LGA versus normal brain	Up	9630013D21Rik	1375	24.97	0.13	0	0	8.80
LGA versus normal brain	Up	Cdkn2c	3928	24.81	0.11	0	0	6.59
LGA versus normal brain	Up	Lxn	9615	24.76	0.06	0	0	2.86
LGA versus normal brain	Up	Cenpi	3978	24.30	0.14	0	0	9.81
LGA versus normal brain	Up	Figl1	6577	23.91	0.15	0	0	11.54
LGA versus normal brain	Up	Kif18a	8920	23.80	0.15	0	0	12.00
LGA versus normal brain	Up	Dhfr	5232	23.59	0.11	0	0	5.83
LGA versus normal brain	Up	Smc4	15108	23.56	0.08	0	0	3.43
LGA versus normal brain	Up	Tcf19	15933	23.55	0.08	0	0	3.76
LGA versus normal brain	Up	Esco2	6021	23.51	0.19	0	0	22.17
LGA versus normal brain	Up	2610021K21Rik	598	23.36	0.12	0	0	7.05
LGA versus normal brain	Up	Tyms-ps	16951	23.25	0.11	0	0	5.45
LGA versus normal brain	Up	Chaf1b	4052	23.03	0.11	0	0	5.85
LGA versus normal brain	Up	Aard	1556	23.01	0.08	0	0	3.86
LGA versus normal brain	Up	Nde1	10701	23.00	0.06	0	0	2.73
LGA versus normal brain	Up	Tyms	16950	22.76	0.08	0	0	3.72
LGA versus normal brain	Up	Cks2	4183	22.59	0.12	0	0	6.86
LGA versus normal brain	Up	Ckap2l	4175	22.44	0.16	0	0	12.83
LGA versus normal brain	Up	Neil3	10775	22.28	0.12	0	0	6.64
LGA versus normal brain	Up	Rad51	13469	21.92	0.12	0	0	5.89
LGA versus normal brain	Up	Ccdc34	3605	21.86	0.09	0	0	3.82
LGA versus normal brain	Up	Sept10	14445	21.85	0.06	0	0	2.66
LGA versus normal brain	Up	Hmgb2	8107	21.81	0.11	0	0	5.53
LGA versus normal brain	Up	Pipox	12506	21.79	0.07	0	0	2.83
LGA versus normal brain	Up	Psph	13215	21.77	0.09	0	0	3.75
LGA versus normal brain	Up	Uhrf1	17083	21.77	0.15	0	0	9.84
LGA versus normal brain	Up	Pcna	12170	21.74	0.09	0	0	3.92
LGA versus normal brain	Up	Cdkn3	3930	21.73	0.11	0	0	5.62

LGA versus normal brain	Up	Cklf	4179	21.72	0.08	0	0	3.50
LGA versus normal brain	Up	Birc5	3083	21.58	0.12	0	0	6.10
LGA versus normal brain	Up	Zfp367	17877	21.36	0.08	0	0	3.13
LGA versus normal brain	Up	Ccnb1	3689	21.31	0.14	0	0	8.45
LGA versus normal brain	Up	Spc25	15330	21.26	0.16	0	0	9.99
LGA versus normal brain	Up	Ect2	5689	21.21	0.13	0	0	7.25
LGA versus normal brain	Up	Zwilch	18207	21.17	0.09	0	0	3.73
LGA versus normal brain	Up	Cenpk	3980	21.13	0.14	0	0	7.72
LGA versus normal brain	Up	Rpa2	13978	21.11	0.07	0	0	2.71
LGA versus normal brain	Up	Spink2	15369	21.04	0.16	0	0	9.61
LGA versus normal brain	Up	Nedd1	10765	20.90	0.07	0	0	2.64
LGA versus normal brain	Up	Kif23	8930	20.87	0.06	0	0	2.26
LGA versus normal brain	Up	Ccnb2	3691	20.84	0.08	0	0	3.00
LGA versus normal brain	Up	Gins1	7010	20.83	0.12	0	0	5.31
LGA versus normal brain	Up	Aurkb	2722	20.80	0.17	0	0	12.23
LGA versus normal brain	Up	Rbl1	13591	20.61	0.10	0	0	4.35
LGA versus normal brain	Up	2810442I21Rik	687	20.61	0.09	0	0	3.48
LGA versus normal brain	Up	Casc5	3482	20.60	0.16	0	0	9.57
LGA versus normal brain	Up	Fam64a	6326	20.55	0.10	0	0	4.16
LGA versus normal brain	Up	Cep55	4000	20.46	0.12	0	0	5.65
LGA versus normal brain	Up	Gas2l3	6880	20.40	0.10	0	0	4.13
LGA versus normal brain	Up	Chek1	4074	20.40	0.16	0	0	9.78
LGA versus normal brain	Up	Gja1	7021	20.38	0.08	0	0	2.89
LGA versus normal brain	Up	Cenph	3977	20.31	0.12	0	0	5.49
LGA versus normal brain	Up	Myb	10480	20.31	0.10	0	0	4.28
LGA versus normal brain	Up	Cdc20	3830	20.26	0.09	0	0	3.61
LGA versus normal brain	Up	Nusap1	11194	20.05	0.13	0	0	6.29
LGA versus normal brain	Up	Lrrc56	9542	19.97	0.10	0	0	4.18
LGA versus normal brain	Up	Fam111a	6165	19.95	0.12	0	0	4.97
LGA versus normal brain	Up	Ppm1m	12861	19.89	0.07	0	0	2.67

LGA versus normal brain	Up	Ncapg	10666	19.83	0.14	0	0	7.15
LGA versus normal brain	Up	Tpx2	16586	19.82	0.11	0	0	4.42
LGA versus normal brain	Up	Cdca8	3863	19.77	0.10	0	0	3.77
LGA versus normal brain	Up	Hells	7984	19.75	0.11	0	0	4.32
LGA versus normal brain	Up	D930014E17Rik	4986	19.71	0.05	0	0	2.05
LGA versus normal brain	Up	Top2a	16539	19.66	0.11	0	0	4.47
LGA versus normal brain	Up	Tacc3	15790	19.61	0.11	0	0	4.27
LGA versus normal brain	Up	Mcm6	9882	19.61	0.13	0	0	5.76
LGA versus normal brain	Up	Mns1	10157	19.45	0.13	0	0	6.15
LGA versus normal brain	Up	Mxd3	10473	19.42	0.11	0	0	4.28
LGA versus normal brain	Up	E2f7	5637	19.38	0.11	0	0	4.66
LGA versus normal brain	Up	Pich1	12588	19.33	0.11	0	0	4.52
LGA versus normal brain	Up	Melk	9965	19.26	0.13	0	0	6.06
LGA versus normal brain	Up	Ascl1	2537	19.19	0.10	0	0	3.57
LGA versus normal brain	Up	Kif4	8940	19.16	0.13	0	0	5.29
LGA versus normal brain	Up	Rad51l1	13472	19.14	0.09	0	0	3.46
LGA versus normal brain	Up	Nek2	10778	19.14	0.14	0	0	6.13
LGA versus normal brain	Up	Rad54l	13476	19.13	0.11	0	0	4.15
LGA versus normal brain	Up	Fam47e	6305	19.13	0.13	0	0	5.93
LGA versus normal brain	Up	Aif1l	1980	19.12	0.09	0	0	3.26
LGA versus normal brain	Up	E130303B06Rik	5610	19.11	0.04	0	0	1.81
LGA versus normal brain	Up	Gins2	7011	18.99	0.11	0	0	4.41
LGA versus normal brain	Up	Kntc1	9061	18.98	0.11	0	0	4.27
LGA versus normal brain	Up	Mis18bp1	10083	18.92	0.09	0	0	3.41
LGA versus normal brain	Up	Ncapg2	10667	18.92	0.12	0	0	4.63
LGA versus normal brain	Up	Ccna2	3688	18.91	0.13	0	0	5.79
LGA versus normal brain	Up	Gmnn	7450	18.80	0.10	0	0	3.77
LGA versus normal brain	Up	Tuba1c	16889	18.69	0.07	0	0	2.37
LGA versus normal brain	Up	Atad2	2569	18.67	0.11	0	0	3.91
LGA versus normal brain	Up	Hist1h2ak	8062	18.65	0.14	0	0	6.37

LGA versus normal brain	Up	Ucma	17058	18.65	0.12	0	0	4.62
LGA versus normal brain	Up	Hn1l	8128	18.64	0.09	0	0	3.05
LGA versus normal brain	Up	Kif20b	8926	18.63	0.13	0	0	5.11
LGA versus normal brain	Up	Dsn1	5510	18.59	0.10	0	0	3.57
LGA versus normal brain	Up	Ezh2	6102	18.56	0.11	0	0	4.20
LGA versus normal brain	Up	Rrm1	14103	18.55	0.08	0	0	2.92
LGA versus normal brain	Up	Cenpf	3976	18.54	0.14	0	0	5.94
LGA versus normal brain	Up	Hmmr	8121	18.53	0.11	0	0	3.92
LGA versus normal brain	Up	Tipin	16156	18.49	0.09	0	0	3.27
LGA versus normal brain	Up	Shcbp1	14641	18.44	0.14	0	0	6.05
LGA versus normal brain	Up	Prim2	12990	18.43	0.08	0	0	2.82
LGA versus normal brain	Up	Hist1h2aa	8056	18.42	0.09	0	0	3.22
LGA versus normal brain	Up	Fbxo5	6460	18.40	0.08	0	0	2.91
LGA versus normal brain	Up	Fanci	6376	18.40	0.13	0	0	5.45
LGA versus normal brain	Up	Kpna2	9063	18.36	0.07	0	0	2.44
LGA versus normal brain	Up	Sgol1	14586	18.34	0.09	0	0	3.02
LGA versus normal brain	Up	Hist1h2af	8060	18.32	0.13	0	0	4.90
LGA versus normal brain	Up	Kif20a	8925	18.32	0.12	0	0	4.84
LGA versus normal brain	Up	Sgol2	14587	18.30	0.13	0	0	5.18
LGA versus normal brain	Up	Racgap1	13461	18.21	0.10	0	0	3.44
LGA versus normal brain	Up	Depdc1b	5199	18.19	0.13	0	0	5.47
LGA versus normal brain	Up	Mcm4	9880	18.15	0.12	0	0	4.72
LGA versus normal brain	Up	Prdx4	12969	18.14	0.07	0	0	2.46
LGA versus normal brain	Up	Tcf7l2	15941	18.14	0.07	0	0	2.32
LGA versus normal brain	Up	Prim1	12989	18.13	0.09	0	0	3.00
LGA versus normal brain	Up	Mcm7	9883	18.07	0.09	0	0	3.00
LGA versus normal brain	Up	Cks1b	4182	18.03	0.11	0	0	3.93
LGA versus normal brain	Up	Echdc2	5679	18.01	0.08	0	0	2.72
LGA versus normal brain	Up	Brip1	3161	17.96	0.11	0	0	3.78
LGA versus normal brain	Up	Rrm2	14104	17.95	0.14	0	0	5.42

LGA versus normal brain	Up	Tmem98	16420	17.91	0.07	0	0	2.26
LGA versus normal brain	Up	Kif14	8916	17.90	0.09	0	0	3.14
LGA versus normal brain	Up	Pole3	12733	17.90	0.05	0	0	1.75
LGA versus normal brain	Up	Aurka	2720	17.89	0.07	0	0	2.41
LGA versus normal brain	Up	Hist1h2ai	8061	17.87	0.15	0	0	6.36
LGA versus normal brain	Up	Foxj1	6674	17.87	0.07	0	0	2.30
LGA versus normal brain	Up	Stx2	15640	17.87	0.05	0	0	1.97
LGA versus normal brain	Up	Pkmyt1	12537	17.85	0.07	0	0	2.30
LGA versus normal brain	Up	Exo1	6067	17.81	0.16	0	0	7.62
LGA versus normal brain	Up	Psmc3ip	13186	17.73	0.08	0	0	2.70
LGA versus normal brain	Up	Cdc6	3854	17.73	0.13	0	0	4.78
LGA versus normal brain	Up	Clspn	4269	17.68	0.14	0	0	5.63
LGA versus normal brain	Up	Plk1	12638	17.66	0.09	0	0	3.02
LGA versus normal brain	Up	Nek5	10781	17.61	0.14	0	0	5.70
LGA versus normal brain	Up	Rfc4	13718	17.59	0.09	0	0	3.00
LGA versus normal brain	Up	Bmper	3110	17.59	0.09	0	0	2.89
LGA versus normal brain	Up	Slbp	14726	17.58	0.08	0	0	2.58
LGA versus normal brain	Up	Ska1	14706	17.57	0.14	0	0	5.80
LGA versus normal brain	Up	Carhsp1	3472	17.55	0.06	0	0	2.15
LGA versus normal brain	Up	Mamdc2	9719	17.54	0.13	0	0	4.81
LGA versus normal brain	Up	Fancb	6370	17.51	0.07	0	0	2.22
LGA versus normal brain	Up	Asf1b	2541	17.49	0.08	0	0	2.56
LGA versus normal brain	Up	Cdt1	3940	17.48	0.14	0	0	5.56
LGA versus normal brain	Up	Psrc1	13217	17.40	0.13	0	0	5.07
LGA versus normal brain	Up	Gsg2	7743	17.35	0.12	0	0	4.00
LGA versus normal brain	Up	Pmp22	12679	17.34	0.08	0	0	2.61
LGA versus normal brain	Up	Cd9	3817	17.33	0.12	0	0	4.06
LGA versus normal brain	Up	Sox9	15284	17.33	0.08	0	0	2.54
LGA versus normal brain	Up	Cdca5	3860	17.32	0.10	0	0	3.31
LGA versus normal brain	Up	St14	15518	17.29	0.06	0	0	2.11

LGA versus normal brain	Up	Mcm2	9877	17.27	0.16	0	0	6.88
LGA versus normal brain	Up	Rfc5	13719	17.27	0.08	0	0	2.52
LGA versus normal brain	Up	Nfia	10825	17.26	0.06	0	0	1.97
LGA versus normal brain	Up	Cenpl	3981	17.23	0.09	0	0	3.10
LGA versus normal brain	Up	Cenpp	3985	17.20	0.08	0	0	2.57
LGA versus normal brain	Up	Gdpd2	6954	17.19	0.10	0	0	3.36
LGA versus normal brain	Up	Mtbp	10389	17.18	0.08	0	0	2.58
LGA versus normal brain	Up	Cdca2	3857	17.15	0.10	0	0	3.14
LGA versus normal brain	Up	Dek	5182	17.15	0.08	0	0	2.44
LGA versus normal brain	Up	Cenpm	3982	17.14	0.09	0	0	2.99
LGA versus normal brain	Up	Bub1	3206	17.10	0.10	0	0	3.11
LGA versus normal brain	Up	Topbp1	16543	17.10	0.11	0	0	3.65
LGA versus normal brain	Up	Ift80	8396	17.07	0.04	0	0	1.52
LGA versus normal brain	Up	Fanca	6369	17.06	0.09	0	0	2.89
LGA versus normal brain	Up	Cdc45	3852	17.03	0.12	0	0	3.96
LGA versus normal brain	Up	Trim59	16683	17.01	0.07	0	0	2.31
LGA versus normal brain	Up	Mcm5	9881	17.01	0.08	0	0	2.61
LGA versus normal brain	Up	Pask	12082	16.99	0.10	0	0	3.40
LGA versus normal brain	Up	Arl4c	2450	16.94	0.07	0	0	2.39
LGA versus normal brain	Up	2810417H13Rik	678	16.94	0.12	0	0	4.19
LGA versus normal brain	Up	Mki67	10087	16.93	0.16	0	0	6.42
LGA versus normal brain	Up	Kif11	8912	16.93	0.08	0	0	2.70
LGA versus normal brain	Up	Mlf1ip	10103	16.92	0.09	0	0	2.92
LGA versus normal brain	Up	2610020H08Rik	596	16.90	0.09	0	0	2.84
LGA versus normal brain	Up	Mcm3	9878	16.87	0.12	0	0	3.94
LGA versus normal brain	Up	Emp1	5885	16.82	0.09	0	0	2.89
LGA versus normal brain	Up	Trip13	16702	16.80	0.11	0	0	3.74
LGA versus normal brain	Up	E2f8	5638	16.79	0.13	0	0	4.31
LGA versus normal brain	Up	2010317E24Rik	433	16.78	0.16	0	0	6.67
LGA versus normal brain	Up	Dna2	5338	16.77	0.10	0	0	3.25

LGA versus normal brain	Up	Mms22l	10153	16.77	0.12	0	0	4.09
LGA versus normal brain	Up	Ptplad2	13272	16.77	0.06	0	0	2.07
LGA versus normal brain	Up	Phf19	12393	16.76	0.12	0	0	3.99
LGA versus normal brain	Up	Tmpo	16429	16.74	0.08	0	0	2.46
LGA versus normal brain	Up	Fam54a	6313	16.73	0.13	0	0	4.30
LGA versus normal brain	Up	Rab13	13388	16.73	0.09	0	0	2.97
LGA versus normal brain	Up	Zfp503	17922	16.73	0.13	0	0	4.77
LGA versus normal brain	Up	Tk1	16163	16.71	0.11	0	0	3.66
LGA versus normal brain	Up	Rpa1	13977	16.69	0.07	0	0	2.36
LGA versus normal brain	Up	Pole2	12732	16.66	0.12	0	0	4.03
LGA versus normal brain	Up	Aspm	2556	16.64	0.13	0	0	4.24
LGA versus normal brain	Up	Icosl	8330	16.63	0.10	0	0	3.11
LGA versus normal brain	Up	Rnaseh2b	13862	16.63	0.08	0	0	2.39
LGA versus normal brain	Up	Gemin8	6962	16.62	0.06	0	0	2.01
LGA versus normal brain	Up	Armc3	2465	16.61	0.16	0	0	6.61
LGA versus normal brain	Up	Cdca3	3858	16.58	0.11	0	0	3.66
LGA versus normal brain	Up	Acot1	1686	16.53	0.13	0	0	4.52
LGA versus normal brain	Up	Naprt1	10633	16.52	0.08	0	0	2.39
LGA versus normal brain	Up	Ddit4l	5110	16.50	0.10	0	0	3.27
LGA versus normal brain	Up	E130306D19Rik	5613	16.47	0.10	0	0	3.15
LGA versus normal brain	Up	Rbbp8	13583	16.46	0.06	0	0	2.05
LGA versus normal brain	Up	Cep57l1	4002	16.45	0.04	0	0	1.50
LGA versus normal brain	Up	Phgdh	12405	16.40	0.05	0	0	1.86
LGA versus normal brain	Up	Iqcg	8606	16.39	0.13	0	0	4.21
LGA versus normal brain	Up	H2afv	7874	16.38	0.08	0	0	2.61
LGA versus normal brain	Up	Ccdc46	3614	16.37	0.06	0	0	2.05
LGA versus normal brain	Up	Katnal2	8771	16.37	0.10	0	0	3.08
LGA versus normal brain	Up	Brca2	3146	16.35	0.07	0	0	2.29
LGA versus normal brain	Up	C330027C09Rik	3305	16.34	0.11	0	0	3.59
LGA versus normal brain	Up	Tmem194	16321	16.33	0.08	0	0	2.56

LGA versus normal brain	Up	4930422G04Rik	841	16.33	0.07	0	0	2.23
LGA versus normal brain	Up	Plk4	12642	16.30	0.13	0	0	4.14
LGA versus normal brain	Up	Ccne2	3698	16.25	0.11	0	0	3.39
LGA versus normal brain	Up	Itgb3bp	8688	16.23	0.07	0	0	2.25
LGA versus normal brain	Up	Prkcdbp	13008	16.22	0.05	0	0	1.77
LGA versus normal brain	Up	Troap	16721	16.21	0.08	0	0	2.47
LGA versus normal brain	Up	Pold1	12725	16.18	0.08	0	0	2.49
LGA versus normal brain	Up	Cdca7	3861	16.15	0.10	0	0	3.06
LGA versus normal brain	Up	Lig1	9311	16.14	0.08	0	0	2.40
LGA versus normal brain	Up	Mcm10	9876	16.12	0.13	0	0	4.18
LGA versus normal brain	Up	Smc2	15106	16.11	0.10	0	0	3.14
LGA versus normal brain	Up	Nek8	10784	16.11	0.08	0	0	2.53
LGA versus normal brain	Up	Oat	11220	16.08	0.05	0	0	1.78
LGA versus normal brain	Up	Depdc1a	5198	16.07	0.15	0	0	5.41
LGA versus normal brain	Up	Soat1	15236	16.07	0.07	0	0	2.11
LGA versus normal brain	Up	Oip5	11258	16.03	0.10	0	0	2.97
LGA versus normal brain	Up	Dut	5558	16.02	0.07	0	0	2.06
LGA versus normal brain	Up	BC055324	2978	16.02	0.11	0	0	3.39
LGA versus normal brain	Up	Chek2	4075	15.99	0.09	0	0	2.83
LGA versus normal brain	Up	Cenpe	3975	15.99	0.14	0	0	4.79
LGA versus normal brain	Up	Zfp36l1	17879	15.98	0.08	0	0	2.41
LGA versus normal brain	Up	Haus4	7913	15.96	0.09	0	0	2.84
LGA versus normal brain	Up	Cntln	4345	15.96	0.07	0	0	2.14
LGA versus normal brain	Up	Syce2	15724	15.96	0.08	0	0	2.48
LGA versus normal brain	Up	Rfc2	13716	15.95	0.05	0	0	1.74
LGA versus normal brain	Up	Hist1h1b	8051	15.94	0.17	0	0	6.73
LGA versus normal brain	Up	Hc	7932	15.92	0.10	0	0	3.10
LGA versus normal brain	Up	C730049O14Rik	3329	15.89	0.07	0	0	2.24
LGA versus normal brain	Up	Cd109	3737	15.88	0.10	0	0	3.03
LGA versus normal brain	Up	Chaf1a	4051	15.87	0.09	0	0	2.68

LGA versus normal brain	Up	Kif22	8929	15.86	0.09	0	0	2.75
LGA versus normal brain	Up	Ube2c	16983	15.85	0.11	0	0	3.32
LGA versus normal brain	Up	Col9a3	4409	15.79	0.09	0	0	2.77
LGA versus normal brain	Up	Fbln7	6409	15.77	0.10	0	0	2.94
LGA versus normal brain	Up	Fam33a	6291	15.76	0.06	0	0	1.89
LGA versus normal brain	Up	Stil	15583	15.73	0.08	0	0	2.48
LGA versus normal brain	Up	Rad51ap1	13470	15.73	0.12	0	0	3.90
LGA versus normal brain	Up	D330028D13Rik	4932	15.71	0.09	0	0	2.67
LGA versus normal brain	Up	Slc43a1	14965	15.68	0.11	0	0	3.33
LGA versus normal brain	Up	Rarres2	13535	15.68	0.11	0	0	3.21
LGA versus normal brain	Up	Gen1	6963	15.68	0.08	0	0	2.28
LGA versus normal brain	Up	Cenpn	3983	15.68	0.10	0	0	2.88
LGA versus normal brain	Up	Hist2h2ac	8077	15.64	0.09	0	0	2.75
LGA versus normal brain	Up	Pole	12731	15.63	0.10	0	0	3.00
LGA versus normal brain	Up	Ropn1l	13968	15.63	0.09	0	0	2.66
LGA versus normal brain	Up	Spc24	15329	15.62	0.14	0	0	4.46
LGA versus normal brain	Up	Haus1	7910	15.59	0.06	0	0	1.90
LGA versus normal brain	Up	Plin3	12635	15.49	0.05	0	0	1.74
LGA versus normal brain	Up	Kif15	8917	15.48	0.12	0	0	3.73
LGA versus normal brain	Up	Nsmce1	11094	15.48	0.05	0	0	1.69
LGA versus normal brain	Up	Dscc1	5501	15.43	0.11	0	0	3.11
LGA versus normal brain	Up	Cenpq	3986	15.40	0.12	0	0	3.42
LGA versus normal brain	Up	Kifc1	8948	15.33	0.13	0	0	3.94
LGA versus normal brain	Up	Thbs4	16094	15.32	0.12	0	0	3.47
LGA versus normal brain	Up	Galnt10	6845	15.30	0.06	0	0	1.99
LGA versus normal brain	Up	Dapp1	5026	15.28	0.12	0	0	3.57
LGA versus normal brain	Up	Dnali1	5397	15.27	0.12	0	0	3.71
LGA versus normal brain	Up	Spata6	15322	15.25	0.07	0	0	2.04
LGA versus normal brain	Up	Mad2l1	9677	15.25	0.12	0	0	3.45
LGA versus normal brain	Up	Sncaip	15161	15.25	0.06	0	0	1.94

LGA versus normal brain	Up	Tspan6	16799	15.22	0.06	0	0	1.95
LGA versus normal brain	Up	4930547N16Rik	948	15.21	0.11	0	0	3.30
LGA versus normal brain	Up	Itgb5	8690	15.17	0.07	0	0	2.06
LGA versus normal brain	Up	Athl1	2602	15.17	0.08	0	0	2.31
LGA versus normal brain	Up	4632434I11Rik	776	15.15	0.14	0	0	4.56
LGA versus normal brain	Up	Nsl1	11092	15.14	0.10	0	0	2.74
LGA versus normal brain	Up	Gtse1	7808	15.12	0.10	0	0	2.97
LGA versus normal brain	Up	Gemin6	6960	15.12	0.07	0	0	2.09
LGA versus normal brain	Up	Gm8096	7398	15.11	0.07	0	0	2.02
LGA versus normal brain	Up	Timeless	16137	15.07	0.11	0	0	3.02
LGA versus normal brain	Up	Ncaph	10668	15.02	0.15	0	0	4.61
LGA versus normal brain	Up	Mybl1	10482	14.99	0.12	0	0	3.39
LGA versus normal brain	Up	BC048355	2962	14.98	0.10	0	0	2.84
LGA versus normal brain	Up	6720463M24Rik	1227	14.96	0.09	0	0	2.66
LGA versus normal brain	Up	Tmem47	16372	14.95	0.06	0	0	1.80
LGA versus normal brain	Up	Lhpp	9301	14.94	0.04	0	0	1.58
LGA versus normal brain	Up	Kif18b	8921	14.92	0.13	0	0	3.90
LGA versus normal brain	Up	Ccdc99	3664	14.89	0.09	0	0	2.60
LGA versus normal brain	Up	Gbp2	6905	14.89	0.11	0	0	3.10
LGA versus normal brain	Up	Gins4	7013	14.85	0.04	0	0	1.53
LGA versus normal brain	Up	Twsg1	16925	14.83	0.03	0	0	1.41
LGA versus normal brain	Up	Hmgn2	8115	14.83	0.09	0	0	2.60
LGA versus normal brain	Up	Tonsl	16536	14.82	0.08	0	0	2.19
LGA versus normal brain	Up	Trim30a	16664	14.79	0.15	0	0	4.59
LGA versus normal brain	Up	Kif2c	8936	14.79	0.10	0	0	2.83
LGA versus normal brain	Up	Col4a4	4394	14.77	0.08	0	0	2.28
LGA versus normal brain	Up	Casp7	3494	14.76	0.09	0	0	2.45
LGA versus normal brain	Up	Cchcr1	3665	14.74	0.07	0	0	2.14
LGA versus normal brain	Up	4933404M02Rik	1019	14.74	0.08	0	0	2.16
LGA versus normal brain	Up	Ttf2	16863	14.73	0.09	0	0	2.57

LGA versus normal brain	Up	Gtf3c5	7797	14.73	0.04	0	0	1.52
LGA versus normal brain	Up	Cenpj	3979	14.73	0.09	0	0	2.52
LGA versus normal brain	Up	Lair1	9161	14.68	0.05	0	0	1.71
LGA versus normal brain	Up	1700040L02Rik	290	14.67	0.08	0	0	2.33
LGA versus normal brain	Up	Ptma	13262	14.67	0.05	0	0	1.71
LGA versus normal brain	Up	Arhgap11a	2377	14.64	0.12	0	0	3.40
LGA versus normal brain	Up	Pola1	12722	14.61	0.12	0	0	3.39
LGA versus normal brain	Up	Ung	17113	14.61	0.10	0	0	2.78
LGA versus normal brain	Up	Ccdc96	3662	14.60	0.08	0	0	2.21
LGA versus normal brain	Up	Lrr1	9505	14.60	0.16	0	0	4.91
LGA versus normal brain	Up	Ptgr1	13250	14.59	0.07	0	0	2.00
LGA versus normal brain	Up	H2afx	7875	14.57	0.10	0	0	2.63
LGA versus normal brain	Up	Gas1	6877	14.55	0.09	0	0	2.39
LGA versus normal brain	Up	Eda2r	5691	14.55	0.12	0	0	3.33
LGA versus normal brain	Up	Ccdc138	3578	14.54	0.05	0	0	1.73
LGA versus normal brain	Up	Ppil6	12847	14.52	0.09	0	0	2.53
LGA versus normal brain	Up	Dtymk	5526	14.52	0.07	0	0	2.08
LGA versus normal brain	Up	2810408B13Rik	673	14.50	0.08	0	0	2.17
LGA versus normal brain	Up	Bcl2l12	3024	14.50	0.08	0	0	2.21
LGA versus normal brain	Up	Cenpa	3972	14.46	0.08	0	0	2.29
LGA versus normal brain	Up	D17H6S56E-5	4903	14.45	0.11	0	0	3.09
LGA versus normal brain	Up	Spag5	15304	14.44	0.14	0	0	3.97
LGA versus normal brain	Up	Mastl	9828	14.43	0.10	0	0	2.60
LGA versus normal brain	Up	Emp2	5886	14.42	0.10	0	0	2.84
LGA versus normal brain	Up	Ccdc61	3627	14.41	0.07	0	0	1.92
LGA versus normal brain	Up	Pycard	13346	14.38	0.12	0	0	3.38
LGA versus normal brain	Up	Efhb	5730	14.34	0.17	0	0	5.18
LGA versus normal brain	Up	Ttk	16866	14.33	0.12	0	0	3.23
LGA versus normal brain	Up	Tead2	15986	14.33	0.08	0	0	2.27
LGA versus normal brain	Up	Dnajc9	5394	14.32	0.06	0	0	1.90

LGA versus normal brain	Up	2700094K13Rik	643	14.31	0.09	0	0	2.35
LGA versus normal brain	Up	Pon3	12780	14.29	0.10	0	0	2.72
LGA versus normal brain	Up	Plk1s1	12639	14.20	0.04	0	0	1.53
LGA versus normal brain	Up	E2f1	5631	14.17	0.08	0	0	2.30
LGA versus normal brain	Up	D2ErtD750e	4927	14.16	0.11	0	0	2.82
LGA versus normal brain	Up	Trim30d	16666	14.15	0.15	0	0	4.29
LGA versus normal brain	Up	Cenpw	3989	14.14	0.10	0	0	2.70
LGA versus normal brain	Up	G2e3	6793	14.14	0.08	0	0	2.09
LGA versus normal brain	Up	1110034A24Rik	64	14.12	0.06	0	0	1.80
LGA versus normal brain	Up	Gli3	7052	14.12	0.05	0	0	1.56
LGA versus normal brain	Up	Dtl	5516	14.09	0.12	0	0	3.18
LGA versus normal brain	Up	2610039C10Rik	612	14.04	0.08	0	0	2.20
LGA versus normal brain	Up	F630043A04Rik	6117	14.03	0.09	0	0	2.39
LGA versus normal brain	Up	Gjc1	7032	14.02	0.07	0	0	2.04
LGA versus normal brain	Up	Lin9	9334	14.01	0.06	0	0	1.82
LGA versus normal brain	Up	Chtf18	4145	13.99	0.08	0	0	2.24
LGA versus normal brain	Up	Ugp2	17073	13.98	0.05	0	0	1.56
LGA versus normal brain	Up	Cenpo	3984	13.97	0.07	0	0	1.91
LGA versus normal brain	Up	Hist1h2ab	8057	13.97	0.15	0	0	4.20
LGA versus normal brain	Up	Eri1	6002	13.96	0.06	0	0	1.83
LGA versus normal brain	Up	Lpar4	9456	13.96	0.08	0	0	2.21
LGA versus normal brain	Up	Lrdd	9479	13.92	0.06	0	0	1.82
LGA versus normal brain	Up	Mlf1	10102	13.92	0.16	0	0	4.66
LGA versus normal brain	Up	Trim56	16682	13.89	0.08	0	0	2.20
LGA versus normal brain	Up	Armc2	2464	13.88	0.10	0	0	2.52
LGA versus normal brain	Up	Idh2	8338	13.86	0.06	0	0	1.86
LGA versus normal brain	Up	Gpx7	7666	13.83	0.09	0	0	2.41
LGA versus normal brain	Up	Phkg1	12410	13.79	0.09	0	0	2.36
LGA versus normal brain	Up	Akr1c19	2029	13.77	0.07	0	0	2.01
LGA versus normal brain	Up	Cpne3	4507	13.77	0.06	0	0	1.78

LGA versus normal brain	Up	Wdhd1	17441	13.74	0.10	0	0	2.53
LGA versus normal brain	Up	Hacl1	7889	13.72	0.07	0	0	1.88
LGA versus normal brain	Up	Cyp39a1	4827	13.68	0.14	0	0	3.89
LGA versus normal brain	Up	Olfml2b	11265	13.68	0.08	0	0	2.06
LGA versus normal brain	Up	Rbm43	13617	13.67	0.05	0	0	1.56
LGA versus normal brain	Up	Igsf10	8429	13.67	0.12	0	0	3.04
LGA versus normal brain	Up	Foxm1	6680	13.65	0.12	0	0	3.04
LGA versus normal brain	Up	Haus8	7917	13.65	0.08	0	0	2.03
LGA versus normal brain	Up	Gna13	7458	13.65	0.08	0	0	2.08
LGA versus normal brain	Up	Mad2l2	9679	13.64	0.07	0	0	1.87
LGA versus normal brain	Up	Nfe2l2	10823	13.61	0.06	0	0	1.72
LGA versus normal brain	Up	Alg14	2073	13.60	0.05	0	0	1.54
LGA versus normal brain	Up	Arhgef26	2419	13.57	0.05	0	0	1.62
LGA versus normal brain	Up	Ube2t	17009	13.55	0.08	0	0	2.14
LGA versus normal brain	Up	Spin4	15367	13.55	0.11	0	0	2.90
LGA versus normal brain	Up	Skp2	14716	13.54	0.07	0	0	1.91
LGA versus normal brain	Up	Fam167a	6231	13.53	0.11	0	0	2.79
LGA versus normal brain	Up	Iqgap3	8611	13.53	0.11	0	0	2.74
LGA versus normal brain	Up	6720489N17Rik	1232	13.52	0.05	0	0	1.65
LGA versus normal brain	Up	Zfp185	17812	13.51	0.07	0	0	2.01
LGA versus normal brain	Up	Tspo	16803	13.51	0.06	0	0	1.68
LGA versus normal brain	Up	Pmf1	12674	13.48	0.06	0	0	1.81
LGA versus normal brain	Up	Ruvbl2	14172	13.46	0.03	0	0	1.35
LGA versus normal brain	Up	Zfp41	17894	13.45	0.07	0	0	1.93
LGA versus normal brain	Up	Ccdc153	3587	13.44	0.23	0	0	8.72
LGA versus normal brain	Up	Capsl	3447	13.44	0.14	0	0	3.59
LGA versus normal brain	Up	Cox6b2	4476	13.43	0.09	0	0	2.29
LGA versus normal brain	Up	BC051019	2970	13.43	0.11	0	0	2.78
LGA versus normal brain	Up	Slc43a3	14967	13.40	0.11	0	0	2.67
LGA versus normal brain	Up	Fam83d	6351	13.38	0.07	0	0	1.93

LGA versus normal brain	Up	Ccdc111	3558	13.38	0.08	0	0	2.06
LGA versus normal brain	Up	Wdr16	17447	13.37	0.10	0	0	2.53
LGA versus normal brain	Up	Olfml1	11264	13.36	0.08	0	0	2.19
LGA versus normal brain	Up	Egfr	5755	13.35	0.10	0	0	2.63
LGA versus normal brain	Up	Vrk1	17392	13.34	0.07	0	0	1.90
LGA versus normal brain	Up	Bub1b	3207	13.33	0.10	0	0	2.45
LGA versus normal brain	Up	Dnajb13	5358	13.32	0.12	0	0	3.15
LGA versus normal brain	Up	Cdc25b	3833	13.32	0.05	0	0	1.62
LGA versus normal brain	Up	Nt5dc2	11108	13.28	0.11	0	0	2.87
LGA versus normal brain	Up	Slc25a10	14814	13.28	0.04	0	0	1.46
LGA versus normal brain	Up	1700029F09Rik	267	13.28	0.07	0	0	1.93
LGA versus normal brain	Up	Chic2	4084	13.28	0.05	0	0	1.64
LGA versus normal brain	Up	Vim	17267	13.27	0.11	0	0	2.73
LGA versus normal brain	Up	Frem2	6705	13.26	0.11	0	0	2.70
LGA versus normal brain	Up	Cxcr4	4752	13.25	0.07	0	0	1.90
LGA versus normal brain	Up	Prdx6	12971	13.22	0.06	0	0	1.66
LGA versus normal brain	Up	Ssr3	15501	13.19	0.04	0	0	1.41
LGA versus normal brain	Up	2810055G20Rik	667	13.15	0.05	0	0	1.59
LGA versus normal brain	Up	Tmed10	16223	13.14	0.04	0	0	1.49
LGA versus normal brain	Up	Lmnb1	9367	13.12	0.15	0	0	4.02
LGA versus normal brain	Up	Haus3	7912	13.09	0.10	0	0	2.54
LGA versus normal brain	Up	Cdk2	3900	13.07	0.11	0	0	2.78
LGA versus normal brain	Up	Cdk5rap2	3910	13.02	0.07	0	0	1.87
LGA versus normal brain	Up	4932438H23Rik	1009	13.01	0.09	0	0	2.24
LGA versus normal brain	Up	Vwa5a	17409	13.00	0.07	0	0	1.80
LGA versus normal brain	Up	Gng5	7486	13.00	0.07	0	0	1.93
LGA versus normal brain	Up	Lmf2	9364	13.00	0.06	0	0	1.74
LGA versus normal brain	Up	Cd63	3800	12.99	0.05	0	0	1.56
LGA versus normal brain	Up	Zfp936	18085	12.99	0.07	0	0	1.84
LGA versus normal brain	Up	Acsl3	1715	12.97	0.06	0	0	1.78

LGA versus normal brain	Up	4933436C20Rik	1059	12.97	0.12	0	0	2.95
LGA versus normal brain	Up	Hist1h2bp	8068	12.97	0.11	0	0	2.73
LGA versus normal brain	Up	Enkur	5899	12.96	0.14	0	0	3.43
LGA versus normal brain	Up	Zfp934	18083	12.96	0.04	0	0	1.45
LGA versus normal brain	Up	Ctf1	4670	12.93	0.06	0	0	1.69
LGA versus normal brain	Up	Haus7	7916	12.91	0.08	0	0	2.05
LGA versus normal brain	Up	Fads2	6136	12.88	0.08	0	0	2.09
LGA versus normal brain	Up	Fen1	6507	12.87	0.08	0	0	1.98
LGA versus normal brain	Up	Cbs	3528	12.86	0.05	0	0	1.63
LGA versus normal brain	Up	Fam100b	6148	12.86	0.06	0	0	1.78
LGA versus normal brain	Up	Ccna1	3687	12.85	0.09	0	0	2.27
LGA versus normal brain	Up	2310015B20Rik	488	12.84	0.16	0	0	4.10
LGA versus normal brain	Up	Prdx6b	12972	12.82	0.07	0	0	1.87
LGA versus normal brain	Up	Rcbtb2	13647	12.80	0.04	0	0	1.45
LGA versus normal brain	Up	Rnf125	13883	12.78	0.06	0	0	1.77
LGA versus normal brain	Up	Serpinh1	14513	12.78	0.08	0	0	2.10
LGA versus normal brain	Up	Scml2	14309	12.76	0.12	0	0	2.82
LGA versus normal brain	Up	Asrgl1	2560	12.75	0.05	0	0	1.60
LGA versus normal brain	Up	Ednrb	5705	12.75	0.07	0	0	1.89
LGA versus normal brain	Up	Retsat	13708	12.74	0.08	0	0	1.99
LGA versus normal brain	Up	P2ry1	11976	12.74	0.11	0	0	2.53
LGA versus normal brain	Up	4833427G06Rik	801	12.73	0.23	0	0	7.41
LGA versus normal brain	Up	Rtkn2	14145	12.72	0.07	0	0	1.85
LGA versus normal brain	Up	Limd1	9320	12.72	0.06	0	0	1.63
LGA versus normal brain	Up	Ak7	2000	12.70	0.24	0	0	8.55
LGA versus normal brain	Up	Sox6	15281	12.69	0.09	0	0	2.15
LGA versus normal brain	Up	Tnc	16453	12.69	0.07	0	0	1.82
LGA versus normal brain	Up	Fkbp10	6585	12.69	0.06	0	0	1.72
LGA versus normal brain	Up	Acat3	1660	12.67	0.06	0	0	1.65
LGA versus normal brain	Up	Tmem48	16373	12.67	0.08	0	0	1.95

LGA versus normal brain	Up	Akr1c12	2026	12.67	0.08	0	0	2.00
LGA versus normal brain	Up	Depdc7	5201	12.67	0.10	0	0	2.32
LGA versus normal brain	Up	Cmtm2a	4294	12.65	0.09	0	0	2.17
LGA versus normal brain	Up	H2-Q8	7867	12.63	0.19	0	0	5.16
LGA versus normal brain	Up	Mdfic	9898	12.63	0.16	0	0	4.04
LGA versus normal brain	Up	Erh	6001	12.62	0.05	0	0	1.49
LGA versus normal brain	Up	D330045A20Rik	4935	12.61	0.17	0	0	4.33
LGA versus normal brain	Up	Npepl1	11008	12.60	0.08	0	0	1.95
LGA versus normal brain	Up	Mt2	10370	12.59	0.11	0	0	2.71
LGA versus normal brain	Up	Tceanc	15925	12.58	0.08	0	0	1.96
LGA versus normal brain	Up	4930427A07Rik	842	12.58	0.11	0	0	2.61
LGA versus normal brain	Up	Kdelr2	8881	12.56	0.05	0	0	1.54
LGA versus normal brain	Up	Ccdc37	3607	12.54	0.08	0	0	1.98
LGA versus normal brain	Up	Smo	15123	12.53	0.06	0	0	1.62
LGA versus normal brain	Up	Lpin3	9469	12.52	0.10	0	0	2.44
LGA versus normal brain	Up	Ncapd2	10664	12.52	0.10	0	0	2.47
LGA versus normal brain	Up	Usp1	17152	12.51	0.09	0	0	2.12
LGA versus normal brain	Up	Mif4gd	10070	12.51	0.07	0	0	1.84
LGA versus normal brain	Up	Heph	7992	12.50	0.14	0	0	3.39
LGA versus normal brain	Up	Fas	6388	12.49	0.10	0	0	2.29
LGA versus normal brain	Up	Nmi	10941	12.49	0.09	0	0	2.26
LGA versus normal brain	Up	Rdh11	13665	12.49	0.03	0	0	1.33
LGA versus normal brain	Up	Ang3	2152	12.49	0.08	0	0	1.94
LGA versus normal brain	Up	Nckap5	10681	12.48	0.11	0	0	2.66
LGA versus normal brain	Up	Ikbip	8442	12.48	0.04	0	0	1.44
LGA versus normal brain	Up	Nqo1	11035	12.47	0.09	0	0	2.11
LGA versus normal brain	Up	Gm16499	7197	12.47	0.10	0	0	2.38
LGA versus normal brain	Up	Rfc3	13717	12.45	0.08	0	0	2.04
LGA versus normal brain	Up	Rplp0	14033	12.44	0.04	0	0	1.37
LGA versus normal brain	Up	Dbx2	5048	12.43	0.09	0	0	2.14

LGA versus normal brain	Up	Mlxipl	10122	12.42	0.08	0	0	1.91
LGA versus normal brain	Up	Ccdc102a	3549	12.40	0.05	0	0	1.58
LGA versus normal brain	Up	Rdbp	13663	12.40	0.05	0	0	1.48
LGA versus normal brain	Up	Lingo4	9338	12.39	0.09	0	0	2.11
LGA versus normal brain	Up	Tom1l1	16525	12.38	0.04	0	0	1.45
LGA versus normal brain	Up	Rad54b	13475	12.37	0.08	0	0	1.92
LGA versus normal brain	Up	Cdkn2b	3927	12.36	0.15	0	0	3.51
LGA versus normal brain	Up	H3f3a	7880	12.36	0.05	0	0	1.54
LGA versus normal brain	Up	Prrx1	13111	12.35	0.07	0	0	1.76
LGA versus normal brain	Up	Rftn2	13727	12.33	0.05	0	0	1.60
LGA versus normal brain	Up	Brca1	3145	12.32	0.09	0	0	2.22
LGA versus normal brain	Up	Hmg20b	8101	12.30	0.08	0	0	1.95
LGA versus normal brain	Up	Psat1	13150	12.30	0.06	0	0	1.71
LGA versus normal brain	Up	Polh	12737	12.30	0.07	0	0	1.82
TR(P) versus T(P) LGA	Down	2310022B05Rik	492	-8.15	0.09	0	0	0.59
TR(P) versus T(P) LGA	Down	Pdlim7	12262	-7.84	0.05	0	0	0.78
TR(P) versus T(P) LGA	Down	Senp2	14432	-6.99	0.05	5.49E-07	3.46E-05	0.79
TR(P) versus T(P) LGA	Down	Rheb	13782	-6.75	0.04	5.49E-07	3.46E-05	0.83
TR(P) versus T(P) LGA	Down	1700094D03Rik	336	-6.71	0.13	5.49E-07	3.46E-05	0.55
TR(P) versus T(P) LGA	Down	Morn5	10189	-6.61	0.12	5.49E-07	3.46E-05	0.57
TR(P) versus T(P) LGA	Down	Ube2w	17012	-6.44	0.04	1.10E-06	5.02E-05	0.82
TR(P) versus T(P) LGA	Down	Gli1	7050	-6.43	0.04	1.10E-06	5.02E-05	0.84
TR(P) versus T(P) LGA	Down	Morn4	10188	-6.39	0.06	1.10E-06	5.02E-05	0.75
TR(P) versus T(P) LGA	Down	Ccdc65	3631	-6.38	0.08	1.10E-06	5.02E-05	0.69
TR(P) versus T(P) LGA	Down	Uox	17116	-6.36	0.09	1.10E-06	5.02E-05	0.68
TR(P) versus T(P) LGA	Down	Parp6	12075	-6.27	0.08	1.65E-06	6.19E-05	0.71
TR(P) versus T(P) LGA	Down	Prkar1a	13000	-6.19	0.06	1.65E-06	6.19E-05	0.78
TR(P) versus T(P) LGA	Down	Nkain4	10891	-6.18	0.10	1.65E-06	6.19E-05	0.65
TR(P) versus T(P) LGA	Down	Fam154b	6213	-6.16	0.10	1.65E-06	6.19E-05	0.65
TR(P) versus T(P) LGA	Down	Tex264	16029	-6.16	0.04	1.65E-06	6.19E-05	0.86

TR(P) versus T(P) LGA	Down	Atp6v0d1	2665	-6.06	0.05	2.20E-06	7.83E-05	0.82
TR(P) versus T(P) LGA	Down	Dmkn	5324	-6.05	0.12	2.20E-06	7.83E-05	0.60
TR(P) versus T(P) LGA	Down	1700007G11Rik	167	-6.03	0.18	2.74E-06	8.50E-05	0.46
TR(P) versus T(P) LGA	Down	Celsr3	3970	-6.02	0.06	2.74E-06	8.50E-05	0.78
TR(P) versus T(P) LGA	Down	Fbxl2	6423	-5.99	0.07	2.74E-06	8.50E-05	0.73
TR(P) versus T(P) LGA	Down	Cd24a	3761	-5.99	0.16	2.74E-06	8.50E-05	0.52
TR(P) versus T(P) LGA	Down	Got1l1	7526	-5.83	0.15	4.94E-06	1.39E-04	0.54
TR(P) versus T(P) LGA	Down	Crygn	4600	-5.82	0.14	4.94E-06	1.39E-04	0.57
TR(P) versus T(P) LGA	Down	Aph1b	2293	-5.81	0.07	5.49E-06	1.50E-04	0.76
TR(P) versus T(P) LGA	Down	Letm2	9275	-5.78	0.08	6.04E-06	1.56E-04	0.72
TR(P) versus T(P) LGA	Down	Hsph1	8287	-5.77	0.13	6.04E-06	1.56E-04	0.60
TR(P) versus T(P) LGA	Down	Dnm1l	5407	-5.71	0.04	7.14E-06	1.69E-04	0.85
TR(P) versus T(P) LGA	Down	Fam183b	6258	-5.68	0.23	7.14E-06	1.69E-04	0.41
TR(P) versus T(P) LGA	Down	Hspa4l	8270	-5.68	0.09	7.14E-06	1.69E-04	0.70
TR(P) versus T(P) LGA	Down	Atp6v1h	2678	-5.64	0.07	7.14E-06	1.69E-04	0.77
TR(P) versus T(P) LGA	Down	Spag6	15305	-5.63	0.11	7.14E-06	1.69E-04	0.64
TR(P) versus T(P) LGA	Down	Myst1	10566	-5.61	0.04	7.69E-06	1.78E-04	0.85
TR(P) versus T(P) LGA	Down	Nxn	11200	-5.61	0.12	7.69E-06	1.78E-04	0.62
TR(P) versus T(P) LGA	Down	Rpl27a	14012	-5.61	0.07	7.69E-06	1.78E-04	0.77
TR(P) versus T(P) LGA	Down	Ccdc75	3640	-5.60	0.05	9.88E-06	2.18E-04	0.84
TR(P) versus T(P) LGA	Down	Zfp773	18030	-5.59	0.09	9.88E-06	2.18E-04	0.72
TR(P) versus T(P) LGA	Down	1700028P14Rik	266	-5.58	0.18	9.88E-06	2.18E-04	0.49
TR(P) versus T(P) LGA	Down	Atp6v1d	2672	-5.56	0.09	1.10E-05	2.40E-04	0.72
TR(P) versus T(P) LGA	Down	Rdh5	13671	-5.56	0.10	1.15E-05	2.45E-04	0.68
TR(P) versus T(P) LGA	Down	Gcg	6923	-5.56	0.09	1.15E-05	2.45E-04	0.71
TR(P) versus T(P) LGA	Down	Hprt	8205	-5.55	0.10	1.15E-05	2.45E-04	0.67
TR(P) versus T(P) LGA	Down	Appl1	2335	-5.55	0.04	1.21E-05	2.53E-04	0.87
TR(P) versus T(P) LGA	Down	Ube2v2	17011	-5.55	0.06	1.21E-05	2.53E-04	0.79
TR(P) versus T(P) LGA	Down	Zmynd10	18160	-5.52	0.15	1.26E-05	2.61E-04	0.57
TR(P) versus T(P) LGA	Down	T2	15778	-5.51	0.11	1.32E-05	2.70E-04	0.66

TR(P) versus T(P) LGA	Down	Ift88	8398	-5.48	0.07	1.48E-05	2.89E-04	0.77
TR(P) versus T(P) LGA	Down	Atg16l1	2590	-5.48	0.07	1.48E-05	2.89E-04	0.76
TR(P) versus T(P) LGA	Down	Kif6	8944	-5.45	0.08	1.54E-05	2.89E-04	0.75
TR(P) versus T(P) LGA	Down	Pgrmc1	12370	-5.44	0.07	1.54E-05	2.89E-04	0.78
TR(P) versus T(P) LGA	Down	Greb1l	7682	-5.43	0.12	1.54E-05	2.89E-04	0.64
TR(P) versus T(P) LGA	Down	Mycbpap	10492	-5.43	0.17	1.54E-05	2.89E-04	0.53
TR(P) versus T(P) LGA	Down	Tspyl2	16806	-5.42	0.07	1.54E-05	2.89E-04	0.77
TR(P) versus T(P) LGA	Down	Ccdc113	3560	-5.35	0.16	1.65E-05	2.93E-04	0.56
TR(P) versus T(P) LGA	Down	Dnajb6	5364	-5.35	0.05	1.65E-05	2.93E-04	0.82
TR(P) versus T(P) LGA	Down	Vti1b	17405	-5.32	0.08	1.81E-05	3.09E-04	0.74
TR(P) versus T(P) LGA	Down	Morf4l2	10184	-5.32	0.07	1.81E-05	3.09E-04	0.79
TR(P) versus T(P) LGA	Down	5730469M10Rik	1124	-5.31	0.06	1.81E-05	3.09E-04	0.79
TR(P) versus T(P) LGA	Down	Atp6ap2	2660	-5.29	0.08	1.87E-05	3.10E-04	0.74
TR(P) versus T(P) LGA	Down	Clip1	4245	-5.29	0.06	1.92E-05	3.10E-04	0.79
TR(P) versus T(P) LGA	Down	Zfp523	17933	-5.28	0.07	1.92E-05	3.10E-04	0.77
TR(P) versus T(P) LGA	Down	Bbs5	2898	-5.27	0.09	1.92E-05	3.10E-04	0.73
TR(P) versus T(P) LGA	Down	Cluap1	4277	-5.27	0.05	1.92E-05	3.10E-04	0.82
TR(P) versus T(P) LGA	Down	Chia	4082	-5.25	0.12	1.98E-05	3.10E-04	0.66
TR(P) versus T(P) LGA	Down	Lmod1	9374	-5.23	0.10	1.98E-05	3.10E-04	0.69
TR(P) versus T(P) LGA	Down	Klf16	8974	-5.21	0.07	2.09E-05	3.19E-04	0.78
TR(P) versus T(P) LGA	Down	B4galnt4	2818	-5.21	0.09	2.09E-05	3.19E-04	0.73
TR(P) versus T(P) LGA	Down	Odf3b	11240	-5.21	0.19	2.09E-05	3.19E-04	0.50
TR(P) versus T(P) LGA	Down	Trim2	16654	-5.20	0.08	2.14E-05	3.27E-04	0.75
TR(P) versus T(P) LGA	Down	Al428936	1950	-5.19	0.09	2.25E-05	3.42E-04	0.72
TR(P) versus T(P) LGA	Down	Ddx25	5129	-5.18	0.09	2.42E-05	3.58E-04	0.73
TR(P) versus T(P) LGA	Down	Mllt11	10114	-5.18	0.15	2.42E-05	3.58E-04	0.59
TR(P) versus T(P) LGA	Down	Synj2bp	15745	-5.17	0.06	2.47E-05	3.66E-04	0.81
TR(P) versus T(P) LGA	Down	1700024G13Rik	249	-5.16	0.12	2.53E-05	3.67E-04	0.65
TR(P) versus T(P) LGA	Down	Ypel5	17652	-5.15	0.08	2.58E-05	3.72E-04	0.75
TR(P) versus T(P) LGA	Down	Ryr2	14188	-5.14	0.07	2.58E-05	3.72E-04	0.79

TR(P) versus T(P) LGA	Down	Mdh1b	9902	-5.14	0.14	2.74E-05	3.93E-04	0.60
TR(P) versus T(P) LGA	Down	Plin4	12636	-5.13	0.20	2.80E-05	3.97E-04	0.49
TR(P) versus T(P) LGA	Down	Riia1	13817	-5.12	0.20	2.85E-05	4.04E-04	0.49
TR(P) versus T(P) LGA	Down	Tmtc4	16446	-5.12	0.10	2.91E-05	4.07E-04	0.69
TR(P) versus T(P) LGA	Down	Asb6	2530	-5.12	0.04	2.91E-05	4.07E-04	0.86
TR(P) versus T(P) LGA	Down	Sfxn3	14571	-5.11	0.09	2.91E-05	4.07E-04	0.73
TR(P) versus T(P) LGA	Down	5033411D12Rik	1071	-5.11	0.08	2.91E-05	4.07E-04	0.77
TR(P) versus T(P) LGA	Down	Ecsit	5688	-5.09	0.04	3.18E-05	4.21E-04	0.86
TR(P) versus T(P) LGA	Down	Polr2g	12755	-5.08	0.05	3.18E-05	4.21E-04	0.85
TR(P) versus T(P) LGA	Down	Fam166b	6230	-5.08	0.18	3.18E-05	4.21E-04	0.54
TR(P) versus T(P) LGA	Down	Snx16	15214	-5.08	0.08	3.18E-05	4.21E-04	0.75
TR(P) versus T(P) LGA	Down	Inpp5a	8553	-5.08	0.06	3.18E-05	4.21E-04	0.80
TR(P) versus T(P) LGA	Down	Zfp772	18029	-5.07	0.08	3.18E-05	4.21E-04	0.75
TR(P) versus T(P) LGA	Down	Ppp1r32	12891	-5.07	0.14	3.18E-05	4.21E-04	0.62
TR(P) versus T(P) LGA	Down	CYTB	4856	-5.07	0.09	3.18E-05	4.21E-04	0.72
TR(P) versus T(P) LGA	Down	Polb	12724	-5.06	0.09	3.18E-05	4.21E-04	0.72
TR(P) versus T(P) LGA	Down	Gm13629	7158	-5.05	0.11	3.29E-05	4.34E-04	0.69
TR(P) versus T(P) LGA	Down	Fdps	6498	-5.04	0.06	3.46E-05	4.51E-04	0.81
TR(P) versus T(P) LGA	Down	Dhx57	5259	-5.04	0.08	3.46E-05	4.51E-04	0.75
TR(P) versus T(P) LGA	Down	Efhc2	5732	-5.03	0.09	3.57E-05	4.60E-04	0.74
TR(P) versus T(P) LGA	Down	Efh2	5734	-5.03	0.08	3.62E-05	4.64E-04	0.76
TR(P) versus T(P) LGA	Down	Sln	15071	-5.02	0.17	3.68E-05	4.70E-04	0.56
TR(P) versus T(P) LGA	Down	Pex13	12318	-5.02	0.05	3.79E-05	4.77E-04	0.85
TR(P) versus T(P) LGA	Down	Slco4a1	15052	-5.02	0.13	3.79E-05	4.77E-04	0.64
TR(P) versus T(P) LGA	Down	1500011H22Rik	121	-5.02	0.05	3.79E-05	4.77E-04	0.84
TR(P) versus T(P) LGA	Down	Pgbd5	12353	-5.01	0.07	3.79E-05	4.77E-04	0.77
TR(P) versus T(P) LGA	Down	A430108G06Rik	1464	-5.01	0.13	3.79E-05	4.77E-04	0.64
TR(P) versus T(P) LGA	Down	BC022687	2929	-5.01	0.07	3.90E-05	4.89E-04	0.77
TR(P) versus T(P) LGA	Down	Armex1	2471	-5.01	0.13	3.95E-05	4.93E-04	0.64
TR(P) versus T(P) LGA	Down	Socs2	15240	-5.00	0.12	3.95E-05	4.93E-04	0.65

TR(P) versus T(P) LGA	Down	Ubash3b	16978	-4.99	0.09	4.12E-05	5.02E-04	0.73
TR(P) versus T(P) LGA	Down	Fam189b	6268	-4.99	0.07	4.12E-05	5.02E-04	0.79
TR(P) versus T(P) LGA	Down	Dnajb2	5360	-4.98	0.08	4.12E-05	5.02E-04	0.76
TR(P) versus T(P) LGA	Down	Setd4	14530	-4.97	0.09	4.12E-05	5.02E-04	0.75
TR(P) versus T(P) LGA	Down	Spef2	15349	-4.97	0.14	4.12E-05	5.02E-04	0.62
TR(P) versus T(P) LGA	Down	Sirt7	14697	-4.97	0.05	4.23E-05	5.11E-04	0.85
TR(P) versus T(P) LGA	Down	Aox4	2251	-4.96	0.08	4.28E-05	5.16E-04	0.76
TR(P) versus T(P) LGA	Down	Fam98c	6367	-4.96	0.09	4.28E-05	5.16E-04	0.74
TR(P) versus T(P) LGA	Down	Cfp	4038	-4.95	0.09	4.34E-05	5.16E-04	0.73
TR(P) versus T(P) LGA	Down	Fam164a	6227	-4.95	0.11	4.34E-05	5.16E-04	0.68
TR(P) versus T(P) LGA	Down	Rap1gds1	13518	-4.95	0.07	4.34E-05	5.16E-04	0.78
TR(P) versus T(P) LGA	Down	Rgs11	13753	-4.95	0.09	4.34E-05	5.16E-04	0.74
TR(P) versus T(P) LGA	Down	Cnn1	4316	-4.95	0.10	4.34E-05	5.16E-04	0.70
TR(P) versus T(P) LGA	Down	Fhad1	6560	-4.94	0.08	4.50E-05	5.34E-04	0.77
TR(P) versus T(P) LGA	Down	Ccdc39	3609	-4.94	0.13	4.56E-05	5.39E-04	0.63
TR(P) versus T(P) LGA	Down	C85492	3335	-4.94	0.09	4.61E-05	5.44E-04	0.74
TR(P) versus T(P) LGA	Down	Pim2	12491	-4.94	0.06	4.61E-05	5.44E-04	0.83
TR(P) versus T(P) LGA	Down	Gm88	7405	-4.93	0.09	4.67E-05	5.46E-04	0.73
TR(P) versus T(P) LGA	Down	Spryd3	15417	-4.93	0.10	4.67E-05	5.46E-04	0.72
TR(P) versus T(P) LGA	Down	Wdr16	17447	-4.92	0.12	4.94E-05	5.73E-04	0.66
TR(P) versus T(P) LGA	Down	A830019P07Rik	1513	-4.90	0.09	5.44E-05	6.17E-04	0.75
TR(P) versus T(P) LGA	Down	Kcnab2	8789	-4.90	0.11	5.44E-05	6.17E-04	0.68
TR(P) versus T(P) LGA	Down	Dalrd3	5017	-4.89	0.06	5.49E-05	6.17E-04	0.83
TR(P) versus T(P) LGA	Down	Fam92b	6362	-4.89	0.22	5.49E-05	6.17E-04	0.48
TR(P) versus T(P) LGA	Down	Zmat2	18147	-4.89	0.08	5.49E-05	6.17E-04	0.75
TR(P) versus T(P) LGA	Down	Dynlrb2	5575	-4.89	0.10	5.49E-05	6.17E-04	0.70
TR(P) versus T(P) LGA	Down	Tmem212	16338	-4.89	0.31	5.49E-05	6.17E-04	0.35
TR(P) versus T(P) LGA	Down	Tspan15	16789	-4.88	0.09	5.54E-05	6.21E-04	0.74
TR(P) versus T(P) LGA	Down	Acot7	1694	-4.88	0.11	5.60E-05	6.24E-04	0.69
TR(P) versus T(P) LGA	Down	Prepl	12978	-4.88	0.08	5.60E-05	6.24E-04	0.77

TR(P) versus T(P) LGA	Down	Ccdc148	3582	-4.87	0.12	5.82E-05	6.43E-04	0.66
TR(P) versus T(P) LGA	Down	Kif9	8946	-4.87	0.14	5.82E-05	6.43E-04	0.63
TR(P) versus T(P) LGA	Down	B930095I24Rik	2838	-4.87	0.12	5.82E-05	6.43E-04	0.66
TR(P) versus T(P) LGA	Down	Farp2	6384	-4.87	0.07	5.87E-05	6.47E-04	0.80
TR(P) versus T(P) LGA	Down	Rusc2	14170	-4.86	0.06	5.93E-05	6.52E-04	0.81
TR(P) versus T(P) LGA	Down	Ccdc74a	3639	-4.86	0.15	6.04E-05	6.60E-04	0.61
TR(P) versus T(P) LGA	Down	Card10	3467	-4.85	0.07	6.15E-05	6.66E-04	0.80
TR(P) versus T(P) LGA	Down	Ube2b	16982	-4.85	0.05	6.15E-05	6.66E-04	0.84
TR(P) versus T(P) LGA	Down	Rb1cc1	13577	-4.84	0.06	6.42E-05	6.87E-04	0.83
TR(P) versus T(P) LGA	Down	Meig1	9961	-4.84	0.21	6.42E-05	6.87E-04	0.49
TR(P) versus T(P) LGA	Down	Ttc19	16831	-4.84	0.07	6.42E-05	6.87E-04	0.79
TR(P) versus T(P) LGA	Down	Mthfsd	10409	-4.84	0.06	6.42E-05	6.87E-04	0.81
TR(P) versus T(P) LGA	Down	Nme1	10934	-4.83	0.09	6.48E-05	6.91E-04	0.75
TR(P) versus T(P) LGA	Down	Coq4	4448	-4.83	0.06	6.53E-05	6.96E-04	0.82
TR(P) versus T(P) LGA	Down	Ptchd1	13230	-4.83	0.12	6.70E-05	7.08E-04	0.67
TR(P) versus T(P) LGA	Down	Calm1	3395	-4.82	0.07	6.70E-05	7.08E-04	0.80
TR(P) versus T(P) LGA	Down	1700026D08Rik	257	-4.81	0.24	6.86E-05	7.20E-04	0.45
TR(P) versus T(P) LGA	Down	Spns2	15385	-4.81	0.09	7.08E-05	7.38E-04	0.74
TR(P) versus T(P) LGA	Down	A230006K03Rik	1423	-4.80	0.09	7.19E-05	7.44E-04	0.75
TR(P) versus T(P) LGA	Down	Camk4	3415	-4.80	0.16	7.19E-05	7.44E-04	0.59
TR(P) versus T(P) LGA	Down	Tmem64	16391	-4.79	0.06	7.41E-05	7.63E-04	0.81
TR(P) versus T(P) LGA	Down	Ppp2r5b	12919	-4.79	0.07	7.41E-05	7.63E-04	0.78
TR(P) versus T(P) LGA	Down	Insl5	8566	-4.79	0.08	7.69E-05	7.89E-04	0.77
TR(P) versus T(P) LGA	Down	Dgat2	5214	-4.78	0.07	7.74E-05	7.89E-04	0.80
TR(P) versus T(P) LGA	Down	Srxn1	15484	-4.77	0.07	7.85E-05	7.97E-04	0.78
TR(P) versus T(P) LGA	Down	Pmvk	12684	-4.77	0.05	7.96E-05	8.03E-04	0.85
TR(P) versus T(P) LGA	Down	Hmga1	8102	-4.77	0.08	8.02E-05	8.03E-04	0.78
TR(P) versus T(P) LGA	Down	Spata7	15323	-4.76	0.09	8.02E-05	8.03E-04	0.73
TR(P) versus T(P) LGA	Down	Puf60	13318	-4.76	0.04	8.02E-05	8.03E-04	0.87
TR(P) versus T(P) LGA	Down	Map3k6	9762	-4.76	0.11	8.07E-05	8.06E-04	0.69

TR(P) versus T(P) LGA	Down	Morc2b	10180	-4.76	0.10	8.07E-05	8.06E-04	0.72
TR(P) versus T(P) LGA	Down	Zfp692	18002	-4.75	0.05	8.23E-05	8.17E-04	0.84
TR(P) versus T(P) LGA	Down	Calml4	3399	-4.75	0.27	8.23E-05	8.17E-04	0.42
TR(P) versus T(P) LGA	Down	4930506M07Rik	906	-4.75	0.09	8.34E-05	8.27E-04	0.74
TR(P) versus T(P) LGA	Down	Fibin	6571	-4.74	0.15	8.51E-05	8.42E-04	0.62
TR(P) versus T(P) LGA	Down	Wdr13	17446	-4.73	0.06	8.78E-05	8.61E-04	0.81
TR(P) versus T(P) LGA	Down	B230217C12Rik	2779	-4.73	0.09	9.17E-05	8.95E-04	0.74
TR(P) versus T(P) LGA	Down	Mdh1	9901	-4.72	0.07	9.33E-05	9.06E-04	0.80
TR(P) versus T(P) LGA	Down	Igfbp5	8413	-4.72	0.13	9.33E-05	9.06E-04	0.66
TR(P) versus T(P) LGA	Down	1700049E17Rik1	299	-4.72	0.15	9.61E-05	9.25E-04	0.61
TR(P) versus T(P) LGA	Down	Inpp5f	8557	-4.72	0.07	9.61E-05	9.25E-04	0.80
TR(P) versus T(P) LGA	Down	6330406I15Rik	1183	-4.71	0.11	9.66E-05	9.28E-04	0.70
TR(P) versus T(P) LGA	Down	Rsph10b2	14127	-4.71	0.08	9.66E-05	9.28E-04	0.77
TR(P) versus T(P) LGA	Down	Map3k12	9754	-4.70	0.07	1.02E-04	9.75E-04	0.81
TR(P) versus T(P) LGA	Down	Pak3	12018	-4.69	0.12	1.04E-04	9.84E-04	0.69
TR(P) versus T(P) LGA	Down	Cldn2	4208	-4.69	0.08	1.06E-04	9.97E-04	0.76
TR(P) versus T(P) LGA	Down	Sub1	15657	-4.68	0.06	1.06E-04	9.97E-04	0.82
TR(P) versus T(P) LGA	Down	Ttll5	16875	-4.68	0.05	1.07E-04	1.00E-03	0.86
TR(P) versus T(P) LGA	Down	Snap47	15152	-4.68	0.10	1.07E-04	1.00E-03	0.72
TR(P) versus T(P) LGA	Down	Madd	9681	-4.68	0.10	1.07E-04	1.00E-03	0.71
TR(P) versus T(P) LGA	Down	Zfp341	17865	-4.68	0.09	1.08E-04	1.00E-03	0.76
TR(P) versus T(P) LGA	Down	Acot5	1692	-4.66	0.12	1.17E-04	1.09E-03	0.67
TR(P) versus T(P) LGA	Down	Kcnj14	8822	-4.66	0.11	1.17E-04	1.09E-03	0.70
TR(P) versus T(P) LGA	Down	Klhl8	9023	-4.65	0.07	1.21E-04	1.12E-03	0.80
TR(P) versus T(P) LGA	Down	Dixdc1	5286	-4.65	0.08	1.25E-04	1.15E-03	0.78
TR(P) versus T(P) LGA	Down	Sh3glb2	14621	-4.65	0.08	1.26E-04	1.16E-03	0.78
TR(P) versus T(P) LGA	Down	Wdr44	17468	-4.65	0.07	1.26E-04	1.16E-03	0.79
TR(P) versus T(P) LGA	Down	Ccdc92	3659	-4.64	0.11	1.28E-04	1.17E-03	0.70
TR(P) versus T(P) LGA	Down	Rbfox2	13588	-4.63	0.11	1.32E-04	1.20E-03	0.70
TR(P) versus T(P) LGA	Down	Ankrd42	2202	-4.63	0.07	1.33E-04	1.21E-03	0.81

TR(P) versus T(P) LGA	Down	Mfi2	10017	-4.62	0.13	1.37E-04	1.24E-03	0.67
TR(P) versus T(P) LGA	Down	Rps6kl1	14083	-4.62	0.09	1.38E-04	1.24E-03	0.75
TR(P) versus T(P) LGA	Down	Lpar1	9453	-4.61	0.12	1.40E-04	1.24E-03	0.68
TR(P) versus T(P) LGA	Down	1700029J07Rik	272	-4.61	0.13	1.41E-04	1.24E-03	0.66
TR(P) versus T(P) LGA	Down	4931428F04Rik	990	-4.61	0.04	1.41E-04	1.25E-03	0.88
TR(P) versus T(P) LGA	Down	Fam132a	6196	-4.60	0.11	1.42E-04	1.25E-03	0.71
TR(P) versus T(P) LGA	Down	Wipi2	17538	-4.60	0.03	1.43E-04	1.26E-03	0.92
TR(P) versus T(P) LGA	Down	Fhdc1	6561	-4.60	0.09	1.44E-04	1.26E-03	0.76
TR(P) versus T(P) LGA	Down	Pclo	12165	-4.59	0.10	1.44E-04	1.26E-03	0.73
TR(P) versus T(P) LGA	Down	Dnahc5	5345	-4.59	0.10	1.45E-04	1.27E-03	0.73
TR(P) versus T(P) LGA	Down	Atpif1	2693	-4.59	0.06	1.45E-04	1.27E-03	0.83
TR(P) versus T(P) LGA	Down	1190002N15Rik	89	-4.59	0.09	1.47E-04	1.28E-03	0.76
TR(P) versus T(P) LGA	Down	Wdr63	17485	-4.59	0.15	1.48E-04	1.29E-03	0.61
TR(P) versus T(P) LGA	Down	Fbxo33	6449	-4.58	0.09	1.51E-04	1.31E-03	0.76
TR(P) versus T(P) LGA	Down	Orc4	11896	-4.58	0.05	1.53E-04	1.32E-03	0.85
TR(P) versus T(P) LGA	Down	Pcgf6	12161	-4.58	0.07	1.53E-04	1.32E-03	0.81
TR(P) versus T(P) LGA	Down	Meaf6	9914	-4.57	0.04	1.56E-04	1.34E-03	0.89
TR(P) versus T(P) LGA	Down	1700009P17Rik	180	-4.57	0.17	1.57E-04	1.34E-03	0.58
TR(P) versus T(P) LGA	Down	Prnp	13048	-4.56	0.09	1.57E-04	1.34E-03	0.75
TR(P) versus T(P) LGA	Down	Cyb561	4761	-4.56	0.12	1.59E-04	1.34E-03	0.67
TR(P) versus T(P) LGA	Down	Eno4	5903	-4.56	0.14	1.59E-04	1.35E-03	0.64
TR(P) versus T(P) LGA	Down	Ttc8	16858	-4.56	0.10	1.60E-04	1.35E-03	0.72
TR(P) versus T(P) LGA	Down	Cdk5r1	3907	-4.56	0.08	1.60E-04	1.35E-03	0.78
TR(P) versus T(P) LGA	Down	Arid3a	2432	-4.55	0.09	1.61E-04	1.35E-03	0.76
TR(P) versus T(P) LGA	Down	Wnt10a	17548	-4.55	0.10	1.61E-04	1.35E-03	0.72
TR(P) versus T(P) LGA	Down	Grm7	7722	-4.55	0.10	1.61E-04	1.35E-03	0.74
TR(P) versus T(P) LGA	Down	Ttc33	16845	-4.55	0.09	1.61E-04	1.35E-03	0.76
TR(P) versus T(P) LGA	Down	Dnrtip1	5418	-4.55	0.04	1.63E-04	1.35E-03	0.88
TR(P) versus T(P) LGA	Down	4930451C15Rik	864	-4.55	0.18	1.63E-04	1.36E-03	0.57
TR(P) versus T(P) LGA	Down	Bbs4	2897	-4.54	0.10	1.64E-04	1.37E-03	0.74

TR(P) versus T(P) LGA	Down	Ppp1r42	12901	-4.54	0.18	1.65E-04	1.37E-03	0.57
TR(P) versus T(P) LGA	Down	Nop56	10978	-4.54	0.06	1.65E-04	1.37E-03	0.82
TR(P) versus T(P) LGA	Down	Eno2	5901	-4.54	0.11	1.65E-04	1.37E-03	0.71
TR(P) versus T(P) LGA	Down	Gm9856	7430	-4.53	0.09	1.67E-04	1.37E-03	0.76
TR(P) versus T(P) LGA	Down	Ube2q2	17005	-4.53	0.06	1.67E-04	1.37E-03	0.82
TR(P) versus T(P) LGA	Down	Ttll7	16877	-4.53	0.11	1.67E-04	1.37E-03	0.70
TR(P) versus T(P) LGA	Down	Nae1	10605	-4.53	0.06	1.68E-04	1.37E-03	0.82
TR(P) versus T(P) LGA	Down	Nek1	10776	-4.53	0.05	1.69E-04	1.38E-03	0.86
TR(P) versus T(P) LGA	Down	Unc13a	17097	-4.52	0.06	1.70E-04	1.38E-03	0.83
TR(P) versus T(P) LGA	Down	Zmym5	18158	-4.52	0.05	1.70E-04	1.38E-03	0.86
TR(P) versus T(P) LGA	Down	Bnip3l	3121	-4.52	0.05	1.71E-04	1.38E-03	0.85
TR(P) versus T(P) LGA	Down	Ift46	8392	-4.52	0.04	1.71E-04	1.38E-03	0.89
TR(P) versus T(P) LGA	Down	Ric8b	13814	-4.52	0.06	1.71E-04	1.38E-03	0.83
TR(P) versus T(P) LGA	Down	Zfp512	17926	-4.52	0.04	1.71E-04	1.38E-03	0.89
TR(P) versus T(P) LGA	Down	1700003E16Rik	162	-4.52	0.10	1.71E-04	1.38E-03	0.73
TR(P) versus T(P) LGA	Down	Cpeb1	4496	-4.52	0.13	1.71E-04	1.38E-03	0.67
TR(P) versus T(P) LGA	Down	9030425E11Rik	1268	-4.52	0.16	1.71E-04	1.38E-03	0.60
TR(P) versus T(P) LGA	Down	Entpd2	5918	-4.51	0.18	1.72E-04	1.39E-03	0.56
TR(P) versus T(P) LGA	Down	Anxa7	2243	-4.51	0.09	1.74E-04	1.39E-03	0.76
TR(P) versus T(P) LGA	Down	Xbp1	17583	-4.50	0.07	1.77E-04	1.41E-03	0.80
TR(P) versus T(P) LGA	Down	Pcyt2	12195	-4.49	0.06	1.81E-04	1.43E-03	0.83
TR(P) versus T(P) LGA	Down	Nmt2	10947	-4.49	0.08	1.83E-04	1.45E-03	0.79
TR(P) versus T(P) LGA	Down	Dlk2	5307	-4.48	0.12	1.88E-04	1.47E-03	0.69
TR(P) versus T(P) LGA	Down	Ppp2r2b	12911	-4.47	0.07	1.91E-04	1.48E-03	0.80
TR(P) versus T(P) LGA	Down	Ccdc89	3654	-4.47	0.08	1.91E-04	1.48E-03	0.77
TR(P) versus T(P) LGA	Down	Ddhd2	5106	-4.47	0.07	1.93E-04	1.50E-03	0.80
TR(P) versus T(P) LGA	Down	Clec3b	4229	-4.46	0.10	1.97E-04	1.52E-03	0.74
TR(P) versus T(P) LGA	Down	Hrk	8223	-4.46	0.10	1.97E-04	1.52E-03	0.73
TR(P) versus T(P) LGA	Down	Rbm4b	13620	-4.46	0.05	1.97E-04	1.52E-03	0.84
TR(P) versus T(P) LGA	Down	Arm9	2470	-4.46	0.07	1.97E-04	1.52E-03	0.81

TR(P) versus T(P) LGA	Down	Hdac5	7953	-4.45	0.10	2.03E-04	1.56E-03	0.73
TR(P) versus T(P) LGA	Down	6820408C15Rik	1235	-4.45	0.08	2.03E-04	1.56E-03	0.78
TR(P) versus T(P) LGA	Down	Syngn3	15741	-4.45	0.10	2.04E-04	1.56E-03	0.74
TR(P) versus T(P) LGA	Down	Nfil3	10828	-4.45	0.10	2.04E-04	1.56E-03	0.73
TR(P) versus T(P) LGA	Down	Nenf	10789	-4.45	0.09	2.04E-04	1.56E-03	0.76
TR(P) versus T(P) LGA	Down	Flrt3	6613	-4.45	0.11	2.05E-04	1.57E-03	0.72
TR(P) versus T(P) LGA	Down	Fam92a	6361	-4.44	0.06	2.09E-04	1.59E-03	0.84
TR(P) versus T(P) LGA	Down	2210408I21Rik	458	-4.44	0.06	2.10E-04	1.59E-03	0.84
TR(P) versus T(P) LGA	Down	Lass4	9198	-4.44	0.08	2.10E-04	1.59E-03	0.79
TR(P) versus T(P) LGA	Down	8430410K20Rik	1251	-4.44	0.06	2.10E-04	1.59E-03	0.84
TR(P) versus T(P) LGA	Down	Slc45a1	14972	-4.44	0.07	2.10E-04	1.59E-03	0.80
TR(P) versus T(P) LGA	Down	Ankrd13b	2180	-4.43	0.13	2.13E-04	1.61E-03	0.66
TR(P) versus T(P) LGA	Down	Atp1b1	2628	-4.43	0.11	2.14E-04	1.61E-03	0.71
TR(P) versus T(P) LGA	Down	Zscan18	18191	-4.43	0.06	2.14E-04	1.61E-03	0.82
TR(P) versus T(P) LGA	Down	Lrrc48	9535	-4.43	0.16	2.14E-04	1.61E-03	0.62
TR(P) versus T(P) LGA	Down	Ccdc81	3645	-4.42	0.22	2.16E-04	1.62E-03	0.51
TR(P) versus T(P) LGA	Down	Hdc	7958	-4.42	0.17	2.16E-04	1.62E-03	0.60
TR(P) versus T(P) LGA	Down	9330159F19Rik	1307	-4.42	0.10	2.16E-04	1.62E-03	0.74
TR(P) versus T(P) LGA	Down	Ankzf1	2220	-4.42	0.05	2.17E-04	1.62E-03	0.85
TR(P) versus T(P) LGA	Down	Ift81	8397	-4.42	0.09	2.18E-04	1.62E-03	0.75
TR(P) versus T(P) LGA	Down	Ube2e2	16989	-4.41	0.08	2.22E-04	1.65E-03	0.77
TR(P) versus T(P) LGA	Down	Ppid	12838	-4.41	0.06	2.22E-04	1.65E-03	0.83
TR(P) versus T(P) LGA	Down	Acan	1654	-4.41	0.11	2.22E-04	1.65E-03	0.72
TR(P) versus T(P) LGA	Down	Bag5	2855	-4.41	0.06	2.25E-04	1.66E-03	0.84
TR(P) versus T(P) LGA	Down	Ube2q1	17004	-4.40	0.04	2.26E-04	1.67E-03	0.88
TR(P) versus T(P) LGA	Down	March11	9800	-4.40	0.09	2.29E-04	1.68E-03	0.75
TR(P) versus T(P) LGA	Down	Tmem216	16341	-4.40	0.06	2.33E-04	1.70E-03	0.82
TR(P) versus T(P) LGA	Down	Ube2k	16998	-4.39	0.04	2.35E-04	1.71E-03	0.88
TR(P) versus T(P) LGA	Down	Ttll3	16873	-4.39	0.14	2.36E-04	1.71E-03	0.65
TR(P) versus T(P) LGA	Down	Sorbs2	15252	-4.39	0.10	2.38E-04	1.73E-03	0.73

TR(P) versus T(P) LGA	Down	Efcab1	5717	-4.39	0.14	2.39E-04	1.73E-03	0.65
TR(P) versus T(P) LGA	Down	Jkamp	8736	-4.39	0.05	2.39E-04	1.73E-03	0.85
TR(P) versus T(P) LGA	Down	Ccl25	3676	-4.38	0.09	2.42E-04	1.74E-03	0.76
TR(P) versus T(P) LGA	Down	9630003H22Rik	1373	-4.38	0.15	2.43E-04	1.75E-03	0.64
TR(P) versus T(P) LGA	Down	Cdcp1	3864	-4.38	0.06	2.43E-04	1.75E-03	0.84
TR(P) versus T(P) LGA	Down	C230091D08Rik	3285	-4.38	0.07	2.44E-04	1.75E-03	0.80
TR(P) versus T(P) LGA	Down	Trp53bp1	16725	-4.38	0.06	2.44E-04	1.75E-03	0.84
TR(P) versus T(P) LGA	Down	St3gal1	15520	-4.37	0.07	2.50E-04	1.78E-03	0.80
TR(P) versus T(P) LGA	Down	Dus3l	5535	-4.36	0.06	2.50E-04	1.78E-03	0.84
TR(P) versus T(P) LGA	Down	Pitpna	12510	-4.36	0.07	2.53E-04	1.79E-03	0.82
TR(P) versus T(P) LGA	Down	Chordc1	4105	-4.36	0.09	2.56E-04	1.81E-03	0.77
TR(P) versus T(P) LGA	Down	Rnmt	13953	-4.36	0.06	2.56E-04	1.81E-03	0.84
TR(P) versus T(P) LGA	Down	Pcsk1	12181	-4.36	0.13	2.56E-04	1.81E-03	0.67
TR(P) versus T(P) LGA	Down	BC005764	2911	-4.35	0.10	2.57E-04	1.81E-03	0.74
TR(P) versus T(P) LGA	Down	Abca8a	1576	-4.35	0.09	2.57E-04	1.81E-03	0.76
TR(P) versus T(P) LGA	Down	Adra1a	1860	-4.34	0.08	2.67E-04	1.87E-03	0.80
TR(P) versus T(P) LGA	Down	Rnft2	13949	-4.34	0.07	2.68E-04	1.88E-03	0.81
TR(P) versus T(P) LGA	Down	Trnp1	16718	-4.34	0.09	2.70E-04	1.89E-03	0.76
TR(P) versus T(P) LGA	Down	Dnalc1	5395	-4.33	0.10	2.78E-04	1.93E-03	0.74
TR(P) versus T(P) LGA	Down	5033430I15Rik	1075	-4.33	0.14	2.78E-04	1.93E-03	0.66
TR(P) versus T(P) LGA	Down	Slc25a14	14818	-4.33	0.08	2.78E-04	1.93E-03	0.78
TR(P) versus T(P) LGA	Down	Dctn3	5087	-4.33	0.08	2.80E-04	1.95E-03	0.78
TR(P) versus T(P) LGA	Down	2900009J20Rik	698	-4.32	0.11	2.91E-04	2.01E-03	0.71
TR(P) versus T(P) LGA	Down	Agpat4	1911	-4.32	0.08	2.95E-04	2.03E-03	0.78
TR(P) versus T(P) LGA	Down	Rprd1a	14043	-4.32	0.05	2.95E-04	2.03E-03	0.86
TR(P) versus T(P) LGA	Down	Mapre3	9796	-4.32	0.09	2.95E-04	2.03E-03	0.77
TR(P) versus T(P) LGA	Down	Fam179a	6253	-4.31	0.07	3.00E-04	2.06E-03	0.80
TR(P) versus T(P) LGA	Down	Dcc	5065	-4.31	0.08	3.00E-04	2.06E-03	0.80
TR(P) versus T(P) LGA	Down	Armc3	2465	-4.31	0.23	3.01E-04	2.06E-03	0.50
TR(P) versus T(P) LGA	Down	Lpgat1	9463	-4.31	0.11	3.02E-04	2.07E-03	0.71

TR(P) versus T(P) LGA	Down	Dnaja1	5351	-4.31	0.06	3.04E-04	2.07E-03	0.83
TR(P) versus T(P) LGA	Down	Necap1	10763	-4.31	0.08	3.05E-04	2.07E-03	0.79
TR(P) versus T(P) LGA	Down	Hyou1	8315	-4.31	0.07	3.05E-04	2.08E-03	0.80
TR(P) versus T(P) LGA	Down	Krt222	9090	-4.30	0.12	3.06E-04	2.08E-03	0.69
TR(P) versus T(P) LGA	Down	0610010O12Rik	15	-4.30	0.13	3.09E-04	2.10E-03	0.68
TR(P) versus T(P) LGA	Down	Fkbp3	6592	-4.30	0.07	3.13E-04	2.12E-03	0.82
TR(P) versus T(P) LGA	Down	Api5	2295	-4.29	0.04	3.13E-04	2.12E-03	0.88
TR(P) versus T(P) LGA	Down	LOC100504423	9405	-4.29	0.11	3.13E-04	2.12E-03	0.72
TR(P) versus T(P) LGA	Down	Syt13	15760	-4.29	0.13	3.13E-04	2.12E-03	0.68
TR(P) versus T(P) LGA	Down	Tmem191c	16319	-4.29	0.08	3.14E-04	2.12E-03	0.78
TR(P) versus T(P) LGA	Down	Cc2d1a	3540	-4.29	0.05	3.14E-04	2.12E-03	0.85
TR(P) versus T(P) LGA	Down	Sc4mol	14268	-4.29	0.09	3.16E-04	2.13E-03	0.76
TR(P) versus T(P) LGA	Down	Ywhaz	17663	-4.29	0.06	3.20E-04	2.15E-03	0.83
TR(P) versus T(P) LGA	Down	Gnl3l	7493	-4.29	0.08	3.21E-04	2.15E-03	0.79
TR(P) versus T(P) LGA	Down	Ankrd34b	2196	-4.29	0.12	3.21E-04	2.15E-03	0.70
TR(P) versus T(P) LGA	Down	Ppm1l	12860	-4.28	0.09	3.22E-04	2.15E-03	0.75
TR(P) versus T(P) LGA	Down	Uckl1	17057	-4.28	0.05	3.25E-04	2.16E-03	0.85
TR(P) versus T(P) LGA	Down	Mtap6	10383	-4.28	0.12	3.26E-04	2.16E-03	0.71
TR(P) versus T(P) LGA	Down	S100a10	14191	-4.28	0.10	3.26E-04	2.16E-03	0.75
TR(P) versus T(P) LGA	Down	Kcnj6	8828	-4.28	0.10	3.26E-04	2.16E-03	0.73
TR(P) versus T(P) LGA	Down	Wls	17543	-4.28	0.09	3.26E-04	2.16E-03	0.76
TR(P) versus T(P) LGA	Down	Arl16	2445	-4.27	0.08	3.29E-04	2.18E-03	0.80
TR(P) versus T(P) LGA	Down	Pip5k1b	12503	-4.27	0.13	3.33E-04	2.20E-03	0.68
TR(P) versus T(P) LGA	Down	Lime1	9322	-4.27	0.09	3.35E-04	2.22E-03	0.76
TR(P) versus T(P) LGA	Down	Nap1l2	10625	-4.26	0.15	3.44E-04	2.27E-03	0.65
TR(P) versus T(P) LGA	Down	Enpp5	5912	-4.26	0.10	3.46E-04	2.27E-03	0.75
TR(P) versus T(P) LGA	Down	Neu2	10797	-4.26	0.12	3.46E-04	2.27E-03	0.70
TR(P) versus T(P) LGA	Down	Fank1	6379	-4.26	0.14	3.49E-04	2.28E-03	0.67
TR(P) versus T(P) LGA	Down	Ttc18	16830	-4.25	0.12	3.52E-04	2.30E-03	0.70
TR(P) versus T(P) LGA	Down	Abhd14b	1614	-4.25	0.07	3.52E-04	2.30E-03	0.81

TR(P) versus T(P) LGA	Down	Gckr	6928	-4.25	0.11	3.54E-04	2.30E-03	0.73
TR(P) versus T(P) LGA	Down	Trappc4	16616	-4.25	0.05	3.56E-04	2.31E-03	0.86
TR(P) versus T(P) LGA	Down	1190003J15Rik	90	-4.24	0.15	3.58E-04	2.32E-03	0.64
TR(P) versus T(P) LGA	Down	Sbno1	14264	-4.24	0.06	3.61E-04	2.33E-03	0.85
TR(P) versus T(P) LGA	Down	Sc5d	14269	-4.24	0.07	3.61E-04	2.33E-03	0.81
TR(P) versus T(P) LGA	Down	Ces5a	4024	-4.24	0.06	3.61E-04	2.33E-03	0.83
TR(P) versus T(P) LGA	Down	Tekt1	15997	-4.24	0.12	3.62E-04	2.33E-03	0.70
TR(P) versus T(P) LGA	Down	Mterfd3	10396	-4.23	0.09	3.67E-04	2.35E-03	0.77
TR(P) versus T(P) LGA	Down	Uhrf1bp1l	17085	-4.23	0.06	3.69E-04	2.36E-03	0.83
TR(P) versus T(P) LGA	Down	Zfr	18114	-4.23	0.06	3.69E-04	2.36E-03	0.83
TR(P) versus T(P) LGA	Down	Dpm1	5460	-4.23	0.07	3.72E-04	2.37E-03	0.80
TR(P) versus T(P) LGA	Down	Rnf214	13925	-4.23	0.06	3.73E-04	2.37E-03	0.84
TR(P) versus T(P) LGA	Down	Ppp1r36	12893	-4.23	0.15	3.73E-04	2.37E-03	0.64
TR(P) versus T(P) LGA	Down	Ap1s2	2259	-4.23	0.09	3.76E-04	2.39E-03	0.76
TR(P) versus T(P) LGA	Down	Sdpr	14362	-4.22	0.09	3.76E-04	2.39E-03	0.78
TR(P) versus T(P) LGA	Down	Fytd1	6780	-4.22	0.06	3.76E-04	2.39E-03	0.84
TR(P) versus T(P) LGA	Down	Lgi2	9288	-4.22	0.15	3.77E-04	2.39E-03	0.64
TR(P) versus T(P) LGA	Down	Morf4l1	10183	-4.22	0.05	3.81E-04	2.41E-03	0.86
TR(P) versus T(P) LGA	Down	Rrn3	14106	-4.22	0.05	3.84E-04	2.42E-03	0.87
TR(P) versus T(P) LGA	Down	Wdr65	17487	-4.22	0.14	3.85E-04	2.42E-03	0.67
TR(P) versus T(P) LGA	Down	Ufsp1	17067	-4.22	0.07	3.86E-04	2.43E-03	0.81
TR(P) versus T(P) LGA	Down	Avpi1	2730	-4.21	0.11	3.90E-04	2.44E-03	0.74
TR(P) versus T(P) LGA	Down	Capsl	3447	-4.21	0.19	3.91E-04	2.45E-03	0.57
TR(P) versus T(P) LGA	Down	Pdp1	12263	-4.21	0.13	3.96E-04	2.47E-03	0.69
TR(P) versus T(P) LGA	Down	1700026L06Rik	259	-4.21	0.23	3.99E-04	2.48E-03	0.51
TR(P) versus T(P) LGA	Down	Rpl11	13995	-4.20	0.05	4.06E-04	2.52E-03	0.87
TR(P) versus T(P) LGA	Down	Inpp4a	8551	-4.20	0.08	4.07E-04	2.52E-03	0.78
TR(P) versus T(P) LGA	Down	Mb	9840	-4.19	0.10	4.13E-04	2.54E-03	0.74
TR(P) versus T(P) LGA	Down	Stk39	15604	-4.19	0.10	4.14E-04	2.54E-03	0.76
TR(P) versus T(P) LGA	Down	1110004E09Rik	38	-4.19	0.09	4.14E-04	2.54E-03	0.78

TR(P) versus T(P) LGA	Down	Sema3a	14411	-4.19	0.09	4.15E-04	2.54E-03	0.77
TR(P) versus T(P) LGA	Down	B4galt6	2824	-4.19	0.10	4.15E-04	2.54E-03	0.74
TR(P) versus T(P) LGA	Down	Paip2	12013	-4.19	0.07	4.17E-04	2.55E-03	0.82
TR(P) versus T(P) LGA	Down	Fam110b	6163	-4.19	0.10	4.18E-04	2.56E-03	0.74
TR(P) versus T(P) LGA	Down	Casc1	3479	-4.19	0.08	4.19E-04	2.56E-03	0.78
TR(P) versus T(P) LGA	Down	Cyb561d1	4762	-4.18	0.09	4.19E-04	2.56E-03	0.77
TR(P) versus T(P) LGA	Down	Hagh	7893	-4.18	0.09	4.23E-04	2.58E-03	0.78
TR(P) versus T(P) LGA	Down	Tmem218	16343	-4.18	0.07	4.25E-04	2.59E-03	0.82
TR(P) versus T(P) LGA	Down	Tctn2	15968	-4.18	0.11	4.25E-04	2.59E-03	0.72
TR(P) versus T(P) LGA	Down	L3mbtl4	9153	-4.18	0.09	4.25E-04	2.59E-03	0.78
TR(P) versus T(P) LGA	Down	Msx1	10365	-4.18	0.11	4.29E-04	2.60E-03	0.72
TR(P) versus T(P) LGA	Down	Rtn4	14149	-4.18	0.10	4.29E-04	2.60E-03	0.74
TR(P) versus T(P) LGA	Down	Chchd7	4061	-4.18	0.13	4.30E-04	2.60E-03	0.69
TR(P) versus T(P) LGA	Down	Srrm4	15470	-4.18	0.12	4.32E-04	2.61E-03	0.70
TR(P) versus T(P) LGA	Down	Nkiras1	10897	-4.17	0.11	4.35E-04	2.62E-03	0.73
TR(P) versus T(P) LGA	Down	Ift57	8394	-4.17	0.07	4.38E-04	2.63E-03	0.83
TR(P) versus T(P) LGA	Down	Ncoa7	10692	-4.17	0.12	4.38E-04	2.63E-03	0.70
TR(P) versus T(P) LGA	Down	Rab3a	13419	-4.16	0.10	4.39E-04	2.64E-03	0.74
TR(P) versus T(P) LGA	Down	Sars	14248	-4.16	0.06	4.40E-04	2.64E-03	0.85
TR(P) versus T(P) LGA	Down	Akd1	2016	-4.16	0.17	4.44E-04	2.66E-03	0.61
TR(P) versus T(P) LGA	Down	A030010E16Rik	1404	-4.16	0.10	4.46E-04	2.67E-03	0.75
TR(P) versus T(P) LGA	Down	Hdac11	7949	-4.16	0.09	4.47E-04	2.67E-03	0.77
TR(P) versus T(P) LGA	Down	Camk2n2	3414	-4.16	0.12	4.50E-04	2.67E-03	0.71
TR(P) versus T(P) LGA	Down	Gipr	7018	-4.16	0.11	4.50E-04	2.67E-03	0.74
TR(P) versus T(P) LGA	Down	Cacng2	3370	-4.15	0.12	4.51E-04	2.68E-03	0.71
TR(P) versus T(P) LGA	Down	Clstn3	4272	-4.15	0.16	4.52E-04	2.68E-03	0.63
TR(P) versus T(P) LGA	Down	Stx18	15637	-4.15	0.06	4.55E-04	2.69E-03	0.85
TR(P) versus T(P) LGA	Down	Ccrn4l	3725	-4.15	0.13	4.56E-04	2.69E-03	0.69
TR(P) versus T(P) LGA	Down	A930011O12Rik	1535	-4.15	0.07	4.57E-04	2.69E-03	0.81
TR(P) versus T(P) LGA	Down	Epor	5965	-4.15	0.11	4.57E-04	2.69E-03	0.73

TR(P) versus T(P) LGA	Down	B3galt2	2797	-4.15	0.08	4.58E-04	2.69E-03	0.79
TR(P) versus T(P) LGA	Down	Jakmip1	8727	-4.15	0.11	4.62E-04	2.71E-03	0.73
TR(P) versus T(P) LGA	Down	Cltb	4274	-4.14	0.06	4.66E-04	2.72E-03	0.85
TR(P) versus T(P) LGA	Down	Dcn	5076	-4.14	0.16	4.68E-04	2.73E-03	0.63
TR(P) versus T(P) LGA	Down	Pde4a	12221	-4.14	0.09	4.68E-04	2.73E-03	0.76
TR(P) versus T(P) LGA	Down	Mapk10	9772	-4.14	0.07	4.71E-04	2.74E-03	0.83
TR(P) versus T(P) LGA	Down	Nr2f2	11049	-4.14	0.10	4.74E-04	2.75E-03	0.75
TR(P) versus T(P) LGA	Down	Mirg	10081	-4.13	0.15	4.79E-04	2.78E-03	0.66
TR(P) versus T(P) LGA	Down	Fbxo9	6464	-4.13	0.09	4.81E-04	2.79E-03	0.78
TR(P) versus T(P) LGA	Down	3110047P20Rik	743	-4.12	0.10	4.86E-04	2.82E-03	0.74
TR(P) versus T(P) LGA	Down	Katnb1	8772	-4.12	0.04	4.88E-04	2.82E-03	0.90
TR(P) versus T(P) LGA	Down	2410004A20Rik	544	-4.12	0.11	4.88E-04	2.82E-03	0.72
TR(P) versus T(P) LGA	Down	BC010981	2914	-4.12	0.10	4.93E-04	2.84E-03	0.74
TR(P) versus T(P) LGA	Down	Ttc16	16828	-4.12	0.11	4.95E-04	2.85E-03	0.73
TR(P) versus T(P) LGA	Down	2900011G08Rik	700	-4.11	0.12	5.05E-04	2.90E-03	0.70
TR(P) versus T(P) LGA	Down	Fkbp1a	6589	-4.11	0.06	5.06E-04	2.90E-03	0.85
TR(P) versus T(P) LGA	Down	Cby3	3539	-4.11	0.09	5.06E-04	2.90E-03	0.77
TR(P) versus T(P) LGA	Down	Rad23b	13467	-4.11	0.05	5.08E-04	2.91E-03	0.86
TR(P) versus T(P) LGA	Down	Paqr6	12051	-4.11	0.12	5.10E-04	2.92E-03	0.71
TR(P) versus T(P) LGA	Down	Plekha5	12608	-4.11	0.11	5.11E-04	2.92E-03	0.74
TR(P) versus T(P) LGA	Down	Plekhg4	12619	-4.11	0.10	5.12E-04	2.92E-03	0.75
TR(P) versus T(P) LGA	Down	Cnfn	4306	-4.10	0.07	5.18E-04	2.95E-03	0.81
TR(P) versus T(P) LGA	Down	Csnk1a1	4625	-4.10	0.05	5.19E-04	2.95E-03	0.87
TR(P) versus T(P) LGA	Down	Cnksr2	4314	-4.10	0.11	5.20E-04	2.95E-03	0.72
TR(P) versus T(P) LGA	Down	Pnpo	12706	-4.09	0.12	5.24E-04	2.96E-03	0.71
TR(P) versus T(P) LGA	Down	1500011B03Rik	120	-4.09	0.10	5.25E-04	2.96E-03	0.75
TR(P) versus T(P) LGA	Down	Cacnb2	3366	-4.09	0.07	5.25E-04	2.96E-03	0.82
TR(P) versus T(P) LGA	Down	Wrb	17564	-4.09	0.06	5.25E-04	2.96E-03	0.83
TR(P) versus T(P) LGA	Down	Nkpd1	10899	-4.09	0.12	5.25E-04	2.96E-03	0.72
TR(P) versus T(P) LGA	Down	Mia1	10052	-4.09	0.11	5.25E-04	2.96E-03	0.74

TR(P) versus T(P) LGA	Down	Armcx3	2473	-4.09	0.05	5.30E-04	2.98E-03	0.87
TR(P) versus T(P) LGA	Down	2010003D24Rik	408	-4.09	0.12	5.39E-04	3.03E-03	0.72
TR(P) versus T(P) LGA	Down	Rhou	13799	-4.08	0.13	5.45E-04	3.05E-03	0.69
TR(P) versus T(P) LGA	Down	4921509J17Rik	810	-4.08	0.10	5.46E-04	3.05E-03	0.75
TR(P) versus T(P) LGA	Down	Iqcg	8606	-4.08	0.19	5.46E-04	3.05E-03	0.59
TR(P) versus T(P) LGA	Down	Orai2	11890	-4.08	0.08	5.47E-04	3.05E-03	0.80
TR(P) versus T(P) LGA	Down	Snx32	15228	-4.08	0.04	5.51E-04	3.07E-03	0.89
TR(P) versus T(P) LGA	Down	Itm2c	8704	-4.08	0.06	5.51E-04	3.07E-03	0.84
TR(P) versus T(P) LGA	Down	Prpf39	13074	-4.07	0.07	5.58E-04	3.09E-03	0.82
TR(P) versus T(P) LGA	Down	Zdhhc1	17746	-4.07	0.08	5.58E-04	3.09E-03	0.81
TR(P) versus T(P) LGA	Down	Ppp3ca	12923	-4.07	0.14	5.61E-04	3.11E-03	0.67
TR(P) versus T(P) LGA	Down	Pank4	12035	-4.07	0.04	5.62E-04	3.11E-03	0.88
TR(P) versus T(P) LGA	Down	Rsph1	14126	-4.07	0.14	5.63E-04	3.11E-03	0.68
TR(P) versus T(P) LGA	Down	Tacc1	15788	-4.07	0.07	5.65E-04	3.12E-03	0.83
TR(P) versus T(P) LGA	Down	Cdh8	3885	-4.07	0.13	5.65E-04	3.12E-03	0.69
TR(P) versus T(P) LGA	Down	5330426P16Rik	1081	-4.07	0.07	5.66E-04	3.12E-03	0.81
TR(P) versus T(P) LGA	Down	2900006K08Rik	697	-4.06	0.11	5.69E-04	3.12E-03	0.73
TR(P) versus T(P) LGA	Down	Ip6k2	8586	-4.06	0.08	5.72E-04	3.13E-03	0.80
TR(P) versus T(P) LGA	Down	Zcchc7	17740	-4.06	0.09	5.74E-04	3.15E-03	0.77
TR(P) versus T(P) LGA	Down	Arpm1	2488	-4.06	0.10	5.75E-04	3.15E-03	0.76
TR(P) versus T(P) LGA	Down	Kif5a	8941	-4.06	0.09	5.84E-04	3.19E-03	0.79
TR(P) versus T(P) LGA	Down	Usp33	17176	-4.06	0.05	5.85E-04	3.19E-03	0.86
TR(P) versus T(P) LGA	Down	Pip4k2c	12501	-4.05	0.06	5.92E-04	3.22E-03	0.84
TR(P) versus T(P) LGA	Down	Cdk9	3915	-4.05	0.05	5.92E-04	3.22E-03	0.87
TR(P) versus T(P) LGA	Down	Ttc25	16837	-4.05	0.12	5.92E-04	3.22E-03	0.71
TR(P) versus T(P) LGA	Down	2810032G03Rik	660	-4.05	0.15	5.94E-04	3.23E-03	0.66
TR(P) versus T(P) LGA	Down	D16H22S680E	4900	-4.05	0.09	5.98E-04	3.25E-03	0.78
TR(P) versus T(P) LGA	Down	Timm9	16148	-4.05	0.05	5.99E-04	3.25E-03	0.87
TR(P) versus T(P) LGA	Down	Usp29	17171	-4.05	0.11	6.03E-04	3.26E-03	0.74
TR(P) versus T(P) LGA	Down	Fam78b	6345	-4.05	0.11	6.03E-04	3.26E-03	0.74

TR(P) versus T(P) LGA	Down	Gnl2	7491	-4.04	0.05	6.05E-04	3.26E-03	0.87
TR(P) versus T(P) LGA	Down	Col6a1	4400	-4.04	0.09	6.08E-04	3.27E-03	0.78
TR(P) versus T(P) LGA	Down	Ociad2	11232	-4.04	0.13	6.14E-04	3.30E-03	0.69
TR(P) versus T(P) LGA	Down	Kptn	9069	-4.04	0.07	6.14E-04	3.30E-03	0.83
TR(P) versus T(P) LGA	Down	Kifap3	8947	-4.04	0.09	6.14E-04	3.30E-03	0.78
TR(P) versus T(P) LGA	Down	Bend6	3054	-4.03	0.15	6.18E-04	3.31E-03	0.66
TR(P) versus T(P) LGA	Down	Mlf1	10102	-4.03	0.22	6.24E-04	3.33E-03	0.53
TR(P) versus T(P) LGA	Down	Ccdc11	3557	-4.03	0.12	6.30E-04	3.35E-03	0.72
TR(P) versus T(P) LGA	Down	Fbxo25	6442	-4.02	0.09	6.36E-04	3.38E-03	0.77
TR(P) versus T(P) LGA	Down	Fabp3	6130	-4.02	0.15	6.38E-04	3.39E-03	0.65
TR(P) versus T(P) LGA	Down	Pdxdp	12275	-4.02	0.12	6.43E-04	3.41E-03	0.72
TR(P) versus T(P) LGA	Down	Olfr1093	11292	-4.02	0.08	6.43E-04	3.41E-03	0.81
TR(P) versus T(P) LGA	Down	Ccdc108	3554	-4.02	0.08	6.45E-04	3.42E-03	0.81
TR(P) versus T(P) LGA	Down	Cd200	3750	-4.02	0.09	6.46E-04	3.42E-03	0.77
TR(P) versus T(P) LGA	Down	Fn3k	6634	-4.01	0.07	6.51E-04	3.44E-03	0.82
TR(P) versus T(P) LGA	Down	1700045119Rik	295	-4.01	0.17	6.52E-04	3.44E-03	0.62
TR(P) versus T(P) LGA	Down	Crelid1	4555	-4.01	0.06	6.57E-04	3.45E-03	0.84
TR(P) versus T(P) LGA	Down	Zbbx	17669	-4.01	0.15	6.61E-04	3.47E-03	0.65
TR(P) versus T(P) LGA	Down	Slmo1	15070	-4.01	0.05	6.61E-04	3.47E-03	0.87
TR(P) versus T(P) LGA	Down	A330076H08Rik	1448	-4.01	0.16	6.62E-04	3.47E-03	0.65
TR(P) versus T(P) LGA	Down	Dlec1	5294	-4.01	0.12	6.64E-04	3.47E-03	0.72
TR(P) versus T(P) LGA	Down	Ddx55	5150	-4.01	0.06	6.64E-04	3.47E-03	0.85
TR(P) versus T(P) LGA	Down	Hs6st2	8232	-4.00	0.12	6.67E-04	3.48E-03	0.72
TR(P) versus T(P) LGA	Down	P4ha2	11983	-4.00	0.10	6.68E-04	3.48E-03	0.76
TR(P) versus T(P) LGA	Down	1700019L03Rik	225	-4.00	0.11	6.68E-04	3.48E-03	0.74
TR(P) versus T(P) LGA	Down	Prosapip1	13062	-4.00	0.08	6.76E-04	3.51E-03	0.81
TR(P) versus T(P) LGA	Down	Elp3	5867	-4.00	0.05	6.77E-04	3.52E-03	0.86
TR(P) versus T(P) LGA	Down	Gcc2	6919	-4.00	0.07	6.80E-04	3.53E-03	0.82
TR(P) versus T(P) LGA	Down	Zmat1	18146	-3.99	0.07	6.82E-04	3.53E-03	0.82
TR(P) versus T(P) LGA	Down	Ccdc103	3550	-3.99	0.13	6.88E-04	3.56E-03	0.70

TR(P) versus T(P) LGA	Down	Tspyl1	16805	-3.99	0.12	6.93E-04	3.58E-03	0.72
TR(P) versus T(P) LGA	Down	Dlg2	5297	-3.99	0.10	6.96E-04	3.58E-03	0.76
TR(P) versus T(P) LGA	Down	Zmynd8	18166	-3.99	0.09	6.96E-04	3.58E-03	0.77
TR(P) versus T(P) LGA	Down	Elavl2	5837	-3.98	0.16	6.99E-04	3.60E-03	0.64
TR(P) versus T(P) LGA	Up	Prokr1	13056	11.57	0.21	0	0	5.46
TR(P) versus T(P) LGA	Up	Hoxa1	8164	11.43	0.27	0	0	8.21
TR(P) versus T(P) LGA	Up	Etv4	6051	10.96	0.16	0	0	3.49
TR(P) versus T(P) LGA	Up	Spry1	15413	9.69	0.19	0	0	3.50
TR(P) versus T(P) LGA	Up	Chst7	4141	9.63	0.19	0	0	3.66
TR(P) versus T(P) LGA	Up	Bves	3212	9.50	0.25	0	0	5.09
TR(P) versus T(P) LGA	Up	Aldh1l1	2052	9.38	0.09	0	0	1.76
TR(P) versus T(P) LGA	Up	Igfbp2	8410	9.24	0.21	0	0	3.91
TR(P) versus T(P) LGA	Up	Hoxa7	8173	9.20	0.29	0	0	6.54
TR(P) versus T(P) LGA	Up	Sept9	14456	9.18	0.09	0	0	1.83
TR(P) versus T(P) LGA	Up	Igfbp3	8411	9.03	0.11	0	0	1.97
TR(P) versus T(P) LGA	Up	Frk	6707	8.86	0.14	0	0	2.37
TR(P) versus T(P) LGA	Up	Gsc	7732	8.83	0.22	0	0	3.76
TR(P) versus T(P) LGA	Up	Apobec1	2309	8.76	0.14	0	0	2.41
TR(P) versus T(P) LGA	Up	Traf4	16597	8.74	0.21	0	0	3.53
TR(P) versus T(P) LGA	Up	Lgals3bp	9281	8.39	0.18	0	0	2.84
TR(P) versus T(P) LGA	Up	Akr1b10	2022	8.33	0.10	0	0	1.76
TR(P) versus T(P) LGA	Up	Lgals9	9286	8.32	0.12	0	0	2.04
TR(P) versus T(P) LGA	Up	Fam5c	6322	8.30	0.09	0	0	1.72
TR(P) versus T(P) LGA	Up	Slfn10-ps	15053	8.28	0.19	0	0	3.02
TR(P) versus T(P) LGA	Up	Rsad2	14118	8.24	0.20	0	0	3.15
TR(P) versus T(P) LGA	Up	Skap2	14708	8.22	0.14	0	0	2.18
TR(P) versus T(P) LGA	Up	Fgfr11	6553	8.16	0.10	0	0	1.74
TR(P) versus T(P) LGA	Up	Gng12	7481	8.16	0.13	0	0	2.04
TR(P) versus T(P) LGA	Up	Lpar6	9458	8.12	0.08	0	0	1.60
TR(P) versus T(P) LGA	Up	Cst7	4650	8.06	0.30	0	0	5.39

TR(P) versus T(P) LGA	Up	Cspg4	4634	8.02	0.12	0	0	2.00
TR(P) versus T(P) LGA	Up	Stat1	15566	8.01	0.15	0	0	2.30
TR(P) versus T(P) LGA	Up	Hoxa2	8168	7.99	0.31	0	0	5.67
TR(P) versus T(P) LGA	Up	Dusp6	5554	7.98	0.13	0	0	2.08
TR(P) versus T(P) LGA	Up	Raet1a	13482	7.91	0.15	0	0	2.29
TR(P) versus T(P) LGA	Up	Usp18	17160	7.88	0.19	0	0	2.80
TR(P) versus T(P) LGA	Up	Irf7	8629	7.87	0.20	0	0	3.02
TR(P) versus T(P) LGA	Up	Creb5	4549	7.86	0.07	0	0	1.50
TR(P) versus T(P) LGA	Up	Herc6	7997	7.85	0.15	0	0	2.24
TR(P) versus T(P) LGA	Up	Niacr1	10865	7.84	0.22	0	0	3.33
TR(P) versus T(P) LGA	Up	Acadl	1649	7.83	0.11	0	0	1.82
TR(P) versus T(P) LGA	Up	Klhl5	9020	7.79	0.08	0	0	1.57
TR(P) versus T(P) LGA	Up	Ctsc	4697	7.79	0.18	0	0	2.62
TR(P) versus T(P) LGA	Up	Tmem176b	16300	7.78	0.13	0	0	2.03
TR(P) versus T(P) LGA	Up	Pmaip1	12670	7.77	0.23	0	0	3.41
TR(P) versus T(P) LGA	Up	Rasa13	13544	7.77	0.09	0	0	1.60
TR(P) versus T(P) LGA	Up	Parp9	12077	7.69	0.13	0	0	2.01
TR(P) versus T(P) LGA	Up	F2r	6111	7.63	0.12	0	0	1.92
TR(P) versus T(P) LGA	Up	Tmem37	16360	7.58	0.20	0	0	2.85
TR(P) versus T(P) LGA	Up	Trib2	16643	7.58	0.12	0	0	1.87
TR(P) versus T(P) LGA	Up	Hoxa5	8171	7.56	0.33	0	0	5.69
TR(P) versus T(P) LGA	Up	Trim25	16658	7.48	0.13	0	0	1.93
TR(P) versus T(P) LGA	Up	Zranb3	18186	7.47	0.05	0	0	1.33
TR(P) versus T(P) LGA	Up	Ttpa	16881	7.46	0.19	0	0	2.68
TR(P) versus T(P) LGA	Up	Pdgfra	12241	7.44	0.09	0	0	1.58
TR(P) versus T(P) LGA	Up	Ddx58	5152	7.43	0.13	0	0	1.96
TR(P) versus T(P) LGA	Up	Tmem176a	16299	7.43	0.13	0	0	1.92
TR(P) versus T(P) LGA	Up	Lpcat1	9459	7.42	0.10	0	0	1.68
TR(P) versus T(P) LGA	Up	Metrn1	9983	7.41	0.10	0	0	1.68
TR(P) versus T(P) LGA	Up	Kctd12b	8862	7.36	0.09	0	0	1.60

TR(P) versus T(P) LGA	Up	Dll3	5309	7.33	0.14	0	0	2.00
TR(P) versus T(P) LGA	Up	Irf8	8630	7.31	0.12	0	0	1.87
TR(P) versus T(P) LGA	Up	Fam83d	6351	7.30	0.07	0	0	1.46
TR(P) versus T(P) LGA	Up	Plekhhf2	12615	7.29	0.09	0	0	1.60
TR(P) versus T(P) LGA	Up	Ercc6l	5992	7.26	0.11	0	0	1.77
TR(P) versus T(P) LGA	Up	Shmt1	14654	7.25	0.10	0	0	1.67
TR(P) versus T(P) LGA	Up	Tmem144	16270	7.24	0.13	0	0	1.95
TR(P) versus T(P) LGA	Up	Suc1g2	15660	7.24	0.11	0	0	1.75
TR(P) versus T(P) LGA	Up	Irgm1	8634	7.24	0.20	0	0	2.69
TR(P) versus T(P) LGA	Up	Vav3	17242	7.21	0.12	0	0	1.83
TR(P) versus T(P) LGA	Up	Hexb	8007	7.19	0.09	0	0	1.55
TR(P) versus T(P) LGA	Up	Zc3hav1	17724	7.18	0.09	0	0	1.53
TR(P) versus T(P) LGA	Up	Oas1f	11215	7.15	0.21	0	0	2.77
TR(P) versus T(P) LGA	Up	Oas2	11216	7.13	0.20	0	0	2.66
TR(P) versus T(P) LGA	Up	E2f2	5632	7.11	0.11	0	0	1.75
TR(P) versus T(P) LGA	Up	Papss1	12046	7.10	0.05	0	0	1.27
TR(P) versus T(P) LGA	Up	Tgif2	16067	7.09	0.17	0	0	2.27
TR(P) versus T(P) LGA	Up	BC064078	2986	7.08	0.25	0	0	3.47
TR(P) versus T(P) LGA	Up	Kras	9070	7.08	0.07	0	0	1.39
TR(P) versus T(P) LGA	Up	Mdfic	9898	7.05	0.18	0	0	2.40
TR(P) versus T(P) LGA	Up	Arhgap24	2387	7.05	0.06	0	0	1.34
TR(P) versus T(P) LGA	Up	Sp100	15286	7.02	0.10	5.49E-07	3.46E-05	1.62
TR(P) versus T(P) LGA	Up	Galnt3	6851	6.98	0.12	5.49E-07	3.46E-05	1.78
TR(P) versus T(P) LGA	Up	Prr11	13088	6.97	0.09	5.49E-07	3.46E-05	1.53
TR(P) versus T(P) LGA	Up	Ifi47	8363	6.96	0.21	5.49E-07	3.46E-05	2.76
TR(P) versus T(P) LGA	Up	Arhgap18	2381	6.95	0.15	5.49E-07	3.46E-05	2.02
TR(P) versus T(P) LGA	Up	Ifih1	8364	6.94	0.15	5.49E-07	3.46E-05	2.06
TR(P) versus T(P) LGA	Up	Gpnmb	7564	6.94	0.06	5.49E-07	3.46E-05	1.35
TR(P) versus T(P) LGA	Up	Tspan12	16786	6.93	0.14	5.49E-07	3.46E-05	1.93
TR(P) versus T(P) LGA	Up	Txn1	16930	6.92	0.09	5.49E-07	3.46E-05	1.52

TR(P) versus T(P) LGA	Up	Cxcl11	4745	6.91	0.20	5.49E-07	3.46E-05	2.61
TR(P) versus T(P) LGA	Up	Megf6	9956	6.91	0.19	5.49E-07	3.46E-05	2.52
TR(P) versus T(P) LGA	Up	Galnt4	6852	6.90	0.11	5.49E-07	3.46E-05	1.71
TR(P) versus T(P) LGA	Up	Isg15	8648	6.89	0.23	5.49E-07	3.46E-05	2.97
TR(P) versus T(P) LGA	Up	Trim21	16655	6.88	0.15	5.49E-07	3.46E-05	2.01
TR(P) versus T(P) LGA	Up	Mpeg1	10201	6.86	0.11	5.49E-07	3.46E-05	1.65
TR(P) versus T(P) LGA	Up	Bst2	3180	6.85	0.23	5.49E-07	3.46E-05	2.95
TR(P) versus T(P) LGA	Up	Oas1a	11210	6.84	0.18	5.49E-07	3.46E-05	2.37
TR(P) versus T(P) LGA	Up	Rtp4	14157	6.82	0.27	5.49E-07	3.46E-05	3.63
TR(P) versus T(P) LGA	Up	6720463M24Rik	1227	6.82	0.11	5.49E-07	3.46E-05	1.68
TR(P) versus T(P) LGA	Up	Etv6	6053	6.82	0.07	5.49E-07	3.46E-05	1.40
TR(P) versus T(P) LGA	Up	Slc15a3	14749	6.82	0.12	5.49E-07	3.46E-05	1.78
TR(P) versus T(P) LGA	Up	Rab31	13408	6.82	0.12	5.49E-07	3.46E-05	1.73
TR(P) versus T(P) LGA	Up	Tlcd1	16166	6.80	0.09	5.49E-07	3.46E-05	1.53
TR(P) versus T(P) LGA	Up	Hus1	8305	6.77	0.07	5.49E-07	3.46E-05	1.41
TR(P) versus T(P) LGA	Up	Dhx58	5260	6.77	0.16	5.49E-07	3.46E-05	2.13
TR(P) versus T(P) LGA	Up	Itpril2	8713	6.76	0.10	5.49E-07	3.46E-05	1.61
TR(P) versus T(P) LGA	Up	Reep3	13682	6.76	0.08	5.49E-07	3.46E-05	1.49
TR(P) versus T(P) LGA	Up	Sh3bp4	14613	6.76	0.10	5.49E-07	3.46E-05	1.63
TR(P) versus T(P) LGA	Up	Gm1966	7227	6.75	0.15	5.49E-07	3.46E-05	1.99
TR(P) versus T(P) LGA	Up	Ppic	12837	6.73	0.19	5.49E-07	3.46E-05	2.40
TR(P) versus T(P) LGA	Up	Slfn8	15056	6.73	0.21	5.49E-07	3.46E-05	2.67
TR(P) versus T(P) LGA	Up	Ctsz	4710	6.73	0.07	5.49E-07	3.46E-05	1.41
TR(P) versus T(P) LGA	Up	Xaf1	17582	6.72	0.19	5.49E-07	3.46E-05	2.40
TR(P) versus T(P) LGA	Up	Eps8	5970	6.72	0.17	5.49E-07	3.46E-05	2.16
TR(P) versus T(P) LGA	Up	Ifi44	8362	6.71	0.23	5.49E-07	3.46E-05	2.91
TR(P) versus T(P) LGA	Up	Dpf3	5454	6.71	0.12	5.49E-07	3.46E-05	1.77
TR(P) versus T(P) LGA	Up	Cav3	3511	6.71	0.20	5.49E-07	3.46E-05	2.48
TR(P) versus T(P) LGA	Up	Trip13	16702	6.70	0.12	5.49E-07	3.46E-05	1.78
TR(P) versus T(P) LGA	Up	X99384	17580	6.70	0.12	5.49E-07	3.46E-05	1.75

TR(P) versus T(P) LGA	Up	Ltbr	9603	6.70	0.11	5.49E-07	3.46E-05	1.70
TR(P) versus T(P) LGA	Up	Cdkn2a	3924	6.70	0.15	5.49E-07	3.46E-05	2.00
TR(P) versus T(P) LGA	Up	Tbccd1	15888	6.68	0.03	5.49E-07	3.46E-05	1.17
TR(P) versus T(P) LGA	Up	Ifit1	8365	6.65	0.25	5.49E-07	3.46E-05	3.15
TR(P) versus T(P) LGA	Up	Tor1aip1	16546	6.65	0.07	5.49E-07	3.46E-05	1.38
TR(P) versus T(P) LGA	Up	C1qtnf6	3269	6.62	0.17	5.49E-07	3.46E-05	2.13
TR(P) versus T(P) LGA	Up	Slfn9	15057	6.61	0.28	5.49E-07	3.46E-05	3.57
TR(P) versus T(P) LGA	Up	C2	3275	6.61	0.10	5.49E-07	3.46E-05	1.56
TR(P) versus T(P) LGA	Up	Phf11	12386	6.61	0.24	5.49E-07	3.46E-05	2.94
TR(P) versus T(P) LGA	Up	Vcan	17247	6.61	0.10	5.49E-07	3.46E-05	1.58
TR(P) versus T(P) LGA	Up	Fcgr1	6483	6.60	0.15	5.49E-07	3.46E-05	1.97
TR(P) versus T(P) LGA	Up	Adora2b	1854	6.60	0.10	5.49E-07	3.46E-05	1.57
TR(P) versus T(P) LGA	Up	Itpr2	8710	6.59	0.12	1.10E-06	5.02E-05	1.74
TR(P) versus T(P) LGA	Up	Rrs1	14116	6.59	0.06	1.10E-06	5.02E-05	1.32
TR(P) versus T(P) LGA	Up	Cbfb	3515	6.58	0.11	1.10E-06	5.02E-05	1.68
TR(P) versus T(P) LGA	Up	Fabp5	6132	6.57	0.20	1.10E-06	5.02E-05	2.45
TR(P) versus T(P) LGA	Up	Plek	12602	6.57	0.10	1.10E-06	5.02E-05	1.59
TR(P) versus T(P) LGA	Up	LOC100504864	9412	6.57	0.23	1.10E-06	5.02E-05	2.85
TR(P) versus T(P) LGA	Up	1500001M20Rik	110	6.56	0.08	1.10E-06	5.02E-05	1.42
TR(P) versus T(P) LGA	Up	Tm7sf3	16196	6.55	0.10	1.10E-06	5.02E-05	1.58
TR(P) versus T(P) LGA	Up	2010002N04Rik	407	6.55	0.17	1.10E-06	5.02E-05	2.16
TR(P) versus T(P) LGA	Up	LOC100504230	9403	6.54	0.12	1.10E-06	5.02E-05	1.69
TR(P) versus T(P) LGA	Up	Fen1	6507	6.53	0.09	1.10E-06	5.02E-05	1.47
TR(P) versus T(P) LGA	Up	Abtb2	1638	6.52	0.16	1.10E-06	5.02E-05	2.02
TR(P) versus T(P) LGA	Up	Prkcq	13012	6.52	0.13	1.10E-06	5.02E-05	1.81
TR(P) versus T(P) LGA	Up	Lims2	9326	6.51	0.12	1.10E-06	5.02E-05	1.70
TR(P) versus T(P) LGA	Up	Rfc3	13717	6.51	0.09	1.10E-06	5.02E-05	1.52
TR(P) versus T(P) LGA	Up	Cd48	3791	6.50	0.16	1.10E-06	5.02E-05	2.09
TR(P) versus T(P) LGA	Up	Mrpl51	10293	6.50	0.08	1.10E-06	5.02E-05	1.41
TR(P) versus T(P) LGA	Up	Tnfrsf1a	16472	6.50	0.16	1.10E-06	5.02E-05	2.04

TR(P) versus T(P) LGA	Up	Mastl	9828	6.50	0.11	1.10E-06	5.02E-05	1.62
TR(P) versus T(P) LGA	Up	Epn2	5963	6.49	0.10	1.10E-06	5.02E-05	1.53
TR(P) versus T(P) LGA	Up	Tesk2	16013	6.47	0.08	1.10E-06	5.02E-05	1.41
TR(P) versus T(P) LGA	Up	Alpl	2100	6.46	0.15	1.10E-06	5.02E-05	1.92
TR(P) versus T(P) LGA	Up	Smpdl3b	15132	6.46	0.19	1.10E-06	5.02E-05	2.36
TR(P) versus T(P) LGA	Up	H2-Ab1	7846	6.46	0.18	1.10E-06	5.02E-05	2.20
TR(P) versus T(P) LGA	Up	Hip1	8042	6.40	0.13	1.10E-06	5.02E-05	1.76
TR(P) versus T(P) LGA	Up	Sulf2	15667	6.39	0.15	1.10E-06	5.02E-05	1.91
TR(P) versus T(P) LGA	Up	Fbp1	6412	6.38	0.23	1.10E-06	5.02E-05	2.81
TR(P) versus T(P) LGA	Up	Lyn	9637	6.37	0.18	1.10E-06	5.02E-05	2.26
TR(P) versus T(P) LGA	Up	D14Ert668e	4897	6.37	0.20	1.10E-06	5.02E-05	2.38
TR(P) versus T(P) LGA	Up	C430049B03Rik	3309	6.35	0.17	1.10E-06	5.02E-05	2.09
TR(P) versus T(P) LGA	Up	Impa2	8524	6.35	0.12	1.10E-06	5.02E-05	1.73
TR(P) versus T(P) LGA	Up	Acap1	1655	6.34	0.10	1.10E-06	5.02E-05	1.57
TR(P) versus T(P) LGA	Up	5430427O19Rik	1100	6.34	0.17	1.10E-06	5.02E-05	2.12
TR(P) versus T(P) LGA	Up	Spry4	15416	6.34	0.21	1.10E-06	5.02E-05	2.56
TR(P) versus T(P) LGA	Up	Ppp1r14b	12877	6.32	0.10	1.10E-06	5.02E-05	1.56
TR(P) versus T(P) LGA	Up	Ccl4	3680	6.32	0.22	1.10E-06	5.02E-05	2.57
TR(P) versus T(P) LGA	Up	Gbp3	6906	6.32	0.27	1.10E-06	5.02E-05	3.27
TR(P) versus T(P) LGA	Up	1300014I06Rik	105	6.31	0.12	1.10E-06	5.02E-05	1.67
TR(P) versus T(P) LGA	Up	Prkd3	13017	6.31	0.10	1.10E-06	5.02E-05	1.56
TR(P) versus T(P) LGA	Up	Aplf	2298	6.31	0.08	1.10E-06	5.02E-05	1.40
TR(P) versus T(P) LGA	Up	Parp12	12069	6.30	0.14	1.10E-06	5.02E-05	1.88
TR(P) versus T(P) LGA	Up	Tlr2	16178	6.29	0.17	1.10E-06	5.02E-05	2.10
TR(P) versus T(P) LGA	Up	Eda2r	5691	6.29	0.14	1.10E-06	5.02E-05	1.86
TR(P) versus T(P) LGA	Up	Ms4a6c	10341	6.28	0.13	1.10E-06	5.02E-05	1.78
TR(P) versus T(P) LGA	Up	Ms4a6d	10342	6.27	0.15	1.10E-06	5.02E-05	1.95
TR(P) versus T(P) LGA	Up	Cacng4	3372	6.27	0.10	1.10E-06	5.02E-05	1.55
TR(P) versus T(P) LGA	Up	Serpinb5	14493	6.27	0.19	1.65E-06	6.19E-05	2.29
TR(P) versus T(P) LGA	Up	Masp1	9822	6.27	0.06	1.65E-06	6.19E-05	1.27

TR(P) versus T(P) LGA	Up	Mad2l1	9677	6.26	0.13	1.65E-06	6.19E-05	1.75
TR(P) versus T(P) LGA	Up	Mob1a	10160	6.26	0.08	1.65E-06	6.19E-05	1.40
TR(P) versus T(P) LGA	Up	Mnda	10156	6.25	0.24	1.65E-06	6.19E-05	2.78
TR(P) versus T(P) LGA	Up	H2-Aa	7845	6.25	0.20	1.65E-06	6.19E-05	2.42
TR(P) versus T(P) LGA	Up	Piwil4	12521	6.25	0.11	1.65E-06	6.19E-05	1.58
TR(P) versus T(P) LGA	Up	Srd5a1	15436	6.24	0.11	1.65E-06	6.19E-05	1.62
TR(P) versus T(P) LGA	Up	Tnfsf10	16482	6.23	0.16	1.65E-06	6.19E-05	2.01
TR(P) versus T(P) LGA	Up	Fadd	6134	6.22	0.08	1.65E-06	6.19E-05	1.44
TR(P) versus T(P) LGA	Up	Mosc2	10191	6.22	0.08	1.65E-06	6.19E-05	1.40
TR(P) versus T(P) LGA	Up	Arl11	2442	6.22	0.14	1.65E-06	6.19E-05	1.81
TR(P) versus T(P) LGA	Up	Ptpcr	13293	6.22	0.10	1.65E-06	6.19E-05	1.53
TR(P) versus T(P) LGA	Up	Pde4b	12222	6.21	0.06	1.65E-06	6.19E-05	1.32
TR(P) versus T(P) LGA	Up	Ifit2	8366	6.21	0.12	1.65E-06	6.19E-05	1.64
TR(P) versus T(P) LGA	Up	Angpt2	2157	6.21	0.28	1.65E-06	6.19E-05	3.30
TR(P) versus T(P) LGA	Up	Irf9	8631	6.21	0.18	1.65E-06	6.19E-05	2.17
TR(P) versus T(P) LGA	Up	Lims1	9325	6.21	0.09	1.65E-06	6.19E-05	1.49
TR(P) versus T(P) LGA	Up	Palb2	12021	6.19	0.07	1.65E-06	6.19E-05	1.34
TR(P) versus T(P) LGA	Up	Gm2a	7271	6.18	0.10	1.65E-06	6.19E-05	1.56
TR(P) versus T(P) LGA	Up	Tmem71	16398	6.16	0.13	1.65E-06	6.19E-05	1.75
TR(P) versus T(P) LGA	Up	Gramd3	7671	6.16	0.12	1.65E-06	6.19E-05	1.64
TR(P) versus T(P) LGA	Up	Dctd	5084	6.16	0.09	1.65E-06	6.19E-05	1.49
TR(P) versus T(P) LGA	Up	Fgfr1op2	6549	6.16	0.08	1.65E-06	6.19E-05	1.44
TR(P) versus T(P) LGA	Up	Gbp5	6908	6.15	0.15	1.65E-06	6.19E-05	1.93
TR(P) versus T(P) LGA	Up	F630043A04Rik	6117	6.13	0.10	1.65E-06	6.19E-05	1.54
TR(P) versus T(P) LGA	Up	Eif2ak2	5785	6.13	0.14	1.65E-06	6.19E-05	1.81
TR(P) versus T(P) LGA	Up	Samd9l	14233	6.13	0.19	1.65E-06	6.19E-05	2.20
TR(P) versus T(P) LGA	Up	Ptgr2	13251	6.13	0.05	1.65E-06	6.19E-05	1.22
TR(P) versus T(P) LGA	Up	Cmtm3	4296	6.12	0.11	1.65E-06	6.19E-05	1.59
TR(P) versus T(P) LGA	Up	4632434I11Rik	776	6.12	0.17	1.65E-06	6.19E-05	2.02
TR(P) versus T(P) LGA	Up	Efemp2	5727	6.11	0.09	1.65E-06	6.19E-05	1.46

TR(P) versus T(P) LGA	Up	Rad18	13464	6.11	0.13	1.65E-06	6.19E-05	1.74
TR(P) versus T(P) LGA	Up	Ccdc69	3635	6.11	0.12	1.65E-06	6.19E-05	1.66
TR(P) versus T(P) LGA	Up	Vegfc	17257	6.10	0.08	1.65E-06	6.19E-05	1.42
TR(P) versus T(P) LGA	Up	Tmem209	16336	6.10	0.07	2.20E-06	7.83E-05	1.33
TR(P) versus T(P) LGA	Up	Lyz2	9660	6.09	0.16	2.20E-06	7.83E-05	1.98
TR(P) versus T(P) LGA	Up	1700066M21Rik	318	6.09	0.11	2.20E-06	7.83E-05	1.57
TR(P) versus T(P) LGA	Up	Mkl	10107	6.09	0.13	2.20E-06	7.83E-05	1.70
TR(P) versus T(P) LGA	Up	Slc12a4	14736	6.09	0.13	2.20E-06	7.83E-05	1.76
TR(P) versus T(P) LGA	Up	Cdc42ep1	3845	6.08	0.12	2.20E-06	7.83E-05	1.69
TR(P) versus T(P) LGA	Up	Gstcd	7755	6.08	0.10	2.20E-06	7.83E-05	1.53
TR(P) versus T(P) LGA	Up	Ctss	4708	6.07	0.17	2.20E-06	7.83E-05	2.05
TR(P) versus T(P) LGA	Up	Prnd	13047	6.07	0.32	2.20E-06	7.83E-05	3.80
TR(P) versus T(P) LGA	Up	4930547N16Rik	948	6.05	0.12	2.20E-06	7.83E-05	1.69
TR(P) versus T(P) LGA	Up	Entpd1	5917	6.04	0.09	2.74E-06	8.50E-05	1.46
TR(P) versus T(P) LGA	Up	Tmem106b	16236	6.03	0.09	2.74E-06	8.50E-05	1.43
TR(P) versus T(P) LGA	Up	Dhrs13	5238	6.03	0.09	2.74E-06	8.50E-05	1.47
TR(P) versus T(P) LGA	Up	Dck	5069	6.03	0.08	2.74E-06	8.50E-05	1.41
TR(P) versus T(P) LGA	Up	Tube1	16901	6.03	0.05	2.74E-06	8.50E-05	1.24
TR(P) versus T(P) LGA	Up	Slfn2	15054	6.03	0.19	2.74E-06	8.50E-05	2.19
TR(P) versus T(P) LGA	Up	Mmp15	10138	6.02	0.18	2.74E-06	8.50E-05	2.11
TR(P) versus T(P) LGA	Up	Irf5	8627	6.02	0.10	2.74E-06	8.50E-05	1.53
TR(P) versus T(P) LGA	Up	Ccl2	3724	6.02	0.11	2.74E-06	8.50E-05	1.57
TR(P) versus T(P) LGA	Up	Cdca3	3858	6.02	0.14	2.74E-06	8.50E-05	1.78
TR(P) versus T(P) LGA	Up	Atp13a4	2623	6.02	0.09	2.74E-06	8.50E-05	1.46
TR(P) versus T(P) LGA	Up	E330016A19Rik	5643	6.01	0.09	2.74E-06	8.50E-05	1.45
TR(P) versus T(P) LGA	Up	Tmem194	16321	6.00	0.09	2.74E-06	8.50E-05	1.47
TR(P) versus T(P) LGA	Up	BC013712	2916	6.00	0.11	2.74E-06	8.50E-05	1.58
TR(P) versus T(P) LGA	Up	Rbpms2	13639	5.99	0.11	2.74E-06	8.50E-05	1.60
TR(P) versus T(P) LGA	Up	Fzd9	6790	5.99	0.11	2.74E-06	8.50E-05	1.56
TR(P) versus T(P) LGA	Up	B2m	2792	5.99	0.16	2.74E-06	8.50E-05	1.94

TR(P) versus T(P) LGA	Up	Clec7a	4238	5.98	0.37	2.74E-06	8.50E-05	4.61
TR(P) versus T(P) LGA	Up	Gbp7	6910	5.98	0.21	2.74E-06	8.50E-05	2.43
TR(P) versus T(P) LGA	Up	Slc25a43	14848	5.97	0.10	2.74E-06	8.50E-05	1.51
TR(P) versus T(P) LGA	Up	5730559C18Rik	1132	5.97	0.10	2.74E-06	8.50E-05	1.48
TR(P) versus T(P) LGA	Up	Eme1	5872	5.96	0.13	2.74E-06	8.50E-05	1.71
TR(P) versus T(P) LGA	Up	Epx	5976	5.96	0.35	2.74E-06	8.50E-05	4.30
TR(P) versus T(P) LGA	Up	Dennd2a	5187	5.95	0.13	2.74E-06	8.50E-05	1.72
TR(P) versus T(P) LGA	Up	Myo1f	10540	5.95	0.15	2.74E-06	8.50E-05	1.88
TR(P) versus T(P) LGA	Up	Nrm	11076	5.95	0.13	2.74E-06	8.50E-05	1.68
TR(P) versus T(P) LGA	Up	Epsti1	5974	5.94	0.17	2.74E-06	8.50E-05	2.00
TR(P) versus T(P) LGA	Up	Kcnp3	8816	5.94	0.14	2.74E-06	8.50E-05	1.79
TR(P) versus T(P) LGA	Up	Zbp1	17672	5.93	0.19	2.74E-06	8.50E-05	2.16
TR(P) versus T(P) LGA	Up	Htra2	8300	5.93	0.05	2.74E-06	8.50E-05	1.22
TR(P) versus T(P) LGA	Up	Cd86	3814	5.92	0.13	2.74E-06	8.50E-05	1.73
TR(P) versus T(P) LGA	Up	Ctsd	4698	5.92	0.11	2.74E-06	8.50E-05	1.56
TR(P) versus T(P) LGA	Up	Cxcl10	4744	5.91	0.38	3.29E-06	9.94E-05	4.76
TR(P) versus T(P) LGA	Up	Calcr1	3392	5.91	0.16	3.29E-06	9.94E-05	1.91
TR(P) versus T(P) LGA	Up	Tmem106a	16235	5.91	0.09	3.29E-06	9.94E-05	1.47
TR(P) versus T(P) LGA	Up	Irgm2	8635	5.91	0.20	3.29E-06	9.94E-05	2.25
TR(P) versus T(P) LGA	Up	Cdc42se1	3850	5.90	0.09	3.29E-06	9.94E-05	1.44
TR(P) versus T(P) LGA	Up	Nasp	10640	5.90	0.10	3.29E-06	9.94E-05	1.53
TR(P) versus T(P) LGA	Up	Jam2	8730	5.89	0.10	3.29E-06	9.94E-05	1.51
TR(P) versus T(P) LGA	Up	Itga4	8670	5.87	0.05	4.39E-06	1.32E-04	1.25
TR(P) versus T(P) LGA	Up	Gas1	6877	5.87	0.11	4.94E-06	1.39E-04	1.54
TR(P) versus T(P) LGA	Up	Fam84b	6357	5.86	0.09	4.94E-06	1.39E-04	1.43
TR(P) versus T(P) LGA	Up	Lrrc25	9518	5.86	0.11	4.94E-06	1.39E-04	1.58
TR(P) versus T(P) LGA	Up	Adam12	1763	5.86	0.16	4.94E-06	1.39E-04	1.89
TR(P) versus T(P) LGA	Up	Itgax	8680	5.86	0.15	4.94E-06	1.39E-04	1.83
TR(P) versus T(P) LGA	Up	Ifi2712a	8359	5.86	0.31	4.94E-06	1.39E-04	3.57
TR(P) versus T(P) LGA	Up	Golph3	7514	5.85	0.07	4.94E-06	1.39E-04	1.34

TR(P) versus T(P) LGA	Up	Htra3	8301	5.84	0.05	4.94E-06	1.39E-04	1.25
TR(P) versus T(P) LGA	Up	Arhgap31	2393	5.84	0.06	4.94E-06	1.39E-04	1.26
TR(P) versus T(P) LGA	Up	Klf3	8977	5.84	0.09	4.94E-06	1.39E-04	1.47
TR(P) versus T(P) LGA	Up	Rnf122	13881	5.84	0.11	4.94E-06	1.39E-04	1.57
TR(P) versus T(P) LGA	Up	Fbxo5	6460	5.84	0.10	4.94E-06	1.39E-04	1.51
TR(P) versus T(P) LGA	Up	Tmem173	16296	5.83	0.11	4.94E-06	1.39E-04	1.56
TR(P) versus T(P) LGA	Up	Pik3cg	12478	5.83	0.10	4.94E-06	1.39E-04	1.50
TR(P) versus T(P) LGA	Up	Exoc4	6073	5.82	0.08	4.94E-06	1.39E-04	1.39
TR(P) versus T(P) LGA	Up	Ulbp1	17088	5.82	0.16	4.94E-06	1.39E-04	1.94
TR(P) versus T(P) LGA	Up	Gpc4	7547	5.82	0.11	4.94E-06	1.39E-04	1.55
TR(P) versus T(P) LGA	Up	Al607873	1960	5.82	0.19	4.94E-06	1.39E-04	2.18
TR(P) versus T(P) LGA	Up	Slc16a10	14752	5.81	0.04	5.49E-06	1.50E-04	1.20
TR(P) versus T(P) LGA	Up	Kif15	8917	5.81	0.14	5.49E-06	1.50E-04	1.75
TR(P) versus T(P) LGA	Up	Gna14	7459	5.81	0.13	5.49E-06	1.50E-04	1.67
TR(P) versus T(P) LGA	Up	Eri1	6002	5.81	0.07	5.49E-06	1.50E-04	1.33
TR(P) versus T(P) LGA	Up	Pros1	13061	5.81	0.10	5.49E-06	1.50E-04	1.49
TR(P) versus T(P) LGA	Up	Wipf1	17534	5.79	0.11	5.49E-06	1.50E-04	1.56
TR(P) versus T(P) LGA	Up	Fam89a	6359	5.79	0.21	5.49E-06	1.50E-04	2.30
TR(P) versus T(P) LGA	Up	Bcl2l13	3025	5.78	0.08	5.49E-06	1.50E-04	1.38
TR(P) versus T(P) LGA	Up	Cybb	4773	5.77	0.18	6.04E-06	1.56E-04	2.07
TR(P) versus T(P) LGA	Up	Rhoq	13796	5.77	0.15	6.04E-06	1.56E-04	1.81
TR(P) versus T(P) LGA	Up	Acot1	1686	5.76	0.16	6.04E-06	1.56E-04	1.91
TR(P) versus T(P) LGA	Up	Car3	3459	5.75	0.26	6.04E-06	1.56E-04	2.79
TR(P) versus T(P) LGA	Up	6530418L21Rik	1219	5.75	0.17	6.04E-06	1.56E-04	1.97
TR(P) versus T(P) LGA	Up	Mpzl1	10227	5.75	0.14	6.04E-06	1.56E-04	1.74
TR(P) versus T(P) LGA	Up	Bcl6b	3031	5.74	0.15	6.04E-06	1.56E-04	1.83
TR(P) versus T(P) LGA	Up	Cbr3	3526	5.74	0.19	6.04E-06	1.56E-04	2.10
TR(P) versus T(P) LGA	Up	Ifi271l	8358	5.73	0.18	6.04E-06	1.56E-04	2.01
TR(P) versus T(P) LGA	Up	Stk17b	15591	5.73	0.16	6.04E-06	1.56E-04	1.85
TR(P) versus T(P) LGA	Up	Vrk1	17392	5.73	0.09	6.04E-06	1.56E-04	1.41

TR(P) versus T(P) LGA	Up	2210411K11Rik	461	5.73	0.13	6.04E-06	1.56E-04	1.71
TR(P) versus T(P) LGA	Up	H2-Q10	7862	5.72	0.14	6.04E-06	1.56E-04	1.77
TR(P) versus T(P) LGA	Up	Hes6	8004	5.72	0.09	6.04E-06	1.56E-04	1.41
TR(P) versus T(P) LGA	Up	H2-K1	7853	5.72	0.17	6.04E-06	1.56E-04	1.96
TR(P) versus T(P) LGA	Up	Slc37a2	14933	5.72	0.14	6.59E-06	1.69E-04	1.71
TR(P) versus T(P) LGA	Up	Ccdc14	3579	5.71	0.08	6.59E-06	1.69E-04	1.40
TR(P) versus T(P) LGA	Up	Il1rn	8486	5.71	0.09	7.14E-06	1.69E-04	1.42
TR(P) versus T(P) LGA	Up	Specc1	15337	5.70	0.09	7.14E-06	1.69E-04	1.41
TR(P) versus T(P) LGA	Up	Lix1l	9350	5.70	0.10	7.14E-06	1.69E-04	1.46
TR(P) versus T(P) LGA	Up	Ddx60	5155	5.70	0.25	7.14E-06	1.69E-04	2.67
TR(P) versus T(P) LGA	Up	Tnfrsf8	16459	5.70	0.08	7.14E-06	1.69E-04	1.39
TR(P) versus T(P) LGA	Up	Tlr6	16182	5.70	0.18	7.14E-06	1.69E-04	2.06
TR(P) versus T(P) LGA	Up	Icam1	8323	5.70	0.18	7.14E-06	1.69E-04	2.01
TR(P) versus T(P) LGA	Up	Plcb2	12579	5.69	0.05	7.14E-06	1.69E-04	1.21
TR(P) versus T(P) LGA	Up	Eci2	5683	5.69	0.09	7.14E-06	1.69E-04	1.44
TR(P) versus T(P) LGA	Up	Oip5	11258	5.68	0.10	7.14E-06	1.69E-04	1.49
TR(P) versus T(P) LGA	Up	Nkx2-2	10904	5.68	0.14	7.14E-06	1.69E-04	1.73
TR(P) versus T(P) LGA	Up	Plk4	12642	5.67	0.16	7.14E-06	1.69E-04	1.86
TR(P) versus T(P) LGA	Up	Trem2	16628	5.67	0.15	7.14E-06	1.69E-04	1.77
TR(P) versus T(P) LGA	Up	Sowahc	15265	5.67	0.10	7.14E-06	1.69E-04	1.48
TR(P) versus T(P) LGA	Up	Tdp2	15975	5.66	0.04	7.14E-06	1.69E-04	1.19
TR(P) versus T(P) LGA	Up	Slc27a6	14870	5.64	0.12	7.14E-06	1.69E-04	1.60
TR(P) versus T(P) LGA	Up	Tmem229a	16350	5.64	0.15	7.14E-06	1.69E-04	1.77
TR(P) versus T(P) LGA	Up	Bax	2881	5.64	0.11	7.14E-06	1.69E-04	1.53
TR(P) versus T(P) LGA	Up	Arl6ip6	2459	5.64	0.10	7.14E-06	1.69E-04	1.46
TR(P) versus T(P) LGA	Up	Rnf213	13924	5.64	0.14	7.14E-06	1.69E-04	1.75
TR(P) versus T(P) LGA	Up	Alg13	2072	5.64	0.07	7.14E-06	1.69E-04	1.33
TR(P) versus T(P) LGA	Up	Smad5	15083	5.64	0.10	7.14E-06	1.69E-04	1.46
TR(P) versus T(P) LGA	Up	Dlgap5	5305	5.63	0.07	7.14E-06	1.69E-04	1.33
TR(P) versus T(P) LGA	Up	Gvin1	7826	5.62	0.14	7.69E-06	1.78E-04	1.76

TR(P) versus T(P) LGA	Up	Chst3	4138	5.62	0.11	7.69E-06	1.78E-04	1.53
TR(P) versus T(P) LGA	Up	Eci3	5684	5.62	0.09	7.69E-06	1.78E-04	1.44
TR(P) versus T(P) LGA	Up	Gas2	6878	5.61	0.08	7.69E-06	1.78E-04	1.38
TR(P) versus T(P) LGA	Up	Myc	10489	5.60	0.08	8.78E-06	2.02E-04	1.38
TR(P) versus T(P) LGA	Up	BC055324	2978	5.60	0.13	8.78E-06	2.02E-04	1.65
TR(P) versus T(P) LGA	Up	H2-D1	7848	5.60	0.18	8.78E-06	2.02E-04	1.98
TR(P) versus T(P) LGA	Up	Gm8995	7406	5.60	0.16	9.88E-06	2.18E-04	1.86
TR(P) versus T(P) LGA	Up	Elovl5	5863	5.59	0.09	9.88E-06	2.18E-04	1.42
TR(P) versus T(P) LGA	Up	Nrp1	11079	5.59	0.09	9.88E-06	2.18E-04	1.39
TR(P) versus T(P) LGA	Up	I830012O16Rik	8316	5.59	0.20	9.88E-06	2.18E-04	2.17
TR(P) versus T(P) LGA	Up	Slc11a1	14732	5.58	0.11	9.88E-06	2.18E-04	1.52
TR(P) versus T(P) LGA	Up	2810417H13Rik	678	5.58	0.15	9.88E-06	2.18E-04	1.79
TR(P) versus T(P) LGA	Up	Dsn1	5510	5.58	0.12	9.88E-06	2.18E-04	1.57
TR(P) versus T(P) LGA	Up	Pyhin1	13355	5.58	0.13	9.88E-06	2.18E-04	1.63
TR(P) versus T(P) LGA	Up	Ggh	6984	5.58	0.11	9.88E-06	2.18E-04	1.53
TR(P) versus T(P) LGA	Up	Lsm11	9579	5.58	0.11	9.88E-06	2.18E-04	1.53
TR(P) versus T(P) LGA	Up	Gbp4	6907	5.58	0.20	9.88E-06	2.18E-04	2.19
TR(P) versus T(P) LGA	Up	Ms4a4d	10338	5.58	0.19	9.88E-06	2.18E-04	2.11
TR(P) versus T(P) LGA	Up	Bmp4	3104	5.58	0.13	9.88E-06	2.18E-04	1.65
TR(P) versus T(P) LGA	Up	Batf2	2879	5.58	0.19	9.88E-06	2.18E-04	2.10
TR(P) versus T(P) LGA	Up	Mars2	9817	5.57	0.07	1.04E-05	2.29E-04	1.31
TR(P) versus T(P) LGA	Up	Cd180	3746	5.56	0.11	1.15E-05	2.45E-04	1.52
TR(P) versus T(P) LGA	Up	Sardh	14245	5.56	0.09	1.15E-05	2.45E-04	1.39
TR(P) versus T(P) LGA	Up	Slc39a8	14957	5.56	0.13	1.15E-05	2.45E-04	1.66
TR(P) versus T(P) LGA	Up	Brip1	3161	5.56	0.12	1.15E-05	2.45E-04	1.61
TR(P) versus T(P) LGA	Up	Ncf2	10675	5.56	0.12	1.15E-05	2.45E-04	1.58
TR(P) versus T(P) LGA	Up	Mtap	10377	5.56	0.09	1.15E-05	2.45E-04	1.43
TR(P) versus T(P) LGA	Up	Osmr	11926	5.55	0.10	1.15E-05	2.45E-04	1.45
TR(P) versus T(P) LGA	Up	Ogfr	11253	5.55	0.08	1.15E-05	2.45E-04	1.36
TR(P) versus T(P) LGA	Up	6230424C14Rik	1178	5.55	0.16	1.21E-05	2.53E-04	1.82

TR(P) versus T(P) LGA	Up	Afmid	1888	5.55	0.08	1.21E-05	2.53E-04	1.33
TR(P) versus T(P) LGA	Up	Cmtm6	4299	5.54	0.08	1.21E-05	2.53E-04	1.35
TR(P) versus T(P) LGA	Up	Gm11127	7116	5.54	0.17	1.21E-05	2.53E-04	1.94
TR(P) versus T(P) LGA	Up	Tlr7	16183	5.54	0.15	1.21E-05	2.53E-04	1.78
TR(P) versus T(P) LGA	Up	Twsg1	16925	5.54	0.04	1.26E-05	2.61E-04	1.16
TR(P) versus T(P) LGA	Up	5930416I19Rik	1163	5.53	0.09	1.26E-05	2.61E-04	1.40
TR(P) versus T(P) LGA	Up	Ccbl2	3546	5.53	0.12	1.26E-05	2.61E-04	1.59
TR(P) versus T(P) LGA	Up	Ick	8327	5.53	0.05	1.26E-05	2.61E-04	1.23
TR(P) versus T(P) LGA	Up	Calu	3404	5.52	0.09	1.32E-05	2.70E-04	1.41
TR(P) versus T(P) LGA	Up	Ndufa9	10728	5.51	0.06	1.32E-05	2.70E-04	1.27
TR(P) versus T(P) LGA	Up	C330027C09Rik	3305	5.51	0.14	1.32E-05	2.70E-04	1.72
TR(P) versus T(P) LGA	Up	Tap1	15833	5.50	0.19	1.43E-05	2.89E-04	2.09
TR(P) versus T(P) LGA	Up	Gm22	7256	5.50	0.09	1.43E-05	2.89E-04	1.43
TR(P) versus T(P) LGA	Up	Nek8	10784	5.50	0.10	1.43E-05	2.89E-04	1.47
TR(P) versus T(P) LGA	Up	Lcp1	9238	5.49	0.08	1.43E-05	2.89E-04	1.34
TR(P) versus T(P) LGA	Up	Prkd1	13015	5.49	0.14	1.43E-05	2.89E-04	1.71
TR(P) versus T(P) LGA	Up	Ifit3	8367	5.49	0.14	1.48E-05	2.89E-04	1.68
TR(P) versus T(P) LGA	Up	Fyb	6777	5.48	0.13	1.48E-05	2.89E-04	1.61
TR(P) versus T(P) LGA	Up	Lrig1	9487	5.48	0.19	1.48E-05	2.89E-04	2.09
TR(P) versus T(P) LGA	Up	Slamf6	14722	5.48	0.07	1.48E-05	2.89E-04	1.32
TR(P) versus T(P) LGA	Up	Cd72	3805	5.48	0.20	1.48E-05	2.89E-04	2.11
TR(P) versus T(P) LGA	Up	Bcdin3d	3011	5.48	0.05	1.48E-05	2.89E-04	1.20
TR(P) versus T(P) LGA	Up	Mtbp	10389	5.48	0.10	1.48E-05	2.89E-04	1.44
TR(P) versus T(P) LGA	Up	Gpr65	7630	5.47	0.16	1.48E-05	2.89E-04	1.80
TR(P) versus T(P) LGA	Up	Spry2	15414	5.47	0.13	1.48E-05	2.89E-04	1.63
TR(P) versus T(P) LGA	Up	Fyn	6779	5.47	0.09	1.48E-05	2.89E-04	1.43
TR(P) versus T(P) LGA	Up	Hcls1	7938	5.47	0.09	1.48E-05	2.89E-04	1.39
TR(P) versus T(P) LGA	Up	Abhd2	1618	5.46	0.11	1.54E-05	2.89E-04	1.52
TR(P) versus T(P) LGA	Up	H2-Q5	7865	5.46	0.18	1.54E-05	2.89E-04	1.97
TR(P) versus T(P) LGA	Up	Haus6	7915	5.45	0.08	1.54E-05	2.89E-04	1.36

TR(P) versus T(P) LGA	Up	Pola2	12723	5.44	0.08	1.54E-05	2.89E-04	1.34
TR(P) versus T(P) LGA	Up	Gpr84	7637	5.44	0.15	1.54E-05	2.89E-04	1.75
TR(P) versus T(P) LGA	Up	Hoxa4	8170	5.43	0.17	1.54E-05	2.89E-04	1.92
TR(P) versus T(P) LGA	Up	E030003E18Rik	5589	5.43	0.21	1.54E-05	2.89E-04	2.19
TR(P) versus T(P) LGA	Up	Fam195a	6274	5.43	0.09	1.54E-05	2.89E-04	1.41
TR(P) versus T(P) LGA	Up	Hpse	8211	5.43	0.11	1.54E-05	2.89E-04	1.52
TR(P) versus T(P) LGA	Up	Il4ra	8507	5.43	0.11	1.54E-05	2.89E-04	1.49
TR(P) versus T(P) LGA	Up	Rab8b	13442	5.43	0.12	1.54E-05	2.89E-04	1.57
TR(P) versus T(P) LGA	Up	D630039A03Rik	4960	5.42	0.11	1.54E-05	2.89E-04	1.50
TR(P) versus T(P) LGA	Up	H2-Q8	7867	5.42	0.23	1.54E-05	2.89E-04	2.38
TR(P) versus T(P) LGA	Up	Fsbp	6723	5.41	0.10	1.59E-05	2.93E-04	1.45
TR(P) versus T(P) LGA	Up	Ppat	12821	5.40	0.05	1.59E-05	2.93E-04	1.20
TR(P) versus T(P) LGA	Up	1810010H24Rik	369	5.40	0.14	1.65E-05	2.93E-04	1.68
TR(P) versus T(P) LGA	Up	Ets1	6047	5.40	0.11	1.65E-05	2.93E-04	1.52
TR(P) versus T(P) LGA	Up	Cenpq	3986	5.39	0.14	1.65E-05	2.93E-04	1.71
TR(P) versus T(P) LGA	Up	Tnfsf9	16489	5.39	0.06	1.65E-05	2.93E-04	1.25
TR(P) versus T(P) LGA	Up	Mtmr14	10418	5.39	0.07	1.65E-05	2.93E-04	1.29
TR(P) versus T(P) LGA	Up	Chrdl1	4111	5.38	0.19	1.65E-05	2.93E-04	2.02
TR(P) versus T(P) LGA	Up	Lpin3	9469	5.38	0.12	1.65E-05	2.93E-04	1.56
TR(P) versus T(P) LGA	Up	Olig2	11865	5.38	0.14	1.65E-05	2.93E-04	1.68
TR(P) versus T(P) LGA	Up	Lin9	9334	5.38	0.07	1.65E-05	2.93E-04	1.29
TR(P) versus T(P) LGA	Up	Klhdc5	8989	5.38	0.08	1.65E-05	2.93E-04	1.35
TR(P) versus T(P) LGA	Up	Lpo	9471	5.38	0.32	1.65E-05	2.93E-04	3.30
TR(P) versus T(P) LGA	Up	Sirt2	14692	5.37	0.08	1.65E-05	2.93E-04	1.33
TR(P) versus T(P) LGA	Up	Trim30a	16664	5.37	0.19	1.65E-05	2.93E-04	2.05
TR(P) versus T(P) LGA	Up	Oasl2	11219	5.37	0.29	1.65E-05	2.93E-04	2.99
TR(P) versus T(P) LGA	Up	H2-Q2	7863	5.36	0.18	1.65E-05	2.93E-04	1.95
TR(P) versus T(P) LGA	Up	Elovl2	5860	5.36	0.12	1.65E-05	2.93E-04	1.58
TR(P) versus T(P) LGA	Up	Kif2c	8936	5.36	0.12	1.65E-05	2.93E-04	1.54
TR(P) versus T(P) LGA	Up	Meox1	9968	5.35	0.25	1.65E-05	2.93E-04	2.54

TR(P) versus T(P) LGA	Up	Abcb1b	1582	5.35	0.06	1.65E-05	2.93E-04	1.27
TR(P) versus T(P) LGA	Up	Tbxas1	15916	5.35	0.11	1.65E-05	2.93E-04	1.49
TR(P) versus T(P) LGA	Up	Tmem111	16243	5.34	0.09	1.65E-05	2.93E-04	1.40
TR(P) versus T(P) LGA	Up	Cflar	4037	5.34	0.05	1.65E-05	2.93E-04	1.22
TR(P) versus T(P) LGA	Up	Axl	2748	5.34	0.12	1.76E-05	3.09E-04	1.57
TR(P) versus T(P) LGA	Up	1700040I03Rik	289	5.34	0.10	1.81E-05	3.09E-04	1.45
TR(P) versus T(P) LGA	Up	Elk3	5846	5.33	0.10	1.81E-05	3.09E-04	1.43
TR(P) versus T(P) LGA	Up	Pcdh12	12117	5.33	0.11	1.81E-05	3.09E-04	1.48
TR(P) versus T(P) LGA	Up	Mcm8	9884	5.33	0.10	1.81E-05	3.09E-04	1.46
TR(P) versus T(P) LGA	Up	Fgr	6558	5.33	0.18	1.81E-05	3.09E-04	1.93
TR(P) versus T(P) LGA	Up	1700029F09Rik	267	5.33	0.09	1.81E-05	3.09E-04	1.38
TR(P) versus T(P) LGA	Up	Hyal2	8310	5.32	0.04	1.81E-05	3.09E-04	1.18
TR(P) versus T(P) LGA	Up	Pld4	12598	5.32	0.12	1.81E-05	3.09E-04	1.58
TR(P) versus T(P) LGA	Up	Klhl6	9021	5.32	0.15	1.81E-05	3.09E-04	1.75
TR(P) versus T(P) LGA	Up	Lmo2	9370	5.32	0.10	1.81E-05	3.09E-04	1.45
TR(P) versus T(P) LGA	Up	H2-D4	7849	5.32	0.17	1.81E-05	3.09E-04	1.90
TR(P) versus T(P) LGA	Up	H2-T23	7869	5.31	0.21	1.81E-05	3.09E-04	2.19
TR(P) versus T(P) LGA	Up	Pdha1	12244	5.31	0.04	1.81E-05	3.09E-04	1.18
TR(P) versus T(P) LGA	Up	Thumpd3	16119	5.31	0.07	1.81E-05	3.09E-04	1.28
TR(P) versus T(P) LGA	Up	Tgtp1	16078	5.31	0.20	1.81E-05	3.09E-04	2.09
TR(P) versus T(P) LGA	Up	H2-Q7	7866	5.30	0.20	1.81E-05	3.09E-04	2.09
TR(P) versus T(P) LGA	Up	Lmf1	9363	5.30	0.05	1.81E-05	3.09E-04	1.19
TR(P) versus T(P) LGA	Up	Hsdl2	8251	5.30	0.10	1.87E-05	3.10E-04	1.42
TR(P) versus T(P) LGA	Up	Tdg	15970	5.30	0.05	1.87E-05	3.10E-04	1.20
TR(P) versus T(P) LGA	Up	Atad2	2569	5.29	0.12	1.87E-05	3.10E-04	1.57
TR(P) versus T(P) LGA	Up	Emr1	5888	5.29	0.08	1.92E-05	3.10E-04	1.35
TR(P) versus T(P) LGA	Up	Chst2	4137	5.29	0.14	1.92E-05	3.10E-04	1.64
TR(P) versus T(P) LGA	Up	Mest	9977	5.29	0.19	1.92E-05	3.10E-04	2.02
TR(P) versus T(P) LGA	Up	Hvcn1	8308	5.29	0.13	1.92E-05	3.10E-04	1.64
TR(P) versus T(P) LGA	Up	2410003K15Rik	543	5.28	0.07	1.92E-05	3.10E-04	1.30

TR(P) versus T(P) LGA	Up	A130010J15Rik	1411	5.28	0.08	1.92E-05	3.10E-04	1.33
TR(P) versus T(P) LGA	Up	Pla2g7	12564	5.28	0.10	1.92E-05	3.10E-04	1.45
TR(P) versus T(P) LGA	Up	Irf1	8621	5.28	0.11	1.92E-05	3.10E-04	1.49
TR(P) versus T(P) LGA	Up	Mx2	10471	5.28	0.19	1.92E-05	3.10E-04	2.02
TR(P) versus T(P) LGA	Up	Naif1	10612	5.28	0.04	1.92E-05	3.10E-04	1.17
TR(P) versus T(P) LGA	Up	Rrm2	14104	5.27	0.18	1.92E-05	3.10E-04	1.90
TR(P) versus T(P) LGA	Up	Cdh11	3868	5.27	0.07	1.92E-05	3.10E-04	1.28
TR(P) versus T(P) LGA	Up	Rad51ap1	13470	5.27	0.17	1.92E-05	3.10E-04	1.83
TR(P) versus T(P) LGA	Up	C3ar1	3307	5.26	0.11	1.98E-05	3.10E-04	1.49
TR(P) versus T(P) LGA	Up	Rad54l	13476	5.26	0.13	1.98E-05	3.10E-04	1.60
TR(P) versus T(P) LGA	Up	Tmem48	16373	5.26	0.10	1.98E-05	3.10E-04	1.43
TR(P) versus T(P) LGA	Up	Ephx1	5956	5.26	0.14	1.98E-05	3.10E-04	1.66
TR(P) versus T(P) LGA	Up	Vhl	17264	5.26	0.08	1.98E-05	3.10E-04	1.34
TR(P) versus T(P) LGA	Up	Fam181a	6256	5.25	0.09	1.98E-05	3.10E-04	1.39
TR(P) versus T(P) LGA	Up	Igtp	8438	5.25	0.26	1.98E-05	3.10E-04	2.54
TR(P) versus T(P) LGA	Up	Pdlim5	12261	5.25	0.07	1.98E-05	3.10E-04	1.28
TR(P) versus T(P) LGA	Up	Fancd2	6372	5.25	0.09	1.98E-05	3.10E-04	1.38
TR(P) versus T(P) LGA	Up	Frrs1	6717	5.24	0.11	1.98E-05	3.10E-04	1.47
TR(P) versus T(P) LGA	Up	H2afb1	7872	5.24	0.15	1.98E-05	3.10E-04	1.76
TR(P) versus T(P) LGA	Up	Arhgap11a	2377	5.24	0.16	1.98E-05	3.10E-04	1.79
TR(P) versus T(P) LGA	Up	Cdk2	3900	5.24	0.14	1.98E-05	3.10E-04	1.67
TR(P) versus T(P) LGA	Up	Gpr160	7597	5.24	0.11	1.98E-05	3.10E-04	1.50
TR(P) versus T(P) LGA	Up	Fam111a	6165	5.23	0.14	1.98E-05	3.10E-04	1.69
TR(P) versus T(P) LGA	Up	Haus3	7912	5.23	0.13	1.98E-05	3.10E-04	1.61
TR(P) versus T(P) LGA	Up	Zcchc24	17736	5.23	0.09	1.98E-05	3.10E-04	1.36
TR(P) versus T(P) LGA	Up	Tor3a	16550	5.23	0.10	1.98E-05	3.10E-04	1.41
TR(P) versus T(P) LGA	Up	Cd84	3813	5.23	0.18	1.98E-05	3.10E-04	1.90
TR(P) versus T(P) LGA	Up	Dfna5	5212	5.23	0.03	1.98E-05	3.10E-04	1.12
TR(P) versus T(P) LGA	Up	Lym5	9652	5.22	0.10	2.03E-05	3.17E-04	1.45
TR(P) versus T(P) LGA	Up	Slc27a3	14867	5.22	0.14	2.03E-05	3.17E-04	1.64

TR(P) versus T(P) LGA	Up	Lyl1	9636	5.22	0.10	2.03E-05	3.17E-04	1.42
TR(P) versus T(P) LGA	Up	Kank1	8760	5.21	0.13	2.09E-05	3.19E-04	1.59
TR(P) versus T(P) LGA	Up	Cyp24a1	4792	5.21	0.25	2.09E-05	3.19E-04	2.43
TR(P) versus T(P) LGA	Up	Cd40	3786	5.21	0.10	2.09E-05	3.19E-04	1.44
TR(P) versus T(P) LGA	Up	Tnfrsf19	16471	5.21	0.13	2.09E-05	3.19E-04	1.62
TR(P) versus T(P) LGA	Up	Slc25a15	14819	5.21	0.14	2.09E-05	3.19E-04	1.65
TR(P) versus T(P) LGA	Up	Tmpo	16429	5.21	0.10	2.09E-05	3.19E-04	1.44
TR(P) versus T(P) LGA	Up	Parp14	12070	5.21	0.17	2.09E-05	3.19E-04	1.82
TR(P) versus T(P) LGA	Up	C230035116Rik	3277	5.20	0.12	2.14E-05	3.27E-04	1.53
TR(P) versus T(P) LGA	Up	Apoc1	2313	5.20	0.20	2.20E-05	3.34E-04	2.04
TR(P) versus T(P) LGA	Up	Cxcl16	4749	5.20	0.14	2.20E-05	3.34E-04	1.64
TR(P) versus T(P) LGA	Up	Iigp1	8440	5.19	0.32	2.31E-05	3.49E-04	3.14
TR(P) versus T(P) LGA	Up	Vav1	17240	5.19	0.08	2.36E-05	3.56E-04	1.32
TR(P) versus T(P) LGA	Up	Pcyox1	12191	5.19	0.06	2.36E-05	3.56E-04	1.24
TR(P) versus T(P) LGA	Up	Foxc1	6663	5.19	0.18	2.36E-05	3.56E-04	1.93
TR(P) versus T(P) LGA	Up	9930014A18Rik	1390	5.18	0.13	2.42E-05	3.58E-04	1.59
TR(P) versus T(P) LGA	Up	Cd68	3801	5.18	0.11	2.42E-05	3.58E-04	1.50
TR(P) versus T(P) LGA	Up	Neu4	10799	5.18	0.16	2.42E-05	3.58E-04	1.76
TR(P) versus T(P) LGA	Up	Orc1	11893	5.18	0.13	2.42E-05	3.58E-04	1.59
TR(P) versus T(P) LGA	Up	Gjc3	7034	5.18	0.12	2.42E-05	3.58E-04	1.53
TR(P) versus T(P) LGA	Up	P2ry6	11981	5.17	0.13	2.42E-05	3.58E-04	1.58
TR(P) versus T(P) LGA	Up	Cdk2ap1	3902	5.17	0.09	2.42E-05	3.58E-04	1.36
TR(P) versus T(P) LGA	Up	Cfb	4029	5.17	0.30	2.53E-05	3.67E-04	2.93
TR(P) versus T(P) LGA	Up	Mlec	10101	5.17	0.07	2.53E-05	3.67E-04	1.30

Table S2.3. One versus rest SAM analysis of T(RP) LGA transcriptomes at 2 m after induction. One versus rest significance of microarray (SAM) analyses identified 7949 and 2460 genes with significantly increased (Up) and decreased (Down) expression in LGA versus histologically normal brain and LGA with [TR(P)] versus without [T(P)] Kras^{G12D} at FDR of 0.001 and 0.01, respectively. This table lists the 500 most increased and decreased genes in each comparison.

Table S2.4. Kras^{G12D} immune LGA signature (300 genes)

Orthologous human genes used in ssGSEA (Fig. 3C)	
PROKR1	
HOXA1	
ETV4	
SPRY1	
CHST7	
BVES	
ALDH1L1	
IGFBP2	
HOXA7	
SEPT9	
IGFBP3	
FRK	
GSC	
APOBEC1	
TRAF4	
LGALS3BP	
AKR1B10	
LGALS9	
FAM5C	
RSAD2	
SKAP2	
FGFRL1	
GNG12	
LPAR6	
CST7	
CSPG4	
STAT1	
HOXA2	
DUSP6	
USP18	
IRF7	
CREB5	
HERC6	
HCAR2	
ACADL	
KLHL5	
CTSC	
TMEM176B	
PMAIP1	

RASAL3	
PARP9	
F2R	
TMEM37	
TRIB2	
HOXA5	
TRIM25	
ZRANB3	
TTPA	
PDGFRA	
DDX58	
TMEM176A	
LPCAT1	
METRNL	
DLL3	
IRF8	
FAM83D	
PLEKHF2	
ERCC6L	
SHMT1	
TMEM144	
SUCLG2	
IRGM	
VAV3	
HEXB	
ZC3HAV1	
OAS2	
E2F2	
PAPSS1	
TGIF2	
KRAS	
MDFIC	
ARHGAP24	
SP100	
GALNT3	
PRR11	
ARHGAP18	
IFIH1	
GPNMB	
TSPAN12	
TXN	
CXCL11	
MEGF6	
GALNT4	
ISG15	

TRIM21
MPEG1
BST2
RTP4
BORA
ETV6
SLC15A3
RAB31
TLCD1
HUS1
DHX58
ITPRIPL2
REEP3
SH3BP4
PPIC
SLFN13
CTS2
XAF1
EPS8
IFI44
DPF3
CAV3
TRIP13
KIAA1274
LTBR
CDKN2A
TBCCD1
IFIT1
TOR1AIP1
C1QTNF6
C2
VCAN
FCGR1A
ADORA2B
ITPR2
RRS1
CBFB
FABP5
PLEK
TAMM41
TM7SF3
C5orf62
FEN1
ABTB2
PRKCQ

LIMS2	
RFC3	
CD48	
MRPL51	
TNFRSF1A	
MASTL	
EPN2	
TESK2	
ALPL	
SMPDL3B	
HLA-DQB1	
HIP1	
SULF2	
FBP1	
LYN	
IMPA2	
ACAP1	
CXorf21	
SPRY4	
PPP1R14B	
CCL4	
GBP4	
C6orf145	
PRKD3	
APLF	
PARP12	
TLR2	
EDA2R	
CACNG4	
SERPINB5	
MASP1	
MAD2L1	
HLA-DQA1	
PIWIL4	
SRD5A1	
TNFSF10	
FADD	
MOSC2	
ARL11	
PTPRC	
PDE4B	
IFIT2	
ANGPT2	
IRF9	
LIMS1	

PALB2
GM2A
TMEM71
GRAMD3
DCTD
FGFR1OP2
GBP5
SKA3
EIF2AK2
SAMD9L
PTGR2
CMTM3
C11orf82
EFEMP2
RAD18
CCDC69
VEGFC
TMEM209
C2orf69
MLKL
SLC12A4
CDC42EP1
GSTCD
CTSS
PRND
C12orf48
ENTPD1
TMEM106B
DHRS13
DCK
TUBE1
SLFN12L
MMP15
IRF5
CCRL2
CDCA3
ATP13A4
MB21D1
TMEM194A
C1orf38
RBPMS2
FZD9
B2M
CLEC7A
GBP7

SLC25A43

C1orf106

EME1

EPX

DENND2A

MYO1F

NRM

EPSTI1

KCNIP3

ZBP1

HTRA2

CD86

CTSD

CXCL10

CALCRL

TMEM106A

CDC42SE1

NASP

JAM2

ITGA4

GAS1

FAM84B

LRRC25

ADAM12

ITGAX

IFI27L2

GOLPH3

HTRA3

ARHGAP31

KLF3

RNF122

FBXO5

TMEM173

PIK3CG

EXOC4

ULBP1

GPC4

SLC16A10

KIF15

GNA14

ERI1

PROS1

WIPF1

FAM89A

BCL2L13

CYBB
RHOQ
CA3
C1orf183
MPZL1
BCL6B
CBR3
IFI27
STK17B
VRK1
TMEM238
HLA-A
HES6
SLC37A2
CCDC14
IL1RN
SPECC1
LIX1L
DDX60
TNFAIP8
TLR6
ICAM1
PLCB2
ECI2
OIP5
NKX2-2
PLK4
TREM2
TDP2
SLC27A6
TMEM229A
BAX
ARL6IP6
RNF213
ALG13
SMAD5

Table S2.4. Kras^{G12D} immune LGA signature. A 300 gene Kras^{G12D} immune signature was identified by SAM of LGA transcriptomes with and without Kras^{G12D} (Table S2.3). Orthologous human genes used in ssGSEA (Fig. 3C) are listed.

Table S2.5. TRP HGA cohort: Mice aged to neurological morbidity						
Summary						
GFAP-CreER	4OHT induction	Genotype	Diagnosis	Total aCGH samples	Total transcriptome samples	Total Mice
No	Yes	P ^{+/-}	Normal			1
		TR	Normal			2
		TRP ^{+/-}	Normal			2
		TRP ^{-/-}	Normal			2
Yes	No	R	Normal			1
		RP ^{-/-}	Normal			1
	Yes	WT	Normal			2
		P ^{-/-}	Normal			4
		R	Normal			6
		RP ^{+/-}	Normal			7
		RP ^{-/-}	Normal			10
		T	A2			11
			A3			3
		TP ^{+/-}	A2			20
			A3			4
		TP ^{-/-}	A2			15
			A3			3
		TR	A2			10
			A3	3	3	20
			GBM	5	6	11

TRP ^{+/-}	A2			16
	A3	6	6	18
	GBM	19	20	21
TRP ^{-/-}	A2			9
	A3	3	3	11
	GBM	5	5	16
Total		41	43	226

	Mean	SD	Min	Max
Age at induction (days)	107.9	22.2	31	183

Table S2.5. TRP HGA cohort: Mice aged to neurological morbidity. Adult GFAP-CreER mice with various combinations of T, R, and P alleles were induced with 4OHT at ~3 m of age (mean 108, SD 22 d) and aged to neurological morbidity or sacrificed healthy at 7-19 m. Uninduced GFAP-CreER mice (N=2), induced mice lacking GFAP-CreER (N=7), and induced GFAP-CreER mice with wild-type (WT), P, R, or RP oncogenic alleles (N=29) showed no evidence of tumorigenesis. In contrast, all induced, GFAP-CreER mice with T(P) or TR(P) developed astrocytomas (N=188).

Table S2.6. CNA in core pathway genes in TR(P) HGA

179	Rb Pathway				RTK Pathway				MAPK Pathway				PI3K Pathway				Trp53 Pathway			
	Gene	Mutated Samples (%)			Gene	Mutated Samples (%)			Gene	Mutated Samples (%)			Gene	Mutated Samples (%)			Gene	Mutated Samples (%)		
		Gain	Loss	Total		Gain	Loss	Total		Gain	Loss	Total		Gain	Loss	Total		Gain	Loss	Total
	Ccnd2	67	67	67	Met	67	0	67	Braf	69	0	69	Foxo2	5	0	5	Mdm4	24	0	24
	Stat1	21	0	21	Egfr	2	5	7	Kras	69	0	69	Pten	0	5	5	Trp53	2	7	10
	E2f6	0	7	7	ErbB2	2	5	7	Raf1	67	0	67	Akt2	0	2	2	Cdkn2a	0	2	2
	E2f7	0	7	7	Pdgfb	7	0	7	Map2k4	2	10	12	Akt2s2	0	2	2	Mdm2	0	2	2
	Myc	7	0	7	Pdgfa	5	0	5	Dab2	10	0	10	Akt5	2	0	2	Trp53bp1	2	0	2
	Stat3	2	5	7	Fgf1	2	0	2	Mapk9	2	7	10	Pik3ca	2	0	2				
	Stat5a	2	5	7	Fgfr1	2	0	2	Map2k3	2	5	7	Pik3r5	2	0	2				
	Stat5b	2	5	7	Igf1r	0	2	2	Map3k3	2	5	7	Pdpk2	0	0	0				
	Ccna1	5	0	5	Pdgfrb	2	0	2	Mapk12	5	2	7	Pik3r2	0	0	0				
	E2f2	2	2	5	ErbB3	0	0	0	Mapk7	2	5	7	Rheb	0	0	0				
	E2f8	0	5	5	Igf1	0	0	0	Rab25	5	0	5	Tsc2	0	0	0				
	Jak2	0	5	5	Kdr	0	0	0	Hras1	0	2	2	Tsc5	0	0	0				
	Ccnd1	0	2	2	Kit	0	0	0	Map3k2	2	0	2								
	Ccne1	0	2	2	Pdgfra	0	0	0	Mapk1	2	0	2								
	Cdk6	0	2	2	Vegfa	0	0	0	Mapk3	0	2	2								
	Cdkn2a	0	2	2	Vegfb	0	0	0	Map2k1	0	0	0								
	E2f1	2	0	2					Map2k2	0	0	0								
	E2f3	0	2	2					Map2k5	0	0	0								
	E2f5	2	0	2					Map3k1	0	0	0								
	Jak1	0	2	2					Map3k4	0	0	0								
	Rbl1	2	0	2					Map3k5	0	0	0								
	Src	2	0	2					Mapk14	0	0	0								
	Ccnb1	0	0	0					Mapk4	0	0	0								
	Cdc25a	0	0	0					Mapk6	0	0	0								

Cdk2	0	0	0
Cdk4	0	0	0
Cdkn1a	0	0	0
E2f4	0	0	0
Rb1	0	0	0
Rbl2	0	0	0
Stat2	0	0	0

Mapk8	0	0	0
Rassf1	0	0	0

Table S2.6. CNA in Rb, RTK, MAPK, PI3K, and Trp53 pathway genes in TR(P) HGA. Copy number gains and losses for the indicated Rb, RTK, MAPK, PI3K, and Trp53 pathway genes in 41 HGA samples from 35 TR(P) mice (Table S2.5) are shown (Fig. 2.5J-L).

Table S2.7. CNA in spatially distinct TR(P) HGA show evidence of clonal evolution

Mouse ID	CNA	HGA 1 Location			HGA 2 Location		
		Chromosome	Start	End	Chromosome	Start	End
235344	Gain	BS			DI		
		6	3407797	149520604	1	84771143	96148343
					5	24498907	40604784
					5	43178200	45514283
					6	3386664	125527378
					13	55502290	74249044
	Loss	2	86040946	90813486	11	52603926	121796672
		8	49770240	69609457	14	68219133	68432377
		10	91355355	116504740	15	42866402	54539782
		13	17168563	29133133			
		13	116505113	120606172			
		14	79020241	115431576			
		16	66635653	86219861			
		17	35948984	42090956			
236024	Gain	CTX			OFB		
		4	111551341	112104179	4	111634766	112114746
		6	3734548	138332452	6	3373820	106180182
	Loss	1	109642970	119351601	None		
		2	85392180	89836288			
		5	9630570	19355183			
		8	99365014	106947658			
		10	99835535	106828005			

	13	116761502	120606172
	14	78985869	91624735
	14	105500491	112936324
	15	13453095	24598294
	15	42245596	54539782
	16	59482110	83786212

		OFB			BS		
244706	Gain	6	3763705	138332452	1	9863	169875650
					6	3024849	131473159
	Loss	1	159251360	170278139	2	137186961	149502225
		1	175677083	176180255	4	144867593	146628899
		2	137634657	149072625	8	14227242	17834414
		4	144867593	146659327	11	33530019	47916916
		11	71035484	71319408	11	62582530	72429309
		13	116761502	118916994	12	26428637	31422158
					13	116754485	119063864
					16	59406082	90816204

	CTX				OFB		
244939	Gain	17	30169694	30650214	6	3024849	105935318
	Loss	5	104804922	105242139	5	104488686	105176403

		CTX			DI		
245116	Loss	4	111579573	112104179	2	136784609	149072625
		4	112114745	113386023	4	111579573	112091073
		12	16353603	30880108	4	112304580	113356036
					12	16353603	31508274
					13	116743684	119063864

246270	CTX		OFB	
	Loss	13	116754485	119072276
			None	

CNA in Rb, RTK/MAPK/PI3K, and Trp53 pathway genes			
Mouse ID	Genotype	Common CNA	Unique CNA
235344	TR	Ccnd2, Braf, Kras, Raf1	E2f7, Stat3, Stat5a, Stat5b, Erbb2, Met, Map2k3, Map2k4, Map3k3, Mapk7, Trp53
236024	TRP ^{+/-}	Ccnd2, Met, Braf, Kras, Raf1	E2f2
244706	TRP ^{+/-}	Ccnd2, Met, Braf, Kras, Raf1	Stat1, Map2k4, Mdm4, Trp53
244939	TRP ^{+/-}	None	Ccnd2, Met, Braf, Kras, Raf1
245116	TRP ^{+/-}	None	E2f6
246270	TRP ^{-/-}	None	None

Table S2.7. CNA in spatially distinct TR(P) HGA show evidence of clonal evolution. Six mice from Table S2.6 had HGA in two spatially distinct brain regions and all HGA pairs had distinct CNA landscapes.

Table S2.8. TR(P) HGA transcriptome samples

Sample Name	Mouse ID	Genotype	Location	HGA Subtype (S1-S3) (Fig. 6A)	TCGA GBM Subtype Prediction (Fig. 6C)	Core Sample (Fig. S15D)	Survival (months) (Fig. S16 B)	Censored Survival	Diagnosis
245304_BS	245304	TRP ^{+/-}	BS	S1	Classical	Yes	4.27	No	A3
232366_BS	232366	TR	BS	S1	Mesenchymal	Yes	3.52	No	GBM
235316_BS	235316	TR	BS	S1	Mesenchymal	Yes	4.93	No	GBM
246742_CTX	246742	TR	CTX	S1	Mesenchymal	Yes	4.83	No	GBM
236070_CTX	236070	TRP ^{-/-}	CTX	S1	Mesenchymal	Yes	3.12	No	A3
245586_BS	245586	TRP ^{-/-}	BS	S1	Mesenchymal	Yes	2.33	No	A3
233106_BS	233106	TRP ^{+/-}	BS	S1	Mesenchymal	Yes	4.7	No	GBM
234451_OFB	234451	TRP ^{+/-}	OFB	S1	Mesenchymal	Yes	4.24	No	GBM
236024_1_CTX	236024	TRP ^{+/-}	CTX	S1	Mesenchymal	Yes	3.94	No	GBM
244190_BS	244190	TRP ^{+/-}	BS	S1	Mesenchymal	Yes	3.06	No	A3
244706_2_BS	244706	TRP ^{+/-}	BS	S1	Mesenchymal	Yes	3.32	No	GBM
245016_BS	245016	TRP ^{+/-}	BS	S1	Mesenchymal	Yes	3.55	No	A3
245660_1_BS	245660	TRP ^{+/-}	BS	S1	Mesenchymal	Yes	3.81	No	GBM
245662_BS	245662	TRP ^{+/-}	BS	S1	Mesenchymal	Yes	3.48	No	GBM
245936_BS	245936	TRP ^{+/-}	BS	S1	Mesenchymal	Yes	3.52	No	GBM
246300_BS	246300	TRP ^{+/-}	BS	S1	Mesenchymal	Yes	4.17	No	GBM
246302_BS	246302	TRP ^{+/-}	BS	S1	Mesenchymal	Yes	3.35	No	GBM
234458_DI	234458	TRP ^{+/-}	DI	S1	Neural	No (Excluded)	4.7	No	GBM
235344_2_DI	235344	TR	DI	S2	Classical	Yes	4.47	No	GBM
236024_2_OFB	236024	TRP ^{+/-}	OFB	S2	Classical	Yes	3.94	No	GBM
235791_BS	235791	TR	BS	S2	Proneural	Yes	4.27	No	A3
245665_OFB	245665	TRP ^{-/-}	OFB	S2	Proneural	Yes	1.97	Yes	A3
233117_OFB	233117	TRP ^{+/-}	OFB	S2	Proneural	Yes	3.68	No	GBM
241898_BS	241898	TRP ^{+/-}	BS	S2	Proneural	Yes	4.6	No	GBM
244706_1_OFB	244706	TRP ^{+/-}	OFB	S2	Proneural	Yes	3.32	No	GBM
245660_2_OFB	245660	TRP ^{+/-}	CTX	S2	Proneural	Yes	3.81	No	GBM
242092_BS	242092	TR	BS	S3	Mesenchymal	Yes	4.17	No	A3
234750_BS	234750	TR	BS	S3	Neural	Yes	4.5	No	GBM
245861_DI	245861	TR	DI	S3	Neural	Yes	3.94	No	A3

241102_DI	241102	TRP ^{-/-}	DI	S3	Neural	Yes	3.25	No	GBM
242486_DI	242486	TRP ^{-/-}	DI	S3	Neural	Yes	3.22	No	GBM
245237_DI	245237	TRP ^{-/-}	DI	S3	Neural	Yes	2.1	No	GBM
246270_2_OFB	246270	TRP ^{-/-}	OFB	S3	Neural	Yes	1.91	No	GBM
244189_DI	244189	TRP ^{+/-}	DI	S3	Neural	Yes	3.91	No	A3
244605_CTX	244605	TRP ^{+/-}	CTX	S3	Neural	Yes	4.14	No	GBM
244939_2_OFB	244939	TRP ^{+/-}	OFB	S3	Neural	Yes	3.94	No	A3
245116_1_CTX	245116	TRP ^{+/-}	CTX	S3	Neural	Yes	3.48	No	GBM
245116_2_DI	245116	TRP ^{+/-}	DI	S3	Neural	Yes	3.48	No	GBM
235344_1_BS	235344	TR	BS	S3	Proneural	Yes	4.47	No	GBM
246270_1_CTX	246270	TRP ^{-/-}	CTX	S3	Proneural	Yes	1.91	No	GBM
233352_OFB	233352	TRP ^{+/-}	OFB	S3	Proneural	Yes	4.24	No	GBM
243852_OFB	243852	TRP ^{+/-}	OFB	S3	Proneural	Yes	4.17	No	GBM
244939_1_CTX	244939	TRP ^{+/-}	CTX	S3	Proneural	Yes	3.94	No	A3

Table S2.8. TR(P) HGA transcriptome samples. Forty-three HGA samples from 36 TR(P) mice were utilized for transcriptome analyses in Figs. 6 and S17-19. Initiating genotype did not correlate with HGA location or subtype (Fisher $P \leq 0.6$). HGA subtype correlated with location ($P=0.004$) and human GBM (TCGA) subtype ($P<0.0001$). Seven mice developed spatially distinct HGA; four pairs showed different HGA S1-S3 subtypes and six pairs showed different human GBM (TCGA) subtypes.

Table S2.9. HGA subtypes S1-S3 600-gene classifier**Genes ordered as depicted in Fig. 6 heatmaps**

Gadd45a
Cp
Cald1
Gpnmb
Ctgf
Mgp
Crip2
Itgb5
Ephx1
Mr1
Hfe
Fgfr1
Itm2b
Plxnb2
Sypl
Igdcc4
Prex2
Inf2
Fxyd1
Timp2
Anxa7
Fth1
Stx3
Foxo1
Pnpla7
Bcl6
Phf15
Fam174a
Mllt6
Arhgap23
Plekhm2
Hagh
Rabac1
Ift172
Nub1
Spnb2
Zbtb4
Ezh1
Inpp5k
Mnt
Rnf6
Pacsin3

Tacc1
Fyco1
Rab11fip5
Hipk3
Lats2
Aff1
Tnip1
Acvr1b
Ftsjd2
Hgsnat
Npr2
Ccs
Fnbp1
Osmr
Hspb1
Micall1
Col11a1
Lyz1
Lyz2
Abcg2
Ppic
Gnb4
Tmem176a
Tmem176b
Dusp6
Eps8
Skap2
Ppfibp1
Lmnb1
Suv39h2
2700094K13Rik
6720463M24Rik
Cks1b
Mdm1
Eri1
Hnrnpf
Csda
2810417H13Rik
Rad51ap1
Itgb1
Lpar6
Rhbdf1
Haus4
Zwilch
Fam111a
Cav2
Casp8

Lrrfip1	
Plod2	
Cdr2l	
Scarb1	
Rhoc	
Rod1	
Elk3	
Hspg2	
Lims1	
Ostf1	
Ets1	
Litaf	
Stard13	
Vcan	
Fgfr1l	
Krcc1	
Orai1	
Lin9	
Tmem167	
Cbx3	
Sec61a1	
2610001J05Rik	
Adam10	
Lman1	
Golt1b	
Tpm4	
2610020H08Rik	
Ppib	
Tram1	
Plekha8	
Lsm5	
Phf14	
Lsm3	
Snrpg	
Rpa3	
Naa38	
Nup205	
Errfi1	
Cast	
Rbms1	
Ank	
Man2a1	
Bicc1	
Ifngr1	
Mxra8	
Fkbp9	
Ltbp3	

Arhgap29
Gpsm3
Ifnar2
Tgfb2
Arhgef6
Fkbp7
Ston1
Pgcp
Phldb2
Flna
Tmem43
Nfkb1
Ttc7
Crtap
Wasf2
Ap3b1
Eapp
Tln1
Esyt1
Mgat1
Ebp
Gxylt1
Surf4
Nt5dc1
Stx16
Vcl
Ptpn14
Atl3
Etv6
Capns1
Ppap2a
P2rx4
Tradd
Scpep1
Il10rb
Anxa4
Tmem123
Nck2
Ano6
Fbxo4
Ncoa3
Bpgm
Glb1
Crlf2
Sumf1
Lpp
Rbms2

Csgalnact2

Lrp1

2810474O19Rik

Znrf2

Ddi2

Spty2d1

Igf2r

Fam114a1

Fndc3b

Mxra7

Edem1

Nucb1

H2-K1

B2m

Ifi35

Tgm2

Ctsh

Srgn

Cybb

Cyba

Grn

Tlr13

Ehd4

Syngr2

Bag3

Capg

Dap

Fzd1

Etv5

Arhgap31

Map4k4

Tnfrsf1a

Cd302

Mdfic

Cpne8

Igfbp7

Ifi30

Lamc1

Nid1

Fbxl7

Fli1

Spats2l

Rhoj

Col9a1

Xpnpep1

Atp1b1

Got1

Cacna2d1
Fbxl16
Pgm2l1
Chst1
Stxbp5
Tsc22d3
Acsl3
Phyhd1
Ogfrl1
Cd59a
Ndrgr1
C2cd2l
Trank1
Kalrn
Ppp3cb
Ap2a2
Ubqln2
Epm2aip1
Gsk3b
Clip3
1700019D03Rik
Pbx1
Atp6ap2
Nceh1
Atp6v1c1
Atp6v1a
Atp6v1d
Ppp2r5b
Ttc19
Kifap3
Mapre2
1500031L02Rik
Ttc7b
Atp6v1b2
Rtn4
Ywhah
Nkiras1
Rap1gds1
Ppapdc2
Spryd3
2900097C17Rik
Pja2
Mapk8ip3
Ap1b1
Prkacb
Slc25a22
Synj1

Sirt3	
Eif4a2	
Serinc1	
Ppip5k1	
Fam126b	
Gls	
Atg2b	
Bbs4	
Tmx4	
Ncdn	
Scamp1	
Atp6v1g2	
Inpp4a	
Calm1	
Reep5	
Fam164a	
Ankrd13d	
Habp4	
Adcy9	
Map1lc3a	
Zrsr1	
Morn4	
Slu7	
Trim44	
Ccdc104	
Nicn1	
Oscp1	
Mink1	
Surf1	
Adrbk1	
Vti1b	
Atp6v0a1	
Vamp2	
Kidins220	
Atp6v0d1	
Kctd13	
Dgcr6	
Fis1	
Ggnbp2	
Vti1a	
Tmem85	
Herc1	
Usp20	
Agtpbp1	
Napg	
Rnf14	
Ensa	

Wdr13
Dnajib14
Smpd1
BC031181
Wbp2
2510003E04Rik
Mgrn1
Rogdi
Pip4k2c
Tmem66
Bcas3
Znhit2-ps
Pex11b
Golga2
Use1
1110003E01Rik
Trappc6b
Mat2b
Tbc1d22a
Mbnl2
Zfyve27
Cyth1
5430411K18Rik
Cdc42bpa
Megf8
Coro2b
Fam134b
Clu
Csrp1
Prnp
Ypel2
Lpgat1
Nrbp2
Pitpnm1
Stxbp1
Fam110b
Mllt11
Gabbr1
Snap47
Trim2
Pde4dip
Araf
Atl1
Napb
Trim37
Kif21a
Reps2

Dnalc1

Arf3

Dlg4

Nelf

Syt7

Sgtb

Syne1

Olfm1

Arrb1

Ids

Pfkp

Wdr47

Nedd4l

Tspan7

Zdhhc8

Chn1

Strbp

Dlg3

Parp6

Cpe

Cx3cl1

Pdp1

Marcks1

Rnf180

Mex3b

Phtf2

Caprin1

Gspt1

Dhcr7

Bzw2

Tbc1d7

Tpm1

Polg

Isoc1

Map3k1

Rev3l

Ppp1r14b

Pus7l

Actl6a

Myef2

Nasp

Hnrnpab

Srsf3

Mtap

Alg13

Dctpp1

1110034A24Rik

2410127L17Rik
Strap
Srsf9
Polr2d
Ybx1
Eif4g2
Phf5a
Zbtb10
Gtf2h3
Zbed4
Kti12
Fbl
Snrpd3
Hnrnpa1
Nudt21
Cdk4
Hmgn1
Isg20l2
Prpf40a
Dhx15
Ilf3
Tdg
Trib2
Rpp30
Sephs1
Ppat
Gtf2a2
Ppih
Ercc8
Cpsf4
Hspa14
Cstf2
Ythdf2
1500001M20Rik
Snrpa1
Phf6
Ap3m1
Eif1ad
Nudt5
Slmo2
G3bp1
Cse1l
Set
Srd5a1
Galnt10
Nol7
1700066M21Rik

Hdac2
Papss1
Arl2bp
Hnrnpk
Prpf4
Ankrd49
Rnf138
Rbmx
Srsf1
Gtf2f2
1600012F09Rik
Pdss1
Abcb7
Usp38
Bri3bp
Hnrnpul1
Nap1l1
Snrpd1
Erh
Lsm6
Ilf2
Mrpl50
Clns1a
Gpn1
Fam118b
Cct8
Abce1
Ncbp1
Hmgb3
Midn
Fam108c
Clcn5
Kif13a
Mum1l1
Ccnd2
Mex3a
Flrt3
Gpr85
Pak3
Pkia
Ppp2r2b
Sox11
Sh3gl3
Tmeff1
Bcl7a
Fbxo21
Dbn1

Mmd
Gcsh
Apc
Cwf19l1
Bod1
Naa30
Nckap1
Timm8b
Lcmt1
Camsap1
Ube2k
Hdhd2
Ikbkap
Timm9
Eif1b
Ppp2ca
Ube2n
Ept1
Ppp2cb
Rab39b
Usp22
9330151L19Rik
Ncoa1
Exoc3
Nhlrc1
Atxn7l3b
Slc39a3
Irgq
Klc1
Pafah1b1
Ppme1
Dclk1
Plxnc1
Fasn
Tle4
B3gat1
Mcart6
Phyhipl
Cacna1h
Ptbp2
Phgdh
Tfrc
Enoph1
Alg2
Pfn2
Calm3
Ube2v2

Sub1
Yaf2
1810041L15Rik
Ptplad1
Sall2
S100a1
Bdh1
Ednrb
Gphn
Cadm2
Macrod2
Daam1
Zdhhc14
Fam49b
Fam69b
Celf2
Lrp8
Asphd2
Fez1
Nipa1
Hdac9
Kif21b
Dgat2
Flrt1
Ppm1l
Asxl3
Dlat
Tsr2
Clcn3
Rab4a
Ss18l1
Trim32
Gnl1
Pdpx
Fam171b
Gpm6a
Chst10
Lrrtm2
Smarca1
BC068157
Wasf1

Table S2.9. HGA subtypes S1-S3 600-gene classifier. A 600 gene classifier was identified by ClANC of S1-S3 TR(P) HGA transcriptomes.

Table S2.7A. GO lists from HGA S1 (Mesenchymal) Subtype SAM analysis

Gene Set Name	# Genes in Gene Set (K)	# Genes in Overlap (k)	k/K	p value
HEMATOPOIETIN_INTERFERON_CLASSD200_DOMAIN_CYTOKINE_RECEPTOR_ACTIVITY	32	12	0.375	2.11E-04
CYTOKINE_BINDING	46	15	0.3261	2.18E-04
EXTRACELLULAR_MATRIX_PART	57	16	0.2807	8.99E-04
REGULATION_OF_PROTEIN_IMPORT_INTO_NUCLEUS	16	7	0.4375	1.61E-03
PROTEINACEOUS_EXTRACELLULAR_MATRIX	98	22	0.2245	2.85E-03
REGULATION_OF_NUCLEOCYTOPLASMIC_TRANSPORT	22	8	0.3636	3.06E-03
EXTRACELLULAR_MATRIX	100	22	0.22	3.70E-03
POSITIVE_REGULATION_OF_I_KAPPAB_KINASE_NF_KAPPAB_CASCADE	80	18	0.225	6.44E-03
REGULATION_OF_INTRACELLULAR_TRANSPORT	25	8	0.32	7.43E-03
BASAL_LAMINA	21	7	0.3333	9.49E-03
BASEMENT_MEMBRANE	37	10	0.2703	1.07E-02
REGULATION_OF_I_KAPPAB_KINASE_NF_KAPPAB_CASCADE	86	18	0.2093	1.38E-02
LIPOPROTEIN_BINDING	18	6	0.3333	1.61E-02
POSITIVE_REGULATION_OF_JNK_ACTIVITY	18	6	0.3333	1.61E-02
POSITIVE_REGULATION_OF_MAP_KINASE_ACTIVITY	46	11	0.2391	1.93E-02
INTERLEUKIN_RECEPTOR_ACTIVITY	19	6	0.3158	2.12E-02
REGULATION_OF_JNK_ACTIVITY	20	6	0.3	2.72E-02
I_KAPPAB_KINASE_NF_KAPPAB_CASCADE	107	20	0.1869	3.15E-02
GROWTH_FACTOR_BINDING	32	8	0.25	3.36E-02
NON_MEMBRANE_SPANNING_PROTEIN_TYROSINE_KINASE_ACTIVITY	11	4	0.3636	3.53E-02
ACTIVATION_OF_JNK_ACTIVITY	16	5	0.3125	3.62E-02
ORGAN_MORPHOGENESIS	144	25	0.1736	4.01E-02
PROTEIN_KINASE_CASCADE	282	44	0.156	4.62E-02
RAS_PROTEIN_SIGNAL_TRANSDUCTION	65	13	0.2	4.62E-02
ACTIVATION_OF_MAPK_ACTIVITY	40	9	0.225	4.67E-02
GLYCOPROTEIN_CATABOLIC_PROCESS	12	4	0.3333	4.80E-02
LOW_DENSITY_LIPOPROTEIN_BINDING	12	4	0.3333	4.80E-02
POSITIVE_REGULATION_OF_SIGNAL_TRANSDUCTION	119	21	0.1765	4.87E-02

Table S2.7B. GO lists from HGA S2 (Proneural) Subtype SAM analysis

Gene Set Name	# Genes in Gene Set (K)	# Genes in Overlap (k)	k/K	p value
M_PHASE_OF_MITOTIC_CELL_CYCLE	83	26	0.3133	2.92E-08
MITOTIC_CELL_CYCLE	148	37	0.25	3.46E-08
MITOSIS	81	25	0.3086	7.48E-08
RNA_SPLICING	82	25	0.3049	9.80E-08
CELL_CYCLE_PROCESS	188	41	0.2181	3.73E-07
CELL_CYCLE_PHASE	168	38	0.2262	3.77E-07
M_PHASE	112	29	0.2589	4.77E-07
RNA_PROCESSING	156	35	0.2244	1.33E-06
CELL_CYCLE_GO_0007049	306	56	0.183	1.42E-06
RIBONUCLEOPROTEIN_COMPLEX	129	30	0.2326	3.49E-06

MRNA_METABOLIC_PROCESS	79	21	0.2658	1.16E-05
MRNA_PROCESSING_GO_0006397	68	19	0.2794	1.39E-05
CHROMOSOMAL_PART	96	23	0.2396	2.87E-05
SMALL_NUCLEAR_RIBONUCLEOPROTEIN_COMPLEX	20	9	0.45	4.31E-05
CHROMOSOME	123	26	0.2114	8.89E-05
NUCLEAR_PART	548	78	0.1423	2.15E-04
ENDONUCLEASE_ACTIVITY_GO_0016893	11	6	0.5455	2.37E-04
REGULATION_OF_MITOSIS	40	12	0.3	2.58E-04
CHROMOSOMEPERICENTRIC_REGION	31	10	0.3226	4.40E-04
INTERPHASE_OF_MITOTIC_CELL_CYCLE	62	15	0.2419	6.18E-04
SPLICEOSOME	44	12	0.2727	6.79E-04
ENDORIBONUCLEASE_ACTIVITY	13	6	0.4615	7.43E-04
NUCLEUS	1367	163	0.1192	1.23E-03
DNA_REPLICATION	101	20	0.198	1.33E-03
INTERPHASE	68	15	0.2206	1.71E-03
SPINDLE	37	10	0.2703	2.03E-03
MITOCHONDRIAL_SMALL_RIBOSOMAL_SUBUNIT	11	5	0.4545	2.31E-03
ORGANELLAR_SMALL_RIBOSOMAL_SUBUNIT	11	5	0.4545	2.31E-03
SMALL_RIBOSOMAL_SUBUNIT	11	5	0.4545	2.31E-03
INTRACELLULAR_NON_MEMBRANE_BOUND_ORGANELLE	617	80	0.1297	3.00E-03
NON_MEMBRANE_BOUND_ORGANELLE	617	80	0.1297	3.00E-03
G1_S_TRANSITION_OF_MITOTIC_CELL_CYCLE	27	8	0.2963	3.01E-03
REGULATION_OF_CELL_CYCLE	177	28	0.1582	5.72E-03
PYRIMIDINE_NUCLEOTIDE_METABOLIC_PROCESS	9	4	0.4444	7.25E-03
KINETOCHORE	25	7	0.28	7.66E-03
RIBONUCLEASE_ACTIVITY	25	7	0.28	7.66E-03
NUCLEAR_LUMEN	371	50	0.1348	8.60E-03
RNA_SPLICINGVIA_TRANSESTERIFICATION_REACTIONS	32	8	0.25	9.28E-03
RIBOSOMAL_SUBUNIT	20	6	0.3	9.34E-03
RIBOSOME	39	9	0.2308	1.03E-02
NUCLEOBASENUCLEOSIDENUCLEOTIDE_AND_NUCLEIC_ACID_METABOLIC_PROCESS	1208	139	0.1151	1.08E-02
COENZYME_BIOSYNTHETIC_PROCESS	10	4	0.4	1.12E-02
MEMBRANE_ENCLOSED_LUMEN	440	57	0.1295	1.17E-02
ORGANELLE_LUMEN	440	57	0.1295	1.17E-02
MITOTIC_CELL_CYCLE_CHECKPOINT	21	6	0.2857	1.20E-02
REGULATION_OF_MITOTIC_CELL_CYCLE	21	6	0.2857	1.20E-02
CELL_CYCLE_CHECKPOINT_GO_0000075	47	10	0.2128	1.25E-02
PROTEIN_DNA_COMPLEX_ASSEMBLY	48	10	0.2083	1.45E-02
NUCLEOLAR_PART	16	5	0.3125	1.45E-02
POSITIVE_REGULATION_OF_CELL_CYCLE	16	5	0.3125	1.45E-02

Table S2.7C. GO lists from HGA S3 (Neural) Subtype SAM analysis

Gene Set Name	# Genes in Gene Set (K)	# Genes in Overlap (k)	k/K	p value
GLUTAMATE_RECEPTOR_ACTIVITY	20	10	0.5	1.00E-03

SYNAPTIC_TRANSMISSION	172	46	0.2674	2.04E-03
GROWTH_CONE	10	6	0.6	3.42E-03
METABOTROPIC_GLUTAMATEGABA_B_LIKE_RECEPTOR_ACTIVITY	10	6	0.6	3.42E-03
PROTEIN_SERINE_THREONINE_PHOSPHATASE_COMPLEX	10	6	0.6	3.42E-03
NEUROTRANSMITTER_SECRETION	13	7	0.5385	3.50E-03
TRANSMISSION_OF_NERVE_IMPULSE	187	48	0.2567	4.03E-03
SITE_OF_POLARIZED_GROWTH	11	6	0.5455	6.39E-03
GENERATION_OF_A_SIGNAL_INVOLVED_IN_CELL_CELL_SIGNALING	29	11	0.3793	8.17E-03
REGULATED_SECRETORY_PATHWAY	15	7	0.4667	9.43E-03
VOLTAGE_GATED_CALCIUM_CHANNEL_COMPLEX	15	7	0.4667	9.43E-03
SYNAPSE	27	10	0.3704	1.38E-02
NEURON_PROJECTION	20	8	0.4	1.64E-02
L_AMINO_ACID_TRANSMEMBRANE_TRANSPORTER_ACTIVITY	17	7	0.4118	2.06E-02
CALCIUM_CHANNEL_ACTIVITY	33	11	0.3333	2.31E-02
KINESIN_COMPLEX	14	6	0.4286	2.57E-02
VOLTAGE_GATED_CALCIUM_CHANNEL_ACTIVITY	18	7	0.3889	2.86E-02
MICROTUBULE_ASSOCIATED_COMPLEX	47	14	0.2979	3.01E-02
CATION_TRANSPORTING_ATPASE_ACTIVITY	11	5	0.4545	3.17E-02
GLUTATHIONE_TRANSFERASE_ACTIVITY	15	6	0.4	3.65E-02
SYNAPTIC_VESICLE	15	6	0.4	3.65E-02
GLYCOPHINGOLIPID_METABOLIC_PROCESS	12	5	0.4167	4.66E-02
DENDRITE	16	6	0.375	4.99E-02
MICROTUBULE_BASED_MOVEMENT	16	6	0.375	4.99E-02

Table S2.10. Gene ontology (GO) terms from TR(P) HGA subtype SAM analyses. The top significant ($p < 0.05$) GO terms for TR(P) HGA subtypes S1 (A), S2 (B), and S3 (C) are listed.

Table S2.11. Transcriptomal subtypes in GEM HGA test set

GEM HGA versus human GBM (TCGA) subtypes						
HGA Subtype	TCGA Subtype					Total
	PN	N	NL	CL	MES	
S1	0	0	0	0	28	28
S2	23	0	0	2	3	28
S3	9	12	11	1	2	35
Total	32	12	11	3	33	91
Fisher's $P < 0.0001$						

Table S2.11. Transcriptomal subtypes in GEM HGA test set. The GEM HGA test set consists of 38, 23, and 30 HGA from GSE22927, GSE29458, and GSE35917, respectively (100, 142, 144). The TCGA subtype described in the original reports and the TR(P) HGA subtype (S1-S3) predicted with the 600-gene classifier (Table S2.9) are shown. HGA subtype correlated with human GBM (TCGA) subtype (Fisher $P < 0.0001$).

Table S2.12. GFAP-CreER mice with *p53* deletion and combinations of T_{121} , *Kras*^{G12D}, and *Pten* deletion

Mouse ID	Genotype	Sex	Age at induction (days)	Cause of death	Survival (days)	Diagnosis	aCGH samples (Figs. S19 and S20)
250645	<i>p53</i> ^{+/-}	F	91	Sac	63	Normal	
250868	<i>p53</i> ^{+/-}	M	91	Sac	63	Normal	
250647	R; <i>p53</i> ^{+/-}	F	91	Sac	63	Normal	
250867	R; <i>p53</i> ^{+/-}	M	91	Sac	63	Normal	
247825	RP ^{+/-} ; <i>p53</i> ^{+/-}	F	211	Sac	64	Normal	
248111	RP ^{+/-} ; <i>p53</i> ^{+/-}	M	188	Sac	64	Normal	
249666	RP ^{+/-} ; <i>p53</i> ^{+/-}	F	79	Sac	64	Normal	
241718	T; <i>p53</i> ^{+/-}	M	130	Brain tumor	301	GBM	Fig. S20
250643	T; <i>p53</i> ^{+/-}	F	91	Sac	63	A2	CTX (Fig. S19)
248104	TP ^{+/-} ; <i>p53</i> ^{+/-}	F	188	Sac	64	A2	OFB (Fig. S19)
249301	TP ^{+/-} ; <i>p53</i> ^{+/-}	F	103	Sac	64	A2	OFB (Fig. S19)
251674	TP ^{+/-} ; <i>p53</i> ^{+/-}	F	113	Sac	184	A2	
251676	TP ^{+/-} ; <i>p53</i> ^{+/-}	F	113	Sac	184	A2	
250644	TR; <i>p53</i> ^{+/-}	F	91	Sac	63	A2	CTX, OFB (Fig. S19)
250651	TR; <i>p53</i> ^{+/-}	F	91	Sac	63	A2	CTX (Fig. S19)
251213	TR; <i>p53</i> ^{+/-}	F	102	Sac	64	A2	
247731	TRP ^{+/-} ; <i>p53</i> ^{+/-}	M	166	Brain tumor	39	A2	
249669	TRP ^{+/-} ; <i>p53</i> ^{+/-}	M	79	Sac	64	A3	CTX, OFB (Fig. S19)
249670	TRP ^{+/-} ; <i>p53</i> ^{+/-}	M	79	Sac	64	A3	CTX, OFB (Fig. S19)
251226	TRP ^{+/-} ; <i>p53</i> ^{+/-}	M	102	Sac	64	A2	
251685	TRP ^{+/-} ; <i>p53</i> ^{+/-}	M	113	Brain tumor	81	A3	

Summary

Genotype	Diagnosis	Total aCGH samples	Total mice	
p53 ^{+/-}	Normal		2	
R;p53 ^{+/-}	Normal		2	
RP ^{+/-} ;p53 ^{+/-}	Normal		3	
T;p53 ^{+/-}	LGA (A2)	1	1	
	HGA (GBM)	1	1	
TP ^{+/-} ;p53 ^{+/-}	LGA (A2)	2	4	
TR;p53 ^{+/-}	LGA (A2)	3	3	
TRP ^{+/-} ;p53 ^{+/-}	LGA (A2)		2	
	HGA (A3)	4	3	
Total		11	21	
	Mean	SD	Min	Max
Age at induction (days)	114.4	39.4	79	211
Post-induction Survival (days)	86.0	61.5	39	301

Table S2.12. GFAP-CreER mice with p53 deletion and combinations of T121, KrasG12D, Pten deletion. Adult p53^{+/flox};GFAP-CreER mice with combinations of T, R, and P alleles were induced as previously described with 4OHT at ~3 m of age (mean 114, SD 39 d). These mice were sacrificed between 2-6 m (mean 86, SD 61 d). Astrocytomas from a subset of these mice were additionally analyzed by aCGH (Figs. S2.19 and S2.20).

CHAPTER III

Cooperativity between MAPK and PI3K signaling activation is required for glioblastoma pathogenesis³

INTRODUCTION

Glioblastomas (GBM, WHO Grade IV) account for more than 85% of astrocytomas and are uniformly lethal.(179) Their diffuse infiltration of normal brain makes complete surgical resection impossible and further eradicating tumor cells with radiation or chemotherapy remains difficult. Thus, recurrence is almost certain, occurring in at least 90% of cases near the resection site.(180, 181) This sobering clinical reality has fueled investigation of the biological mechanisms responsible for GBM migration and invasion, particularly the intracellular signaling pathways that govern these phenotypes. The Cancer Genome Atlas (TCGA) catalogued oncogenic mutations and copy number alterations in GBM and showed that these abnormalities occur primarily in genes of three core intracellular pathways, namely the RB regulated G1/S cell cycle checkpoint, receptor tyrosine kinase (RTK) signaling, and TP53. Approximately 74% of human GBM harbored events in all three pathways, while less than 5% harbored events in only one of the three.(29) In contrast, over 90% contained mutations in both RB and RTK pathway genes (<http://tcga-data.nci.nih.gov/tcga/>).

RTK and their downstream effectors, RAS/MAPK and PI3K/AKT/mTOR, have received particular interest, as kinases within these pathways represent potential targets for therapeutic intervention (182).

³ A version of this was previously published as Vitucci, M., N. O. Karpnich, R. E. Bash, A. M. Werneke, R. S. Schmid, K. K. White, R. S. McNeill, B. Huff, S. Wang, T. Van Dyke and C. R. Miller (2013). "Cooperativity between MAPK and PI3K signaling activation is required for glioblastoma pathogenesis." Neuro-Oncology: 2013;15(10):1317-29.

RTK pathway kinases encoded by the *EGFR*, *ERBB2*, *PDGFRA*, *MET*, *KRAS*, *PIK3CA*, and *AKT1* genes are frequently amplified or mutationally activated, whereas negative regulators of RAS and PI3K signaling, *NF1* and *PTEN*, are frequently deleted or mutationally inactivated, respectively.(29) Based upon these genetic alterations, 88% of GBM are predicted to harbor activated RTK signaling through these two effector arms and virtually all show RAS activation.(168, 169)

However, clinical trial results with RTK-targeted therapeutics, particularly EGFR tyrosine kinase inhibitors (TKI), have been disappointing.(183) *EGFR* is amplified or mutated in 36-45% of GBM,(29, 184) but only a small percentage of these tumors respond to EGFR TKI. GBM exhibit both inter- and intra-tumoral genetic heterogeneity and both neighboring and individual tumor cells can harbor amplifications in more than one distinct RTK gene.(185) A recent mouse model study showed that *Met* may functionally compensate for EGFR signaling upon EGFR TKI-mediated inhibition, suggesting one potential resistance mechanism, particularly in the subset of GBM with *EGFR* and *MET* co-amplification.(186) In addition, co-expression of the constitutively active EGFRvIII extracellular domain truncation mutant and PTEN correlated with EGFR TKI response. In contrast, loss of PTEN expression was associated with treatment failure, suggesting that uncoupling of PI3K signaling from EGFR may be an additional EGFR TKI resistance mechanism.(187)

Since its discovery over ten years ago, the *PTEN* tumor suppressor gene has been extensively investigated. The embryonic lethality observed in *Pten*-null mice underscores its importance during development.(74, 188) *PTEN* is also critical in many cellular functions relevant to tumorigenesis, including proliferation, survival, migration, and invasion.(189) Inactivating *PTEN* mutations or deletions are present in 30-40% of human GBM and TCGA identified it as the second most commonly mutated GBM gene.(29, 49) A more complete understanding of the combinatorial roles of RTK signaling through RAS and PI3K effectors in GBM pathogenesis, particularly the migratory and invasive phenotypes that make treatment difficult, is therefore required to develop more effective, targeted therapies.(181)

To overcome this limitation, we have generated primary astrocytes from a series of conditional, genetically engineered mouse (GEM) models in which two of the three core GBM pathways were genetically targeted, either alone or in combination, all on a common C57Bl/6-based genetic background. After Cre-mediated recombination, these mice express an N-terminal 121 amino acid truncation mutant of SV40 large T antigen (T₁₂₁, hereafter called T) from the human glial fibrillary acidic protein (GFAP) promoter,(79) which inactivates all three Rb family proteins - Rb, p107, p130 - and ablates the G1/S cell cycle checkpoint.(190) In addition, these mice have a constitutively active Kras^{G12D} mutant (R)(147) and/or either heterozygous or homozygous *Pten* deletion (P^{+/-} or P^{-/-}).(40) Our previous studies have shown that particular combinations of these three alleles recapitulate the histopathological progression from low-grade (WHO Grade II, A2) to high-grade astrocytomas (WHO grade III and IV, A3 and GBM, respectively) upon recombination in adult GFAP⁺ mouse brain cells.(40) Therefore, we hypothesized that these primary GEM astrocytes would provide a unique opportunity to dissect the individual and combinatorial roles of activated MAPK and PI3K signaling in biological processes relevant to GBM pathogenesis, including cellular growth (proliferation and apoptosis), migration, and invasion *in vitro* and tumorigenesis *in vivo*.

MATERIALS AND METHODS

Genetically-engineered mice

Heterozygous *TgGZT*₁₂₁ mice were maintained on a BDF1 background.(79) Heterozygous *Kras*^{G12D} conditional knock-in and *Pten*^{loxP/loxP} mice were maintained on a C57/Bl6 background.(92, 147) All experimental animals were >94% C57/Bl6. PCR genotyping was performed as previously described.(79, 92, 147) Animal studies were approved by the University of North Carolina Institutional Animal Care and Use Committee.

Primary astrocyte cultures

Primary astrocytes were cultured as previously described.(79) Briefly, cells were selectively harvested from the cortices of post-natal day 1-4 pups, manually dissociated by trituration in trypsin, and incubated at 37°C for 20 minutes. Cells were pelleted, resuspended, and cultured in DMEM supplemented with 10% fetal bovine serum and 1% penicillin-streptomycin (complete media). At 50% confluence, cells were infected at an MOI of 50 for 6 hours in complete media with a recombinant adenoviral vector expressing Cre recombinase from the constitutive cytomegalovirus promoter (Ad5CMVCre, University of Iowa Gene Transfer Vector Core).(191) Following infection, cells were rinsed in PBS and cultured in complete media at 37°C in 5% CO₂. All immunoblot, cell growth, apoptosis, wound closure, collagen invasion, time lapse microscopy, microarray, and orthotopic allograft experiments were performed with genotype-confirmed primary astrocytes, under passage 10 post-Ad5CMVCre infection, in log phase growth and cultured in complete media unless otherwise stated.

Microarray analyses

All original microarray data are publically available at the UNC Microarray Database (<http://genome.unc.edu>) and Gene Expression Omnibus, accession number GSE40265.

Orthotopic allografts

Adult wild type C57Bl/6 mice (≥ 3 months old) were anesthetized with Avertin (250 mg/kg) and placed into a stereotactic frame (Kopf, Tujunga, CA). Following a 0.5 cm scalp incision, 10^5 cells in 5 μ L of 5% methylcellulose were injected into the right basal ganglia using coordinates 1, -2, and -4 mm (A, L, D) from the Bregma suture as previously described.(114)

Statistics

Apoptosis, viability, and time lapse microscopy data were analyzed using one-way ANOVA with Tukey's multiple comparisons correction in GraphPad Prism 5 (GraphPad, San Diego, CA). Wound closure data were analyzed using pairwise Student's T tests. Doubling times from cell growth assays were compared using one-way ANOVA with Tukey's correction in Stata 10 (College Station, TX). Multiple linear regression, Kaplan-Meier plots, and log-rank analyses were conducted in Stata. All comparisons were significant at $\alpha=0.05$.

Immunoblots

One week post-Ad5CMVCre infection, primary astrocytes were harvested, lysed, and analyzed for induction of recombination using immunoblots to detect expression of T₁₂₁ and Pten. Immunoblot analyses of MAPK and PI3K signaling were also performed. Briefly, equal amounts of protein were resolved by gradient (4-20%) SDS-PAGE (Bio-Rad, Hercules, CA) and transferred to nitrocellulose membranes. Blots were probed overnight at 4°C using primary antibodies against SV40 T Antigen (Ab-2, 1:1000, Calbiochem, San Diego, CA), Pten (1:1000, clone 6H2.1, Cascade Bioscience, Winchester, MA), GFP (B-2) (1:200, Santa Cruz Biotechnology, Santa Cruz, CA), and Gapdh (ab8245, 1:10000, Abcam Inc., Cambridge, MA), and Akt (#2967, 1:1000), p-Akt (Ser473, #9271, 1:500), p-S6 (Ser240/244, #2215,

1:2000), p-MEK1/2 (Ser221, #2338, 1:1000), and p-Erk1/2 (Thr202/Tyr204, #9101, 1:1000), all from Cell Signaling Technology, Danvers, MA. Following incubation with HRP-conjugated secondary antibodies, blots were developed by enhanced chemiluminescence (Pierce Biotechnology, Thermo Fisher Scientific, Rockford, IL). Films were scanned using a CanoScan8400F scanner (Canon, Lake Success, NY) and band intensities were quantified using ImageJ (NIH, Bethesda, MD).

Cell growth

In vitro proliferation of cultured primary astrocytes (3-4 independent isolates per genotype) was assessed using Guava ViaCount (Millipore, Billerica, MA) according to manufacturer's instructions. Briefly, astrocytes were seeded in 24-well plates at 2.2×10^5 cells per well. On days one, two, three, four, and seven, cells were stained with ViaCount. Total viable cell numbers were determined using a Guava EasyCyte Plus flow cytometer using the ViaCount package of CytoSoft v5.3. Doubling times were calculated using an exponential growth equation in GraphPad Prism 5 (GraphPad, San Diego, CA).

Apoptosis and viability

Apoptosis and viability were measured by flow cytometry using the Guava ViaCount Assay per manufacturer's instructions. After data acquisition on a Guava EasyPlus, gates for viable, apoptotic and dead cells were set according to the manufacturer's instructions. Percent apoptotic cells were calculated from at least two independent isolates per genotype in three replicate experiments. For wild-type and T astrocytes, apoptosis was quantified using the Caspase-Glo 3/7 Assay system (Promega, Madison, WI). Cells were seeded in quadruplicate at 15,000 cells per well on optical-grade 96-well plates (BD Biosciences, Franklin Lakes, NJ) and luminescence was measured on an Ascent FL plate reader (Thermo Fisher Scientific). Cell viability was determined on duplicate plates using the Cell Titer Glo assay (Promega) to control for potential differences in baseline metabolic activity. Relative

apoptosis (ratio of luminescence for apoptosis and viability) was then calculated. Mean relative apoptosis levels were determined in 4-10 replicate experiments per isolate from at least two independent isolates per genotype.

Wound healing

Wound healing assays were conducted as previously described.(192, 193) Briefly, a scratch wound was created on confluent cell monolayers in 6-well plates using a 100 µl pipette tip and photographs were taken at 0 and 24 hours post-scratch using an Olympus IX81-ZDC inverted fluorescence microscope (Olympus Imaging America Inc., Center Valley, PA) equipped with a QImaging Retiga 4000R camera (QImaging, Surrey, BC, Canada). The percentage of wound closure was calculated by measuring the open area using ImageJ. Mean percent wound closure was determined in quadruplicate wells using 3-4 independent isolates per genotype.

Time lapse microscopy

Primary astrocytes were seeded in laminin-coated 6-well plates at 50,000 cells per well and allowed to adhere overnight. Cell were imaged on an Olympus IX70 inverted microscope equipped with a LEP Precision Bioscan motorized stage and a Hamamatsu ORCA 7424 camera (Hamamatsu, Hamamatsu City, Japan). During imaging, cells were incubated at 37°C with 70% relative humidity and CO₂ was supplied by custom made culture dish lids fitted with tubes for each well. Images were taken every 3 minutes for 1 hour, exported as TIFF images, and compressed into QuickTime movies (Apple, Cupertino, CA). Cell velocity was calculated frame by frame using the manual tracking module in ImageJ software (NIH, Bethesda, MD). Cells that divided or moved out of frame during image acquisition were excluded from analysis. Mean velocities were calculated from at least 100 cells in 3-8 replicate experiments per isolate from a minimum of two independent isolates per genotype.

Collagen invasion

Experiments were performed as previously described.⁽¹⁹⁴⁾ Briefly, astrocytes were seeded at 50,000 cells per well in 200 μ l of complete media in 96-well plates pre-coated with 100 μ l of freshly autoclaved 1.5% Noble Agar (Sigma-Aldrich, St. Louis, MO). Cells were incubated for 2 days at 37° C in 5% CO₂ or until they formed spheroids. Using a 1000 μ l pipette, spheroids were implanted in a mixture of bovine collagen (Organogenesis, Canton, MA), 10X EMEM (Lonza, Walkersville, MD), 200mM L-glutamine (Mediatech, Inc., Manassas, VA), 2% fetal calf serum (Life Technologies, Grand Island, NY), and 7.5% NaHCO₃ (Mediatech, Inc., Manassas, VA). Embedded spheroids were overlaid with 1 mL of complete media and images of spheroid outgrowth were acquired daily for up to 5 days as described above for wound healing. Percent invasion was quantified in 3-9 independent isolates per genotype using the threshold function in ImageJ.

Pten plasmids

Pten plasmids (xloxP(GFP)-wtPten) were generously provided by Dr. Serguei Kozlov (NCI-Frederick, MD). These vectors contain a modified MSCV promoter to drive wild-type Pten expression and include a separate PGK-GFP cassette to monitor transfection efficiency. The corresponding empty vector (xloxP(GFP)) was used as a negative control. For retroviral production, Phoenix packaging cells were transfected with the Pten constructs using FuGENE HD (Promega) according to manufacturer's instructions. Viral supernatants were collected and used to transduce astrocyte cultures for 24-48 hours in 4 μ g/mL polybrene at approximately 60% efficiency.

Microarrays

Total RNA was isolated from astrocytes using an RNeasy Mini Kit (QIAGEN, Valencia, CA), RNA quality was confirmed with the Agilent Bioanalyzer (RNA Integrity Number > 7), labeled with the Agilent Low RNA Input Linear Amplification Kit (Agilent Technologies, Santa Clara, CA), and hybridized to Agilent Whole Mouse Genome 4×44 K microarrays (G4122-60520) per the manufacturer's protocol. Stratagene Universal Mouse Reference RNA (Agilent, #740100) was co-hybridized to each array as a reference. Microarrays were scanned on an Agilent DNA Microarray Scanner with SureScan High-Resolution Technology (G2565CA). Images were analyzed using Agilent Feature Extraction Software.

Microarray analyses

Microarray data was normalized using Lowess on the Cy3 and Cy5 channels. Analyses were performed on data present in at least 70% of experimental samples using genes with an absolute signal intensity of at least 10 units in both dye channels.⁽¹⁵⁴⁾ Replicate probes were collapsed to genes by averaging. Further analyses were performed using R system for statistical computing (R Development Core Team, 2006, <http://www.R-project.org>). Samples from two batches scanned on different dates were combined using a nonparametric adjustment *combat*⁽¹⁹⁵⁾ to form a data matrix on which cluster analysis was performed. Probes were annotated with gene symbols using the Ensembl database through Biomart.⁽¹⁹⁶⁾ Genes were median centered and the 2000 most variable genes across all cell lines were identified by median absolute deviation (MAD) scores. Consensus clustering⁽¹⁵⁸⁾ was performed using the R package *ConsensusClusterPlus*⁽¹⁵⁹⁾ with 1000 iterations and 80% resample rate. Gene Set Analysis (GSA)⁽¹⁹⁷⁾ was performed with 1000 permutations. Single sample Gene Set Enrichment Analysis (ssGSEA) was performed as described previously.⁽¹⁶²⁾ For human TCGA GBM signatures, the top 250 genes most highly expressed in each subtype versus the remaining subtypes were used, as determined by Significance Analysis of Microarrays pairwise comparisons in Verhaak.⁽¹⁷⁾

High grade astrocytoma (HGA) signatures from Phillips, et al. were used as described.(18) Neural lineage-specific gene signatures were composed of the top 500 genes associated with each distinct murine brain cell type as described in Cahoy.(108) Curated gene sets version 3.0 were acquired from the Broad Institute (<http://www.broad.mit.edu/gsea/msigdb>). For comparison to human gene sets, mouse genes were converted to the human orthologs according to the MGI database (<ftp://ftp.informatics.jax.org/pub/reports/index.html#orthology>). All original raw microarray data are publically available at the UNC Microarray Database (<http://genome.unc.edu>) and have been deposited in Gene Expression Omnibus, accession number GSE40265.

Inhibition of the PI3K pathway in TRP^{-/-} astrocytes

TRP^{-/-} astrocytes at 50-60% confluence were treated with PI-103 (Cayman Chemical, Ann Arbor, MI), LY294002 (Cayman), and rapamycin (Sigma-Aldrich) at the lowest concentrations required to maximally inhibit their target kinases. Immunoblots were probed for Akt, phospho-Akt, and phospho-S6 as described above. Fluorescent secondary antibodies from Invitrogen (A21429, A11029) were used to label mouse and rabbit primary antibodies. Blots were scanned on Typhoon 9200 (GE Healthcare, Pittsburgh, PA) and analyzed using ImageQuant TL 7.0. Protein levels in treated versus vehicle control treated astrocytes were normalized to Akt and compared at defined times after treatment to determine the earliest time and duration of maximal inhibition.

Microarray analysis of PI3K inhibition in TRP^{-/-} astrocytes

TRP^{-/-} astrocytes at 50–60% confluence were treated with each drug (inhibited samples). Drug-containing media was removed after 4 hours and replaced with complete media without drug. Total RNA was harvested at 4, 8, and 24 hours after media replacement (released samples). Cells were lysed with RNA lysis buffer and total RNA was extracted as described above. The 4 hour inhibited treated

samples were compared to a pooled untreated TRP^{-/-} reference to look for effects of an inhibitor. To identify a PI3K activation signature after release from each drug, samples released from inhibition (released) were compared to a pooled reference of inhibited samples. Experimental (Cy5 CTP) and reference (Cy3 CTP) samples were mixed and co-hybridized overnight on the same microarrays as described above. Three TRP^{-/-} isolates and microarrays per experimental condition were performed.

Orthotopic allografts

Immediately prior to injection, genotype-confirmed astrocytes were trypsinized, counted with a hemocytometer, washed with PBS, and suspended in serum-free DMEM with 5% methyl cellulose, as previously described.(114) Adult mice (≥ 3 months) were anesthetized with Avertin (250 mg/kg) and placed into a stereotactic frame (Kopf, Tujunga, CA). Following a 0.5 cm scalp incision, 10⁵ cells in 5 µL were delivered intracranially to the right basal ganglia using coordinates 1, -2, and -4 mm (A, L, D) from the Bregma suture via a Hamilton syringe mounted in a repeating antigen dispenser (Hamilton, Reno, NV

Histopathological evaluation

Formalin-fixed, paraffin embedded (FFPE) brains were cut on a rotary microtome in serial 4-5 µm sections, placed on glass slides, and stained with hematoxylin and eosin (H&E) on a Leica Microsystems Autostainer XL (Buffalo Grove, IL). H&E stained slides were scanned on an Aperio ScanScope XT (Vista, CA) using a 20X objective and the resulting svx files were imported into an Aperio Spectrum web database. Histopathological analysis, grading, and photomicrography was performed by CRM according to WHO 2007 criteria for human astrocytomas(5) using an Olympus BX41 microscope equipped with a DP70 digital camera (Center Valley, PA).

RESULTS

PI3K and MAPK signaling and growth of G1/S checkpoint-defective primary astrocytes

To determine how targeted genetic disruption of Rb, Ras, and PI3K signaling affects tumorigenesis, we isolated and cultured primary cortical astrocytes from newborn mouse pups with the following genotypes: T, TR, TP^{wt/loxP}, TP^{loxP/loxP}, TRP^{wt/loxP}, and TRP^{loxP/loxP}. After infection with Ad5CMVCre to induce recombination, we performed a series of *in vitro* experiments to probe how these genetic events affect PI3K and Ras/MAPK signaling, proliferation, apoptosis, migration, invasion, and gene expression.

The Rb family of G1/S cell cycle checkpoint regulatory proteins Rb1, p107, and p130 are encoded in mice by *Rb1*, *Rbl1*, and *Rbl2*. Deletion of all three Rb family genes in mouse embryonic fibroblasts disrupts this checkpoint and enhances cell cycle entry.⁽¹⁹⁰⁾ We confirmed that T-mediated inactivation of all three Rb family proteins disrupted the G1/S checkpoint, as T but not wild-type astrocytes continued to enter S phase and proliferate after serum starvation in media with 0.5% serum (data not shown). Under normal growth conditions, T astrocytes showed essentially no activation of the PI3K pathway effectors Akt and S6 (Fig. 3.1A). Moreover, p-Akt and p-S6 levels were similar to wild-type astrocytes (Fig. S3.1A). These results demonstrate that a defective G1/S checkpoint alone does not activate PI3K signaling (Fig. 3.1A). *Pten* deletion (TP^{+/-} and TP^{-/-}) increased PI3K pathway activation, as p-Akt and p-S6 levels in TP^{-/-} >> TP^{+/-} > T astrocytes. Kras activation (TR and TRP^{+/-}) further increased Akt and S6 phosphorylation. Akt and S6 phosphoprotein levels in at least two of three TR and TRP^{+/-} isolates were similar to astrocytes completely lacking *Pten* (TP^{-/-} and TRP^{-/-}). These results indicate that activated Kras, biallelic *Pten* deletion, or their combination potentiates PI3K pathway signaling in G1/S-defective astrocytes.

We also measured MAPK pathway activation. In at least two of three isolates per genotype, p-Mek1/2 levels were TRP^{-/-} > TRP^{+/-} > TP^{-/-} ≥ TR > TP^{+/-} > T ≥ wild-type astrocytes (Figs. 3.1A and S3.1A).

These data suggest that Kras activation (TR) or *Pten* deletion ($TP^{+/-}$, $TP^{-/-}$) alone induce increased MAPK signaling that is augmented when these mutations are combined ($TRP^{+/-}$, $TRP^{-/-}$). Maximum signaling in $TRP^{-/-}$ astrocytes highlights the combinatorial effects of these mutations on the two main RTK effector pathways.

To determine how Rb, Ras, and/or PI3K pathway alterations affected cellular growth, cultured astrocytes from all six genotype combinations were counted over seven days and apoptosis was quantified. Wild-type astrocyte numbers were essentially unchanged throughout the time course examined (Fig. 3.1B). T astrocytes showed an increased growth rate (5.7 day doubling time) (Figs. 3.1B and C) and approximately 2-fold increased apoptosis (Fig. S3.1B) relative to wild-type astrocytes. Similar results were observed in T-driven astrocytomas *in vivo*.⁽⁷⁹⁾ $TP^{+/-}$ and $TP^{-/-}$ astrocytes grew faster (doubling times 4.1 and 3.4 days) and apoptosis in $TP^{-/-}$ was lower than T astrocytes ($P < 0.05$). Kras activation alone (TR) or in combination with *Pten* deletion ($TRP^{+/-}$, $TRP^{-/-}$) increased growth as TR, $TRP^{+/-}$, and $TRP^{-/-}$ astrocytes displayed the shortest doubling times of 3.8, 3.4, and 2.0 days, respectively (Fig. 3.1C). Apoptosis levels in TR were lower than T ($P < 0.05$) but similar to $TP^{-/-}$ astrocytes ($P > 0.05$) (Figs. 3.1D and S3.2), suggesting that the increased growth in $TP^{-/-}$ versus TR astrocytes is due to a higher proliferation rate in the former. Apoptosis in $TRP^{-/-}$ astrocytes was lower than both $TP^{-/-}$ and TR ($P < 0.001$ and $P = 0.08$, respectively) (Figs. 3.1D and S3.2). Overall, these data suggest that activated Kras or *Pten* loss mitigate the apoptosis induced by T-mediated ablation of the G1/S checkpoint in cultured murine astrocytes. Moreover, the proliferative and anti-apoptotic effects of T, R, and P combined ($TRP^{-/-}$) produced the largest net positive effect on cellular growth.

Both Kras activation and Pten loss contribute to G1/S-defective astrocyte migration in vitro

We have previously shown that TR, $TRP^{+/-}$, $TRP^{-/-}$ mice frequently develop high-grade astrocytomas (HGA), including GBM, whereas T, $TP^{+/-}$, $TP^{-/-}$ mice develop low grade astrocytomas (LGA) that infrequently progress to HGA.⁽⁴⁰⁾ Therefore, we hypothesized that G1/S-defective astrocytes with

activated Kras and/or *Pten* deletion would display enhanced migration *in vitro*. To address these hypotheses, we evaluated migration using two different assays.

Wound closure or “scratch” assays have been extensively used to examine the molecular mechanisms of migration.(198) We used this assay to quantify astrocyte migration after 24 h. Activated Kras, alone or in combination with *Pten* loss, significantly increased migration (Figs. 3.2A and B), as 2.8, 2.8, and 1.9-fold increases in wound closure were evident in TR vs. T, TRP^{+/-} vs. TP^{+/-}, and TRP^{-/-} vs. TP^{-/-} astrocytes ($P \leq 0.0005$). Monoallelic *Pten* deletion did not significantly affect migration of G1/S-defective astrocytes with (TR) and without (T) concomitant Kras activation (TRP^{+/-} vs. TR, $P=0.5$; TP^{+/-} vs. T, $P=0.6$). In contrast, biallelic *Pten* deletion increased migration 2.7-fold in TP^{-/-} compared to T astrocytes ($P=0.009$) and migration nearly doubled (1.8 fold) in TRP^{-/-} compared to TR astrocytes ($P<0.0001$). These results show that either Kras activation alone or biallelic *Pten* deletion, with or without activated Kras, increased G1/S-defective astrocyte migration, and all three alterations resulted in maximal migration.

Because wound closure can be achieved through a combination of cell migration, spreading, proliferation, and interaction with neighboring cells, we examined the cell autonomous genetic contributions to migration by tracking cellular movement over one hour using time lapse video microscopy and calculating the velocities of individual cells (Fig. 3.2C and videos SV1-4). Wild-type astrocytes were relatively non-motile. G1/S checkpoint disruption alone (T) increased mean cellular velocity 4.3-fold compared to wild-type astrocytes. Activated Kras (TR) or *Pten* deletion (TP^{+/-}, TP^{-/-}) only slightly increased migration of G1/S-defective T astrocytes. TR, TRP^{+/-}, and TRP^{-/-} astrocytes migrated faster than their counterparts without activated Kras. Combining all three alterations in TRP^{-/-} astrocytes resulted in maximal migration with a mean velocity of $47 \pm 2 \mu\text{m/h}$. Notably, genotype significantly influenced mean velocity (one-way ANOVA $P<0.0001$) and all pairwise genotype comparisons were significant ($P<0.05$) except T vs. TP^{-/-}. Multivariable regression analysis confirmed the independent contribution of all three alleles ($P<0.001$). Taken together, these results showed that Kras activation

and/or *Pten* loss increased G1/S-defective astrocyte migration and that all three alterations resulted in maximal migration in both multicellular (Fig. 3.2B) and individual cell (Fig. 3.2C) contexts.

We confirmed the effects of activated Ras and PI3K signaling on migration by examining wound closure in TRP^{-/-} astrocytes upon pharmacological inhibition of mTOR, PI3K, and MEK with rapamycin, LY294002, and U0126, respectively (Fig. 3.2D). S6 phosphorylation was virtually eliminated by rapamycin and LY294002 (Fig. S3.6) and decreased wound closure 22% and 45% ($P \leq 0.0004$). U0126 inhibited Erk phosphorylation (Fig. S3.3A) and decreased wound closure 35% ($P < 0.0001$). In contrast, combined inhibition of PI3K and MEK with LY294002 and U0126 decreased TRP^{-/-} astrocyte wound closure 85% relative to untreated TRP^{-/-} astrocytes ($P < 0.0001$). Moreover, combined LY294002/U0126 treatment decreased TRP^{-/-} astrocyte migration to similar levels as T astrocytes without activated *Kras* and deleted *Pten* (Fig. 3.2B), while minimally affecting viability at 24 hours (data not shown) or 5 days (Fig. S3.3B).

Pten loss is necessary for G1/S-defective astrocyte invasion in vitro

Astrocytomas are characterized by their ability to invade the surrounding brain parenchyma. We used our astrocyte panel to ascertain which core signaling pathway alterations were necessary for collagen invasion *in vitro*.(194) T astrocytes showed minimal invasion over seven days (Figs. 3.3A and B). Invasion was only 40% higher in TR astrocytes ($P=0.6$), suggesting that *Kras* activation alone was insufficient for invasion. However, a *Kras* effect was evident when combined with monoallelic *Pten* deletion, as TRP^{+/-} showed 19-fold increased invasion compared to TP^{+/-} astrocytes ($P=0.01$). In contrast, a *Kras*-specific effect was not apparent when combined with biallelic *Pten* deletion, as TRP^{-/-} showed only a 40% increase in invasion compared to TP^{-/-} astrocytes ($P=0.2$). Although monoallelic *Pten* deletion (TP^{+/-}) produced a moderate (6-fold), statistically insignificant increase in invasion ($P=0.09$), biallelic *Pten* deletion (TP^{-/-}) increased invasion 68-fold compared to T astrocytes ($P < 0.0001$, Fig. 3.3B), suggesting that

Pten loss alone is sufficient to induce G1/S-defective astrocyte invasion. Deletion of one (TRP^{+/-}) or both (TRP^{-/-}) *Pten* allele(s) increased invasion 85- ($P=0.01$) and 69-fold ($P=0.001$) over G1/S-defective astrocytes with activated Kras (TR). Thus, while the invasion-related effects of Kras activation were evident in G1/S-defective astrocytes with heterozygous, but not homozygous *Pten* deletion, Pten loss-mediated invasion was independent of Kras activation.

In addition to proliferation and migration, genetic activation of Kras and *Pten* deletion maximally increased G1/S-defective astrocyte invasion *in vitro* (TRP^{-/-}). Therefore, we next confirmed the invasion-related effects of activated PI3K and MEK signaling by examining TRP^{-/-} astrocyte invasion after pharmacological inhibition of mTOR, PI3K, and MEK. Whereas rapamycin, LY294002, and U0126 inhibited TRP^{-/-} astrocyte invasion 47%, 33%, and 49% ($P>0.05$), combined treatment with LY294002/U0126 significantly decreased invasion 90% ($P=0.01$, Fig. 3.3C). Of note, all drug treatments minimally affected viability at 5 days ($P>0.05$, Fig. S3.3B).

Pten restoration reduces proliferation, migration, and invasion

The data above suggest that PI3K pathway activation induced by Pten loss is critical for G1/S-defective astrocyte proliferation, migration, and invasion. To confirm its role in these processes, we restored Pten expression by infecting TRP^{-/-} astrocytes with a retrovirus encoding wild-type murine *Pten*. Pten expression was evident in approximately 60% of cells within 48 hours of infection and attenuated downstream PI3K signaling at p-Akt (56-73%) and p-S6 (68-85%). In contrast, Pten restoration did not significantly alter MAPK signaling at p-Mek and p-Erk (Fig. 3.4A).

Restoring Pten increased TRP^{-/-} astrocyte doubling time from 1.8 to 2.7-3.4 days (Figs. 3.4B and C), growth rates similar to TR astrocytes without *Pten* deletion (Fig. 3.1B). Pten also significantly reduced, but did not completely prevent, migration in the wound closure assay ($P\leq 0.0002$, Fig. 3.4D). GFP transfection did not significantly alter migration (Fig. 3.4D) compared to untransfected TRP^{-/-}

astrocytes (Fig. 3.2B) ($P=0.1$). These data are consistent with wound closure (Fig. 3.2B) and time lapse microscopy (Fig. 3.2C) experiments using TR astrocytes and confirm the Kras contribution to migration. Similarly, invasion was significantly decreased, but not prevented in Pten rescued TRP^{-/-} astrocytes; instead, rescued TRP^{-/-} cells showed 58% and 32% reduction in invasion compared to control, GFP-infected TRP^{-/-} cells at 3 and 5 days, respectively ($P\leq 0.0003$, Fig. 3.4E). These data are consistent with data in Fig. 3.3C where TRP^{-/-} invasion was only partially mitigated after pharmacologically inhibiting PI3K or mTOR.

To confirm the Kras-independent effects of Pten on migration, we restored Pten in cells without activated Kras (TP^{-/-}). Wound closure was reduced to 7.6% (Fig. S3.4), levels comparable to T astrocytes. This demonstrated that Pten loss significantly contributed to migration in the absence of Ras activation.

Activated MAPK and PI3K signaling in G1/S-defective astrocytes produces gene expression profiles similar to human proneural HGA

Results above demonstrate that the phenotypic effects of Ras activation and Pten loss are contextual and complementary. Next, we determined their effects on genome-wide transcriptome patterns using microarrays. These experiments showed that cultured G1/S-defective astrocytes display distinct expression profiles depending upon the presence of activated Kras, Pten loss, or both. Consensus clustering of 23 samples identified 4 classes with high confidence (Fig. S3.5); three of these classes (22 samples) were used in subsequent analyses (see Supplemental methods). Although different isolates from identical genotypes were sometimes present in different clusters, Class 1 contained only T and TP astrocytes, Class 2 contained all analyzed TR astrocytes, and Class 3 contained only TRP astrocytes (Fig. 3.5A). Compared to Class 1 and 2, Class 3 (green bar) astrocyte transcriptomes were significantly enriched for migration, invasion, and stem cell signatures (Fig. 3.5B, Table S3.1). These data are consistent with the above results demonstrating maximal migration and invasion in TRP astrocytes and suggest that these astrocytes may be stem-like and capable of initiating tumorigenesis.

Next, we examined whether these astrocytes were enriched for TCGA human GBM(17) and Phillips prognostic HGA(18) subtype signatures using gene set analysis (GSA) (Table S3.2) and single sample gene set enrichment analysis (ssGSEA) (Fig. 3.5C). Class 3 TRP astrocytes were highly enriched for TCGA proneural and neural signatures ($P \leq 0.003$) and showed particularly low expression of the TCGA ($P = 0.09$) and Phillips ($P = 0.04$) mesenchymal subtype signatures. Individual Class 3 astrocytes were also enriched for Phillips proneural and proliferative signatures, but the entire group was not significantly associated with them ($P \geq 0.1$). None of the HGA signatures were significantly enriched in Class 1 T/TP or Class 2 TR astrocytes, but several samples in these classes expressed low levels of proneural and neural signatures, further highlighting their dissimilarity to Class 3 TRP astrocytes.

We then investigated expression of adult murine neural cell lineage-specific signatures.(108) Class 3 TRP astrocytes showed high expression of oligodendrocyte progenitor (OPC)-specific genes and low expression of cultured astrocytes-specific genes (Fig. 3.5D, Table S3.2), suggesting that the combination of Kras activation and Pten loss induces a more primitive expression pattern in G1/S-defective astrocytes. In contrast, Class 1 (T, TP) astrocytes showed low expression of OPC signature genes, but instead expressed cultured astrocyte-specific genes.

A PI3K activation signature is enriched in human proneural GBM

Because PI3K signaling activation caused by Pten loss was critical for proliferation, migration, and invasion of G1/S-defective TRP^{-/-} astrocytes, we next defined gene signatures specific to activated PI3K signaling. First, PI3K signaling was pharmacologically inhibited in TRP^{-/-} astrocytes using the dual PI3K/mTOR inhibitor PI-103, the PI3K inhibitor LY294002, and the mTOR inhibitor rapamycin. Each drug maximally inhibited Akt-mediated S6 phosphorylation within 2-4 hours of treatment and maximal inhibition lasted at least 24 hours, except LY294002, which lasted 4 hours (Fig. S3.6A-D). To identify PI3K pathway signatures, we analyzed mRNA expression of drug-treated samples after 4 hours of inhibition

(inhibited) and 4, 8, and 24 hours after release from inhibition (released). We used large average submatrices (LAS), an unsupervised significance-based biclustering method, to identify groups of coordinately expressed genes.(199)

The top five biclusters, in order of decreasing statistical significance, consisted of genes highly expressed in the following contexts (data not shown): 1) all times after LY294002 release; 2) all inhibited samples regardless of the specific drug; 3) 24 hours after release from inhibition, regardless of the drug; 4) all times after rapamycin release; and 5) all times after PI-103 release. The fifth bicluster of genes highly expressed after PI-103 release was selected as the PI3K signature for further investigation (Table S3.3). The first bicluster was excluded because the relatively high concentration of LY294002 (50 μ m) required to produce maximal inhibition of PI3K signaling showed slightly reduced viability relative to untreated TRP^{-/-} cells at 24 hours (93 \pm 2%, data not shown), was likely to produce off target effects, and was less efficient than PI-103 in inhibiting Akt phosphorylation (Fig. S3.6D). The second was excluded because we sought to identify genes that defined activated, not inhibited PI3K signaling. The third was excluded because genes expressed only after 24 hours of drug release would not contain genes expressed at earlier time points. The fourth was excluded because rapamycin-mediated inhibition of mTOR complex 1 (mTORC1) ablated S6, but not Akt phosphorylation (Fig. S3.6C). Consequently, genes expressed upon rapamycin release would represent only a distal PI3K pathway activation signature. In contrast, PI-103 inhibits PI3K and both mTOR complexes and it efficiently reduced phosphorylation of both Akt and S6 in TRP^{-/-} astrocytes (Fig. S3.6A). Furthermore, Akt and S6 phosphorylation increased upon PI-103 release, suggesting that both proximal and distal PI3K pathway signaling resumed in TRP^{-/-} astrocytes released from PI-103 (Fig. S3.6A, D, E). We identified 518 genes (Table S3.3) with increased expression upon PI-103 release as a PI3K pathway activation signature and found that these genes clustered G1/S-defective TRP^{-/-} astrocytes on the basis of inhibition or release from each individual drug (Fig. 3.6A).

Expression of PI3K signature genes was next examined in 434 human GBM from the TCGA(167) and was significantly different across the four subtypes (Fig. 3.6B). Proneural GBM, in particular, showed significantly higher expression of PI3K signature genes by ssGSEA (Fig. 3.6C).

Kras activation with or without Pten loss is necessary for G1/S-defective astrocyte tumorigenesis

The complimentary effects of Kras activation and Pten loss produced highly proliferative, migratory, and invasive G1/S-defective astrocytes *in vitro* and their gene expression profiles correlated with human HGA subtypes. Next, we used an allograft model system with syngeneic, immunocompetent hosts to investigate whether Kras activation and/or Pten loss was required for tumorigenesis *in vivo*. Orthotopic injection of T, TR, TRP^{+/-}, and TRP^{-/-} astrocytes produced astrocytomas in 30%, 25%, 64%, and 60% of mice aged up to one year or neurological morbidity (Fig. 3.7A). Three mice injected with T astrocytes developed small foci of LGA that failed to produce neurological symptoms and progress to HGA over the course of a year (Fig. S3.7A-D). Four of six astrocytoma-bearing mice injected with TR astrocytes developed GBM (Figs. 3.7B and S3.7E-H). Thus, while Kras activation was sufficient for malignant progression, TR GBM developed with long latency, as median survival was 207 days (Fig. 3.7C). In contrast, G1/S-defective astrocytes containing both activated Kras and *Pten* deletion progressed to HGA in >97% of mice injected with either TRP^{+/-} or TRP^{-/-} astrocytes and 89% and 83% of these mice developed GBM, respectively (Fig. 3.7B, S3.7I-P). *Pten* deletion also significantly decreased the latency of G1/S-defective, Kras activated HGA, as the median survival of mice injected with TRP^{+/-} and TRP^{-/-} astrocytes was 57 and 36 days, respectively ($P \leq 0.005$) (Fig. 3.7C). These results show that ablation of the G1/S checkpoint is sufficient to produce LGA, Kras activation is required for progression to HGA, and the combination of Kras activation and *Pten* deletion dramatically increases GBM incidence and reduces survival.

TRP (Fig. S3.7IJ and S3.7MN) were significantly more invasive than TR GBM (Fig. S3.7EF), which largely developed as well-circumscribed masses. These findings are consistent with the increased invasion of TRP versus TR astrocytes *in vitro* (Fig. 3.3B). Moreover, TRP GBM contained cells with both astrocytic and oligodendroglial morphology (Fig. S3.7L and S3.7P), a finding consistent with their proneural GBM and murine OPC like gene expression profiles *in vitro*.

To further examine tumor initiation, we injected G1/S-defective astrocytes with (TR, TRP^{+/-}, TRP^{-/-}) and without (TP^{+/-}, TP^{-/-}) activated Kras, sacrificed mice every 7 days for 4 weeks, and evaluated tumor incidence and histological grade. Similar to T astrocytes, TP^{+/-} and TP^{-/-} astrocytes infrequently developed into LGA (Figs. 3.7D and S3.8). In contrast, TRP^{+/-} and TRP^{-/-} astrocytes developed into LGA more efficiently. Mitotically active HGA were evident in 40% and 10% of mice injected with these cells, but only one mouse injected with TRP^{-/-} astrocytes developed a GBM within 28 days. These results suggest that the increased incidence of HGA in mice injected with TRP astrocytes is likely due to more efficient tumor initiation.

DISCUSSION

Virtually all human GBM contain RB pathway gene mutations that dysregulate the G1/S cell cycle checkpoint. Most also contain RTK pathway gene mutations that activate RAS/MAPK and PI3K signaling.(29) We therefore used G1/S checkpoint-defective cortical murine astrocytes to examine the individual and combined effects of Ras/MAPK and/or PI3K pathway dysregulation on multiple cancer-related phenotypes *in vitro*. Both Kras activation and Pten loss induced MAPK and PI3K signaling (Fig. 3.1). Kras activation, but not Pten loss, increased proliferation and reduced apoptosis of cultured T₁₂₁⁺ astrocytes *in vitro* (Fig. 3.1D). We have previously shown that T₁₂₁ induces both proliferation and apoptosis in neonatal, T₁₂₁-driven astrocytomas *in vivo* and that Pten loss potentiates progression by reducing apoptosis.(92) These findings suggest that Kras and Pten signaling perturbations may affect G1/S-defective astrocyte growth by distinct mechanisms depending on their patterns of co-occurrence. The role of Pten in p53-dependent apoptosis has long been recognized, but increasing evidence suggests that nuclear Pten directly regulates mitosis.(200) Decreasing Pten induces expression of cell cycle and chromosome stability genes and proliferation of mouse embryonic fibroblasts.(201) Moreover, *Pten* deletion in embryonic mice increases astrocyte proliferation *in vitro* and *in vivo*.(202) Conversely, exogenous PTEN expression in human glioma cells decreases proliferation and lengthens cell cycle transit from G2/M to G1.(203) Therefore, we conclude that Pten negatively regulates proliferation in G1/S-defective astrocytes.

Kras activation and/or *Pten* deletion not only increased MAPK and PI3K pathway signaling and growth of G1/S-defective astrocytes (Fig. 3.1), but migration as well (Fig. 3.2). However, their effects on invasion were contextual (Fig. 3.3). Kras activation was insufficient for invasion in the absence of *Pten* deletion, suggesting that Ras-mediated invasion requires concurrent activation of PI3K signaling. In contrast, monoallelic *Pten* deletion was sufficient to induce maximal invasion only in the presence of activated Kras (Fig. 3.3B). Biallelic *Pten* deletion caused maximal invasion in both the presence and

absence of activated Kras (Fig. 3.3B) and Pten restoration significantly reduced invasion (Fig. 3.4E). However, Pten restoration did not completely abrogate migration and invasion, likely due to less than 100% transfection efficiency. Thus, a subpopulation of cells in these assays lacked Pten expression and thus retained their migratory and invasive properties. These results indicate that Pten is a primary regulator of G1/S-defective astrocyte invasion and that the invasion-related effects of biallelic, but not monoallelic, *Pten* deletion are independent of activated Kras.

Established human cell lines, such as U87MG, have previously been utilized in genetic gain and loss of function studies to investigate the molecular mechanisms of GBM migration and invasion *in vitro*.(204) PTEN restoration has been shown to inhibit proliferation, migration, and invasion of human *PTEN*-null U87MG astrocytoma cells *in vitro*.(205) PDGF-induced migration of U87MG cells has also been shown to be PI3K-, but not ERK-dependent,(206) and farnesyltransferase-mediated inhibition of Ras reduced U87MG migration in a PI3K dependent manner.(207) However, established cell lines harbor widespread genomic alterations that frequently differ from their original tumor.(115, 208) Therefore, panels of established cell lines, each with distinct genomic landscapes, are typically employed to rule out cell line-specific effects. Our use of an allelic series of genetically-defined astrocytes containing defined core signaling pathway mutations removes ambiguity associated with established human cell lines and provides a unique opportunity to clarify genotype-phenotype relationships in GBM pathogenesis. Our data therefore confirm and extend studies that utilized established human astrocytoma cell lines to demonstrate that PTEN is a critical regulator of migration and invasion, and that RAS-dependent invasion requires PI3K/PTEN signaling.

In addition to their effects on growth, migration, and invasion, mutations that activate Ras/MAPK and PI3K signaling produced three distinct gene expression clusters that correlated with mutation and pathway activation status (Fig. 3.5). Activation of both pathways in cultured TRP astrocytes defined a transcriptomal class (Class 3) enriched for migratory, invasive, and stem-like signatures. TRP astrocytes

also showed high expression of human proneural GBM and murine OPC signatures. These findings are consistent with previous reports demonstrating similarity between proneural GBM and OPC.(17, 108) Conversely, an activated PI3K pathway signature defined in TRP astrocytes released from PI3K pathway inhibition was enriched in human proneural GBM (Fig. 3.6).

The above data suggested that TRP astrocytes would form invasive astrocytomas *in vivo*. We utilized a novel orthotopic allograft model with syngeneic, immunocompetent hosts to show that G1/S-defective astrocytes with activated Kras and/or *Pten* deletion formed astrocytomas with penetrance that correlated with mutational status (Fig. 3.7). Specifically, both Kras activation and *Pten* deletion were required for high penetrance tumorigenesis and efficient progression to HGA. Similar results were obtained in conditional, inducible GEM in which these genetic mutations are targeted specifically to adult GFAP+ cortical astrocytes.(40) These findings suggest that cortical astrocytes may serve as a potential astrocytoma cell of origin, particularly in tumors with G1/S checkpoint dysfunction, activated Kras, and *Pten* deletion.

TRP allografts diffusely invaded normal brain and formed histopathological hallmarks of human astrocytomas, including perineuronal and perivascular satellitosis, migration and invasion along white matter tracks, elevated mitoses, microvascular proliferation, and necrosis (Fig. S3.7). These histopathological features contrast significantly with human U87MG GBM xenografts, which are poorly invasive *in vivo*,(114) and suggest that this model system will be useful for further dissection of the genetics of astrocytoma migration and invasion. We conclude that the syngeneic, orthotopic TRP allograft model represents a significant improvement over traditional xenografts models that employ established human cell lines and immunodeficient mice.

Consistent with the expression profiles of TRP astrocytes *in vitro* (Fig. 3.5) and the presence of oligodendroglial differentiation *in vivo* (Fig. S3.7), TRP allografts also showed enriched expression of human proneural GBM and murine OPC signature genes (manuscript in preparation). The Rb family of

G1/S cell cycle proteins, Nf1, a negative regulator of Ras/MAPK signaling, and Pten have each been shown to regulate neural stem cell self-renewal and fate.(209-211) These results suggest that combined dysregulation of Rb, Ras, and Pten reverts astrocytes to a progenitor-like state of gene expression.

The use of gene expression profiling to characterize the molecular heterogeneity and improve diagnostic classification of specific types of brain tumors has recently brought significant attention to defining their cellular origins. We utilized GEM models to show that the molecular heterogeneity of medulloblastoma, the most common primary brain tumor in children, has a cellular as well as genetic basis.(212) Like HGA, multiple genomic subtypes of human medulloblastoma with distinct mutations exist.(213) Furthermore, GEM models have shown that different initiating oncogenic mutations in specific cells of origin in the developing mouse cerebellum lead to distinct genomic subtypes of medulloblastoma that mimic their human counterparts.

Gene expression profiling of human HGA has suggested that the subtypes may have distinct cellular origins.(17, 142) GEM modeling studies have identified neural stem cells(70) and OPC(142) as potential candidate astrocytoma cells of origin.(139) PDGF-driven murine GBM derived from adult *Pten*-null OPC were shown to have transcriptomes similar to human proneural GBM.(142) Here we identified proneural and OPC-like expression specifically in G1/S-defective neonatal murine astrocytes with activated Kras and *Pten* deletion (Fig. 3.5D). The presence of human proneural GBM and OPC-like expression profiles in both PDGF-driven GBM and TRP astrocyte-derived GBM allografts suggests that molecularly similar GBM can arise from at least two distinct genetic mechanisms and cellular origins. We speculate that multiple cell types can give rise to GBM and that different cells are uniquely susceptible, within defined developmental windows, to the transforming effects of particular combinations of core signaling pathway mutations. These combined factors determine human astrocytoma transcriptomal subtype. Such a unifying hypothesis would explain the associations

between transcriptomal subtype, mutational landscape, signaling pathway alterations, and neural signatures in human GBM.(17, 18, 20)

The *in vitro* experiments described above show that growth, motility, and invasive phenotypes are differentially affected by specific genetic alterations in the RTK core GBM signaling pathway. These alterations may ultimately dictate targeted GBM therapy. As such, we have used MAPK and PI3K targeted drugs to reduce *in vitro* migration, invasion, and signaling in TRP astrocytes transcriptionally similar to human proneural GBM (Fig. 3.2D, 3.3C, S3.6). Release of TRP astrocytes from pharmacological PI3K pathway inhibition identified a PI3K signature significantly enriched in human proneural GBM (Fig. 3.6). The findings that TRP astrocytes contained a PI3K activation signature enriched in proneural human GBM and produced proneural-like HGA allografts upon injection into syngeneic, immunocompetent brains suggest that proneural GBM may be uniquely sensitive to combination therapies targeting both RAS/MAPK and PI3K. The TRP allograft model of human proneural GBM will not only facilitate delineation of the molecular requirements for tumorigenesis and cellular origins of astrocytomas, but will also be useful for preclinical testing of drug combinations and elucidating potential mechanisms of resistance. Moreover, the use of syngeneic, immunocompetent hosts will facilitate preclinical testing of immunotherapies.

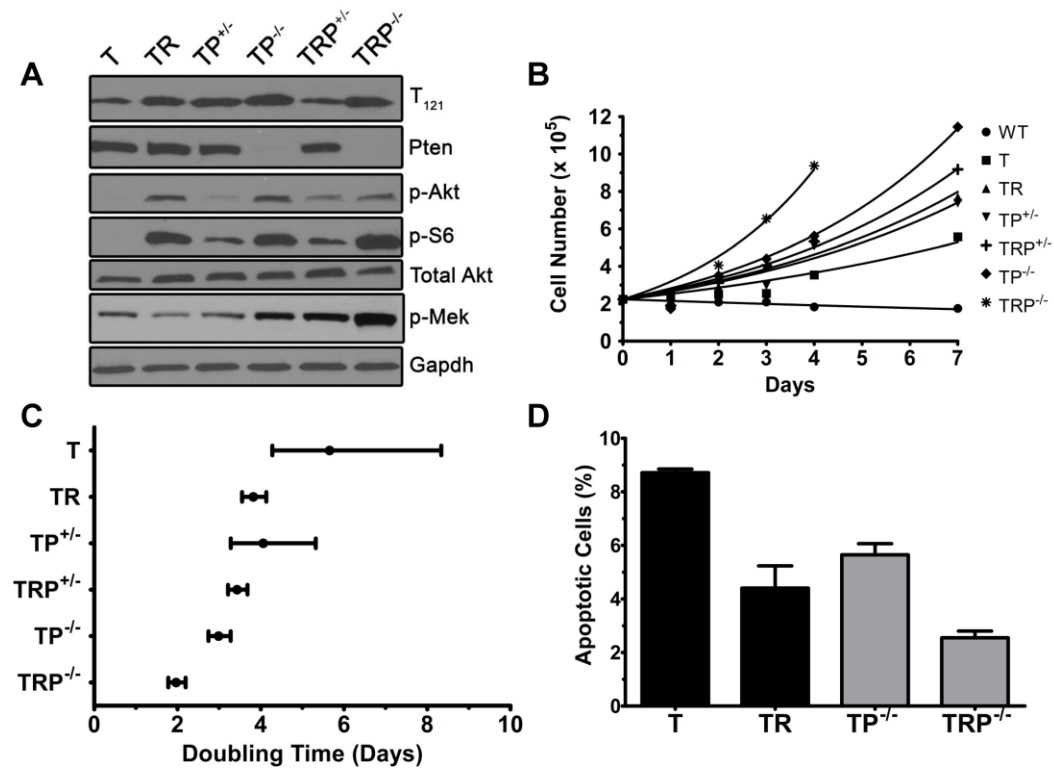


Figure 3.1. MAPK and PI3K signaling and growth of G1/S-defective astrocytes with activated Kras and/or Pten deletion. Representative immunoblots showing MAPK and PI3K pathway signaling in G1/S-defective astrocytes with activated Kras, *Pten* deletion, or both (A). Growth of G1/S defective astrocytes *in vitro*. Cell number was assessed by counting cells at days 1-7. (B). Mean doubling times \pm 95% confidence intervals were calculated from the exponential growth curves in B (C). Growth rates were significantly different across genotypes ($P < 0.0001$). Apoptosis in G1/S defective astrocytes *in vitro* (D). Colors compare genotypes with and without activated Kras. Error bars represent standard error (SEM).

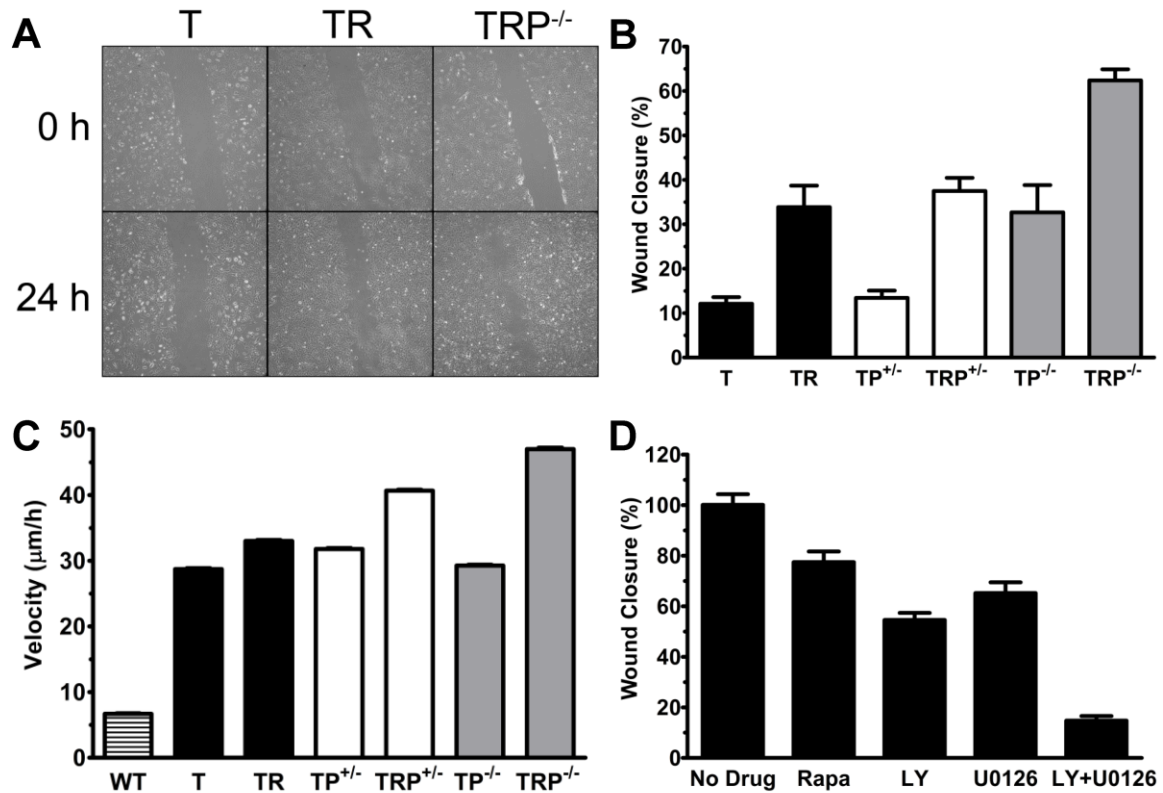


Figure 3.2. Kras activation and Pten loss increase G1/S-defective astrocyte migration.

Representative photomicrographs of wound closure in T, TR, and TRP^{-/-} astrocytes at 0 and 24 hours (A). Mean percent wound closure ± SEM at 24 hours (B). Colors compare genotypes with and without activated Kras. Mean velocity ± SEM of individual astrocytes measured using time lapse microscopy for one hour (C). Colors compare genotypes with and without activated Kras. Wound closure of TRP^{-/-} astrocytes treated with 10 nM rapamycin (Rapa), 50 μM LY294002 (LY), 10 μM U0126, or both LY294002 and U0126 (D). Mean percent wound closure ± SEM is shown relative to untreated (No Drug) TRP^{-/-} astrocytes.

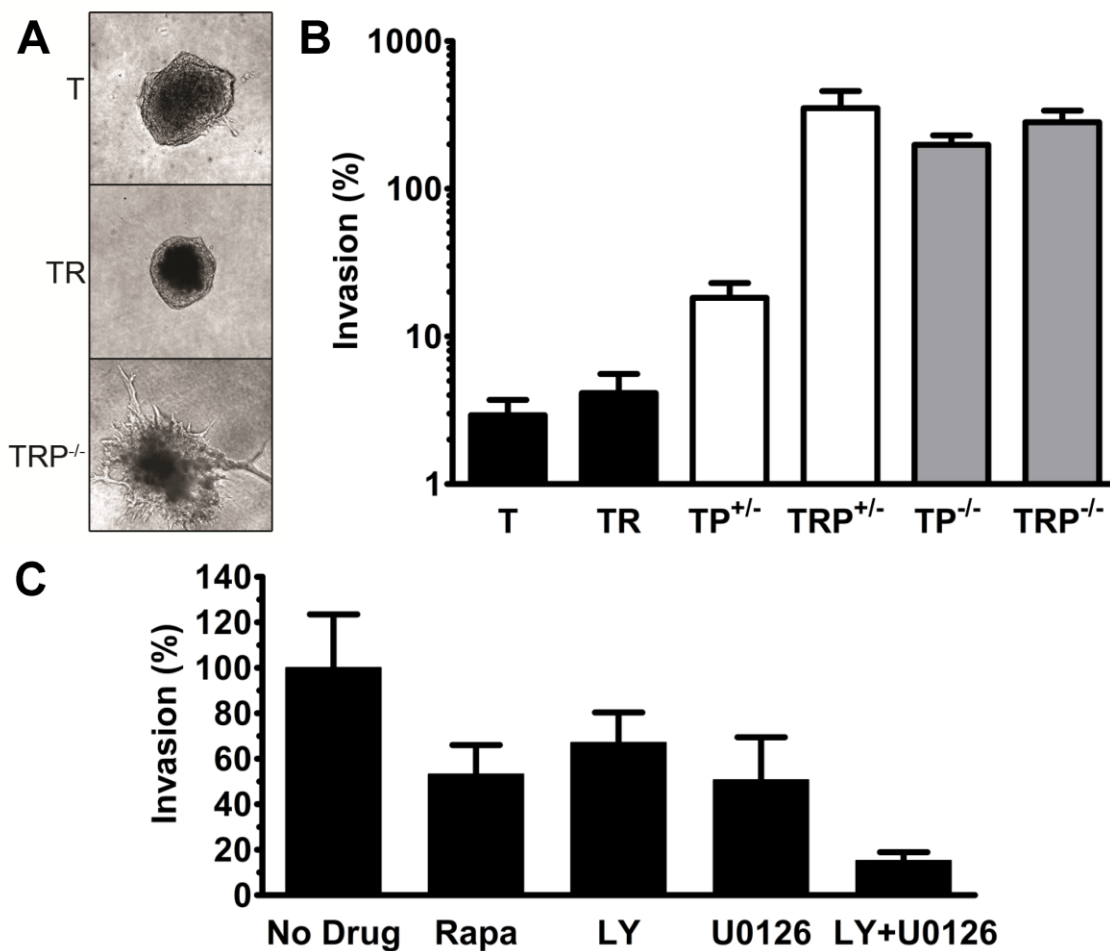


Figure 3.3. Pten deletion is necessary for maximum G1/S-defective astrocyte invasion.

Representative photomicrographs of collagen invasion of T, TR, and TRP^{-/-} astrocytes at 4 days (A). Mean percent invasion \pm SEM into collagen after 4 days (B). Colors compare genotypes with and without activated Kras. Collagen invasion of TRP^{-/-} astrocytes treated with 10 nM rapamycin (Rapa), 50 μ M LY294002 (LY), 10 μ M U0126, or both LY294002 and U0126 (C). Mean percent invasion \pm SEM is shown relative to untreated (No Drug) TRP^{-/-} astrocytes.

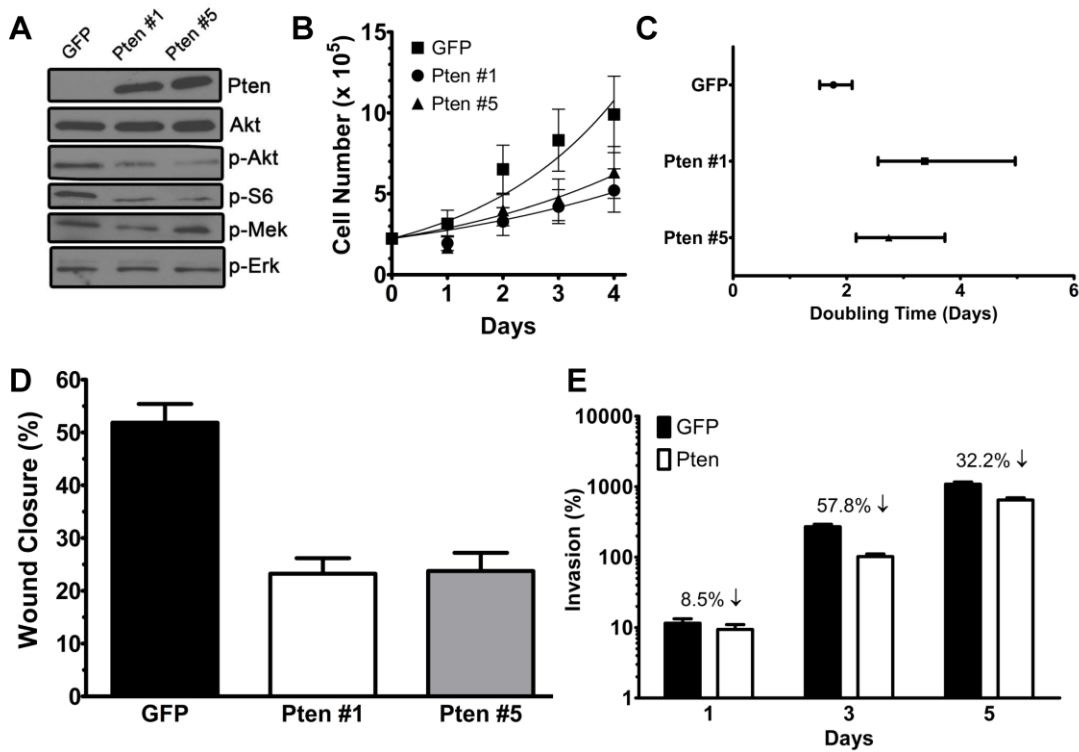


Figure 3.4. Restoration of Pten expression limits growth, migration, and invasion in TRP^{-/-} astrocytes. Representative immunoblot of MAPK and PI3K pathway signaling in TRP^{-/-} astrocytes after infection with retrovirus containing Pten or GFP cDNA (A). Growth (B), doubling time (C), mean percent wound closure at 24 hours (D), and mean percent invasion into collagen at 1, 3, and 5 days (E) of Pten rescued versus non-rescued (GFP) TRP^{-/-} astrocytes. Mean doubling times \pm 95% confidence intervals in C were calculated from the exponential growth curves in B. All experiments are the mean of at least three independent experiments using different astrocyte isolations. Error bars are SEM.

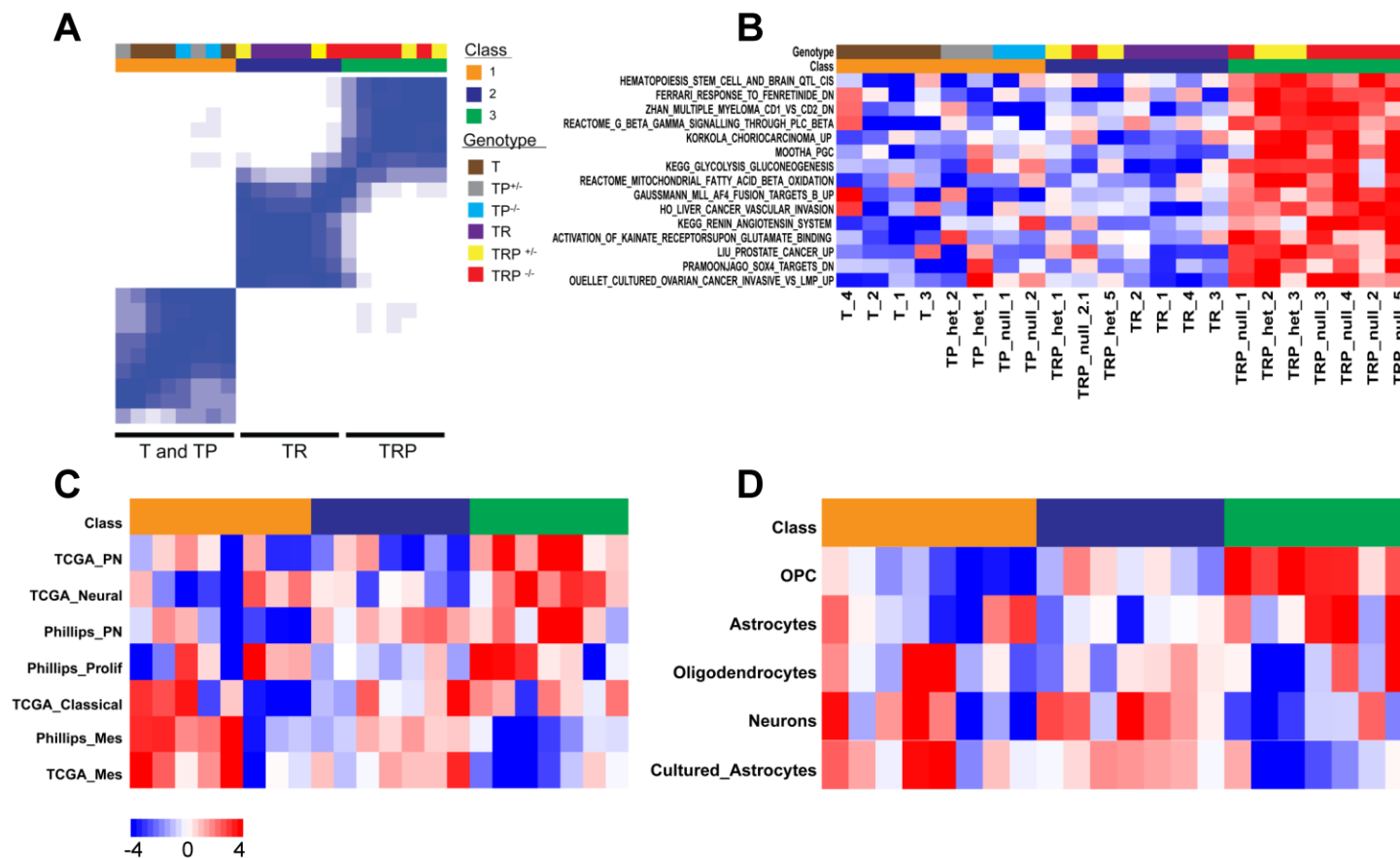


Figure 3.5. Gene expression profiling of G1/S-defective astrocytes with activated Kras and/or Pten deletion. Consensus clustering of 22 independently isolated astrocyte cultures identifies 3 clusters (A). Individual isolates are repeated on the X and Y axes. Darker shades of blue signify isolates that cluster together most often. Single sample GSEA (ssGSEA) of the 15 most significantly enriched gene signatures from MsigDB in Class 3 (green) astrocytes (B). ssGSEA of human GBM signatures (C). ssGSEA of murine neural lineage signatures (D). Red signifies higher enrichment scores of signature genes.

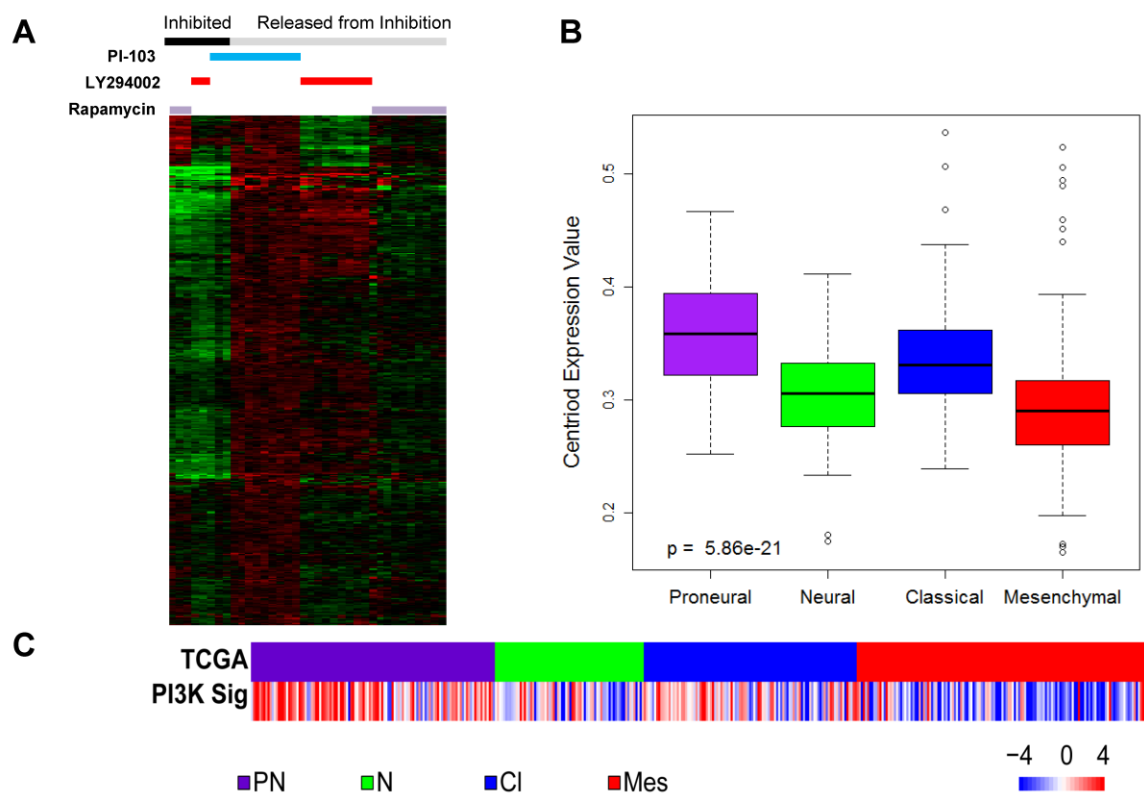


Figure 3.6. A PI3K signature defined in TRP^{-/-} astrocytes upon release from PI-103-mediated inhibition of PI3K signaling is enriched in human proneural GBM. Heatmap of 518 genes with significantly increased expression in TRP^{-/-} astrocytes after release from PI-103 (A). A box and whiskers plot of the distribution of mean expression of PI3K signature genes (centroid) (B) and ssGSEA (C) shows that the PI3K signature is significantly enriched in human proneural (PN), but not neural (N), classical (CI), and mesenchymal (Mes) GBM from TCGA.

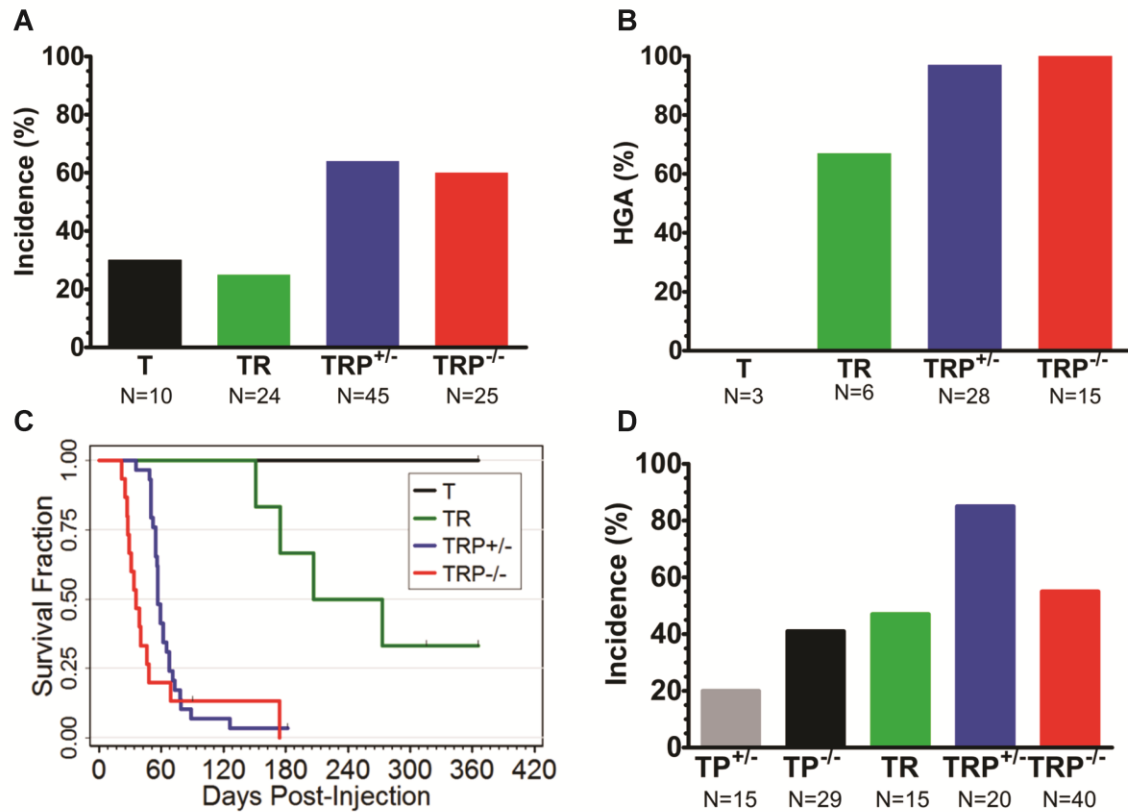


Figure 3.7. G1/S-defective astrocytes form astrocytomas upon orthotopic injection into syngeneic, immunocompetent mouse brains. Astrocytoma incidence in terminally-aged mice upon orthotopic injection of 10^5 astrocytes (A). The number of mice injected per genotype is indicated. The fraction of astrocytomas in panel A with histological features of high-grade astrocytomas (HGA) (B). The number of astrocytomas detected per genotype is indicated. Kaplan-Meier survival analysis of astrocytoma-bearing mice (C). Median survivals were 36, 57, and 207 days for TRP^{-/-}, TRP^{+/-}, and TR astrocytes, respectively ($P < 0.0001$). The incidence of astrocytomas in mice sacrificed between 7 and 28 days post-injection with astrocytes of the indicated genotypes (D).

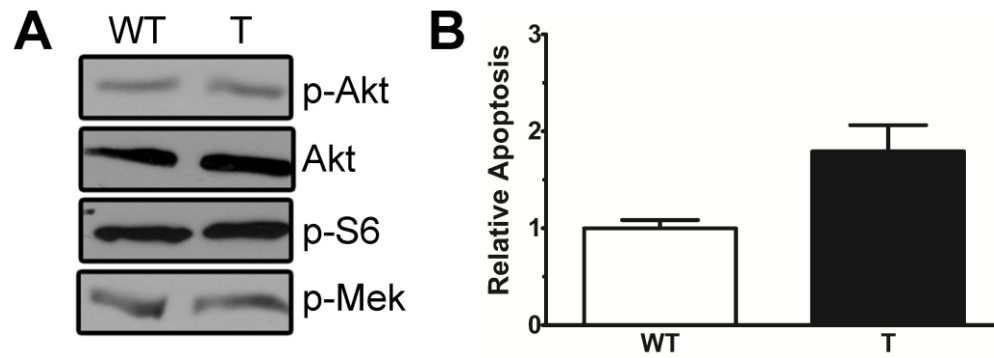


Figure S3.1. MAPK and PI3K signaling and apoptosis in wild-type and G1/S-defective astrocytes. Representative immunoblots showing MAPK and PI3K pathway signaling in wild-type (WT) and G1/S-defective (T) astrocytes (A). Mean apoptosis relative to WT astrocytes (B) ($P=0.03$). Error bars represent standard error (SEM).

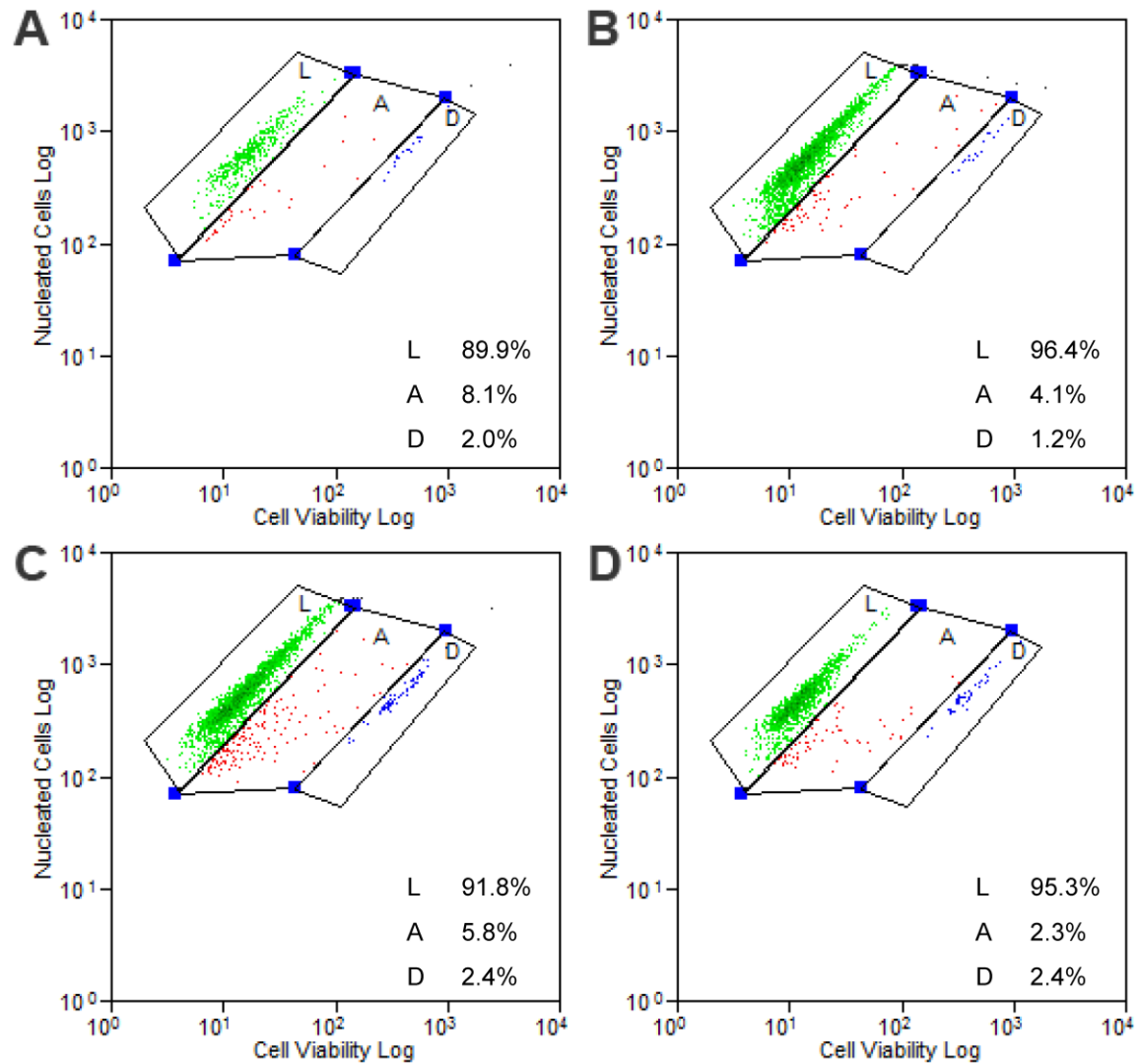


Figure S3.2. Apoptosis in G1/S-defective astrocytes with and without activated Kras and/or Pten deletion. Representative dot plots of live (L, green), apoptotic (A, red), and dead (D, blue) astrocytes of the following genotypes stained with Guava ViaCount and analyzed by flow cytometry: (A) T, (B) TR, (C) TP^{-/-}, and (D) TRP^{-/-}.

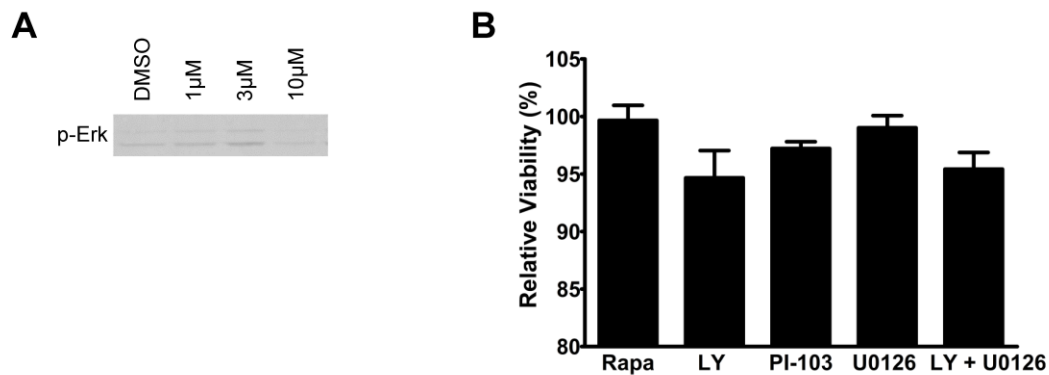


Figure S3.1 Pharmacologic effects on signaling and viability. U0126 (10μM) inhibits Erk phosphorylation in TRP^{-/-} astrocytes 2 hours after treatment (A). Rapamycin (10 nM, Rapa), LY294002 (50 μM, LY), PI-103 (1 μM), U0126 (10 μM), and the combination of LY294002/U0126 minimally affect viability of TRP^{-/-} astrocytes at 5 days after treatment (B). Viability (percent live cells) for each treatment was determined by ViaCount staining and flow cytometry as described for Fig. S2 and was not significantly different across genotypes ($P>0.05$). Values were normalized to untreated TRP^{-/-} astrocytes. Similar results were obtained at 24 hours after treatment (data not shown).

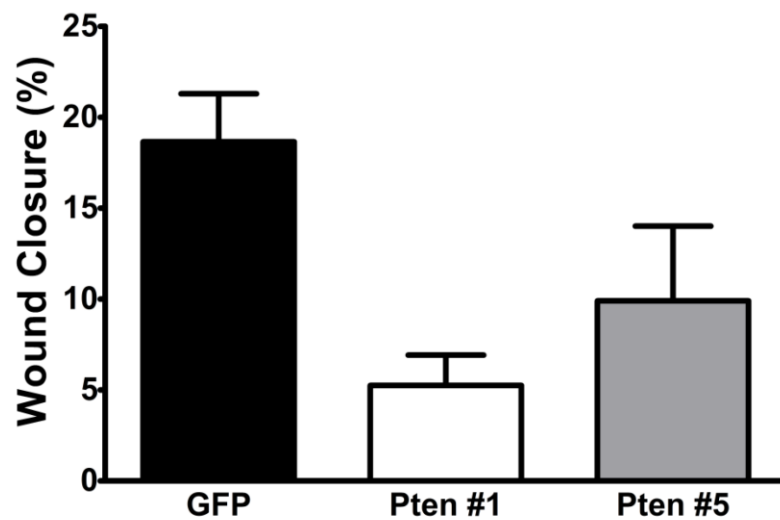


Figure S3.2. Restoration of Pten reduces invasion in TP^{-/-} astrocytes. Mean percent wound closure of TP^{-/-} astrocytes after infection with retrovirus containing Pten or GFP cDNA. The overall mean for all Pten-rescued TP^{-/-} astrocytes was $7.6\% \pm 2.2$ ($P=0.01$). Error bars are SEM.

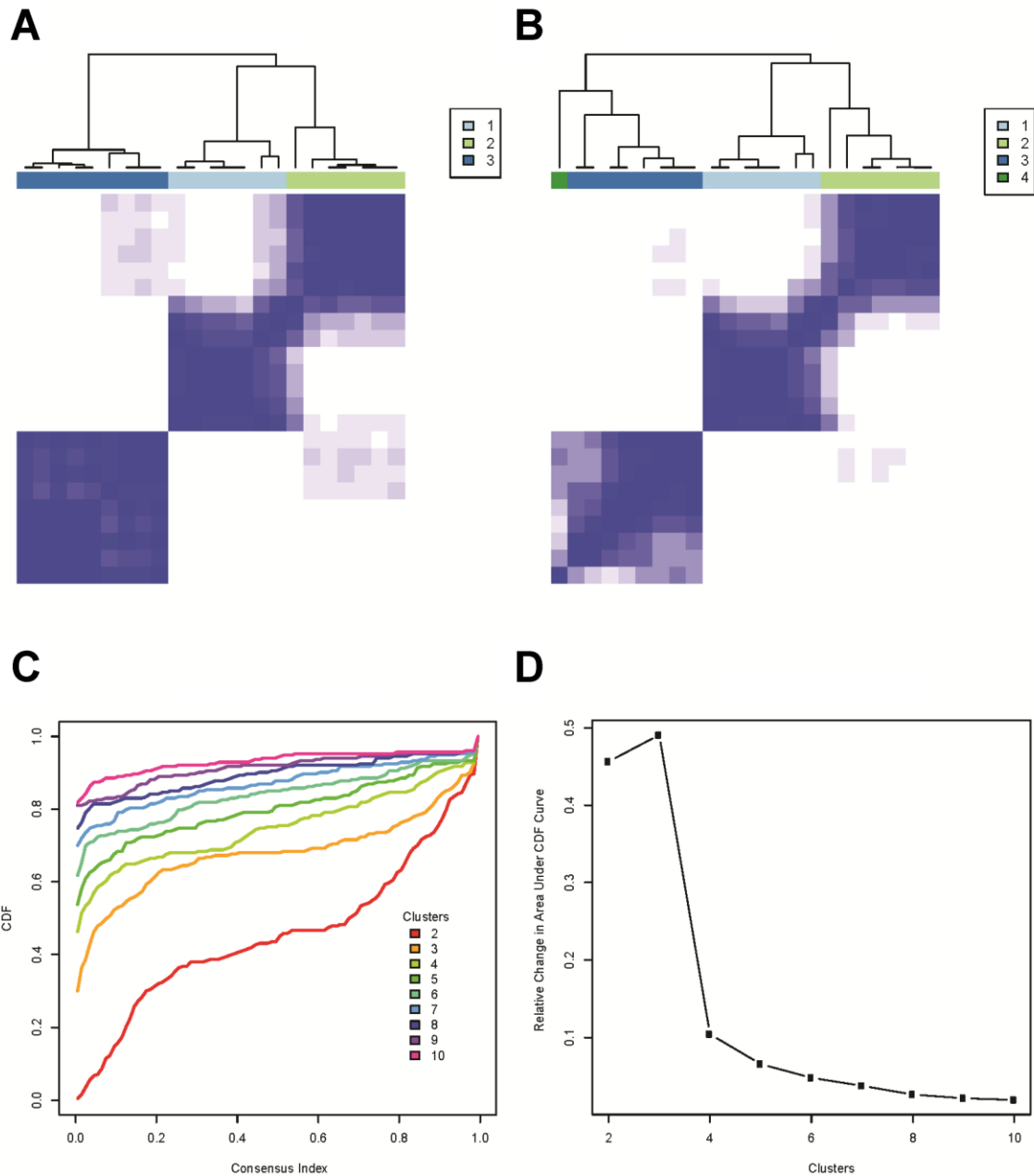


Figure S3.3. Consensus clustering of the transcriptomes of G1/S-defective astrocytes with and without activated Kras and Pten deletion. Twenty-three independently isolated astrocyte cultures were examined (N= 2–5 isolates per genotype). Consensus clustering with $k=3$ (A) and $k=4$ (B). Consensus clustering CDF (C) and delta area plots (D) for $k=2$ to $k=10$.

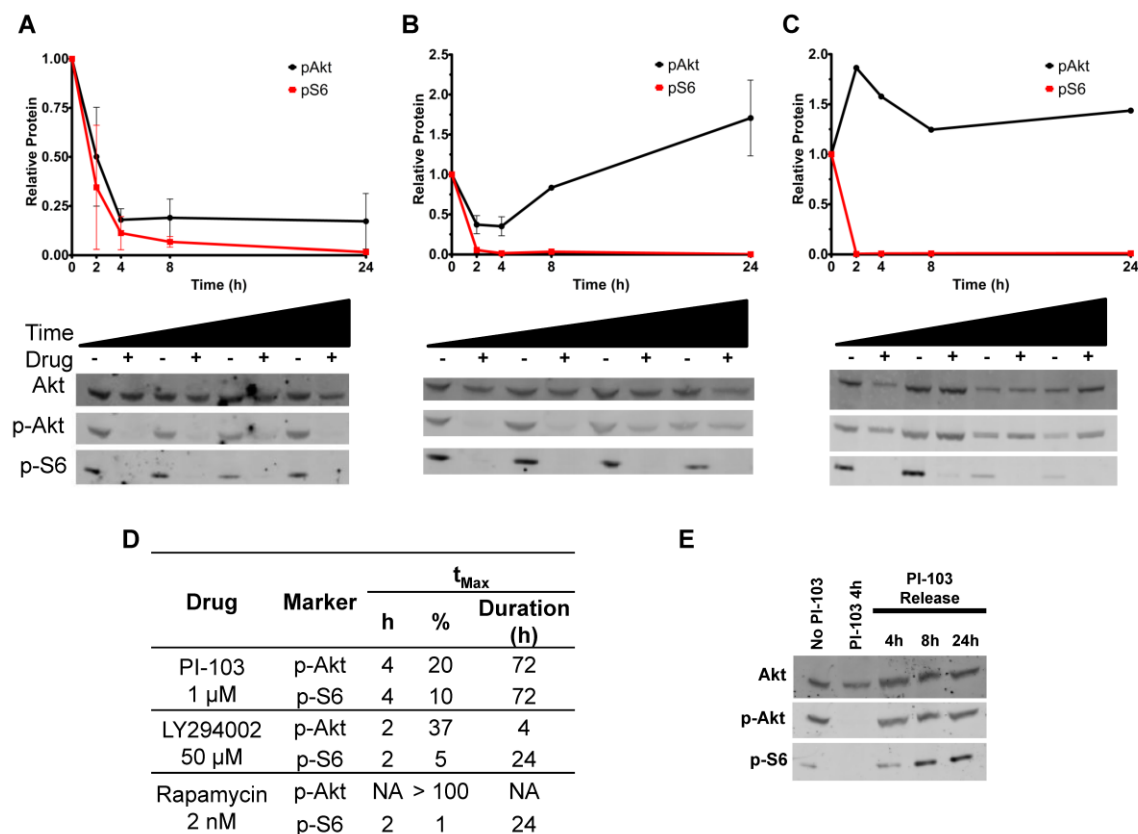


Figure S3.4. Pharmacologic inhibition of PI3K pathway signaling in TRP^{-/-} astrocytes. Time course of Akt and S6 phosphorylation in TRP^{-/-} astrocytes treated for 2-24 hours with PI-103 (A), LY294002 (B), or (C) rapamycin. Ratio of p-Akt normalized to total Akt in treated samples versus controls (black) relative to t=0. Ratio of p-S6 normalized to total Akt in treated samples versus controls (red) relative to t=0. Summary of the time (h) at which maximal inhibition occurred (t_{Max}), the percent inhibition at t_{Max} , and the duration of maximal inhibition (D). Representative immunoblots of Akt, p-Akt, and p-S6 in TRP^{-/-} astrocytes treated with and without PI-103 and after PI-103 release (E).

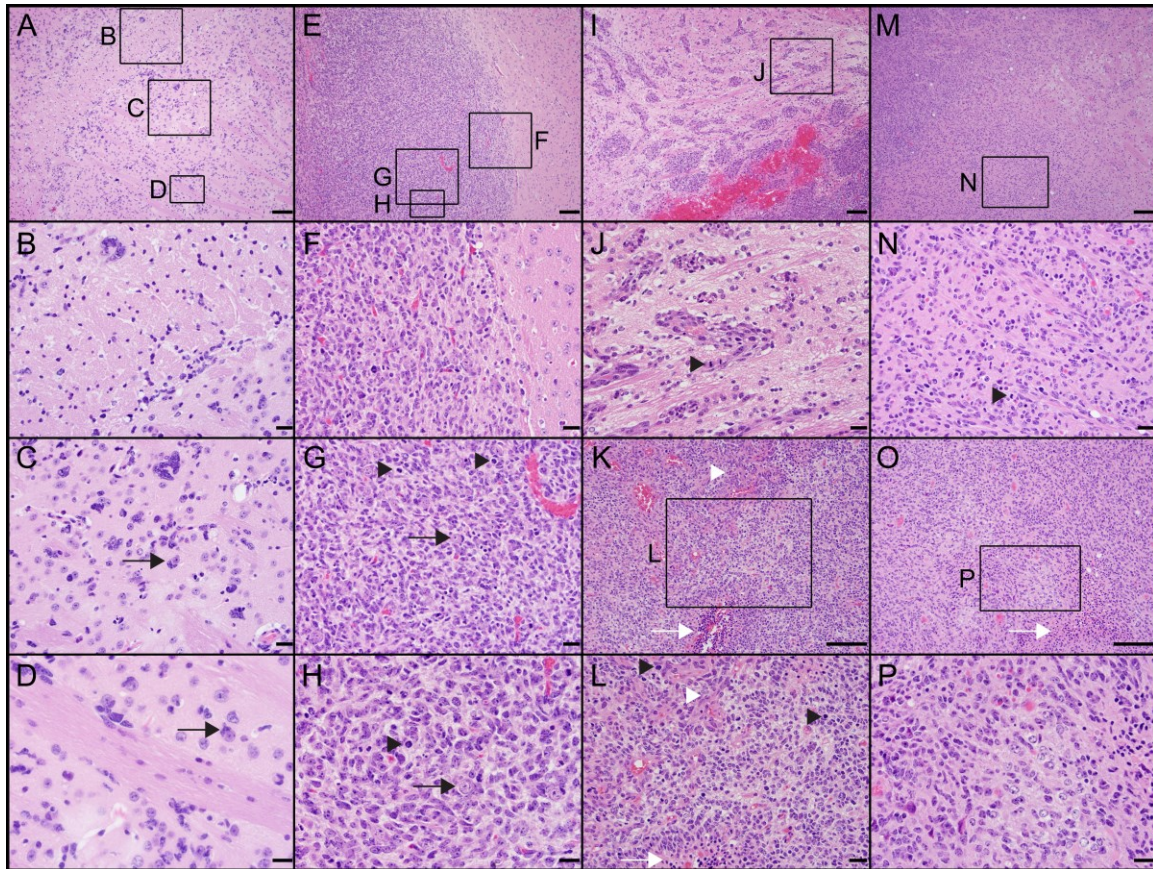


Figure S3.5. Histopathological features of astrocytomas derived from G1/S-defective astrocytes.

Representative H&E stained sections of a grade II T astrocytoma (A-D), a grade IV TR GBM (E-H), two TRP^{+/-} GBM (I-J and K-L), and a TRP^{-/-} GBM (M-P). GBM from both TRP^{+/-} (L) and TRP^{-/-} (P) cells show prominent oligodendroglial features. Black arrows - perineuronal satellites; black arrowheads - mitoses; white arrows - necrosis; white arrowheads - microvascular proliferation. Original magnification: 100X (A, E, I, M); 200X (K, O); 400X (B, C, F, G, J, L, N), 600X (D, H, P). Scale bars for panels A, E, I, and M are 100 μ m; all others are 20 μ m.

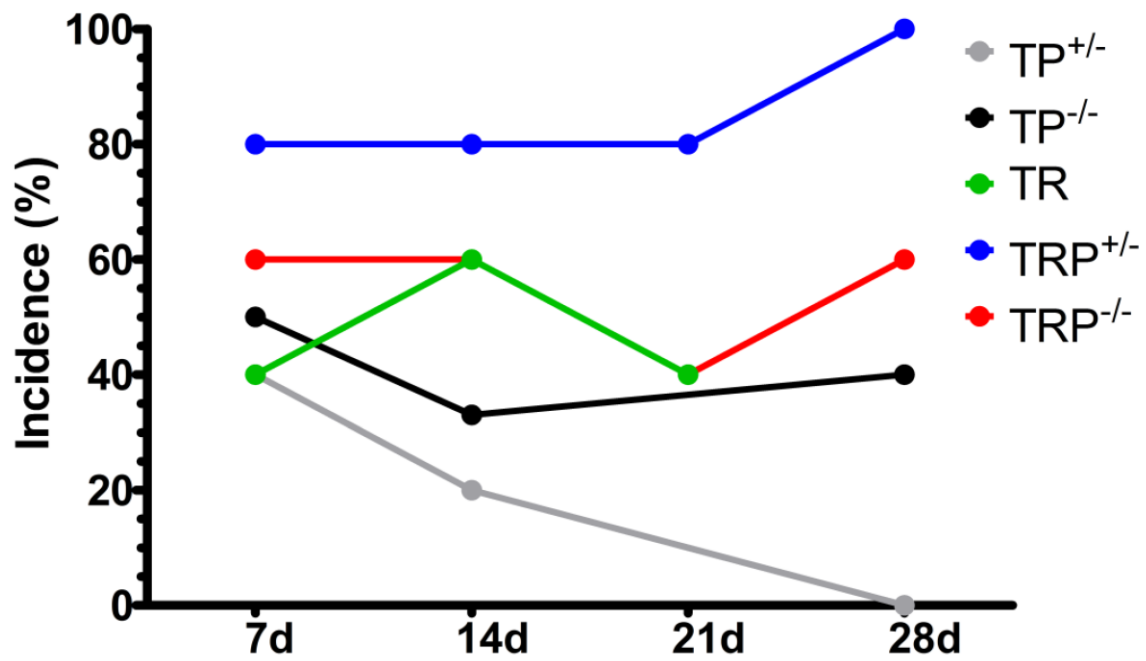


Figure S3.6. Incidence of astrocytomas over the first four weeks post-injection. Tumor incidence at days 7, 14, 21, and 28 for mice injected with astrocytes of the indicated genotypes.

Table S3.1. ssGSEA ROC and P-values for the fifteen most and least enriched MSigDB gene expression signatures in Class 1-3 G1/S defective astrocytes.

	Rank	Signature	ROC	p-value
Class 1 (T, TP)				
Most Enriched	1	WONG_IFNA2_RESISTANCE_DN	0.991	6.25E-06
	2	NICK_RESPONSE_TO_PROC_TREATMENT_UP	0.982	1.25E-05
	3	BIOCARTA_NKT_PATHWAY	0.982	1.25E-05
	4	CHESLER_BRAIN_QTL_TRANS	0.964	3.75E-05
	5	TOMLINS_PROSTATE_CANCER_DN	0.955	5.94E-05
	6	BROWNE_HCMV_INFECTION_16HR_DN	0.955	5.94E-05
	7	ROPERO_HDAC2_TARGETS	0.946	9.38E-05
	8	MARSON_FOXP3_TARGETS_STIMULATED_DN	0.946	9.38E-05
	9	SMID_BREAST_CANCER_NORMAL_LIKE_DN	0.946	9.38E-05
	10	KORKOLA_YOLK_SAC_TUMOR_DN	0.938	0.000141
	11	COLIN_PILOCYTIC_ASTROCYTOMA_VS_GLIOBLASTOMA_DN	0.938	0.000141
	12	GENTILE_UV_RESPONSE_CLUSTER_D2	0.938	0.000141
	13	KORKOLA_CHORIOCARCINOMA_DN	0.929	0.00021
	14	WILLIAMS_ESR2_TARGETS_UP	0.929	0.00021
	15	CLAUS_PGR_POSITIVE_MENINGIOMA_UP	0.929	0.00021
Least Enriched	15	CHEN_LVAD_SUPPORT_OF_FAILING_HEART_DN	0.0536	1
	14	BIOCARTA_SARS_PATHWAY	0.0536	1
	13	KANNAN_TP53_TARGETS_DN	0.0446	1
	12	ZHAN_MULTIPLE_MYELOMA_HP_UP	0.0446	1
	11	BIOCARTA_CARM1_PATHWAY	0.0446	1
	10	KORKOLA_TERATOMA_UP	0.0357	1
	9	NIKOLSKY_BREAST_CANCER_12Q13_Q21_AMPLICON	0.0268	1
	8	GUTIERREZ_MULTIPLE_MYELOMA_DN	0.0268	1
	7	KEGG_GLYCOPHOSPHOLIPID_BIOSYNTHESIS_GANGLIO_SERIES	0.0268	1
	6	KORKOLA_YOLK_SAC_TUMOR_UP	0.0179	1
	5	LU_TUMOR_ENDOTHELIAL_MARKERS_UP	0.0179	1
	4	REACTOME_G1_PHASE	0.0179	1
	3	LU_TUMOR_VASCULATURE_UP	0.00893	1
	2	ZHAN_MULTIPLE_MYELOMA_MF_DN	0.00893	1
	1	VICENT_METASTASIS_UP	0	1
Class 2 (TR)				
Most Enriched	1	MCCABE_HOXC6_TARGETS_CANCER_DN	1	3.13E-06
	2	LEE_NAME_T_LYMPHOCYTE	0.991	6.25E-06
	3	SILIGAN_BOUND_BY_EWS_FLT1_FUSION	0.973	2.19E-05
	4	SHIPP_DLBCL_VS_FOLLICULAR_LYMPHOMA_DN	0.964	3.75E-05
	5	APPEL_IMATINIB_RESPONSE	0.964	3.75E-05
	6	SIG_PIP3_SIGNALING_IN_B_LYMPHOCYTES	0.964	3.75E-05
	7	KEGG_ADHERENS_JUNCTION	0.955	5.94E-05
	8	NOJIMA_SFRP2_TARGETS_DN	0.946	9.38E-05
	9	TONKS_TARGETS_OF_RUNX1_RUNX1T1_FUSION_HSC_UP	0.946	9.38E-05
	10	TOMLINS_PROSTATE_CANCER_UP	0.946	9.38E-05
	11	BOYLAN_MULTIPLE_MYELOMA_C_D_DN	0.946	9.38E-05
	12	ZHOU_INFLAMMATORY_RESPONSE_LPS_UP	0.938	0.000141
	13	KANG_GIST_WITH_PDGFRA_UP	0.938	0.000141
	14	TSAI_DNAJB4_TARGETS_UP	0.938	0.000141
	15	SATO_SILENCED_BY_METHYLATION_IN_PANCREATIC_CANCER	0.938	0.000141
Least Enriched	15	LOPEZ_MESOTELIOMA_SURVIVAL_TIME_UP	0.116	0.999
	14	RODRIGUES_THYROID_CARCINOMA_UP	0.116	0.999
	13	CLAUS_PGR_POSITIVE_MENINGIOMA_UP	0.116	0.999
	12	PETRETTO_BLOOD_PRESSURE_UP	0.107	0.999
	11	VALK_AML_WITH_FLT3_ITD	0.107	0.999
	10	YANAGISAWA_LUNG_CANCER_RECURRENCE	0.107	0.999
	9	KEGG_BIOSYNTHESIS_OF_UNSATURATED_FATTY_ACIDS	0.107	0.999
	8	BIOCARTA_ERYTH_PATHWAY	0.107	0.999
	7	JAERVINEN_AMPLIFIED_IN_LARYNGEAL_CANCER	0.0982	1
	6	KEGG_ALZHEIMERS_DISEASE	0.0893	1
	5	BARIS_THYROID_CANCER_UP	0.0804	1
	4	LI_CYTIDINE_ANALOGS_CYCOTOXICITY	0.0804	1
	3	SPIRA_SMOKERS_LUNG_CANCER_DN	0.0804	1
	2	REACTOME_GLUCOSE_METABOLISM	0.0714	1
	1	LASTOWSKA_NEUROBLASTOMA_COPY_NUMBER_UP	0.0625	1
Class 3 (TRP)				
Signatures Most Enriched	1	BYSTRYKH_HEMATOPOIESIS_STEM_CELL_AND_BRAIN_QTL_CIS	1	5.86E-06
	2	FERRARI_RESPONSE_TO_FENRETINIDE_DN	0.99	1.17E-05
	3	ZHAN_MULTIPLE_MYELOMA_CD1_VS_CD2_DN	0.962	7.04E-05
	4	REACTOME_G_BETA_GAMMA_SIGNALING_THROUGH_PLG_BETA	0.962	7.04E-05
	5	KORKOLA_CHORIOCARCINOMA_UP	0.952	0.000111
	6	MOOTHA_PGC	0.952	0.000111
	7	KEGG_GLYCOLYSIS_GLUONEOGENESIS	0.952	0.000111
	8	REACTOME_MITOCHONDRIAL_FATTY_ACID_BETA_OXIDATION	0.952	0.000111
	9	GAUSSMANN_MLL_AF4_FUSION_TARGETS_B_UP	0.943	0.000176
	10	HO_LIVER_CANCER_VASCULAR_INVASION	0.943	0.000176
	11	KEGG_RENIN_ANGIOTENSIN_SYSTEM	0.943	0.000176
	12	REACTOME_ACTIVATION_OF_KAINATE_RECEPTORS_UPON_GLUTAMATE_BINDING	0.943	0.000176
	13	LIU_PROSTATE_CANCER_UP	0.933	0.000264
	14	PRAMOONJAGO_SOX4_TARGETS_DN	0.933	0.000264
	15	OUELLET_CULTURED_OVARIAN_CANCER_INVASIVE_VS_LMP_UP	0.933	0.000264
Signatures Least Enriched	15	SABATES_COLORECTAL_ADENOMA_SIZE_UP	0.0571	1
	14	SHI_SPARC_TARGETS_DN	0.0571	1
	13	YAO_TEMPORAL_RESPONSE_TO_PROGESTERONE_CLUSTER_3	0.0571	1
	12	BIOCARTA_NFKB_PATHWAY	0.0571	1
	11	ELVIDGE_HIF1A_TARGETS_DN	0.0476	1
	10	AMIT_DELAYED_EARLY_GENES	0.0476	1
	9	NIELSEN_SYNOVIAL_SARCOMA_UP	0.0476	1
	8	KEGG_CYTOKINE_CYTOKINE_RECEPTOR_INTERACTION	0.0476	1
	7	BIOCARTA_LONGEVITY_PATHWAY	0.0476	1
	6	REACTOME_P130CAS_LINKAGE_TO_MAPK_SIGNALING_FOR_INTEGRINS	0.0476	1
	5	KUROKAWA_LIVER_CANCER_CHEMOTHERAPY_DN	0.0381	1
	4	LOPEZ_MESOTHELIOMA_SURVIVAL_UP	0.0381	1
	3	MOREAUX_MULTIPLE_MYELOMA_BY_TACI_UP	0.0286	1
	2	HSC_MATURE_FETAL	0.0286	1
	1	BIOCARTA_INFLAM_PATHWAY	0.019	1

Table S3.2. GSA scores and statistical significance of murine neural ontology and human HGA signatures for Class 1-3 G1/S defective astrocytes

Author	Signature	Class 1		Class 2		Class 3	
		Score	p-value	Score	p-value	Score	p-value
Cahoy	Astrocyte	-0.1108	0.22	-0.2929	0.044	0.2442	0.061
	Oligodendrocyte	0.0227	0.342	-0.0165	0.44	-0.0403	0.251
	Neuron	-0.0354	0.371	0.0251	0.395	0.0411	0.367
	OPC	-0.2484	0.031	-0.059	0.353	0.3101	0.005
	Cultured Astrocytes	0.2028	0.132	0.0694	0.372	-0.3756	0.006
TCGA	Proneural	-0.1505	0.144	-0.0221	0.439	0.1476	0.155
	Neural	-0.108	0.308	-0.0406	0.411	0.2824	0.127
	Classical	-0.1566	0.079	-0.0734	0.265	0.0747	0.242
	Mesenchymal	0.2485	0.175	0.0833	0.389	-0.3857	0.092
Phillips	Proneural	-0.1045	0.235	0.0179	0.427	0.0306	0.42
	Proliferative	0.0403	0.439	-0.0528	0.391	0.0355	0.458
	Mesenchymal	0.2877	0.172	0.0357	0.435	-0.4749	0.043

Signatures with statistically significant enrichment are highlighted for each class.

Highly expressed signatures have positive GSA scores, while lowly expressed signatures have negative GSA scores.

Table S3.3 PI3K signature genes (N=518) defined by release of TRP^{-/-} G1/S defective astrocytes from PI-103 inhibition.

Aacs
Abcb6
Abcf2
Abtb2
Acat2
Actn2
Actr3B
Adamts3
Adcy9
Aebp1
Aen
Agpat6
Akap8
Akirin1
Aldh1L2
Amd1
Ankrd23
Ankrd9
Ap3D1
Aph1A
Apod
Aqp3
Arc
Arl15
Armc6
Armc7
Arntl
Asf1B
Asns
Atad3A
Atf3
Atf4
Atf5
Atg5
Aven
B3Galnt2
Baz1A
Bcat1
Bckdhb
Bdh1

Brd9
Bsn
Btaf1
Btbd10
Btbd11
Bysl
Bzw2
C11Orf94
C12Orf11
C12Orf34
C12Orf41
C12Orf52
C14Orf169
C16Orf59
C18Orf25
C19Orf52
C1Orf189
C1Orf51
C1Orf88
C21Orf59
C2Cd2L
C3Orf23
C3Orf38
C4A
C4Orf32
C4Orf44
C5Orf36
C8Orf30B
C9Orf24
C9Orf80
Cachd1
Cacna2D3
Cacng5
Calca
Cars2
Cbx4
Ccdc134
Ccdc136
Ccdc25
Ccdc64B
Ccdc76
Ccl25
Ccnd1
Ccne1
Cdk2

Cdk2Ap1
Cdk8
Cdr2L
Cep78
Chst3
Ciapin1
Ciita
Clock
Cmtm5
Cntn2
Cntnap2
Cog5
Col16A1
Col7A1
Coro2A
Cox11
Cox6A2
Cplx3
Cpsf6
Creld2
Cry1
Cse1L
Csrnp2
Cxcl2
Cyp1A1
Cyp4F8
Cyp51A1
Darc
Dbnidd2
Dcun1D2
Dcun1D4
Ddit3
Ddx3X
Dfnb31
Dgkb
Dhcr7
Dimt1L
Dis3
Dlgap3
Dnah5
Dnaja4
Dnajc27
Dnajc3
Dnd1
Dock10

Dolpp1
Donson
Dpf3
Dtnbp1
Dusp22
Dynll1
Dynll2
E2F2
E2F8
Eaf1
Eepd1
Efhd2
Eif2Ak2
Eif2B4
Eif2B5
Eif2S2
Elfn2
Eml5
En2
Endog
Enoph1
Enpp2
Ephb2
Eprs
Ercc8
Erlin1
Ero1L
Ets2
Exoc5
Extl1
Fabp3
Fam124B
Fam126A
Fam20C
Fam54B
Fam84A
Fam89B
Farp2
Farsa
Fasn
Fbxw4
Fem1A
Fetub
Fgf9
Fgfr3

Fgfr1
Fhad1
Fkbp4
Fndc5
Foxi2
Foxk2
Foxn2
Foxo6
Fzd9
Gab3
Gadd45G
Galnt14
Gcnt1
Gdap2
Gdf11
Gdf7
Gemin5
Gfod1
Ggnbp2
Ghrhr
Git1
Gls2
Gnl3
Golm1
Gorasp2
Gpaa1
Gpatch4
Gpd1
Gpr155
Grpel2
Grwd1
Has2
Heatr3
Hlf
Hmgcs1
Homer1
Homer2
Hs3St4
Hsd17B1
Hspa5
Hspa8
Idi1
Igsf21
Il6
Ilvbl

Inmt
Inpp5A
Inpp1
Insig1
Insrr
Iqsec3
Isg15
Itih1
Itpa
Jmjd4
Jub
Kbtbd8
Kcnj12
Kcnk5
Kctd15
Kiaa0513
Kiaa0664
Kiaa0895L
Kif21B
Kifc2
Klf16
Klhl32
Kpna1
Kpna4
Kpnb1
Kti12
Lama1
Lcn12
Lhfpl2
Lig4
Limd1
Limk1
Loc10431
Loc646817
Lonrf1
Lrp3
Lrp8
Lrrc10
Lrrc24
Lrrc27
Lrrc59
Lss
Mafb
Magea4
Map1D

Map2K1
Mars2
Mat2A
Mbd3
Mboat2
Med22
Med27
Mertk
Metap1
Mettl1
Mettl11A
Mgll
Mier2
Mlh1
Mllt11
Mmd2
Morc2
Moxd1
Mphosph6
Mrpl12
Mrpl9
Mrps18B
Mthfd2
Mthfsd
Mvd
Mvk
Myo16
Myo19
Myo7A
Nars
Ncln
Ncoa1
Necab3
Nedd4L
Nefh
Nefl
Nefm
Neu1
Nfil3
Nfyc
Nkd1
Nkiras1
Nkx6-2
Nol10
Nppc

Nsun4
Nsun5
Nudt3
Numbl
Nup210
Nup43
Nxf1
Nxn12
Or11H6
Or5E1P
Osgin2
P2Rx3
Pag1
Pcsk4
Pcyt2
Pde2A
Pde9A
Pdrg1
Pdss1
Pdxp
Pfkfb3
Pgbd5
Phgdh
Phlda1
Phlda2
Phospho2
Pik3R1
Pik3R3
Pla2G2E
Plekhg4
Plekho2
Pmm2
Pmvk
Polr3G
Ppan
Ppargc1B
Ppif
Ppm1G
Ppm1L
Ppp2R1B
Ppp2R5A
Ppp4R4
Pprc1
Ppwd1
Prmt1

Prmt3
Prmt5
Prmt7
Psat1
Psmg1
Ptges
Pusl1
Pycr1
Rabep1
Rabggta
Rabggtb
Ranbp17
Rangrf
Rapgef11
Raph1
Rasl12
Rassf2
Rbm15
Rbm4
Rbm45
Rbpms2
Rcor2
Reep6
Relt
Rgs11
Rhbdd2
Rpl9
Rps6Ka2
Rrp12
Rrp1B
Rrp9
Rrs1
Rsl1D1
Ryr2
S1Pr3
Satb2
Sbsn
Sc4Mol
Scn8A
Sdf2L1
Sec24A
Sergef
Sf1
Sfxn2
Sfxn5

Sh2B2
Shq1
Siah2
Sipa1
Slc13A3
Slc18A2
Slc1A4
Slc1A5
Slc22A16
Slc25A29
Slc25A33
Slc30A1
Slc38A5
Slc38A8
Slc3A2
Slc41A2
Slc6A8
Slc7A3
Slc7A5
Slc7A8
Slco4A1
Slfn12L
Sltm
Smcr7
Smoc1
Snap23
Snapc1
Snx8
Sox3
Spats2
Spef1
Spns2
Sprr1A
Sqle
Srm
Srr
Srxn1
Ss18L2
Ssfa2
St3Gal3
St8Sia2
Stc2
Stk17B
Stx1A
Sult2B1

Suv39H2
Taf6L
Tatdn2
Tbx15
Tek1
Tex15
Thoc1
Ticam1
Tmem120B
Tmem151A
Tmem178
Tmem179
Tmem18
Tmem181
Tmem40
Tnfrsf13C
Tnrc6C
Tomm40
Tp53Inp2
Tppp
Trak2
Trappc10
Trib3
Trim29
Trim36
Trim69
Trim9
Tsc22D1
Tsr1
Tsr2
Ttc7A
Ttll11
Ttll7
Ttyh3
Tubg2
Ube2V2
Ube3C
Uchl3
Ufsp1
Uros
Usp10
Usp16
Usp38
Usp39
Vegfa

Vhl
Vps37B
Vwa5B1
Wars
Wdr18
Wdr4
Wdr43
Wfikkn1
Wisp1
Wnk4
Wnt4
Xdh
Yars
Yrdc
Zap70
Zbed4
Zcchc2
Zcchc9
Zfpm1
Zfr2
Zfyve28
Zic5
Zmynd17
Zmynd19
Znf131
Znf512B
Zswim1
Zswim5

CHAPTER IV

Radiation, but not temozolomide, is effective in an orthotopic allograft of proneural glioblastoma

INTRODUCTION

Diffuse gliomas are some of the most devastating and difficult-to-treat of all human cancers.

Glioblastoma (GBM), the most common malignant glioma, has a median survival of 12-15 months, a statistic that has changed little over the last four decades due to relatively few advances in treatment (214). Standard therapy for newly-diagnosed GBM patients currently consists of surgical resection followed by fractionated radiotherapy with concomitant and adjuvant temozolomide (TMZ) chemotherapy. This regimen results in a modest, three-month survival benefit compared to radiation alone, but invariably fails to prevent tumor recurrence (28).

Development of more effective treatments for GBM has been hindered by the intrinsic resistance of glioma stem cells to radiation and cytotoxic chemotherapy (39). In addition, glioma cells isolated from mice or patients are often heterogeneous themselves due to additional acquired mutations.

Comprehensive molecular profiling analyses of GBM have identified four different subtypes that correlate with alterations in commonly altered signaling pathways.(17, 18, 29). In light of these findings, genetically-engineered mouse models (GEMM) of gliomas that recapitulate the genetics and biology of their human counterparts have emerged as essential tools for the investigation of the genetics and cell and molecular biology of glioma initiation and progression (40, 42-46, 139, 215). We have previously isolated and characterized G1/S-defective murine astrocytes with mutations in the commonly altered MAPK and PI3K signaling pathways (163), and showed that orthotopic injection into immunocompetent mice resulted in proneural-like high-grade astrocytoma (HGA) with high reproducibility, suggesting that

these cells can be used as an *in vitro* and *in vivo* model of proneural GBM. Even though the cells had primitive expression profiles, it was undetermined whether they function as neural stem cells or not.

Here, we evaluate the stemness of G1/S-defective astrocytes containing activated *Kras* and *Pten* deletion and demonstrate the utility of our orthotopic allograft by measuring longitudinal growth and response to standard of care treatment.

MATERIALS AND METHODS

Genetically-engineered mice

Compound TRP mice were generated by crossing heterozygous *TgGZT₁₂₁* (79), *Kras^{G12D}* conditional knock-in (147), conditional *Pten* knock-out (92) and conditional-inducible hGFAP-CreER^{T2} (99) mice. All experimental animals were >94% of C57/B6 background. Animal studies were approved by the University of North Carolina Institutional Animal Care and Use Committee (IACUC).

Primary TRP astrocytes

Primary astrocytes were cultured as previously described (79, 163). Briefly, cells were selectively harvested from the cortices of postnatal day 1-4 pups, manually dissociated by trituration in trypsin, and incubated at 37°C for 20 minutes. Cells were pelleted, resuspended, and cultured in DMEM supplemented with 10% fetal bovine serum and 1% penicillin/streptomycin (complete media). At 50% confluence, cells were infected at an MOI of 50 for 6 hours in complete media with a recombinant adenoviral vector expressing Cre-recombinase from the constitutive cytomegalovirus promoter (Ad5CMVCre, University of Iowa Gene Transfer Vector Core) (191). Following infection, cells were rinsed in PBS and cultured in complete media at 37°C in 5% CO₂.

Growth of TRP astrocytes as non-adherent spheroids (neurospheres) was performed by plating cells at clonal density (1 cell/μl) in mouse stem cell medium (SCM, Stemcell Technologies, Vancouver,

Canada) supplemented with 20 ng/ml EGF and 20 ng/ml bFGF (Life Technologies, Grand Island, NY), and counting the number of neurospheres formed as a fraction of cells plated for 7 days. These neurospheres were disassociated and reseeded for 6 consecutive passages as previously described (216). To generate luciferase expressing cells, TRP^{-/-} astrocytes were infected with retroviral particles containing MSCV-*luc* (a kind gift from Scott Lowe, Cold Spring Harbor Laboratory, Addgene #18782), followed by selection with hygromycin (300 µg/ml) and verified for stable luciferase expression with the OneGlo assay kit (Promega, Madison, WI). U87MG cells were a kind gift from G. Yancey Gillespie (University of Alabama at Birmingham) (114). U87MG cells stably expressing luciferase (U87FL) were a kind gift from C. David James (University of California, San Francisco) (217).

Orthotopic allografts

Orthotopic allografts with TRP astrocytes were carried out as previously described (163). Briefly, 10⁵ cells in 5 µL injected into right basal ganglia using coordinates 1, -2, and -4 mm (A, L, D) from the Bregma suture via a Hamilton syringe mounted in a repeating antigen dispenser (Hamilton, Reno, NV).

Anchorage-independent growth

After cells were exposed to ionizing radiation, 50,000 cells were resuspended at 10 ml in growth medium containing 5% agar (Becton-Dickinson, Franklin Lakes, NJ) and plated onto 100mm plates. Plates were supplemented with complete medium weekly and colonies consisting of more than 5 cells were counted 21 days later.

Cell growth

For cell growth studies in response to TMZ, cells were plated on 96-well plates, treated with increasing concentrations of TMZ and O⁶-benzylguanine (Sigma-Adrich, St.Louis, MO) dissolved in DMSO, or with 0.1% DMSO alone, and after 5 days assayed with the CellTiter 96 AQueous One Solution Cell Proliferation Assay (MTS assay, Promega, Madison, WI).

Cell cycle

Cells were harvested 2 days post-treatment. DNA content was analyzed using Guava Cell Cycle Reagent on an Guava Easy Cyte Plus instrument according to the manufacturer's instructions (EMD Millipore Corp, Billerica, MA). Cell cycle analysis was carried out with ModFit LT software (Verity Software House, Topsham, ME).

Bioluminescence in vivo imaging

Bioluminescence *in vivo* images were acquired from anaesthetized mice with an Ivis Kinetic System (PerkinElmer, Waltham, MA) 10-15 min after peritoneal administration of D-luciferin (PerkinElmer), and analyzed using Living Image software (PerkinElmer).

Histopathological evaluation

Animals were monitored multiple times per week and sacrificed upon neurological symptoms such as lethargy, loss of weight, deterioration in body condition, poor grooming, bulging skull, seizures, ataxia, or paralysis. Brains were harvested, cut sagittally through the needle track, immersion fixed in 10% neutral buffered formalin overnight, and stored in 70% ethanol prior to paraffin embedding. Formalin-fixed, paraffin embedded (FFPE) brains were cut on a rotary microtome in serial 4-5 μ m sections, placed on glass slides, and stained with hematoxylin and eosin (H&E) on a Leica Microsystems Autostainer XL (Buffalo Grove, IL). H&E stained slides were scanned on an Aperio ScanScope XT (Vista, CA) using a 20X objective and the resulting .svs files were imported into an Aperio Spectrum web database. Histopathological analysis, grading, and photomicrography was performed by CRM according to WHO 2007 criteria for human astrocytomas (5) using an Olympus BX41 microscope equipped with a DP70 digital camera (Center Valley, PA).

Immunofluorescence

Cell monolayers were fixed with 4% para-formaldehyde for 10min, followed by incubation with primary or secondary antibodies in 0.05% Triton X100 – PBS buffer. All primary antibodies were obtained from EMD Millipore Corp, except GFAP (Dako Inc, Carpinteria, CA) and Tuj1 (Covance, Princeton, NJ), secondary antibodies were Alexa 488, 568 or 647 dye-conjugated antibodies (Life Technologies).

Microarrays

Total RNA was isolated from astrocytes using an RNeasy Mini Kit (QIAGEN, Valencia, CA), RNA quality was confirmed with the Agilent Bioanalyzer (RNA Integrity Number > 7), labeled with the Agilent Low RNA Input Linear Amplification Kit (Agilent Technologies, Santa Clara, CA), and hybridized to Agilent Whole Mouse Genome 4×44 K microarrays (G4122-60520) per the manufacturer's protocol. Stratagene Universal Mouse Reference RNA (Agilent, #740100) was co-hybridized to each array as a reference. Microarrays were scanned on an Agilent DNA Microarray Scanner with SureScan High-Resolution Technology (G2565CA). Images were analyzed using Agilent Feature Extraction Software.

Microarray analyses

Microarray data was normalized using Lowess on the Cy3 and Cy5 channels. Analyses were performed on data present in at least 70% of experimental samples using genes with an absolute signal intensity of at least 10 units in both dye channels. Replicate probes were collapsed to genes by averaging. Further analyses were performed using R system for statistical computing (R Development Core Team, 2006, <http://www.R-project.org>). Probes were annotated with gene symbols using the Ensembl database through Biomart (196). Genes were median centered before principle components analysis. Single sample Gene Set Enrichment Analysis (ssGSEA) was performed as described previously(162). For human TCGA GBM signatures, the top 250 genes most highly expressed in each

subtype versus the remaining subtypes were used, as determined by Significance Analysis of Microarrays one-versus-rest comparisons in Verhaak (17). For comparison to human gene sets, mouse genes were converted to the human orthologs according to the MGI database (<ftp://ftp.informatics.jax.org/pub/reports/index.html#orthology>).

Statistics

Data was analyzed with Prism 5 software (GraphPad Software, Inc, La Jolla, CA) and Stata 10 (StataCorp LP, College Station, TX). All comparisons were significant at $\alpha=0.05$ unless otherwise stated.

RESULTS

G1/S-defective murine astrocytes with constitutively active Kras and Pten deletion display GBM stem cell features in vitro and in vivo

We have previously generated G1/S cell cycle checkpoint-defective murine cortical astrocytes, harboring constitutively active Kras (Kras^{G12D}) and homozygous *Pten* deletion (hereafter referred to as TRP). TRP astrocytes have activated MAPK and PI3K signaling, which potentiates proliferation, migration, and invasion *in vitro*. Upon orthotopic injection into syngeneic, immunocompetent mice, TRP astrocytes produced GBM with primitive, progenitor-like transcriptomal profiles similar to human proneural GBM.(163) Cells with neural stem cell-like properties – variably referred to in the literature as brain tumor stem cells (BTSC), GBM stem cells (GSC), or more generically as cancer stem cells (CSC) - have been identified in human GBM (52) and GSC have been proposed as a source of the intrinsic resistance of GBM to radiation (55) and possibly temozolomide (218-221). We therefore asked whether genetically-defined, TRP astrocytes function as cancer stem cells.

We first examined their capacity for unlimited self-renewal. When TRP astrocytes were grown in stem cell medium (SCM) at clonal density, neurospheres formed within 7 days (Fig. 4.1A) and were passaged at least 6 times. TRP astrocytes maintained their ability to form neurospheres at a frequency comparable to wildtype stem cells isolated from the early post-natal mouse subventricular zone (SVZ) propagated in parallel (Fig. 4.1A). When dissociated TRP neurospheres were returned to serum-containing medium without growth factors, differentiation into neural, astroglial and oligodendroglial lineages was observed (Fig. 4.1B, C). These results suggest that cultured TRP astrocytes possess functional properties of neural stem cells. They also expressed several molecular markers consistent with mouse stem cell characteristics such as Sox2, Nestin, A2B5, CD133 and Ki-67, (Fig. S4.1), which are also often found highly expressed in human glioblastomas (222-224).

If TRP astrocytes were glioblastoma stem cells *in vivo*, a single tumor stem cell should be able to proliferate and generate a heterogeneous GBM. To test this we injected serial dilutions of TRP astrocytes, as low as 100 cells, into mouse brains. All injections resulted in GBM, causing death within 70 days (Fig. 4.1D), which supports our *in vitro* data where 1-2% of TRP astrocytes gave rise to rapidly growing neurospheres. To test if these GBM could be passaged *in vivo*, we homogenized a primary allograft GBM and reinjected a single-cell suspension of 10^5 cells into syngeneic hosts. We observed secondary and tertiary GBM in all injected mice and median survivals were unchanged (Fig. 4.1E). In summary, TRP astrocytes display features of neural stem cells *in vitro*, and function as tumor initiating cells *in vivo*.

Orthotopic injections of TRP astrocytes for a translational mouse model for GBM

To investigate whether this allograft model could serve as translational research model, we injected 10^5 cells in 84 mice over 7 independent experiments and found highly reproducible survival with a median of 26 days and 95% confidence interval 23-28 days, Fig. S4.2). To verify tumor presence, we carried out a thorough histopathological analysis of H&E stained brain sections according to the WHO criteria (5) (Fig. 4.2A, C, D). Tumors were 98% penetrant (76% GBM and 22% astrocytoma grade II or III). In brain sections collected 5 days after injection, the injected cells were T121-positive and visible as a well-defined cell-dense area in the diencephalon (Fig. 4.2A, B). Most tumors were located in near injection sites, but tumor cells also infiltrated the surrounding brain parenchyma (Fig. 4.2C, D). Characteristic hallmarks of GBM histopathology were also evident, including perineuronal and perivascular satellites, mitoses, invasion along white matter tracks, and pseudopalisading necrosis (Fig. 4.2C, D). These data demonstrate a high-incidence translational glioma model that generates GBM with characteristic histopathology, rapid growth, invasiveness, short survival.

TRP cells are sensitive to temozolomide and ionizing radiation treatment in vitro

To assess the utility of the GBM allograft model for evaluation of therapeutic treatment, we first investigated the impact of radiation and chemotherapy *in vitro*. TRP cells demonstrated a 67% decrease of viability in a colony forming assay after a single dose of 2.5 Gy (Fig. 4.3A), which is similar to sensitivities observed using established human glioma cell lines (225, 226). The alkylating agent temozolomide (TMZ) had an IC₅₀ of 539 μ M after 5 days (Fig. 4.3B). However, because the maximal blood plasma concentration in humans after oral TMZ administration does not exceed 50 μ M (227), cell sensitivities *in vitro* above 100 μ M TMZ have little translational relevance. In comparison, human U87 glioma cells showed a higher sensitivity to TMZ compared to TRP cells (IC₅₀ = 24.57 μ M, Fig. 4.3B) and growth was similar at physiologically relevant TMZ concentrations of 50 μ M, similar to previously described experiments (228). TRP cells did not show cell cycle arrest at the G₂/M checkpoint at TMZ concentrations up to 100 μ M. This contrasted with U87 cells which had significant G₂/M arrest after TMZ (Fig. S4.2) (229).

Ionizing radiation but not TMZ treatment results in modest survival benefit

To assess the *in vivo* effect of radiation and TMZ treatment in orthotopic allografts, we treated TRP-injected mice on day 6 with 100 mg/kg/day TMZ for 5 consecutive days, with and without 3 concomitant doses of 5 Gy IR every other day. Survival of TMZ-treated mice (Fig. 4.4A) were not different from untreated animals (OS 22 and 21 days, respectively; $p=0.8404$), whereas animals that received radiation (XRT) showed significantly increased survival (OS = 33 days, $P = 0.0001$). However, concomitant TMZ and XRT did not increase survival compared to XRT alone (OS = 32 days, $P = 0.5351$). Longitudinal magnetic resonance imaging (MRI) showed that tumors were detectable after 10 days in XRT-treated mice compared to 7 days in untreated mice, which reflects tumor growth retardation after treatment (Fig. 4.4B). Volumetric measurements with MRI showed XRT-treated mice had a doubling time of 3.3

days versus 1.8 days for untreated mice, but histopathological analysis confirmed that all mice died with GBM.

We also created luciferase-expressing TRP astrocytes and performed bioluminescence imaging (BLI) in order to account for viable diffuse tumor cells that are undetectable with contrast enhancing MRI. The BL signal from injected tumor cells and their progeny will correlate with the entire tumor size and allow calculation of tumor growth rates. As a positive control for BLI we utilized luciferase-infected U87 human glioma (U87FL) xenografts (Fig. S4.4A) (230). Survival of untreated and XRT-treated U87FL xenografts was not significantly different and they were thus used as a negative control for treatment with XRT. ($P=0.5$, Fig. S4.4B).

TRP cells were retrovirally infected with a luciferase-encoding plasmid to create TRP/*luc* cells and verified that their BL signal remained stable for at least 7 *in vitro* cell passages (data not shown). TRP/*luc* allografts treated with and without XRT showed similar survival to the parental cell line lacking luciferase, indicating that the luciferase plasmid did not affect survival (Fig. S4.4C). *In vivo* BLI of the same cohort indicated exponential growth (Fig. 4.4C). When TRP/*luc* tumors were treated with XRT the BLI signal remained stable for about a week before increasing again, a doubling time of 3.5 days compared to untreated the 1.9 days doubling of TRP/*luc* tumors, which is similar to the data obtained by MRI. Histopathological analysis confirmed that all mice died with GBM.

Radiation treatment leads to a switch from the proneural to the mesenchymal GBM subtype

Having demonstrated that TRP GBM allografts are similar to human GBM in growth characteristics, histopathology, and response radio-chemotherapy, we next analyzed their genome-wide transcriptome patterns using DNA microarrays. Because treatment with XRT showed a survival benefit, we assessed how untreated and XRT-treated tumors compared to human GBM. Principle component analysis showed XRT-related influence in the second and fourth principal components, accounting for 20% of

total variation in the data (Fig. 4.4D). Projection of human GBM subtype signatures on the untreated and XRT-treated GBM allografts using single sample gene set enrichment analysis (ssGSEA) identified significant enrichment of the proneural signature in untreated allografts ($P < 0.001$, Fig. 4.4E). However, XRT-treated GBM were not enriched for the proneural subtype but were enriched in the mesenchymal signature ($P = 0.005$), suggesting that treatment with XRT influenced a change in expression from proneural to mesenchymal.

DISCUSSION

Here we have demonstrated that injection G1/S-defective cortical astrocytes with Kras activation and *Pten* deletion generate GBM in an orthotopic allograft model system. These GBM were highly penetrant and aggressive with a reproducible median survival of 26 days. They resembled human GBM histopathologically and molecularly. TRP GBM allografts were sensitive to radiation but not temozolomide, and relapsed after cessation of radiation which was comparable to human GBM treated with standard of care therapy (28). We also showed that the TRP tumor initiating cells in this model function as neural stem cells and thus are a renewable source of glioma stem cells. This model combines the advantages of GEM and their genetically-defined mutations with a predictable and fast-growing allograft that can be used to discover and evaluate new treatment for GBM.

The allograft described in this manuscript offers several advantages over traditional GEM or xenografts. First, short reproducible latency is an advantage over inducible GEM models, where the latency before tumor detection often exceeds 3 months and median survival can be as long as 5-7 months (reviewed in (139)). Additionally, many previous therapeutic studies tested compounds and different modes of radiation treatment for GBM in xenograft models by flank injection lacks the physiological relevant biology and structure of the brain. Others offer a slight improvement by using orthotopic brain injections into *nude* or SCID mice, but these models are still limited by the use of genomically heterogeneous human cell lines (208, 231), and mice without functioning immune systems. Patient-derived orthotopic xenografts are even better but still require the use of immunosuppressed mice and the genomic alterations are predetermined by the tumor harvested. Notably, we used wildtype C57B6/J mice as orthotopic allograft hosts and inject genetically defined cortical astrocytes. Therefore, in contrast to immunocompromised, xenograft recipients, our allografts more closely resemble the tumor environment found in human patients. This model has the flexibility that other models lack, to incorporate additional gene manipulation through introduction of plasmids, viruses, or

mice with different mutations. In addition, orthotopic injections can target different brain regions in order to model location-related differences in GBM biology or response to therapy. Our previous results with the conditional, inducible GEM described in Chapter II suggest location influences distinct gene expression signatures. These factors may ultimately dictate future therapeutic options as well.

Comparative genetic analysis of The Cancer Genome Atlas (TCGA) has defined abnormally functioning signaling pathways in GBM (17, 29). TCGA identified 4 GBM subtypes based on their gene expression and signature genomic abnormalities. Expression of the GBM allograft described in this manuscript imitates human proneural GBM *in vitro* (163) and *in vivo*. However, after radiation therapy the recurrent GBM resemble mesenchymal subtype rather than proneural, suggesting a radiation-induced change in expression and subtype. A similar proneural to mesenchymal change was observed in patient-matched human GBM samples before and after radiation (18). This feature suggests TRP allografts respond similarly to human GBM at the molecular level, and that in addition to therapeutic and phenotypic readouts, they have the potential to model molecular responses to new compounds or treatment regimens.

In summary, we have developed a translational research mouse model for GBM that can serve as a platform for development of novel therapies against glioma stem cells, or to model response to proneural subtype-specific treatment.

FUNDING

Damon Runyon Cancer Research Foundation (CI-45-09 to C.R.M.)

University of North Carolina University Cancer Research Fund (C.R.M.)

Department of Defense (W81XWH-09-2-0042 to C.R.M.)

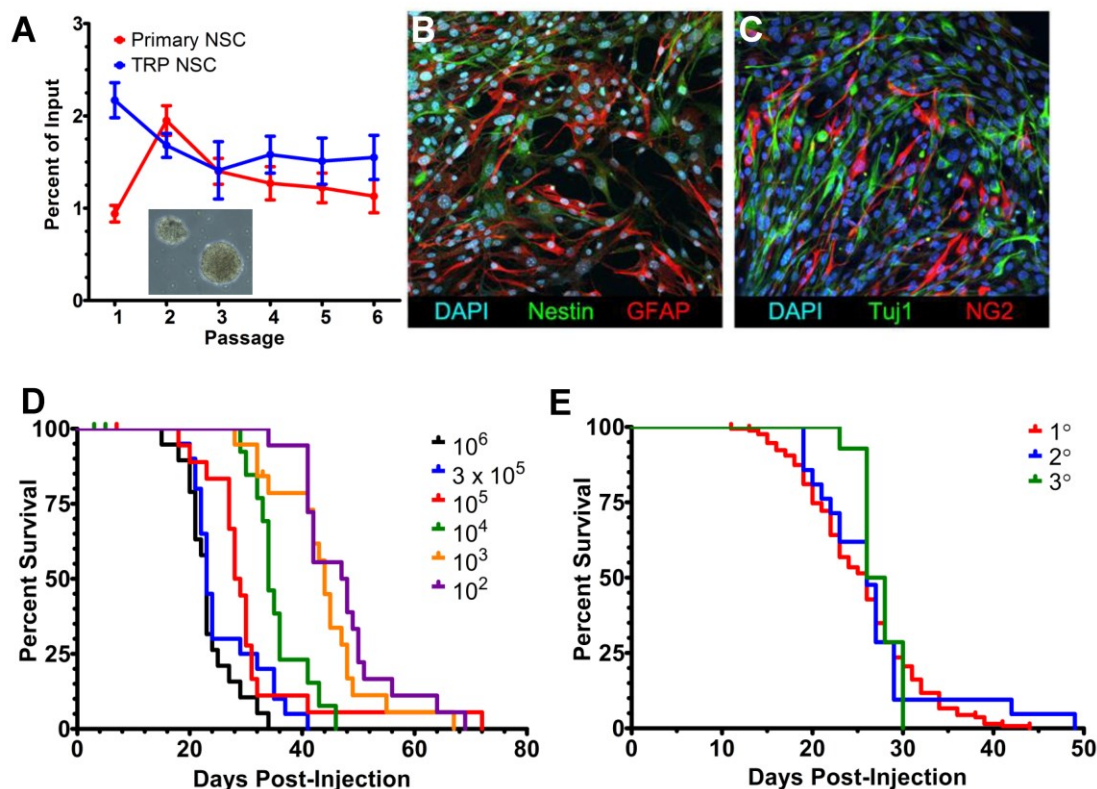


Figure 4.1: TRP cells function as glioma stem cells in vitro and in vivo Adherent TRP cells form neurospheres in stem cell medium (SCM) after 7 days. Over 6 passages, about 1-2% of cells originating from dissociated neurospheres were able to form new neurospheres. In comparison, freshly isolated neural stem cells from the SVZ of 3 day old pups yielded similar numbers in parallel (A). TRP neurospheres differentiated into all neural lineages (GFAP+, astrocytic; Tuji1+, neural; NG2+, oligodendritic; Nestin+, stem cell) within 5 days after NGF and EGF were removed and replaced with 10% FBS (B, C). Allograft tumors were passaged by dissecting the primary tumor and disassociating it into a single cell suspension of 10^5 cells that was immediately re-injected into another cohort to form secondary tumors (D). The same procedure was repeated for tertiary allografts. Mean overall survival time ranged from 25 to 27 days for all 3 cohorts.

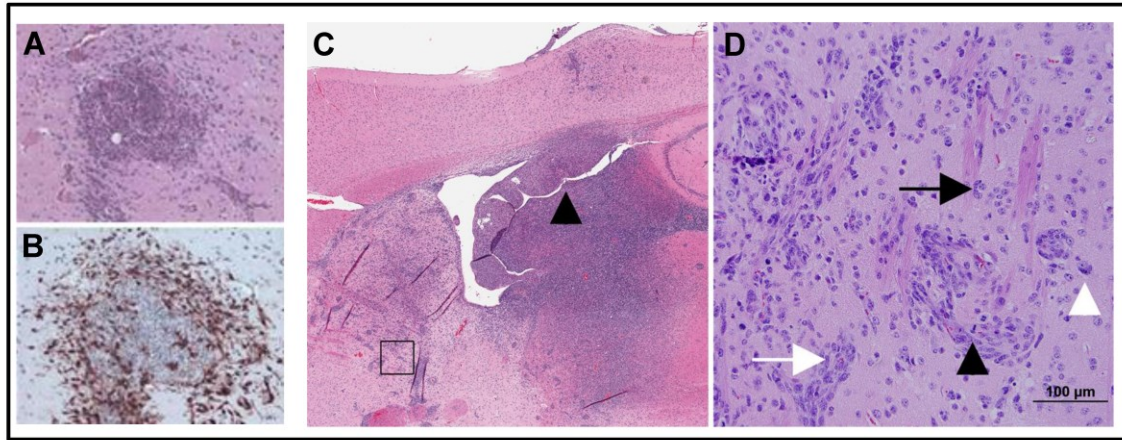


Figure 4.2. TRP allografts develop rapidly proliferating GBM Representative images of TRP allografts with GBM show T121+ cell bolus at the injection site 5 days after injection (A,B). GBM primarily present at injection site in the diencephalon within 3 weeks and are visible as large H&E-dense tumor area, surrounded by less dense areas populated with invasive cells (C, D). TRP allografts are characterized by histopathologic features of GBM, including necrosis (C, black arrowhead), perineural (D, white arrowhead) and perivascular (D, white arrow) satellitosis, mitosis (D, black arrowhead), and migration along white matter tracks (D, black arrow).

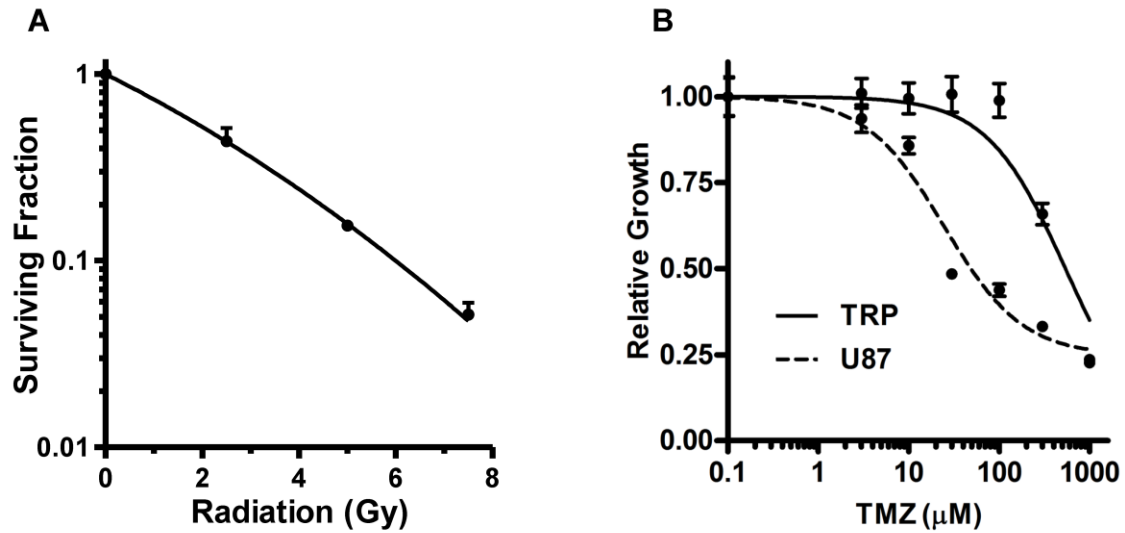


Figure 4.3. TRP cells are sensitive to ionizing radiation and TMZ *in vitro* TRP cells were treated with increasing doses of ionizing radiation, and then plated on soft agar to assess anchorage-independent growth. Quantification of colonies formed after 21 days showed an exponential decrease in surviving cells as radiation increased (A). TRP or U87MG cells were treated with increasing concentrations of temozolomide (TMZ) and assayed 5 days later with the MTS assay. While U87MG cells showed increasingly reduced growth at concentrations over 10 μ M TMZ, the growth rate for TRP cells did not decrease until at least 100 μ M TMZ (B).

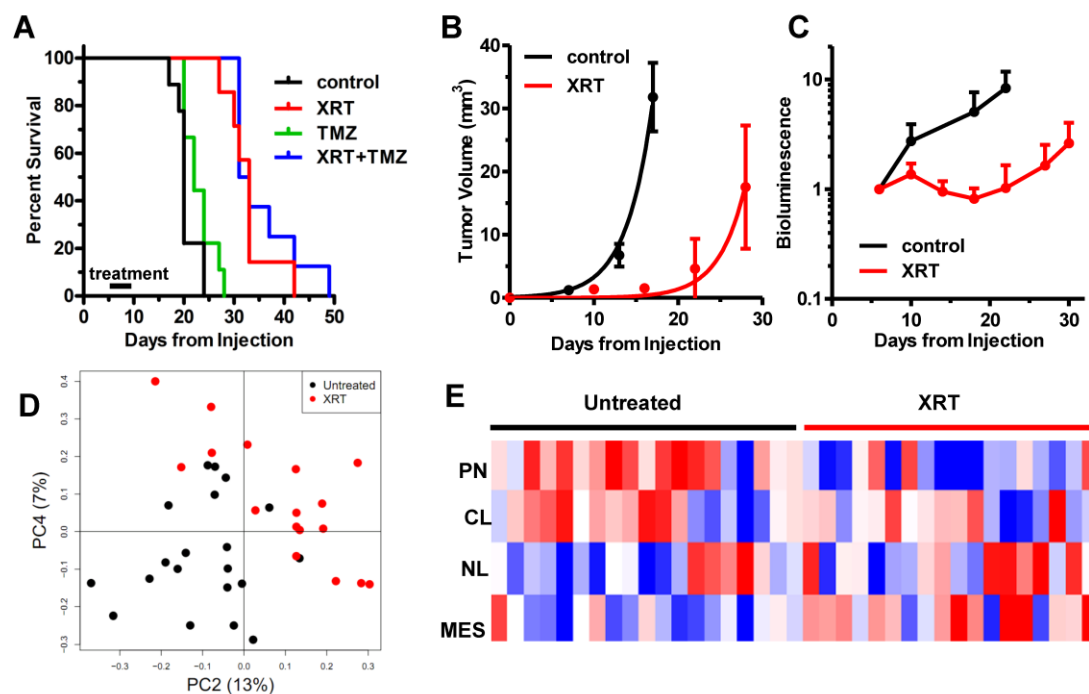


Figure 4.4. TRP allografts response to radiation but not temozolomide therapy Mice (N=40) were randomized to 4 treatment groups and subjected to 5 consecutive treatments with 100mg/kg TMZ on day 6-10 after injection (TMZ, green), or 3 doses of 5 Gy ionizing radiation each on days 6, 8 and 10 (XRT, red), concurrent TMZ+XRT (blue), or control treatment. Survival analysis showed median survival was 20, 22, 33, and 32 days for the controls, TMZ, XRT, and TMZ+XRT groups, respectively, indicating that treatment with XRT ($P < 0.0001$) but not TMZ ($P < 0.5$) showed survival benefit (A). Longitudinal MRI showed control-treated tumors grew exponentially in contrast to significantly retarded growth in XRT-treated mice, though those tumors eventually resumed exponential growth (B). TRP*luc* astrocytes that express luciferase allowed longitudinal bioluminescence imaging (BLI) of 20 mice randomized and treated similarly with control or XRT-treatment to confirm the growth measurements determined by MRI (C). Principle components analysis of untreated and XRT-treated tumors' genome-wide gene expression indicated an influence of XRT in PC2 and PC4, which together accounted for 20% of total expression variation (D). Projection of TCGA subtype signatures on untreated and XRT-treated allografts indicated untreated GBM allografts were enriched for the proneural (PN) signature, but XRT-treated GBM allografts were enriched for mesenchymal (MES) signature (E). CL = classical, NL = neural.

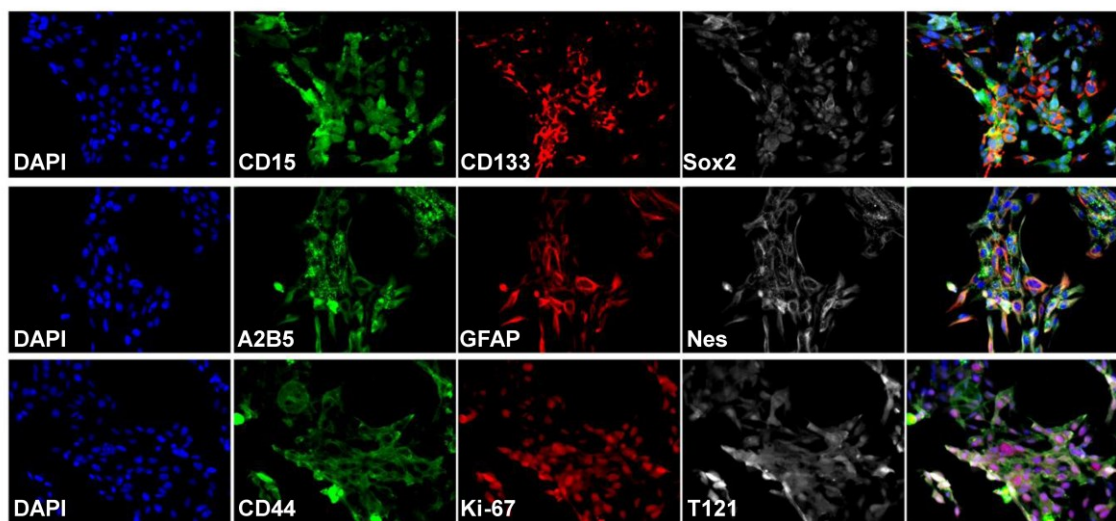


Figure S4.1. TRP astrocytes express stem cell markers. Monolayers of TRP astrocytes were fixed and stained with a panel of molecular markers. Strong expression of neural stem cell markers (e.g. Sox2, Nes, A2B5, CD133) was observed. Cells were CD44-positive and showed weak expression of CD15. All cells expressed GFAP, Ki-67 and T121 (serving as a marker for recombined astrocytes).

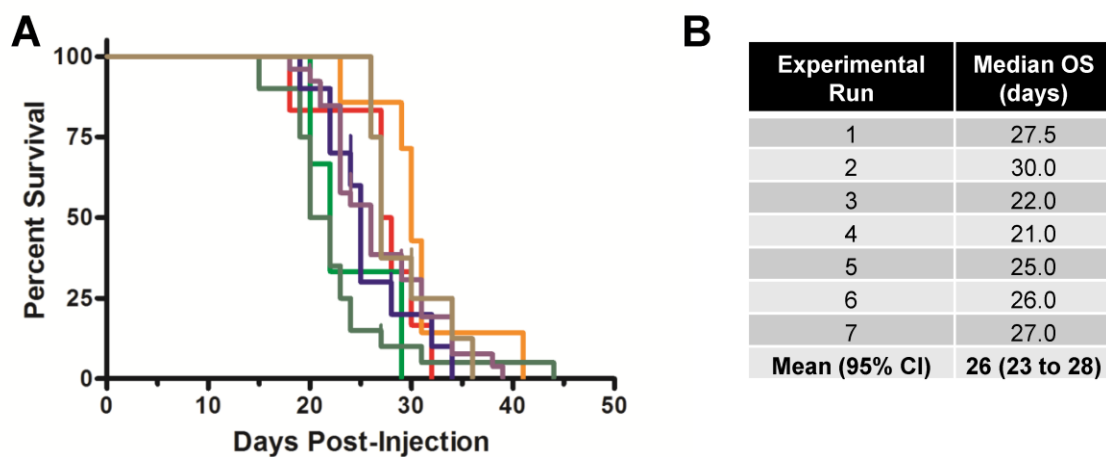


Figure S4.2. Orthotopic allograft injections have reproducible survival. Survival statistics from 7 independent experiments with TRP astrocyte injections (10^5 cells, N=84) (A). Astrocytoma formed with 98% penetrance. Histopathological analysis of H&E stained brain sections using WHO criteria determined 76% of the cohort developed GBM and 22% grade II or III astrocytoma. Median survivals by experiment (B). The overall median survival was 26 days (95% confidence interval: 23-28 days).

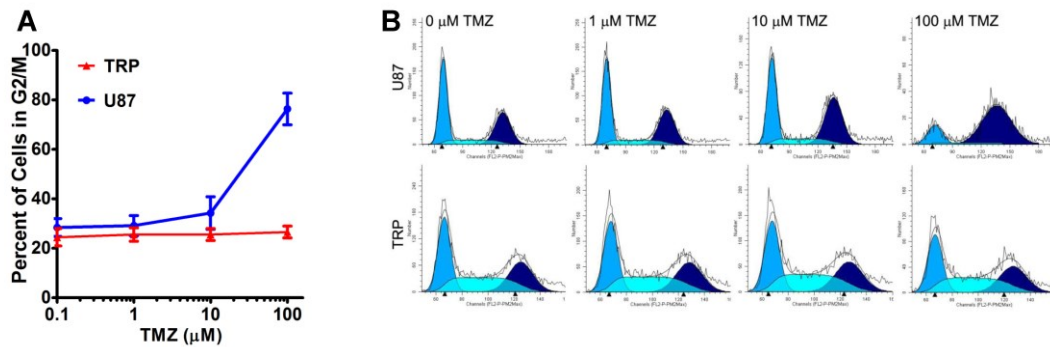


Figure S4.3. TRP astrocytes are insensitive to temozolomide. TRP or U87 cells were analyzed for cell cycle status by flow cytometry. The fraction of TRP cells in G2/M did not increase when treated with up to 100 μM TMZ for 2 days, whereas the number of U87 cells arrested in G2/M increased from 28-34% (0.1-10 μM) to 76% at 100 μM (A). The graph represents the mean percentages and SEM from 3 independent experiments. Representative data for cell cycle distribution in one individual experiment is shown in (B).

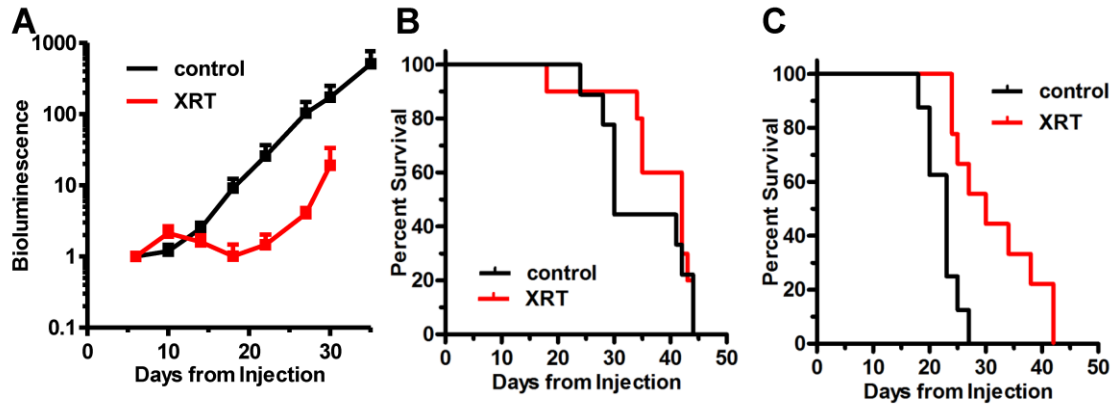


Figure S4.4. Bioluminescent Imaging in U87 and TRP cells. 5×10^5 U87FL cells were injected orthotopically into *nude* mice to monitor tumor growth using bioluminescent imaging (BLI) (A). XRT treatment occurred as described earlier with 5 Gy on day 6, 8, and 10. Median overall survival was 30 days for untreated and 42 for XRT treated mice (B). Survival of mice (N=20) injected with 10^5 TRP/*luc* cells to allow longitudinal bioluminescence imaging (BLI) of the developing tumor. The median overall survival was 23 days and 30 days for the untreated and XRT-treated groups, respectively. This is similar to TRP cells without luciferase, indicating that luciferase expression does not affect survival.

CHAPTER V

Discussion

Summary

The previous chapters detail significant findings that should inform future glioma modeling. Collectively, they help define the requirements for astrocytoma initiation and progression, show the effects of these requirements on genome-wide expression, and suggest methods to evaluate standard and novel therapies in physiologically and molecularly relevant experimental systems. In Chapter II, I described a conditional, inducible, adult GEM astrocytoma model that targeted GFAP-positive cells with disruption of the G1/S-checkpoint and RTK effector pathways using a fragment of SV40 large T antigen and targeted mutations to Kras and/or Pten. Genetic fate mapping showed Kras and Pten mutations potentiated tumor initiation in G1/S-defective astrocytes throughout the brain, including in the cortex, diencephalon, brain stem, and olfactory bulb, to produce LGA. These LGA showed oncogenic driver- and astrocyte location-specific transcriptome profiles, suggesting that both driver mutations and cellular origin contribute to LGA genomic heterogeneity. Progression to high-grade astrocytomas (HGA) was typified by acquisition of CNA and transcriptome analysis of HGA revealed three subtypes that did not correlate with oncogenic driver mutations. These three subtypes resembled human mesenchymal, proneural, and neural GBM and were evident in a test set of GEM HGA with different oncogenic drivers and cellular origins. They expressed distinct neural lineage signatures and were correlated with astrocyte location. These results suggest that oncogenic drivers influence LGA subtype and that regional astrocyte identity and progression-acquired CNA contribute to HGA transcriptomal heterogeneity.

In Chapter III, we used isolated astrocytes from pups used in the above study, and induced recombination in culture to create genetically-defined, G1/S checkpoint-defective cortical murine astrocytes with constitutively active Kras and/or *Pten* deletion. We systematically investigated the individual and combined effects of Kras activation and Pten loss on growth, migration, invasion, and gene expression and evaluated *in vivo* tumorigenesis using a syngeneic orthotopic allograft model system. Activation of both RTK effector arms produced progenitor-like transcriptomal profiles that mimic human proneural GBM. Additionally, allografts injected with these astrocytes resulted in *in vivo* tumorigenesis and produced highly invasive, proneural-like GBM. These results suggest that cortical astrocytes can be transformed into GBM and that combined dysregulation of MAPK and PI3K signaling reverts G1/S-defective astrocytes to a primitive gene expression state. This genetically-defined, immunocompetent model of proneural GBM will be useful for preclinical development of MAPK/PI3K targeted, subtype-specific therapies.

We extended these allograft experiments to evaluate the preclinical utility of TRP allografts by using standard-of-care fractionated radiation and concurrent temozolomide (28). Radiation therapy significantly improved survival but concurrent temozolomide did not provide any additional benefit, nor did temozolomide alone. Expression analysis suggested that radiation-therapy caused proneural allografts to switch to the mesenchymal subtype. This work further validates the allograft as model of proneural GBM which can be used for development of subtype-specific therapies. Furthermore, evidence of subtype switching suggests that, as targeted and subtype-specific therapies become more available, future therapy designs should be customizable and adaptable to account for the dynamic expression of GBM.

The design of models that mimic glioma subtypes

To date, three other studies have examined the transcriptomes of murine, adult HGA (100, 142, 144), and only one of these employed conditional, inducible GEM and also analyzed genomic copy number(100). We were able to make several important interpretations from the work described in Chapter II by using these other GEM HGA in the first documented example of using a validation, or test, set to confirm our discovered subtypes. Since TCGA documented that certain genetic events, in the form of mutations or copy number changes, associated with subtype (17), it is often thought that GEM with mutations in those genes are adequate subtype-specific models. However, this cannot be assumed in the absence of empirical evidence of gene expression that verifies transcriptomal subtype. We showed in our discovery set that the three murine HGA subtypes S1-S3 did not correlate with their initiating oncogenic mutations, suggesting that *Pten* status does not specify subtype and similarly, Chow, Baker, and colleagues also showed that *Rb1* status did not correlate with three murine HGA subtypes (100). Importantly, when *Trp53* was paired with *Nf1* deletion—often thought of as a mesenchymal event—in neural stem cells the transcriptomal subtype of the resulting GBM was proneural (143). This evidence illustrates the point that genotype alone may not be adequate to govern subtype in glioma GEM. Therefore, in order to appropriately contextualize results, experimental transcriptome validation is required to label a GEM model as subtype-specific surrogate, regardless of its genotype. This is of particular importance because the majority of glioma GEM have not been molecularly characterized (139). Even though human glioma molecular characterization has progressed tremendously in the last decade (48), incomplete molecular knowledge of historical glioma GEM currently precludes a complete categorization and understanding of their ability to model disease subtypes.

Brain heterogeneity and its influence on expression and tumorigenesis

However, an important finding of our data in Chapter II was that murine HGA subtypes S1-S3 correlated with tumor location. These results suggest that location, microenvironment, or cell of origin influence molecular subtype. Furthermore, HGA showed location-dependent CNA profiles suggesting that spatial variables might affect susceptibility to specific genomic gains and losses. Current knowledge in these areas is far from conclusive, but continuous refinement of morphological and molecular characterization of different brain regions and cell types should help uncover the role they play in tumorigenesis and heterogeneity.

The cellular and structural composition of the brain is very complex and human gene expression is characterized by distinct co-expression networks that vary according to age, brain region, and the distributions of cell lineages (222, 232). Similarly, murine neural cell lineages have distinct gene expression profiles (108), and these have been shown to be enriched in particular GBM subtypes (17). In Chapter II, however, TR(P) GEM initiated tumorigenesis primarily in astrocytes of adult mice and were still able to molecularly mimic 3 of 4 GBM subtypes. This suggests that unaccounted for astrocyte heterogeneity and perhaps its interaction with regional brain niches influences subtype specificity. Unfortunately, little is known about astrocyte molecular heterogeneity.

Astrocytes were long thought of as a mostly uniform population of cells that supported neurons. Now, however they are recognized to play diverse and complex roles in nearly all aspects of brain biology(146). Moreover, astrocytic, neuronal, and oligodendrocytic molecular heterogeneity varies depending on their brain location (233), and astrocyte heterogeneity persists even within different regions of the cortex (234) and spinal cord (235). Variable expression of oncogenes and tumor suppressors throughout cell lineages and brain regions could indicate regional susceptibility to tumorigenesis (236). As “big data” from microarrays and sequencing becomes more prevalent, it will be critical to design future glioma models based on the discoveries of (intra)regional and (intra)cellular

expression in the brain. Our future studies will focus on identifying the cells of origin for astrocytomas within different brain regions and assess if regions influence tumor subtype.

Identifying the cellular and spatio-temporal features that influence tumorigenesis and glioma molecular heterogeneity

In order to determine if OFB HGA in TRP mice originate from GFAP-positive cells within the SVZ, future experiments will involve restricting recombination to the SVZ using local injection of lentiviral vectors that deliver GFAP-Cre. Fluorescent lineage tracing will confirm that the targeted SVZ astrocytes migrate through the RMS to the OFB, and longitudinal analysis will determine if these cells initiate tumorigenesis in the OFB and progress to HGA. Similar experiments can be done to target tumorigenesis to other brain regions. Furthermore, the lentiviral vector can be packaged so Cre is driven by promoters other than GFAP. Thus, subsequent molecular analysis of any resulting HGA will be used to inform how both regional and cellular specificity contribute to subtype and patterns of CNA. In summary, these proposed experiments will extend the work detailed in Chapter II in three important ways: 1) by locally injecting lentiviral Cre we target a small area within specific brain regions instead of the global recombination in GFAP-positive cells described previously; 2) by adjusting the promoter driving Cre we target specific cell types within these different regions; 3) fluorescent lineage tracing will allow definitive identification of tumor cells, and because the initial injection will be localized this will remove uncertainty in defining the cells of origin if the tumor has migrated and invaded other brain structures.

In addition to an experimental design that allows for greater specificity than our previous experiments, these future experiments will incorporate high-throughput tools such as RNA-seq and exome sequencing. Of these, exome sequencing has more potential to enhance our current knowledge. While RNA-seq will certainly be useful in identifying transcripts that are not printed on arrays and

providing greater resolution of known transcripts, thus far array-based expression analyses have permitted adequate comparisons between mouse and human gliomas. In contrast, exome sequencing will fill a gap that has been largely unmet in murine HGA studies. We and others (100) have examined genomic copy number using array CGH, but comprehensive large-scale sequencing is required to understand the mutation spectrum in GEM HGA models. These two technologies will be particularly useful when applied to fluorescently-labeled targeted cells from mice with and without engineered mutations in order to view acute and longitudinal expression and mutation changes. Such a design will allow analyses at a cellular and spatial resolution previously unavailable, and is the next logical extension from our broad regional analysis of LGA described in Chapter II. We expect that data generated from these experiments aimed at uncovering molecular heterogeneity across brain regions will help address how the spatio-temporal characteristics of astrocytes contribute to tumorigenic susceptibility, progression, acquisition of mutations, and expression subtype.

Genetically-defined models to serve as the basis for designing preclinical models

Experiments in Chapter III describe a genetically defined system in which to evaluate the effects of single and multiple signaling pathway mutations on the phenotypic characteristics of astrocytoma. We have already discussed the difficulties with using human cell lines to examine phenotypic effects of genetic mutations. Namely widespread mutations and alterations (208) preclude attributing individual abnormalities to specific phenotypic qualities, cultured human cells poorly recapitulate the expression of their parent tumor (115), and multiple clones and cell lineages within the tumor (185) complicate pinpointing how specific mutations transform particular cell lineages. Creation of murine cell lines from GEM using lineage-restricted promoters can often address these shortcomings.

As we included more mutation combinations in astrocytes harvested from GEM, their proliferation, migration, and invasion increased, and their transcriptomes became more primitive and stemlike.

Furthermore Kras activation and *Pten* deletion were necessary to efficiently form gliomas in orthotopic allografts. These findings support the hypothesized requirements that GBM have mutations in the three core signaling pathways (17). Therefore, creation of suitable cell lines should focus on meeting this criterion. Using this guideline to create future tumor lines with different mutation permutations will allow “apples to apples comparisons” between cell lines that have different pathway member mutations. Therefore, the determination of functional equivalence between mutations within the same signaling pathways should be able to be more accurately measured.

Also, In Chapter III we defined a PI3k signature by analyzing TRP astrocyte transcription after release from a PI3K inhibitor. This PI3K signature was found to be significantly associated with human proneural GBM. These results reinforce the implication that GBM will require patient, or at least, subtype-centered therapies. One contributing reason many oncology drugs fail clinical trials is because they are administered to all patients with the disease rather than those who have been pre-screened (237), and therefore there is low statistical power to detect a positive result in the patient population that might benefit. At the least, there is a need for larger trials and retrospective subtyping, and at best a more intelligent clinical trial design that includes prospective molecular enrollment criteria (238). Taking advantage of preclinical mouse models that reflect disease subtypes can present opportunities for more sophisticated and multifaceted analyses earlier in the drug development pipeline (117, 123), potentially reducing costs and hastening decisions to proceed with or abandon therapies.

The effect of therapy on gene expression in a preclinical model of HGA

In many ways, Chapter IV is a continuation of the previous chapter, but focuses only on TRP astrocytes. Earlier, we showed gene expression profiling that characterized TRP cells as stem like and proneural. In Chapter IV we went on to verify that in addition to primitive expression patterns, these cells have stem cell properties of multilineage differentiation, self-renewal, are tumor initiating, and

express several key stem cell proteins. Furthermore, TRP HGA allografts were profiled before and after treatment, which extended the analysis in Chapter III that was limited to only astrocyte cell lines. And in contrast to the conditional, inducible GEM HGA described in Chapter II, TRP allograft HGA were all proneural. This suggests that subtype expression is maintained when a subtype-specific cell line is used in an allograft, which can allow prescreening of animal or human cell lines before their inclusion in allografts or xenografts. Follow-up experiments will be undertaken upon the identification of other subtype-specific cell lines, which we are actively generating. Consistent and reproducible survival and subtyping of allograft HGA means they can potentially be used as preclinical models for development or evaluation of molecular therapeutics. To evaluate this we replicated standard of care treatment for GBM and showed that radiation treatment had a significant survival benefit in TRP HGA allografts. After radiation, TRP HGA were most similar to the mesenchymal rather than proneural subtype, which suggests radiation influences subtype switching. It had previously been suggested that recurrent GBM shifted towards the mesenchymal subtype if they were not classified as such previously (18). However, a different analysis of a small sample size of primary and patient-matched recurrent GBM after treatment indicated that there wasn't a switch in subtype upon recurrence (27). This question remains unanswered. However, it is possible that a proneural to mesenchymal shift occurs easier than other subtype shifts, and the starting criteria may not have been met by the samples analyzed in the Murat dataset (27). Alternatively, subtype switching could be a phenomenon that occurs when the recurrence is from a primary grade II or grade III astrocytoma (which are generally classified as proneural (17) that received treatment. In our TRP allografts, radiation treatment occurred shortly after implantation, at which time the proneural tumor would have been lower-grade. But by the time of GBM recurrence and animal death, its subtype was mesenchymal. In support of this hypothesis, two out of three human proneural HGA that switched to mesenchymal were A3 initially and GBM at recurrence (18). Currently, this explanation is little more than speculation, but it is apparent that TRP allograft HGA are more

mesenchymal after radiation. The allograft model provides a means of testing this hypothesis, and the creation and implementation of other subtype-specific cell lines and allografts, or other proneural lines created using different mutations, should provide data to further evaluate this question.

Overall, TRP allografts have most of the features desired in a preclinical model, particularly high penetrance, short latency, reproducibility, immunocompetence, microenvironment, and disease-relevant expression (123).

Preclinical HGA models of the remaining subtypes

Thus far our orthotopic TRP allograft is limited because it only reproduces the proneural GBM subtype. As previously stated we are actively investigating the creation of astrocytes with different mutations, which may yield models of the other subtypes. In lieu of that data, we are attempting to merge the experimental designs of Chapter II and IV in attempts to acquire other subtype-specific allografts. Inducible TR(P) mice described in Chapter 2 are unsuitable as a preclinical model because they are expensive and time consuming to create, and tumor latency is variable at 2-5 months. However, unlike the TRP astrocyte allograft, we have observed all 4 GBM subtypes in this model. Therefore, ongoing experiments involve passaging these induced HGA, by disassociation and direct orthotopic injection, into immunocompetent syngeneic mice as described in Chapter IV. Expression subtyping will determine if the subsequent allograft HGA maintains the original tumor's mouse and human subtype. The creation of GEM that reproduce the other HGA subtypes while maintaining desirable criteria required for preclinical use is a prerequisite to using GEM for discovery and evaluation of subtype-specific responses to therapies, as well as discovering subtype specific therapies themselves.

In the work described above, we used several complimentary approaches to model astrocytoma, define its requirements using GEM and cell lines, and measure response to therapy. Further work must be completed to account for the influence of brain cell lineage and microenvironment on subtypes and

their mutation and CNA susceptibility. Overall, use of specific mutations and molecular subtyping performed here and in other recent studies (100, 142-145) suggests that there may be multiple means to generate similar subtypes. It will be important to determine if there is an undefined commonality between these means to explain their similar ends. Alternatively, subtype susceptibility may be as complicated and heterogeneous as the brain cellular and regional hierarchies from which the subtypes presumably arise. Nonetheless, defining these specificities is a necessary step in the process of creating informative cell lines and preclinical models in which to perform biomarker discovery, drug development, and evaluate therapy.

REFERENCES

1. NCI. RFA CA-98-027 Director's Challenge: Toward a Molecular Classification of Tumors Bethesda: National Cancer Institute; 1999 [June 1, 2010]. Available from: <http://grants.nih.gov/grants/guide/rfa-files/rfa-ca-98-027.html>.
2. Weigelt B, Baehner FL, Reis-Filho JS. The contribution of gene expression profiling to breast cancer classification, prognostication and prediction: a retrospective of the last decade. *J Pathol*. 2009;220(2):263-80.
3. Dupuy A, Simon RM. Critical review of published microarray studies for cancer outcome and guidelines on statistical analysis and reporting. *J Natl Cancer Inst*. 2007;99(2):147-57.
4. Subramanian J, Simon R. What should physicians look for in evaluating prognostic gene-expression signatures? *Nat Rev Clin Oncol*. 2010;7(6):327-34.
5. Louis DN, Ohgaki H, Wiestler OD, Cavenee WK, editors. WHO classification of tumours of the central nervous system. 4th ed. Lyon: IARC; 2007.
6. Miller CR, Perry A. Glioblastoma: Morphological and molecular genetic diversity. *Archives of Pathology and Laboratory Medicine*. 2007;131(3):397-406.
7. Miller CR, Dunham CP, Scheithauer BW, Perry A. Significance of necrosis in grading of oligodendroglial neoplasms: a clinicopathologic and genetic study of newly diagnosed high-grade gliomas. *J Clin Oncol*. 2006;24(34):5419-26.
8. Rickman DS, Bobek MP, Misek DE, Kuick R, Blaivas M, Kurnit DM, et al. Distinctive molecular profiles of high-grade and low-grade gliomas based on oligonucleotide microarray analysis. *Cancer Res*. 2001;61(18):6885-91.
9. Nutt CL, Mani DR, Betensky RA, Tamayo P, Cairncross JG, Ladd C, et al. Gene expression-based classification of malignant gliomas correlates better with survival than histological classification. *Cancer Research*. 2003;63(7):1602-7.
10. Shirahata M, Iwao-Koizumi K, Saito S, Ueno N, Oda M, Hashimoto N, et al. Gene expression-based molecular diagnostic system for malignant gliomas is superior to histological diagnosis. *Clinical Cancer Research*. 2007;13(24):7341-56.
11. Tso CL, Freije WA, Day A, Chen Z, Merriman B, Perlina A, et al. Distinct transcription profiles of primary and secondary glioblastoma subgroups. *Cancer Res*. 2006;66(1):159-67.
12. Godard S, Getz G, Delorenzi M, Farmer P, Kobayashi H, Desbaillets I, et al. Classification of human astrocytic gliomas on the basis of gene expression: a correlated group of genes with angiogenic activity emerges as a strong predictor of subtypes. *Cancer Res*. 2003;63(20):6613-25.
13. Shai R, Shi T, Kremen TJ, Horvath S, Liao LM, Cloughesy TF, et al. Gene expression profiling identifies molecular subtypes of gliomas. *Oncogene*. 2003;22(31):4918-23.

14. Faury D, Nantel A, Dunn SE, Guiot MC, Haque T, Hauser P, et al. Molecular profiling identifies prognostic subgroups of pediatric glioblastoma and shows increased YB-1 expression in tumors. *J Clin Oncol*. 2007;25(10):1196-208.
15. van den Boom J, Wolter M, Kuick R, Misek DE, Youkilis AS, Wechsler DS, et al. Characterization of gene expression profiles associated with glioma progression using oligonucleotide-based microarray analysis and real-time reverse transcription-polymerase chain reaction. *Am J Pathol*. 2003;163(3):1033-43.
16. Li A, Walling J, Ahn S, Kotliarov Y, Su Q, Quezado M, et al. Unsupervised analysis of transcriptomic profiles reveals six glioma subtypes. *Cancer Res*. 2009;69(5):2091-9.
17. Verhaak RG, Hoadley KA, Purdom E, Wang V, Qi Y, Wilkerson MD, et al. Integrated genomic analysis identifies clinically relevant subtypes of glioblastoma characterized by abnormalities in PDGFRA, IDH1, EGFR, and NF1. *Cancer cell*. 2010;17(1):98-110.
18. Phillips HS, Kharbanda S, Chen R, Forrest WF, Soriano RH, Wu TD, et al. Molecular subclasses of high-grade glioma predict prognosis, delineate a pattern of disease progression, and resemble stages in neurogenesis. *Cancer cell*. 2006;9(3):157-73.
19. Madhavan S, Zenklusen JC, Kotliarov Y, Sahni H, Fine HA, Buetow K. Rembrandt: helping personalized medicine become a reality through integrative translational research. *Mol Cancer Res*. 2009;7(2):157-67.
20. Brennan C, Momota H, Hambardzumyan D, Ozawa T, Tandon A, Pedraza A, et al. Glioblastoma subclasses can be defined by activity among signal transduction pathways and associated genomic alterations. *PLoS One*. 2009;4(11):e7752.
21. Freije WA, Castro-Vargas FE, Fang Z, Horvath S, Cloughesy T, Liao LM, et al. Gene expression profiling of gliomas strongly predicts survival. *Cancer Research*. 2004;64(18):6503-10.
22. Kriegstein A, Alvarez-Buylla A. The glial nature of embryonic and adult neural stem cells. *Annu Rev Neurosci*. 2009;32:149-84.
23. Liang Y, Diehn M, Watson N, Bollen AW, Aldape KD, Nicholas MK, et al. Gene expression profiling reveals molecularly and clinically distinct subtypes of glioblastoma multiforme. *Proceedings of the National Academy of Sciences of the United States of America*. 2005;102(16):5814-9.
24. Lee Y, Scheck AC, Cloughesy TF, Lai A, Dong J, Farooqi HK, et al. Gene expression analysis of glioblastomas identifies the major molecular basis for the prognostic benefit of younger age. *BMC Med Genomics*. 2008;1:52.
25. Gravendeel LA, Kouwenhoven MC, Gevaert O, de Rooij JJ, Stubbs AP, Duijm JE, et al. Intrinsic gene expression profiles of gliomas are a better predictor of survival than histology. *Cancer Res*. 2009;69(23):9065-72.

26. Yan H, Parsons DW, Jin G, McLendon R, Rasheed BA, Yuan W, et al. IDH1 and IDH2 mutations in gliomas. *The New England journal of medicine*. 2009;360(8):765-73.
27. Murat A, Migliaiavacca E, Gorlia T, Lambiv WL, Shay T, Hamou MF, et al. Stem cell-related "self-renewal" signature and high epidermal growth factor receptor expression associated with resistance to concomitant chemoradiotherapy in glioblastoma. *Journal of clinical oncology : official journal of the American Society of Clinical Oncology*. 2008;26(18):3015-24.
28. Stupp R, Mason WP, van den Bent MJ, Weller M, Fisher B, Taphoorn MJ, et al. Radiotherapy plus concomitant and adjuvant temozolomide for glioblastoma. *N Engl J Med*. 2005;352(10):987-96.
29. TCGA. Comprehensive genomic characterization defines human glioblastoma genes and core pathways. *Nature*. 2008;455(7216):1061-8.
30. Noushmehr H, Weisenberger DJ, Diefes K, Phillips HS, Pujara K, Berman BP, et al. Identification of a CpG island methylator phenotype that defines a distinct subgroup of glioma. *Cancer cell*. 2010;17(5):510-22.
31. Colman H, Zhang L, Sulman EP, McDonald JM, Shooshtari NL, Rivera A, et al. A multigene predictor of outcome in glioblastoma. *Neuro Oncol*. 2010;12(1):49-57.
32. Wang Z, Gerstein M, Snyder M. RNA-Seq: a revolutionary tool for transcriptomics. *Nat Rev Genet*. 2009;10(1):57-63.
33. Furnari FB, Fenton T, Bachoo RM, Mukasa A, Stommel JM, Stegh A, et al. Malignant astrocytic glioma: genetics, biology, and paths to treatment. *Genes Dev*. 2007;21(21):2683-710.
34. Wen PY, Kesari S. Malignant gliomas in adults. *N Engl J Med*. 2008;359(5):492-507.
35. Louis DN, Ohgaki H, Wiestler OD, Cavenee WK, Burger PC, Jouvet A, et al. The 2007 WHO classification of tumours of the central nervous system. *Acta Neuropathol*. 2007;114(2):97-109.
36. Miller CR, Perry A. Glioblastoma. *Arch Pathol Lab Med*. 2007;131(3):397-406.
37. CBTRUS. Primary brain and central nervous system tumors diagnosed in the United States in 2004-2007 Chicago, IL: CBTRUS (Central Brain Tumor Registry of the United States); 2011.
38. Bailey P, Cushing H. A classification of the tumors of the glioma subgroup on a histogenetic basis with a correlated study of prognosis. Philadelphia 1926.
39. Stupp R, Hegi ME, Mason WP, van den Bent MJ, Taphoorn MJ, Janzer RC, et al. Effects of radiotherapy with concomitant and adjuvant temozolomide versus radiotherapy alone on survival in glioblastoma in a randomised phase III study: 5-year analysis of the EORTC-NCIC trial. *Lancet Oncol*. 2009;10(5):459-66.
40. Miller CR, Karpnich NO, Zhang Q, Bullitt E, Kozlov S, Van Dyke T. Modeling Astrocytomas in a Family of Inducible Genetically Engineered Mice: Implications for Preclinical Cancer Drug Developme. In:

Van Meir EG, editor. CNS Cancer, Cancer Drug Discovery and Development: Humana Press; 2009. p. 119-45.

41. Cheon DJ, Orsulic S. Mouse models of cancer. Annual Review of Pathology: Mechanisms of Disease. 2011;6:95-119.

42. de Vries NA, Beijnen JH, van Tellingen O. High-grade glioma mouse models and their applicability for preclinical testing. Cancer Treat Rev. 2009;35(8):714-23.

43. Frese KK, Tuveson DA. Maximizing mouse cancer models. Nat Rev Cancer. 2007;7(9):645-58.

44. Huse JT, Holland EC. Genetically engineered mouse models of brain cancer and the promise of preclinical testing. Brain Pathol. 2009;19(1):132-43.

45. Sharpless NE, Depinho RA. The mighty mouse: genetically engineered mouse models in cancer drug development. Nature Reviews Drug Discovery. 2006;5(9):741-54.

46. Van Dyke T, Jacks T. Cancer modeling in the modern era: progress and challenges. Cell. 2002;108(2):135-44.

47. Marusyk A, Polyak K. Tumor heterogeneity: causes and consequences. Biochim Biophys Acta. 2010;1805(1):105-17.

48. Vitucci M, Hayes DN, Miller CR. Gene expression profiling of gliomas: merging genomic and histopathological classification for personalised therapy. British journal of cancer. 2011;104(4):545-53.

49. Parsons DW, Jones S, Zhang X, Lin JC, Leary RJ, Angenendt P, et al. An integrated genomic analysis of human glioblastoma multiforme. Science. 2008;321(5897):1807-12.

50. Haber DA, Settleman J. Cancer: drivers and passengers. Nature. 2007;446(7132):145-6.

51. Reya T, Morrison SJ, Clarke MF, Weissman IL. Stem cells, cancer, and cancer stem cells. Nature. 2001;414(6859):105-11.

52. Singh SK, Clarke ID, Terasaki M, Bonn VE, Hawkins C, Squire J, et al. Identification of a cancer stem cell in human brain tumors. Cancer Res. 2003;63(18):5821-8.

53. Galli R, Binda E, Orfanelli U, Cipelletti B, Gritti A, De Vitis S, et al. Isolation and characterization of tumorigenic, stem-like neural precursors from human glioblastoma. Cancer Res. 2004;64(19):7011-21.

54. Singh SK, Hawkins C, Clarke ID, Squire JA, Bayani J, Hide T, et al. Identification of human brain tumour initiating cells. Nature. 2004;432(7015):396-401.

55. Bao S, Wu Q, McLendon RE, Hao Y, Shi Q, Hjelmeland AB, et al. Glioma stem cells promote radioresistance by preferential activation of the DNA damage response. Nature. 2006;444(7120):756-60.

56. Zeppernick F, Ahmadi R, Campos B, Dictus C, Helmke BM, Becker N, et al. Stem cell marker CD133 affects clinical outcome in glioma patients. *Clin Cancer Res*. 2008;14(1):123-9.
57. Stiles CD, Rowitch DH. Glioma stem cells: a midterm exam. *Neuron*. 2008;58(6):832-46.
58. Hadjipanayis CG, Van Meir EG. Brain cancer propagating cells: biology, genetics and targeted therapies. *Trends in Molecular Medicine*. 2009;15(11):519-30.
59. Sanai N, Alvarez-Buylla A, Berger MS. Neural stem cells and the origin of gliomas. *The New England journal of medicine*. 2005;353(8):811-22.
60. Ward RJ, Dirks PB. Cancer stem cells: at the headwaters of tumor development. *Annual Review of Pathology: Mechanisms of Disease*. 2007;2:175-89.
61. Visvader JE. Cells of origin in cancer. *Nature*. 2011;469(7330):314-22.
62. Siebzehnrbuhl FA, Reynolds BA, Vescovi A, Steindler DA, Deleyrolle LP. The origins of glioma: E Pluribus Unum? *Glia*. 2011;doi: 10.1002/glia.21143.
63. Gilbertson RJ. Mapping cancer origins. *Cell*. 2011;145(1):25-9.
64. Cheng L, Bao S, Rich JN. Potential therapeutic implications of cancer stem cells in glioblastoma. *Biochem Pharmacol*. 2010;80(5):654-65.
65. Quinones-Hinajosa A, Chaichana K. The human subventricular zone: a source of new cells and a potential source of brain tumors. *Exp Neurol*. 2007;205(2):313-24.
66. Alcantara Llaguno SR, Chen J, Parada LF. Signaling in malignant astrocytomas: role of neural stem cells and its therapeutic implications. *Clin Cancer Res*. 2009;15(23):7124-9.
67. Jacques TS, Swales A, Brzozowski MJ, Henriquez NV, Linehan JM, Mirzadeh Z, et al. Combinations of genetic mutations in the adult neural stem cell compartment determine brain tumour phenotypes. *Embo J*. 2010;29(1):222-35.
68. Barami K, Sloan AE, Rojiani A, Schell MJ, Staller A, Brem S. Relationship of gliomas to the ventricular walls. *Journal of Clinical Neuroscience*. 2009;16(2):195-201.
69. Visvader JE, Lindeman GJ. Cancer stem cells in solid tumours: accumulating evidence and unresolved questions. *Nat Rev Cancer*. 2008;8(10):755-68.
70. Alcantara Llaguno S, Chen J, Kwon CH, Jackson EL, Li Y, Burns DK, et al. Malignant astrocytomas originate from neural stem/progenitor cells in a somatic tumor suppressor mouse model. *Cancer Cell*. 2009;15(1):45-56.
71. Persson AI, Petritsch C, Swartling FJ, Itsara M, Sim FJ, Auvergne R, et al. Non-stem cell origin for oligodendroglioma. *Cancer Cell*. 2010;18(6):669-82.

72. Joyner AL, Zervas M. Genetic inducible fate mapping in mouse: establishing genetic lineages and defining genetic neuroanatomy in the nervous system. *Dev Dyn*. 2006;235(9):2376-85.
73. Beckervordersandforth R, Tripathi P, Ninkovic J, Bayam E, Lepier A, Stempfhuber B, et al. In vivo fate mapping and expression analysis reveals molecular hallmarks of prospectively isolated adult neural stem cells. *Cell Stem Cell*. 2010;7(6):744-58.
74. Di Cristofano A, Pesce B, Cordon-Cardo C, Pandolfi PP. Pten is essential for embryonic development and tumour suppression. *Nature genetics*. 1998;19(4):348-55.
75. Serrano M, Lee H, Chin L, Cordon-Cardo C, Beach D, DePinho RA. Role of the INK4a locus in tumor suppression and cell mortality. *Cell*. 1996;85(1):27-37.
76. Reilly KM, Loisel DA, Bronson RT, McLaughlin ME, Jacks T. Nf1;Trp53 mutant mice develop glioblastoma with evidence of strain-specific effects. *Nature genetics*. 2000;26(1):109-13.
77. Weissenberger J, Steinbach JP, Malin G, Spada S, Rulicke T, Aguzzi A. Development and malignant progression of astrocytomas in GFAP-v-src transgenic mice. *Oncogene*. 1997;14(17):2005-13.
78. Theurillat JP, Hainfellner J, Maddalena A, Weissenberger J, Aguzzi A. Early induction of angiogenetic signals in gliomas of GFAP-v-src transgenic mice. *Am J Pathol*. 1999;154(2):581-90.
79. Xiao A, Wu H, Pandolfi PP, Louis DN, Van Dyke T. Astrocyte inactivation of the pRb pathway predisposes mice to malignant astrocytoma development that is accelerated by PTEN mutation. *Cancer Cell*. 2002;1(2):157-68.
80. Ding H, Roncari L, Shannon P, Wu X, Lau N, Karaskova J, et al. Astrocyte-specific expression of activated p21-ras results in malignant astrocytoma formation in a transgenic mouse model of human gliomas. *Cancer Res*. 2001;61(9):3826-36.
81. Shannon P, Sabha N, Lau N, Kamnasaran D, Gutmann DH, Guha A. Pathological and molecular progression of astrocytomas in a GFAP:12 V-Ha-Ras mouse astrocytoma model. *Am J Pathol*. 2005;167(3):859-67.
82. Wei Q, Clarke L, Scheidenhelm DK, Qian B, Tong A, Sabha N, et al. High-grade glioma formation results from postnatal pten loss or mutant epidermal growth factor receptor expression in a transgenic mouse glioma model. *Cancer Res*. 2006;66(15):7429-37.
83. Orsulic S. An RCAS-TVA-based approach to designer mouse models. *Mamm Genome*. 2002;13(10):543-7.
84. Uhrbom L, Hesselager G, Nister M, Westermarck B. Induction of brain tumors in mice using a recombinant platelet-derived growth factor B-chain retrovirus. *Cancer Res*. 1998;58(23):5275-9.
85. Holland EC, Varmus HE. Basic fibroblast growth factor induces cell migration and proliferation after glia-specific gene transfer in mice. *Proc Natl Acad Sci U S A*. 1998;95(3):1218-23.

86. Dai C, Celestino JC, Okada Y, Louis DN, Fuller GN, Holland EC. PDGF autocrine stimulation dedifferentiates cultured astrocytes and induces oligodendrogliomas and oligoastrocytomas from neural progenitors and astrocytes in vivo. *Genes Dev.* 2001;15(15):1913-25.
87. Shih AH, Dai C, Hu X, Rosenblum MK, Koutcher JA, Holland EC. Dose-dependent effects of platelet-derived growth factor-B on glial tumorigenesis. *Cancer Res.* 2004;64(14):4783-9.
88. Holland EC, Celestino J, Dai C, Schaefer L, Sawaya RE, Fuller GN. Combined activation of Ras and Akt in neural progenitors induces glioblastoma formation in mice. *Nature genetics.* 2000;25(1):55-7.
89. Uhrbom L, Dai C, Celestino JC, Rosenblum MK, Fuller GN, Holland EC. Ink4a-Arf loss cooperates with KRas activation in astrocytes and neural progenitors to generate glioblastomas of various morphologies depending on activated Akt. *Cancer Research.* 2002;62(19):5551-8.
90. Tchougounova E, Kastemar M, Brasater D, Holland EC, Westermarck B, Uhrbom L. Loss of Arf causes tumor progression of PDGFB-induced oligodendroglioma. *Oncogene.* 2007;26(43):6289-96.
91. Jonkers J, Berns A. Conditional mouse models of sporadic cancer. *Nat Rev Cancer.* 2002;2(4):251-65.
92. Xiao A, Yin C, Yang C, Di Cristofano A, Pandolfi PP, Van Dyke T. Somatic induction of Pten loss in a preclinical astrocytoma model reveals major roles in disease progression and avenues for target discovery and validation. *Cancer Research.* 2005;65(12):5172-80.
93. Zhu Y, Harada T, Liu L, Lush ME, Guignard F, Harada C, et al. Inactivation of NF1 in CNS causes increased glial progenitor proliferation and optic glioma formation. *Development.* 2005;132(24):5577-88.
94. Zhu Y, Guignard F, Zhao D, Liu L, Burns DK, Mason RP, et al. Early inactivation of p53 tumor suppressor gene cooperating with NF1 loss induces malignant astrocytoma. *Cancer Cell.* 2005;8(2):119-30.
95. Kwon CH, Zhao D, Chen J, Alcantara S, Li Y, Burns DK, et al. Pten haploinsufficiency accelerates formation of high-grade astrocytomas. *Cancer Research.* 2008;68(9):3286-94.
96. Zhu H, Acquaviva J, Ramachandran P, Boskovitz A, Woolfenden S, Pfannl R, et al. Oncogenic EGFR signaling cooperates with loss of tumor suppressor gene functions in gliomagenesis. *Proc Natl Acad Sci U S A.* 2009;106(8):2712-6.
97. Metzger D, Chambon P. Site- and time-specific gene targeting in the mouse. *Methods.* 2001;24(1):71-80.
98. Feil R, Wagner J, Metzger D, Chambon P. Regulation of Cre recombinase activity by mutated estrogen receptor ligand-binding domains. *Biochem Biophys Res Commun.* 1997;237(3):752-7.
99. Casper KB, Jones K, McCarthy KD. Characterization of astrocyte-specific conditional knockouts. *Genesis.* 2007;45(5):292-9.

100. Chow LM, Endersby R, Zhu X, Rankin S, Qu C, Zhang J, et al. Cooperativity within and among Pten, p53, and Rb Pathways Induces High-Grade Astrocytoma in Adult Brain. *Cancer Cell*. 2011;19(3):305-16.
101. Graeber TG, Sawyers CL. Cross-species comparisons of cancer signaling. *Nature genetics*. 2005;37(1):7-8.
102. Ellwood-Yen K, Graeber TG, Wongvipat J, Iruela-Arispe ML, Zhang J, Matusik R, et al. Myc-driven murine prostate cancer shares molecular features with human prostate tumors. *Cancer Cell*. 2003;4(3):223-38.
103. Sweet-Cordero A, Mukherjee S, Subramanian A, You H, Roix JJ, Ladd-Acosta C, et al. An oncogenic KRAS2 expression signature identified by cross-species gene-expression analysis. *Nature genetics*. 2005;37(1):48-55.
104. Carretero J, Shimamura T, Rikova K, Jackson AL, Wilkerson MD, Borgman CL, et al. Integrative genomic and proteomic analyses identify targets for Lkb1-deficient metastatic lung tumors. *Cancer Cell*. 2010;17(6):547-59.
105. Lee JS, Chu IS, Mikaelyan A, Calvisi DF, Heo J, Reddy JK, et al. Application of comparative functional genomics to identify best-fit mouse models to study human cancer. *Nature genetics*. 2004;36(12):1306-11.
106. Herschkowitz JI, Simin K, Weigman VJ, Mikaelian I, Usary J, Hu Z, et al. Identification of conserved gene expression features between murine mammary carcinoma models and human breast tumors. *Genome Biology*. 2007;8(5):R76.
107. Molyneux G, Geyer FC, Magnay FA, McCarthy A, Kendrick H, Natrajan R, et al. BRCA1 basal-like breast cancers originate from luminal epithelial progenitors and not from basal stem cells. *Cell Stem Cell*. 2010;7(3):403-17.
108. Cahoy JD, Emery B, Kaushal A, Foo LC, Zamanian JL, Christopherson KS, et al. A transcriptome database for astrocytes, neurons, and oligodendrocytes: a new resource for understanding brain development and function. *The Journal of neuroscience : the official journal of the Society for Neuroscience*. 2008;28(1):264-78.
109. Zuo Y, Lubischer JL, Kang H, Tian L, Mikesch M, Marks A, et al. Fluorescent proteins expressed in mouse transgenic lines mark subsets of glia, neurons, macrophages, and dendritic cells for vital examination. *The Journal of neuroscience : the official journal of the Society for Neuroscience*. 2004;24(49):10999-1009.
110. Lein ES, Hawrylycz MJ, Ao N, Ayres M, Bensinger A, Bernard A, et al. Genome-wide atlas of gene expression in the adult mouse brain. *Nature*. 2007;445(7124):168-76.
111. Maire CL, Ligon KL. Glioma Models: New GEMMs Add "Class" with Genomic and Expression Correlations. *Cancer Cell*. 2011;19(3):295-7.

112. Johnson JI, Decker S, Zaharevitz D, Rubinstein LV, Venditti JM, Schepartz S, et al. Relationships between drug activity in NCI preclinical in vitro and in vivo models and early clinical trials. *Br J Cancer*. 2001;84(10):1424-31.
113. Voskoglou-Nomikos T, Pater JL, Seymour L. Clinical predictive value of the in vitro cell line, human xenograft, and mouse allograft preclinical cancer models. *Clin Cancer Res*. 2003;9(11):4227-39.
114. Miller CR, Williams CR, Buchsbaum DJ, Gillespie GY. Intratumoral 5-fluorouracil produced by cytosine deaminase/5-fluorocytosine gene therapy is effective for experimental human glioblastomas. *Cancer Research*. 2002;62(3):773-80.
115. Li A, Walling J, Kotliarov Y, Center A, Steed ME, Ahn SJ, et al. Genomic changes and gene expression profiles reveal that established glioma cell lines are poorly representative of primary human gliomas. *Molecular cancer research : MCR*. 2008;6(1):21-30.
116. Becher OJ, Holland EC. Genetically engineered models have advantages over xenografts for preclinical studies. *Cancer Res*. 2006;66(7):3355-8.
117. Gutmann DH, Hunter-Schaedle K, Shannon KM. Harnessing preclinical mouse models to inform human clinical cancer trials. *The Journal of clinical investigation*. 2006;116(4):847-52.
118. Burchill SA. What do, can and should we learn from models to evaluate potential anticancer agents? *Future oncology*. 2006;2(2):201-11.
119. Koutcher JA, Hu X, Xu S, Gade TP, Leeds N, Zhou XJ, et al. MRI of mouse models for gliomas shows similarities to humans and can be used to identify mice for preclinical trials. *Neoplasia*. 2002;4(6):480-5.
120. McConville P, Hambardzumyan D, Moody JB, Leopold WR, Kreger AR, Woolliscroft MJ, et al. Magnetic resonance imaging determination of tumor grade and early response to temozolomide in a genetically engineered mouse model of glioma. *Clin Cancer Res*. 2007;13(10):2897-904.
121. Uhrbom L, Nerio E, Holland EC. Dissecting tumor maintenance requirements using bioluminescence imaging of cell proliferation in a mouse glioma model. *Nat Med*. 2004;10(11):1257-60.
122. Zhu H, Woolfenden S, Bronson RT, Jaffer ZM, Barluenga S, Winssinger N, et al. The novel Hsp90 inhibitor NXD30001 induces tumor regression in a genetically engineered mouse model of glioblastoma multiforme. *Mol Cancer Ther*. 2010;9(9):2618-26.
123. Heyer J, Kwong LN, Lowe SW, Chin L. Non-germline genetically engineered mouse models for translational cancer research. *Nat Rev Cancer*. 2010;10(7):470-80.
124. Bachoo RM, Maher EA, Ligon KL, Sharpless NE, Chan SS, You MJ, et al. Epidermal growth factor receptor and Ink4a/Arf: convergent mechanisms governing terminal differentiation and transformation along the neural stem cell to astrocyte axis. *Cancer Cell*. 2002;1(3):269-77.

125. Zindy F, Uziel T, Ayrault O, Calabrese C, Valentine M, Rehg JE, et al. Genetic alterations in mouse medulloblastomas and generation of tumors de novo from primary cerebellar granule neuron precursors. *Cancer Research*. 2007;67(6):2676-84.
126. Abel TW, Clark C, Bieri B, Chytil A, Aakre M, Gorska A, et al. GFAP-Cre-mediated activation of oncogenic K-ras results in expansion of the subventricular zone and infiltrating glioma. *Mol Cancer Res*. 2009;7(5):645-53.
127. Charest A, Wilker EW, McLaughlin ME, Lane K, Gowda R, Coven S, et al. ROS fusion tyrosine kinase activates a SH2 domain-containing phosphatase-2/phosphatidylinositol 3-kinase/mammalian target of rapamycin signaling axis to form glioblastoma in mice. *Cancer Research*. 2006;66(15):7473-81.
128. Dunlap SM, Celestino J, Wang H, Jiang R, Holland EC, Fuller GN, et al. Insulin-like growth factor binding protein 2 promotes glioma development and progression. *Proc Natl Acad Sci U S A*. 2007.
129. de Vries NA, Bruggeman SW, Hulsman D, de Vries HI, Zevenhoven J, Buckle T, et al. Rapid and robust transgenic high-grade glioma mouse models for therapy intervention studies. *Clinical Cancer Research*. 2010;16(13):3431-41.
130. Ding H, Shannon P, Lau N, Wu X, Roncari L, Baldwin RL, et al. Oligodendrogliomas result from the expression of an activated mutant epidermal growth factor receptor in a RAS transgenic mouse astrocytoma model. *Cancer Res*. 2003;63(5):1106-13.
131. Lassman AB, Dai C, Fuller GN, Vickers AJ, Holland EC. Overexpression of c-MYC promotes an undifferentiated phenotype in cultured astrocytes and allows elevated Ras and Akt signaling to induce gliomas from GFAP-expressing cells in mice. *Neuron Glia Biology*. 2004;1(2):157-63.
132. Holland EC, Hively WP, DePinho RA, Varmus HE. A constitutively active epidermal growth factor receptor cooperates with disruption of G1 cell-cycle arrest pathways to induce glioma-like lesions in mice. *Genes Dev*. 1998;12(23):3675-85.
133. Holland EC, Li Y, Celestino J, Dai C, Schaefer L, Sawaya RA, et al. Astrocytes give rise to oligodendrogliomas and astrocytomas after gene transfer of polyoma virus middle T antigen in vivo. *Am J Pathol*. 2000;157(3):1031-7.
134. Hu X, Pandolfi PP, Li Y, Koutcher JA, Rosenblum M, Holland EC. mTOR promotes survival and astrocytic characteristics induced by Pten/AKT signaling in glioblastoma. *Neoplasia*. 2005;7(4):356-68.
135. Weiss WA, Burns MJ, Hackett C, Aldape K, Hill JR, Kuriyama H, et al. Genetic determinants of malignancy in a mouse model for oligodendroglioma. *Cancer Res*. 2003;63(7):1589-95.
136. Reilly KM, Tuskan RG, Christy E, Loisel DA, Ledger J, Bronson RT, et al. Susceptibility to astrocytoma in mice mutant for Nf1 and Trp53 is linked to chromosome 11 and subject to epigenetic effects. *Proc Natl Acad Sci U S A*. 2004;101(35):13008-13.

137. Uhrbom L, Kastemar M, Johansson FK, Westermarck B, Holland EC. Cell type-specific tumor suppression by Ink4a and Arf in Kras-induced mouse gliomagenesis. *Cancer Research*. 2005;65(6):2065-9.
138. Dolecek TA, Propp JM, Stroup NE, Kruchko C. CBTRUS statistical report: primary brain and central nervous system tumors diagnosed in the United States in 2005-2009. *Neuro-oncology*. 2012;14 Suppl 5:v1-49.
139. Schmid RS, Vitucci M, Miller CR. Genetically engineered mouse models of diffuse gliomas. *Brain Res Bull*. 2012;88(1):72-9.
140. Bajenaru ML, Zhu Y, Hedrick NM, Donahoe J, Parada LF, Gutmann DH. Astrocyte-specific inactivation of the neurofibromatosis 1 gene (NF1) is insufficient for astrocytoma formation. *Mol Cell Biol*. 2002;22(14):5100-13.
141. Backman SA, Stambolic V, Suzuki A, Haight J, Elia A, Pretorius J, et al. Deletion of Pten in mouse brain causes seizures, ataxia and defects in soma size resembling Lhermitte-Duclos disease. *Nat Genet*. 2001;29(4):396-403.
142. Lei L, Sonabend AM, Guarnieri P, Soderquist C, Ludwig T, Rosenfeld S, et al. Glioblastoma models reveal the connection between adult glial progenitors and the proneural phenotype. *PLoS One*. 2011;6(5):e20041.
143. Liu C, Sage JC, Miller MR, Verhaak RG, Hippenmeyer S, Vogel H, et al. Mosaic analysis with double markers reveals tumor cell of origin in glioma. *Cell*. 2011;146(2):209-21.
144. Friedmann-Morvinski D, Bushong EA, Ke E, Soda Y, Marumoto T, Singer O, et al. Dedifferentiation of neurons and astrocytes by oncogenes can induce gliomas in mice. *Science*. 2012;338(6110):1080-4.
145. Koso H, Takeda H, Yew CC, Ward JM, Nariai N, Ueno K, et al. Transposon mutagenesis identifies genes that transform neural stem cells into glioma-initiating cells. *Proceedings of the National Academy of Sciences of the United States of America*. 2012.
146. Chaboub LS, Deneen B. Developmental origins of astrocyte heterogeneity: the final frontier of CNS development. *Dev Neurosci*. 2012;34(5):379-88.
147. Jackson EL, Willis N, Mercer K, Bronson RT, Crowley D, Montoya R, et al. Analysis of lung tumor initiation and progression using conditional expression of oncogenic K-ras. *Genes Dev*. 2001;15(24):3243-8.
148. Madisen L, Zwingman TA, Sunkin SM, Oh SW, Zariwala HA, Gu H, et al. A robust and high-throughput Cre reporting and characterization system for the whole mouse brain. *Nat Neurosci*. 2010;13(1):133-40.
149. Suzuki A, Yamaguchi MT, Ohteki T, Sasaki T, Kaisho T, Kimura Y, et al. T cell-specific loss of Pten leads to defects in central and peripheral tolerance. *Immunity*. 2001;14(5):523-34.

150. Marino S, Vooijs M, van Der Gulden H, Jonkers J, Berns A. Induction of medulloblastomas in p53-null mutant mice by somatic inactivation of Rb in the external granular layer cells of the cerebellum. *Genes Dev.* 2000;14(8):994-1004.
151. Zhu Y, Romero MI, Ghosh P, Ye Z, Charnay P, Rushing EJ, et al. Ablation of NF1 function in neurons induces abnormal development of cerebral cortex and reactive gliosis in the brain. *Genes Dev.* 2001;15(7):859-76.
152. Dong HW. Allen reference atlas : a digital color brain atlas of the C57Black/6J male mouse. Hoboken, N.J.: Wiley; 2008. ix, 366 p. p.
153. Akella NS, Ding Q, Menegazzo I, Wang W, Gillespie GY, Grammer JR, et al. A novel technique to quantify glioma tumor invasion using serial microscopy sections. *J Neurosci Methods.* 2006;153(2):183-9.
154. Prat A, Parker JS, Karginova O, Fan C, Livasy C, Herschkowitz JI, et al. Phenotypic and molecular characterization of the claudin-low intrinsic subtype of breast cancer. *Breast Cancer Res.* 2010;12(5):R68.
155. Lein E, Hawrylycz M, Ao N, Ayres M, Bensinger A, Bernard A, et al. Genome-wide atlas of gene expression in the adult mouse brain. *Nature.* 2007;445(7124):168-76.
156. Eisen MB, Spellman PT, Brown PO, Botstein D. Cluster analysis and display of genome-wide expression patterns. *Proc Natl Acad Sci U S A.* 1998;95(25):14863-8.
157. Saldanha AJ. Java Treeview--extensible visualization of microarray data. *Bioinformatics.* 2004;20(17):3246-8.
158. Monti S, Tamayo P, Mesirov J, Golub T. Consensus clustering: A resampling-based method for class discovery and visualization of gene expression microarray data. *Mach Learn.* 2003;52(1-2):91-118.
159. Wilkerson MD, Hayes DN. ConsensusClusterPlus: a class discovery tool with confidence assessments and item tracking. *Bioinformatics.* 2010;26(12):1572-3.
160. Rousseeuw PJ. Silhouettes - A graphical aid to the interpretation and validation of cluster-analysis. *Journal of Computational and Applied Mathematics.* 1987;20:53-65.
161. Dabney AR. Classification of microarrays to nearest centroids. *Bioinformatics.* 2005;21(22):4148-54.
162. Barbie DA, Tamayo P, Boehm JS, Kim SY, Moody SE, Dunn IF, et al. Systematic RNA interference reveals that oncogenic KRAS-driven cancers require TBK1. *Nature.* 2009;462(7269):108-12.
163. Vitucci M, Karpnich NO, Bash RE, Werneke AM, Schmid RS, White KK, et al. Cooperativity between MAPK and PI3K signaling activation is required for glioblastoma pathogenesis. *Neuro-oncology.* 2013:Epub 2013 Jul 3.

164. Gorovets D, Kannan K, Shen R, Kasthuber ER, Islamdoust N, Campos C, et al. IDH mutation and neuroglial developmental features define clinically distinct subclasses of lower grade diffuse astrocytic glioma. *Clinical Cancer Research*. 2012;18(9):2490-501.
165. Weigman VJ, Chao HH, Shabalin AA, He X, Parker JS, Nordgard SH, et al. Basal-like breast cancer DNA copy number losses identify genes involved in genomic instability, response to therapy, and patient survival. *Breast cancer research and treatment*. 2012;133(3):865-80.
166. Qiao X, Zhang HH, Liu Y, Todd MJ, Marron JS. Weighted Distance Weighted Discrimination and Its Asymptotic Properties. *J Am Stat Assoc*. 2010;105(489):401-14.
167. Cerami E, Gao J, Dogrusoz U, Gross BE, Sumer SO, Aksoy BA, et al. The cBio cancer genomics portal: an open platform for exploring multidimensional cancer genomics data. *Cancer Discov*. 2012;2(5):401-4.
168. Guha A, Feldkamp MM, Lau N, Boss G, Pawson A. Proliferation of human malignant astrocytomas is dependent on Ras activation. *Oncogene*. 1997;15(23):2755-65.
169. Jeuken J, van den Broecke C, Gijzen S, Boots-Sprenger S, Wesseling P. RAS/RAF pathway activation in gliomas: the result of copy number gains rather than activating mutations. *Acta Neuropathol*. 2007;114(2):121-33.
170. Dasgupta B, Li W, Perry A, Gutmann DH. Glioma formation in neurofibromatosis 1 reflects preferential activation of K-RAS in astrocytes. *Cancer Res*. 2005;65(1):236-45.
171. Tusher VG, Tibshirani R, Chu G. Significance analysis of microarrays applied to the ionizing radiation response. *Proceedings of the National Academy of Sciences of the United States of America*. 2001;98(9):5116-21.
172. Molofsky AV, Slutsky SG, Joseph NM, He S, Pardal R, Krishnamurthy J, et al. Increasing p16INK4a expression decreases forebrain progenitors and neurogenesis during ageing. *Nature*. 2006;443(7110):448-52.
173. Whitfield ML, Sherlock G, Saldanha AJ, Murray JI, Ball CA, Alexander KE, et al. Identification of genes periodically expressed in the human cell cycle and their expression in tumors. *Molecular Biology of the Cell*. 2002;13(6):1977-2000.
174. Negrini S, Gorgoulis VG, Halazonetis TD. Genomic instability--an evolving hallmark of cancer. *Nature Reviews Molecular Cell Biology*. 2010;11(3):220-8.
175. Henson JW, Schnitker BL, Correa KM, von Deimling A, Fassbender F, Xu HJ, et al. The retinoblastoma gene is involved in malignant progression of astrocytomas. *Ann Neurol*. 1994;36(5):714-21.
176. Sottoriva A, Spiteri I, Piccirillo SG, Touloumis A, Collins VP, Marioni JC, et al. Intratumor heterogeneity in human glioblastoma reflects cancer evolutionary dynamics. *Proceedings of the National Academy of Sciences of the United States of America*. 2013;110(10):4009-14.

177. Ge WP, Miyawaki A, Gage FH, Jan YN, Jan LY. Local generation of glia is a major astrocyte source in postnatal cortex. *Nature*. 2012;484(7394):376-80.
178. Eberhart CG. Three down and one to go: modeling medulloblastoma subgroups. *Cancer Cell*. 2012;21(2):137-8.
179. CBTRUS. CBTRUS Statistical Report: Primary Brain and Central Nervous System Tumors Diagnosed in the United States in 2004-2008. Hinsdale, IL: Central Brain Tumor Registry of the United States; 2012.
180. Gaspar LE, Fisher BJ, Macdonald DR, LeBer DV, Halperin EC, Schold SC, Jr., et al. Supratentorial malignant glioma: patterns of recurrence and implications for external beam local treatment. *International journal of radiation oncology, biology, physics*. 1992;24(1):55-7.
181. Giese A, Bjerkvig R, Berens ME, Westphal M. Cost of migration: invasion of malignant gliomas and implications for treatment. *Journal of clinical oncology : official journal of the American Society of Clinical Oncology*. 2003;21(8):1624-36.
182. Workman P, Clarke PA, Raynaud FI, van Montfort RL. Drugging the PI3 kinome: from chemical tools to drugs in the clinic. *Cancer Research*. 2010;70(6):2146-57.
183. Reardon DA, Rich JN, Friedman HS, Bigner DD. Recent advances in the treatment of malignant astrocytoma. *Journal of clinical oncology : official journal of the American Society of Clinical Oncology*. 2006;24(8):1253-65.
184. Ohgaki H, Kleihues P. Genetic pathways to primary and secondary glioblastoma. *American Journal of Pathology*. 2007;170(5):1445-53.
185. Snuderl M, Fazlollahi L, Le LP, Nitta M, Zhelyazkova BH, Davidson CJ, et al. Mosaic amplification of multiple receptor tyrosine kinase genes in glioblastoma. *Cancer cell*. 2011;20(6):810-7.
186. Jun HJ, Acquaviva J, Chi D, Lessard J, Zhu H, Woolfenden S, et al. Acquired MET expression confers resistance to EGFR inhibition in a mouse model of glioblastoma multiforme. *Oncogene*. 2012;31(25):3039-50.
187. Mellinghoff IK, Wang MY, Vivanco I, Haas-Kogan DA, Zhu S, Dia EQ, et al. Molecular determinants of the response of glioblastomas to EGFR kinase inhibitors. *The New England journal of medicine*. 2005;353(19):2012-24.
188. Suzuki A, de la Pompa JL, Stambolic V, Elia AJ, Sasaki T, del Barco Barrantes I, et al. High cancer susceptibility and embryonic lethality associated with mutation of the PTEN tumor suppressor gene in mice. *Current biology : CB*. 1998;8(21):1169-78.
189. Di Cristofano A, Pandolfi PP. The multiple roles of PTEN in tumor suppression. *Cell*. 2000;100(4):387-90.

190. Dannenberg JH, van Rossum A, Schuijff L, te Riele H. Ablation of the retinoblastoma gene family deregulates G(1) control causing immortalization and increased cell turnover under growth-restricting conditions. *Genes Dev.* 2000;14(23):3051-64.
191. Stec DE, Davisson RL, Haskell RE, Davidson BL, Sigmund CD. Efficient liver-specific deletion of a floxed human angiotensinogen transgene by adenoviral delivery of Cre recombinase in vivo. *The Journal of biological chemistry.* 1999;274(30):21285-90.
192. Hulkower KI, Herber RL. Cell migration and invasion assays as tools for drug discovery. *Pharmaceutics.* 2011;3(1):107-24.
193. Liang CC, Park AY, Guan JL. In vitro scratch assay: a convenient and inexpensive method for analysis of cell migration in vitro. *Nat Protoc.* 2007;2(2):329-33.
194. Smalley KS, Haass NK, Brafford PA, Lioni M, Flaherty KT, Herlyn M. Multiple signaling pathways must be targeted to overcome drug resistance in cell lines derived from melanoma metastases. *Mol Cancer Ther.* 2006;5(5):1136-44.
195. Johnson WE, Li C, Rabinovic A. Adjusting batch effects in microarray expression data using empirical Bayes methods. *Biostatistics.* 2007;8(1):118-27.
196. Smedley D, Haider S, Ballester B, Holland R, London D, Thorisson G, et al. BioMart--biological queries made easy. *BMC Genomics.* 2009;10:22.
197. Efron B, Tibshirani R. On testing the significance of sets of genes. *Ann Appl Stat.* 2007;1(1):107-29.
198. Rodriguez LG, Wu X, Guan JL. Wound-healing assay. *Methods in molecular biology.* 2005;294:23-9.
199. Shabalín AA, Weigman VJ, Perou CM, Nobel AB. Finding Large Average Submatrices in High Dimensional Data. *Ann Appl Stat.* 2009;3(3):985-1012.
200. Planchon SM, Waite KA, Eng C. The nuclear affairs of PTEN. *Journal of cell science.* 2008;121(Pt 3):249-53.
201. Alimonti A, Carracedo A, Clohessy JG, Trotman LC, Nardella C, Egia A, et al. Subtle variations in Pten dose determine cancer susceptibility. *Nature genetics.* 2010;42(5):454-8.
202. Fraser MM, Zhu X, Kwon CH, Uhlmann EJ, Gutmann DH, Baker SJ. Pten loss causes hypertrophy and increased proliferation of astrocytes in vivo. *Cancer Research.* 2004;64(21):7773-9.
203. Inaba N, Kimura M, Fujioka K, Ikeda K, Somura H, Akiyoshi K, et al. The effect of PTEN on proliferation and drug-, and radiosensitivity in malignant glioma cells. *Anticancer research.* 2011;31(5):1653-8.

204. Demuth T, Berens ME. Molecular mechanisms of glioma cell migration and invasion. *Journal of neuro-oncology*. 2004;70(2):217-28.
205. Gidekel Friedlander SY, Chu GC, Snyder EL, Girnius N, Dibelius G, Crowley D, et al. Context-dependent transformation of adult pancreatic cells by oncogenic K-Ras. *Cancer Cell*. 2009;16(5):379-89.
206. Cattaneo MG, Gentilini D, Vicentini LM. Deregulated human glioma cell motility: inhibitory effect of somatostatin. *Molecular and cellular endocrinology*. 2006;256(1-2):34-9.
207. Goldberg L, Kloog Y. A Ras inhibitor tilts the balance between Rac and Rho and blocks phosphatidylinositol 3-kinase-dependent glioblastoma cell migration. *Cancer Research*. 2006;66(24):11709-17.
208. Clark MJ, Homer N, O'Connor BD, Chen Z, Eskin A, Lee H, et al. U87MG decoded: the genomic sequence of a cytogenetically aberrant human cancer cell line. *PLoS genetics*. 2010;6(1):e1000832.
209. Jori FP, Galderisi U, Napolitano MA, Cipollaro M, Cascino A, Giordano A, et al. RB and RB2/P130 genes cooperate with extrinsic signals to promote differentiation of rat neural stem cells. *Molecular and cellular neurosciences*. 2007;34(3):299-309.
210. Gregorian C, Nakashima J, Le Belle J, Ohab J, Kim R, Liu A, et al. Pten deletion in adult neural stem/progenitor cells enhances constitutive neurogenesis. *The Journal of neuroscience : the official journal of the Society for Neuroscience*. 2009;29(6):1874-86.
211. Dasgupta B, Gutmann DH. Neurofibromin regulates neural stem cell proliferation, survival, and astroglial differentiation in vitro and in vivo. *The Journal of neuroscience : the official journal of the Society for Neuroscience*. 2005;25(23):5584-94.
212. Pei Y, Moore CE, Wang J, Tewari AK, Eroshkin A, Cho YJ, et al. An animal model of MYC-driven medulloblastoma. *Cancer Cell*. 2012;21(2):155-67.
213. Northcott PA, Korshunov A, Pfister SM, Taylor MD. The clinical implications of medulloblastoma subgroups. *Nature reviews Neurology*. 2012;8(6):340-51.
214. Dolecek TA, Propp JM, Stroup NE, Kruchko C. CBTRUS statistical report: primary brain and central nervous system tumors diagnosed in the United States in 2005-2009. *Neuro Oncol*. 2012;14 Suppl 5:v1-49.
215. Cheon DJ, Orsulic S. Mouse models of cancer. *Annual review of pathology*. 2011;6:95-119.
216. Louis SA, Rietze RL, Deleyrolle L, Wagey RE, Thomas TE, Eaves AC, et al. Enumeration of neural stem and progenitor cells in the neural colony-forming cell assay. *Stem Cells*. 2008;26(4):988-96.
217. Dinca EB, Sarkaria JN, Schroeder MA, Carlson BL, Voicu R, Gupta N, et al. Bioluminescence monitoring of intracranial glioblastoma xenograft: response to primary and salvage temozolomide therapy. *Journal of neurosurgery*. 2007;107(3):610-6.

218. Chen J, Li Y, Yu TS, McKay RM, Burns DK, Kernie SG, et al. A restricted cell population propagates glioblastoma growth after chemotherapy. *Nature*. 2012;488(7412):522-6.
219. Beier D, Schulz JB, Beier CP. Chemoresistance of glioblastoma cancer stem cells--much more complex than expected. *Mol Cancer*. 2011;10:128.
220. Beier D, Rohrl S, Pillai DR, Schwarz S, Kunz-Schughart LA, Leukel P, et al. Temozolomide preferentially depletes cancer stem cells in glioblastoma. *Cancer Research*. 2008;68(14):5706-15.
221. Liu G, Yuan X, Zeng Z, Tunici P, Ng H, Abdulkadir IR, et al. Analysis of gene expression and chemoresistance of CD133+ cancer stem cells in glioblastoma. *Mol Cancer*. 2006;5:67.
222. Kang MK, Kang SK. Tumorigenesis of chemotherapeutic drug-resistant cancer stem-like cells in brain glioma. *Stem Cells Dev*. 2007;16(5):837-47.
223. Tchoghandjian A, Baeza N, Colin C, Cayre M, Metellus P, Beclin C, et al. A2B5 cells from human glioblastoma have cancer stem cell properties. *Brain Pathol*. 2010;20(1):211-21.
224. Hong X, Chedid K, Kalkanis SN. Glioblastoma cell line-derived spheres in serum-containing medium versus serum-free medium: a comparison of cancer stem cell properties. *International journal of oncology*. 2012;41(5):1693-700.
225. Combs SE, Schulz-Ertner D, Roth W, Herold-Mende C, Debus J, Weber KJ. In vitro responsiveness of glioma cell lines to multimodality treatment with radiotherapy, temozolomide, and epidermal growth factor receptor inhibition with cetuximab. *International journal of radiation oncology, biology, physics*. 2007;68(3):873-82.
226. Yang X, Darling JL, McMillan TJ, Peacock JH, Steel GG. Radiosensitivity, recovery and dose-rate effect in three human glioma cell lines. *Radiotherapy and oncology : journal of the European Society for Therapeutic Radiology and Oncology*. 1990;19(1):49-56.
227. Agarwala SS, Kirkwood JM. Temozolomide, a novel alkylating agent with activity in the central nervous system, may improve the treatment of advanced metastatic melanoma. *The oncologist*. 2000;5(2):144-51.
228. Hirose Y, Berger MS, Pieper RO. p53 effects both the duration of G2/M arrest and the fate of temozolomide-treated human glioblastoma cells. *Cancer Research*. 2001;61(5):1957-63.
229. Chalmers AJ, Ruff EM, Martindale C, Lovegrove N, Short SC. Cytotoxic effects of temozolomide and radiation are additive- and schedule-dependent. *International journal of radiation oncology, biology, physics*. 2009;75(5):1511-9.
230. Szentirmai O, Baker CH, Lin N, Szucs S, Takahashi M, Kiryu S, et al. Noninvasive bioluminescence imaging of luciferase expressing intracranial U87 xenografts: correlation with magnetic resonance imaging determined tumor volume and longitudinal use in assessing tumor growth and antiangiogenic treatment effect. *Neurosurgery*. 2006;58(2):365-72; discussion -72.

231. Goldhoff P, Clarke J, Smirnov I, Berger MS, Prados MD, James CD, et al. Clinical stratification of glioblastoma based on alterations in retinoblastoma tumor suppressor protein (RB1) and association with the proneural subtype. *Journal of neuropathology and experimental neurology*. 2012;71(1):83-9.
232. Hawrylycz MJ, Lein ES, Guillozet-Bongaarts AL, Shen EH, Ng L, Miller JA, et al. An anatomically comprehensive atlas of the adult human brain transcriptome. *Nature*. 2012;489(7416):391-9.
233. Doyle JP, Dougherty JD, Heiman M, Schmidt EF, Stevens TR, Ma G, et al. Application of a translational profiling approach for the comparative analysis of CNS cell types. *Cell*. 2008;135(4):749-62.
234. Belgard TG, Marques AC, Oliver PL, Abaan HO, Sirey TM, Hoerder-Suabedissen A, et al. A transcriptomic atlas of mouse neocortical layers. *Neuron*. 2011;71(4):605-16.
235. Tsai HH, Li H, Fuentealba LC, Molofsky AV, Taveira-Marques R, Zhuang H, et al. Regional astrocyte allocation regulates CNS synaptogenesis and repair. *Science*. 2012;337(6092):358-62.
236. Yeh TH, Lee da Y, Gianino SM, Gutmann DH. Microarray analyses reveal regional astrocyte heterogeneity with implications for neurofibromatosis type 1 (NF1)-regulated glial proliferation. *Glia*. 2009;57(11):1239-49.
237. Kirk R, Hutchinson L. Oncology trials--the elephant in the room. *Nat Rev Clin Oncol*. 2012;9(4):185-6.
238. Berry DA. Adaptive clinical trials in oncology. *Nat Rev Clin Oncol*. 2012;9(4):199-207.